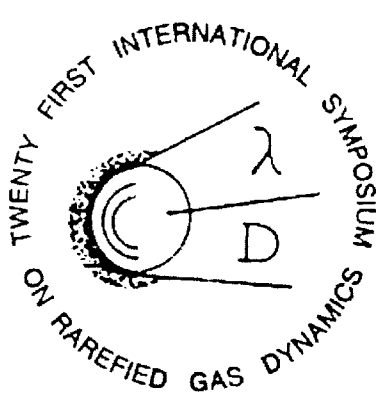

21st International
Symposium on

Rarefied Gas
Dynamics

Marseille (France)
26-31 July 1998

Book of Abstracts
Volume III

Special Session

Molecular Beams

1. AGENCY USE ONLY (Leave blank)	2. REPORT DATE	3. REPORT TYPE AND DATES COVERED
	30 July 1998	Conference Proceedings

4. TITLE AND SUBTITLE

21st International Symposium on Rarefied Gas Dynamics

5. FUNDING NUMBERS

F6170898W0021

6. AUTHOR(S)

Conference Committee

7. PERFORMING ORGANIZATION NAME(S) AND ADDRESS(ES)

I.U.S.T.I.
Technopole de Chateau-Gombert; 5 Rue Enrico Fermi
Marseille 13453
France

8. PERFORMING ORGANIZATION REPORT NUMBER

N/A

9. SPONSORING/MONITORING AGENCY NAME(S) AND ADDRESS(ES)

EOARD
PSC 802 BOX 14
FPO 09499-0200

10. SPONSORING/MONITORING AGENCY REPORT NUMBER

CSP 98-1024

11. SUPPLEMENTARY NOTES

3 Volumes - Oral sessions, Poster sessions, and Special Session

12a. DISTRIBUTION/AVAILABILITY STATEMENT

Approved for public release; distribution is unlimited.

12b. DISTRIBUTION CODE

A

13. ABSTRACT (Maximum 200 words)

The Final Proceedings for 21st International Symposium on Rarefied Gas Dynamics, 26 July 1998 - 31 July 1998

This is an interdisciplinary conference. Topics include Boltzman equation and kinetic theory; Mathematical methods and models; Flow in transitional and rarefied regimes; Numerical simulations of RGD flows; Instrumentation and diagnostics in RGD flows; Free jets and molecular beams; Elementary collisional processes; Transport and relaxation phenomena; Chemical processes; Shock waves; Low density plasmas and ionized gases; Gas-surface interactions; Molecular beams; Clusters; Aerosols; Phase change; Aerodynamics and aerothermochemistry of space vehicles; Industrial applications I (vacuum technology, thin film, microengines...); Industrial applications II (beams, jets, lasers, reactors...); Astrophysics; Environmental aspects.

14. SUBJECT TERMS	15. NUMBER OF PAGES
EOARD, Rarefied Gas Dynamics, Low Density Plasma	875
	16. PRICE CODE N/A

17. SECURITY CLASSIFICATION OF REPORT	18. SECURITY CLASSIFICATION OF THIS PAGE	19. SECURITY CLASSIFICATION OF ABSTRACT	20. LIMITATION OF ABSTRACT
UNCLASSIFIED	UNCLASSIFIED	UNCLASSIFIED	UL

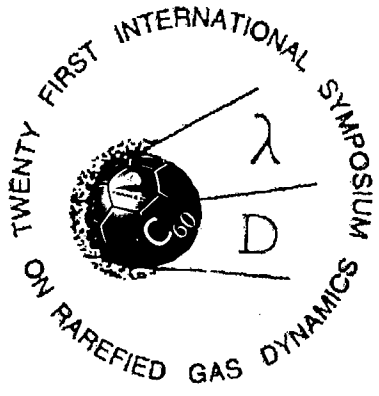

21st International
Symposium on

Rarefied Gas
Dynamics

Marseille (France)
26-31 July 1998

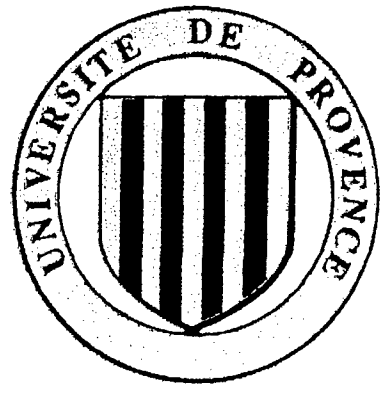

Book of Abstracts
Volume III

Special Session

Molecular Beams

FOREWORD : WHAT IS THE MOLECULAR BEAM SESSION ?

Maintaining a balance between experiment and theory is important to a Symposium including the RGD topics and applications. This has been conveniently obtained during several decades but, at the last meetings, the experimentalists were more and more "rarefied" and replaced by users of the Monte-Carlo methods.

Among about 400 abstracts submitted to the RGD 21, only 15% have presented experimental works. Consequently, at the beginning of the year, the central part of the RGD programme was strongly depopulated, mainly on the following subjects: instrumentation and diagnostics, free jets and molecular beams, plasma flows, relaxation and condensation in expansions, clusters and nanoparticles, elementary collisional processes, interaction with radiation, gas-surface interaction in the style of Lloyd Thomas. These subjects represent essentially the Physics of the RGD which is more and more developed by the Beam and Laser people, now preferring the Conferences on Molecular Beams and Gas-Surface, due to the evolution of the RGD Symposia.

In order to attract again the missing experimentalists, we have organized a special session in the style of the Molecular Beam Symposia issued from the RGD community. This has been possible during the last four months thanks to individual invitations accepted by 34 speakers without financial support. Furthermore, the participation has been enforced by additional contributors making it possible to have finally 62 papers in the Molecular Beam Session covering four full days of the Symposium.

In conclusion, the organization of the Molecular Beam Session already appears as a successful experience to gather together again the RGD people and the Molecular Beam people, as in the past decades. Certainly they are complementary to each other, from various points of view, especially by considering theory and experiment.
After developing for the RGD community most of the diagnostic techniques largely based on the laser methods, now the Physicists and Chemists offer important new topics and applications to the RGD theoreticians as described in the following programme : laser cooling of atoms and molecules, new types of beams and interactions at extremely low energy, collisions with aligned or oriented molecules, clusters and nanoparticles, nanostructure fabrication using laser cooling, thin film deposition, supersonic free-jet expitaxy, and other gas-surface interactions including chemisorption, carbonization, nitrification, etc. which are very promising in the development of industrial applications.
Finally the organization of the Molecular Beam Session has largely enhanced the participation in the RGD-21, mainly from Europe.

Perhaps it is not too late to return to the RGD Symposia in their traditional form including essentially a balance between experiment and theory?

Roger Campargue
Cochairman, RGD-21

GENERAL INFORMATION ON RGD SYMPOSIA

Objectives and Scope

Since their creation in France (Nice, 1958) the International Symposia on Rarefied Gas Dynamics serve as one of the main forums for presentation of recent advances in scientific and technical fields involving physical phenomena and processes in gas flows in the rarefied regimes.

These fields include numerous topics like kinetic theory, direct simulation and various models of transitional and rarefied regimes, instrumentation and diagnostics to investigate flows in wind tunnels, free jets and molecular beams, low density plasmas, gas-surface interactions with or without phase change. Thus, the relaxation and condensation in expansions, the elementary collisional processes, the interaction with radiation, the growth and properties of clusters, nanoparticles, nanostructures, thin films, etc., are on the basis of the RGD research. Applications to hypersonic flights, aerothermochemistry, environment, microelectronics, surface passivation, vacuum technology, are also included as well as gas lasers and astrophysical aspects.

Previous locations of RGD meetings

Nice	France	1958	Cannes	France	1978
Berkeley	U.S.A.	1960	Charlottesville	U.S.A.	1980
Paris	France	1962	Novosibirsk	Russia	1982
Toronto	Canada	1964	Tsukuba	Japan	1984
Oxford	U.K.	1966	Grado	Italy	1986
Cambridge	U.S.A	1968	Pasadena	U.S.A.	1988
Pise	Italy	1970	Aachen	Germany	1990
Stanford	U.S.A.	1972	Vancouver	Canada	1992
Gottingen	Germany	1974	Oxford	U.K.	1994
Aspen	U.S.A	1976	Beijing	China	1996

International Advisory Committee

A.E. BEYLICH	Germany	G. KOPPENWALLNER	Germany
G.A. BIRD	Australia	J. KUNC	U.S.A.
V. BOFFI	Italy	J.C. LENGRAND	France
S.E. BORISOV	Russia	R.G. LORD	U.K.
I. BOYD	U.S.A.	J. MOSS	U.S.A.
R. BRUN	France	K. NANBU	Japan
R. CAMPARGUE	France	A.K. REBROV	Russia
C. CERCIGNANI	Italy	Y.A. RIJOV	Russia
R. GATIGNOL	France	A. SANTOS	Spain
O. HAGENA	Germany	C. SHEN	China
J.K. HARVEY	U.K.	B. SHIZGAL	Canada
L.J.F. HERMANS	The Netherlands	Y. SONE	Japan
F.C. HURLBUT	U.S.A.	J.P. TOENNIES	Germany
M.N. KOGAN	Russia	T. YTREHUS	Norway

21st RAREFIED GAS DYNAMICS SYMPOSIUM

It is worth mentioning that the RGD-21 is held in France just 40 years after the first meeting (Nice,1958) and 20 years after the eleventh meeting (Cannes,1978) the lastest one organized in our country.

Organizers : R. Brun, Chairman, General Organization
R. Campargue, Chairman, Scientific Organization
R. Gatignol, Scientific Committee
A. Lebehot, Scientific Committee
J.C. Lengrand, Scientific Committee
M. Leboisne, Secretary, General Organization

Sponsoring Organizations :

. European Space Agency (ESA)
. European Office of Aerospace Research and Development (EOARD)
. European Research Community on Flow, Turbulence and Combustion (ERCOFTAC)
. Imperial College, London
. Lloyd Thomas Memorial Foundation, USA
. Centre d'Etudes Scientifiques et Techniques d'Aquitaine (CEA/CESTA)
. Centre d'Etudes Spatiales (CNES)
. Aerospatiale
. Ministère de l'Education Nationale, de la Recherche et de la Technologie
. Conseil Régional de Provence-Alpes-Côte d'Azur
. Conseil Général des Bouches du Rhône
. Ville de Marseille
. Association Universitaire de Mécanique (AUM)
. Université de Provence
. Centre National de la Recherche Scientifique (Science & Physique de l'Ingénieur)

MOLECULAR BEAM SESSION AT RGD-21

Organizers : V. Aquilanti (Perugia)
R. Campargue (Saclay)
E.L. Knuth (UCLA)
J.P. Toennies (Gottingen)

Additional Sponsoring devoted to Molecular Beam Session :

Lasers : . Coherent
. Continuum
. Quantel
. Spectra-Physics

Laser & Optical Components : Technoscience

Mechanics : . Physiméca-Technologie

Quantel

17 avenue de l'Atlantique - BP 23 - 91941 Les Ulis cedex - FRANCE
Phone : + 33 (0)1 69 29 17 00 Fax : + 33 (0)1 69 29 17 29 e.mail : quantel@quantel.fr
web : www.quantel.fr

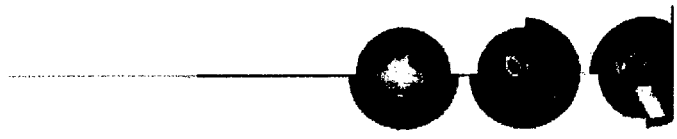

BRILLIANT series

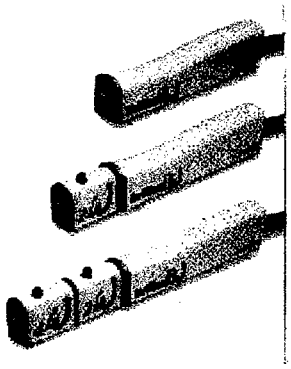

Backed up by a 25 years experience in the field of solid-state pulsed Nd:YAG lasers, the name of Quantel has come to mean reliability and innovation throughout the world.

Quantel's unique know-how has enabled it to develop the original and innovating "BRILLIANT" concept, and a complete range of associated products :

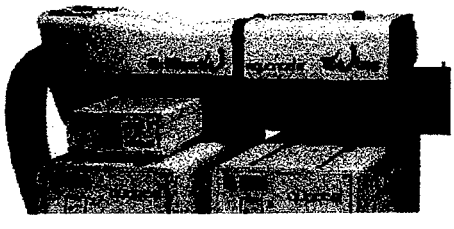

BRILLIANT & BRILLIANT B (compact oscillators) and their harmonic generators,
TWINS (double pulse system),
RAINBOW (tunable broadband OPO - Optical Parametric Oscillator) ...

YG900 & YG980 series

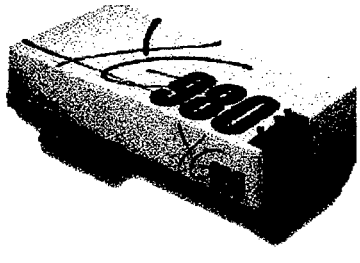

Lasers in the YG980 an YG900 series represent the latest evolution in the modular systems which have made Quantel a success since 1970.
Reliability, quality and innovation are the key words which have guided Quantel's research & development team.
The various laser models - Nd:YAG Q-switched (YG980 series) and mode-locked (YG900 series) - generate high energy, high average power, high stability and optimum beam quality.
Numerous options enable these sources to be adapted to individual user's requirement.

TDL 90 Tunable Dye Laser

The TDL 90 is a modular high efficiency dye laser, pumped by pulsed Q-Switched Nd:YAG lasers. Various extensions allow to cover a wide range of wavelenghts from 198 nm to 4500 nm.

RAINBOW
Optical Parametric Oscillator (OPO)

Rainbow is a plug-in, factory aligned, broadband OPO, with a unique compact and rugged design (sealed ring cavity), pumped by a Brilliant or a Brilliant B Tuning and scanning can be fully monitored through software and a built-in spectrometer.
By pumping at various wavelengths - 1064 nm, 532 nm, 355 nm, 266 nm – and by using UV extension modules, it is possible to cover from 210 nm to more than 2 µm.

Laserblast

Cleaning with laser

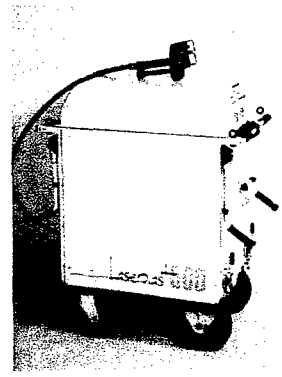

100% Quantel's subsidiary, Laserblast is specialized in laser cleaning systems.
Its line of product is unique worldwide, using optical fibers to transport the light energy. This translates into remarkable ergonomic features and easy integration into automated robot systems.

17 avenue de l'Atlantique - BP 23 - 91941 Les Ulis cedex - FRANCE
Phone : + 33 (0)1 69 29 17 00 Fax : + 33 (0)1 69 29 17 29 e.mail : quantel@quantel.fr web: www.quantel.fr

PROGRAMME OF THE MOLECULAR BEAM SESSION
ROOM: Lavoisier, except otherwise stated

TUESDAY, JULY 28, 1998

8:30 - 9:10 Invited Plenary Lecture
A. ASPECT :*Laser Cooling of Atoms beyond the Limits* **(abstract in page 3)**
Chair: R. Campargue (Saclay)
ROOM: Grand Amphithéâtre

9:15 - 10:35 Session MB 1: Laser Cooling and Manipulation of Atoms and Molecules
Chair: J. Schmiedmayer (Innsbruck)

9:15 ***Making Molecules at MicroKelvin***
W.C. Stwalley

9:45 ***New Excitements in Molecular Optics: Squeezing, Waveguiding, and Reflecting Molecular Beams with Light***
T. Seideman

10:10 ***Progress in Coherent Manipulation of Atoms and Molecules in Beams***
K. Bergmann, H. Theuer, Th. Halfmann

10:35 Coffee Break

10:50 - 12:30 Session MB 2: Effects of Molecule Alignment or Orientation in Scattering Experiments
Chair: J. Fayeton (Orsay)

10:50 ***Aligned Molecules and Intermolecular Forces by Quantum Interference Scattering: O_2-Rare Gases Interactions, Bonding in O_4 and Role of Spin Coupling***
V. Aquilanti, D. Ascenzi, M. Bartolomei, D. Cappelletti, M. de Castro, F. Pirani

11:20 ***Photodissociation of NO_2 at 212.8 nm Yields Aligned $O(^3P_j)$ Atoms***
M. Ahmed, D.S. Peterka, O.S. Vasyutinskii, A.G. Suits

11:45 ***Inelastic Collisions with Oriented Molecules: A Quantitative Exploration of the Steric Effect***
M.J.L. de Lange, M.M.J.E. Drabbels, J. Bulthuis, J.G. Snijders, S. Stolte

12:10 ***Laser Cooling and Reaction Dynamics in Excited Electronic States***
E. Pollak, G. Gershinsky

12:30: Lunch

14:00 - 14:30 Invited Lectures: A.V. Bobylev (Room: Marion)
J.P. Boeuf (Room: Pérès)

14:35 - 16:40 Session MB 3: Theoretical Properties of Clusters.
Gas-Surface I: Interactions of Clusters and Fullerene with Surfaces
Chair: F. Huisken (Göttingen)

14:35 ***Properties of Clusters from the Random Matrix Theory***
V.M. Akulin

15:00 ***Femtosecond Neutralization Dynamics and Electron Emission in Cluster-Surface Collisions***
K.H. Meiwes-Broer, B. Wrenger, M.E. Garcia, O. Speer

15:25 ***Catalytic Reactivity, Mobility, and Electron Dynamics of Deposited Silver Clusters***
T. Leisner, U. Busolt, E. Cottanzin, H. Röhr, L. Socaciu, S. Wolf, L. Wöste

15:50 ***Rotational Distributions of Scattered Molecules from van der Waals Cluster-Surface Collision***
E. Fort, A. De Martino, F. Pradère, M. Châtelet, H. Vach

16:15 ***Charge Transfer Processes in Hyperthermal (5-50 eV) Fullerene-Surface Collisions***
A. Bekkerman, B. Tsipinyuk, E. Kolodney

17:00 - 18:30 POSTER SESSION MB - P
Chair: A. Gonzalez-Urena (Madrid)

- ***Observation and Spectroscopy of Metastable O_4***
  D.S. Peterka, M. Ahmed, A.G. Suits

  Elastic Scattering of Metastable He($2^{1,3}S$) Atomic Beam by the Ground-State Na Beam: Phase Analysis of Scattering Mechanism
  E.Yu. Remeta, V.I. Kelemen, A.V. Snegursky, A.N. Zavilopulo

  Energy Analysis and Model Calculations of Collisional Acceleration in Seeded Molecular Beams: a Study of Xe/He and C_{60}/He
  B. Tsipinyuk, A. Budrevich, A. Bekkerman, E. Kolodney

- ***REMPI Spectroscopy of Internal State Populations in HBr + Ar and HBr + Nitrogen Free Jets: Rotational Relaxation of HBr***
  A.E. Belikov, M.M. Ahern, M.A. Smith

  Femto Second (imaging) Pump Probe Experiments with a High Repetition Rate in a Molecular Beam
  W. Roeterdink, A. Rijs, P. Wasylczyk, A. Wiskerke, S. Stolte, M. Drabbels, M. Janssen

  Molecular Beam Studies of Chiral Molecules
  A. Giardini-Guidoni, S. Piccirillo, A. Latini, D. Toja, A. Paladini, A. Palleschi, M. Satta

  Mixed Clusters Produced in Argon-Nitrogen Coexpansions as Evidenced by two Experimental Methods
  E. Fort, A. De Martino, F. Pradère, M. Châtelet, H. Vach, G. Torchet, M.-F. de Feraudy, Y. Loreaux

- ***Quantum Optics with Atomic Beam Spin Echo***
  M.F.M. DeKieviet, R. Grimm, A. Reiner, M. Zielonkowski

  An Experimental Investigation of Debye-Waller Factor in Hydrogen and Deuterium Scattering from Cu[111] Surface
  M. Varlam, D. Steflea, N. Chiriloaie

  Deposition of Platinum Clusters on HOPG
  A. Bettac, R.-P. Mayer, L. Köller, V. Rank, K.H. Meiwes-Broer

  Collision Dynamics of Water Clusters on a Solid Surface: a Molecular Dynamics and Molecular Beam Studies
  A.A. Vostrikov, I.V. Kazakova, Yu.I. Belousov, D.Yu. Dubov, A.M. Zadorozhny, V.G. Kazakov

  Investigation of Fullerene Thin Fims Deposited with Help of Supersonic Molecular Beam of He
  M.A. Khodorkovski, A.L. Shakhmin, S.V. Murashov, V.Yu. Davydov, Yu.A. Golod, A.M. Alexeev, T.O. Artamonova

WEDNESDAY, JULY 29, 1998

8:30 - 9:00 Invited Lectures: I. Wysong (Room Marion)
D.C. Schram (Room: Pérès)

9:05 - 10:55 Session MB 4: Structure and Relaxation in Molecular Free Jets
Spectroscopy in Cold Molecular Beams
Chair: E.L. Knuth (UCLA)

9:05 ***Raman Studies of Free Jet Expansion***
S. Montero, B. Maté, G. Tejeda, J.M. Fernandez, A. Ramos

9:30 ***Nonequilibrium Distributions of Rotational Energies in a Free-Jet***
H. Hulsman, J. Rozema

9:50 ***The Low Temperature Vibrational Relaxation of OH in the $X^2\Pi$ and $A^2\Sigma$ States in an Argon Free Jet***
M.M. Ahern, M.A. Smith

10:10 ***Thermodynamic Properties of Argon Vapour in a Rarefied Flow at the Onset of Homogeneous Nucleation***
P. Pal

10:30 ***Electronic Spectroscopy of Cold Polycyclic Aromatic Cations in a Molecular Beam***
Ph. Bréchignac, Th. Pino

10:55 Coffee Break

11:10 - 12:30 Session MB 5: Atomic and Molecular Optics
Chair: W.C. Stwalley (Connecticut)

11:10 ***Optics and Interferometry with Atoms and Molecules***
J. Schmiedmayer

11:40 ***Some New Effects in Atom Stern-Gerlach Interferometry***
R. Mathevet, K. Brodsky, F. Perales, K. Rubin, J. Robert, J. Baudon

12:05 ***Wave Packet Interferences in Alkali Atoms and Molecules: Coherent Control and Wave Packet Dynamics***
B. Girard, C. Nicole, M.A. Bouchène

12:30 Lunch

14:00 - 22:00
SYMPOSIUM OUTING

THURSDAY, JULY 30, 1998

8:30 6 9:00 Invited Lectures: A. Beylich (Room: Marion)
M. Capitelli (Room: Pérès)

9:05 - 10:55 Session MB 6: Exotic Session including:
Relaxation of Hot Atoms, Reactivity at Low Temperature,
Structure and Dynamics of Molecule on Surface of Liquid Beam
Chair: A.A. Vostrikov (Novosibirsk)

9:05 ***Relaxation of Electronic Excitation during the Expansion of a Free Jet Generated from a Laser-Sustained Argon-Oxygen Plasma***
A. Lebéhot, J. Kurzyna, R. Campargue, V. Lago, M. Dudeck

9:25 ***Doppler Profiles of the Distribution of $O(^1D)$ Relaxing in Ne: Comparison of Classical and Quantum Cross Sections***
B.D. Shizgal, Y. Matsumi

9:45 ***Optical Emission Spectroscopy of Na Lines in Rarefied Air-Na Plasma Jets***
V. Lago, J. Benier, W. Röck, T. Olivier, M. Dudeck

10:05 ***Recent Developments with the Uniform Supersonic Flow (CRESU) Technique***
B.R. Rowe

10:30 ***Electronic Structure and Dynamics of Solute Molecule on Solution Surface by Use of Liquid Beam Multiphoton Ionization Mass Spectrometry***
T. Kondow, F. Mafuné

10:55 Coffee Break

11:15 - 12:30 Session MB 7: Crossed Molecular Beam Scattering
Chair: V. Aquilanti (Perugia)

11:15 ***New Directions in Reactive Scattering***
A.G. Suits, M. Ahmed, D.S. Peterka, N. Hemmi

11:40 ***Ion-Neutral Collisions in Crossed Beams: Nitrogen Abstraction in the Reaction of Rare Gas Cations and Dications with N_2***
P. Tosi, R. Correale, S. Falcinelli, W.Y. Lu, D. Bassi

12:05 ***Crossed Beam Study of $(NaRb)^+$ Collisional System***
T. Romero, J. De Andrés, M. Alberti, J.M. Lucas, J.M. Bocanegra, A. Aguilar, J. Sogas

12:30 Lunch

THURSDAY, JULY 30, 1998 (continued)

14:00 - 16:00 Session MB 8: Reaction, Coagulation, and Electron Attachment on Clusters or van der Waals Molecules
Chair: G. Meijer (Nijmegen)

14:00 ***Reaction between Barium and N_2O on Large Neon Clusters***
M.A. Gaveau, M. Briant, V. Vallet, J.M. Mestdagh, J.P. Visticot

14:25 ***Chemical Reactions in Small Molecular Clusters***
S. Martrenchard-Barra, D. Solgadi, C. Jouvet, C. Dedonder-Lardeux, G. Grégoire

14:50 ***Resonances in the Reaction Probability and Spectroscopic Probing of the Transition-State Structure of a (van der Waals) Reaction***
S. Skowronek, J.B. Jimenez, A. Gonzales Unrena

15:15 ***Capture and Coagulation of CO Molecules to Small Clusters in Large H_2 Droplets***
E.L. Knuth, S. Schaper, J.P. Toennies

15:35 ***Electron Attachment to Ozone, Oxygen Clusters and Nitric Oxide Clusters***
G. Senn, S. Matejcik, J.D. Skalny, E. Illenberger, N. Mason, Y. Chu, A. Stamatovic, P. Scheier, T.D. Märk

16:00 Coffee Break

16:15 - 18:00 Session MB 9: Diffraction, Polarizability, and Fragmentation of Clusters
Chair: J. Baudon (Paris-Nord)

16:15 ***Diffraction of Cluster Beams from Nano-Transmission Gratings***
W. Schöllkopf, J.P. Toennies

16:45 ***Static Dipole Polarizability and Permanent Dipole of Free Clusters***
Ph. Dugourd, E. Benichou, R. Antoine, D. Rayane, B. Vezin, M. Broyer, C. Ristori, F. Chandezon, B.A. Huber, C. Guet

17:10 ***Collision Induced Fragmentation of Molecules and Small Na^+_n Clusters: Competition between Impulsive and Electronic Mechanisms***
J.A. Fayeton, M. Barat, J.C. Brenot, H. Dunet, Y.J. Picard

17:35 ***Critical Behaviour in Cluster Fragmentation***
B. Farizon, M. Farizon, M.J. Gaillard, F. Gobet, C. Guillermier, J.P. Buchet, M. Carré, P. Scheier, T.D. Märk

20:00 SYMPOSIUM BANQUET

FRIDAY, JULY 31, 1998

8:30 - 9:10 L. Thomas Memorial Lecture (plenary)
Surface Dominated Rarefied Flows and the Potential of Surface Nanomanipulation
Invited Lecturer: E.P. Muntz
Chair: G. Lord
ROOM: Grand Amphitéâtre

9:15 - 10:55 Session MB 10: Gas-Surface II: Deposition, Nanostructure Fabrication, Epitaxy, and Carbonization on Surfaces
Chair: S. Stolte (Amsterdam)

9:15 ***Molecular Beams of Silicon Clusters and Nanoparticles Produced by Laser Pyrolysis of Gas Phase Reactants***
F. Huisken, M. Ehbrecht, B. Kohn

9:40 ***Nanostructure Fabrication by Atom Lithography***
F. Lison, D. Haubrich, D. Meschede

10:05 ***Supersonic Free-Jet Epitaxy of Wide Bandgap Semiconductors***
V.M. Torres, D.C. Jordan, I.S.T. Tsong, R.B. Doak

10:30 ***Chemical Maps and SEM Images of the Reaction Products on Si Surfaces Irradiated with Cold and Hot C_2H_4 Beams***
I. Kusunoki

10:55 Coffee Break

11:15 - 12:30 Session MB 11: Ionization of Fullerenes and of Group III Metal Ammonia Clusters
Chair: E. Kolodney (Haifa)

11:15 ***Infrared Resonance Enhanced Multiphoton Ionization of Fullerenes***
G. Meijer

11:40 ***Radiative Cooling of C_{60} and C^+_{60} in a Beam***
A.A. Vostrikov, D.Yu. Dubov, A.A. Agarkov, S.V. Drozdov, V.A. Galichin

12:05 ***Molecular Beam Studies of Ammonia Clustered with III Group Metals Produced by Laser Reactive Ablation***
T.M. Di Palma, A. Latini, M. Satta, A. Giardini-Guidoni

12:30 Lunch

FRIDAY, JULY 31, 1998 (continued)

14:00 - 14:30 Invited Lectures: D. Gillet (Room: Marion)
R.C. Blanchard, presented by R. Wilmoth (Room: Pérès)

14:35 - 16:30 Session MB12: Gas-Surface III: Chemisorption, Beam Focussing, Quantum Reflection, Spin Echo, van der Waals Cluster Enrichment
Chair: I. Kusunoki (Tohoku)

14:35 ***Probing the Dynamics of Chemisorption though Scattering and Sticking***
A.W. Kleyn

15:00 ***Focussing Helium Atom Beams Using Single Crystal Surfaces***
W. Allison, B. Holst

15:25 ***Sufficient Conditions for Quantum Reflection with Realistic Gas-Surface Interaction Potentials***
R.B. Doak, A.V.G. Chizmeshya

15:45 ***Surface Dynamics Studies using ^{3}He Spin Echo: Coronene on Gold***
M.F.M. DeKieviet, D. Dubbers, S. Hafner, F. Lang

16:10 ***Enrichment of Binary van der Waals Clusters surviving Surface Collision***
E. Fort, A. De Martino, F. Pradère, M. Châtelet, H. Vach

18:00 FAREWELL PARTY

INVITED LECTURES

PLENARY LECTURES

GRAND AMPHITHÉÂTRE

H. GRAD memorial lecture

Monday, July 27, 1998, 9:00

P.L. LIONS: *Mathematical state of the art for Boltzmann equations*
(abstract not available)

L. THOMAS memorial lecture

Friday, July 31, 1998, 8:30

E.P. MUNTZ: *Surface dominated rarefied flows and the potential of surface nanomanipulation*

Additional plenary lecture

Tuesday, July 28, 1998, 8:30

A. ASPECT: *Laser cooling of Atoms beyond the Limits.*

	ROOM MARION	ROOM PÉRÈS
Monday, July 27, 1998 14:00	**S. KAWASHIMA**: *Survey on the initial-boundary value problems for the discrete Boltzmann equation*	**R. G. LORD**: *Modelling of gas-surface interactions and inelastic intermolecular collisions in DSMC calculations*
Tuesday, July 28, 1998 14:00	**A.V. BOBYLEV**: *Relationships between continuous and discrete kinetic theories*	**J.P. BŒUF et al.**: *Physics and modeling of the stationary plasma thruster*
Wednesday, July 29, 1998 8:30	**I. WYSONG**: *Molecular models for reacting flows: should variable collision diameters for internal states be used in DSMC simulations ?*	**D.S. SCHRAM**: *Electronic relaxation in free jet expansions, as generated from arcs, RF, or laser heated plasma sources*
Thursday, July 30, 1998 8:30	**A.E. BEYLICH**: *Structure and applications of jets*	**M. CAPITELLI et al.**: *Non-equilibrium vibrational kinetics and dissociation-recombination processes*
Friday, July 31, 1998 14:00	**D. GILLET**: *On the structure of radiative shock waves in stellar atmospheres*	**R.C. BLANCHARD**: *Review of entry flight measurements during transition from rarefied flow into the hypersonic continuum* (presented by **R. WILMOTH**)

Laser Cooling of Atoms Beyond the Limits *

A. Aspect[1,2]
[1] Groupe d'Optique Atomique - Institut d'Optique Théorique et Appliquée
B.P.147 - F91403 Orsay Cedex- France
[2]previously at : Laboratoire Kastler-Brossel de l'Ecole Normale Supérieure,
24 rue Lhomond, F75005 Paris
in the Laser Cooling Group of Claude Cohen-Tannoudji

In less than two decades, laser cooling of atoms has emerged as a new field of physics, and made major accomplishments, as acknowledged by the 1997 Nobel Prize in Physics awarded to Steven Chu, Claude Cohen-Tannoudji, and W.D. Phillips, "for development of methods to cool and trap atoms with laser light" [1].
In this lecture, I will review the basic principles of laser manipulation of atoms, and show how it has allowed to reach lower and lower temperatures, breaking several so-called "limits":
- the "Doppler limit" (about 100 μK), that was passed thanks to "Sisyphus cooling ", a mechanism resulting from an interplay between optical pumping and light-shifts ;
- the "recoil limit" (about 1 μK), that was passed thanks to "Velocity Selective Dark Resonances", a mechanism resulting from a quantum interference effect in atomic motion.
Laser cooling techniques, which are now standard in many laboratories, have paved the way for the development of atom optics, and in particular the discovery of Bose-Einstein condensates of dilute atomic gases [2, 3, 4], probably as important for atom optics as the discovery of lasers for traditional optics.

References

[1] *Nobel Lectures* , Reviews of Modern Physics, Vol. 70, No3, 1998.

[2] Anderson M.H. et al., Science, Vol.269, p.198, 1995.

[3] Bradley C.C. et al., Phys. Rev. Lett., Vol.75, p.1687, 1995.

[4] Davis K.B. et al., Phys. Rev. Lett., Vol.75, p.3969, 1995.

*Abstract 6935 submitted to the 21st International Symposium on Rarefied Gas Dynamics, Marseille, France, July 26-31, 1998

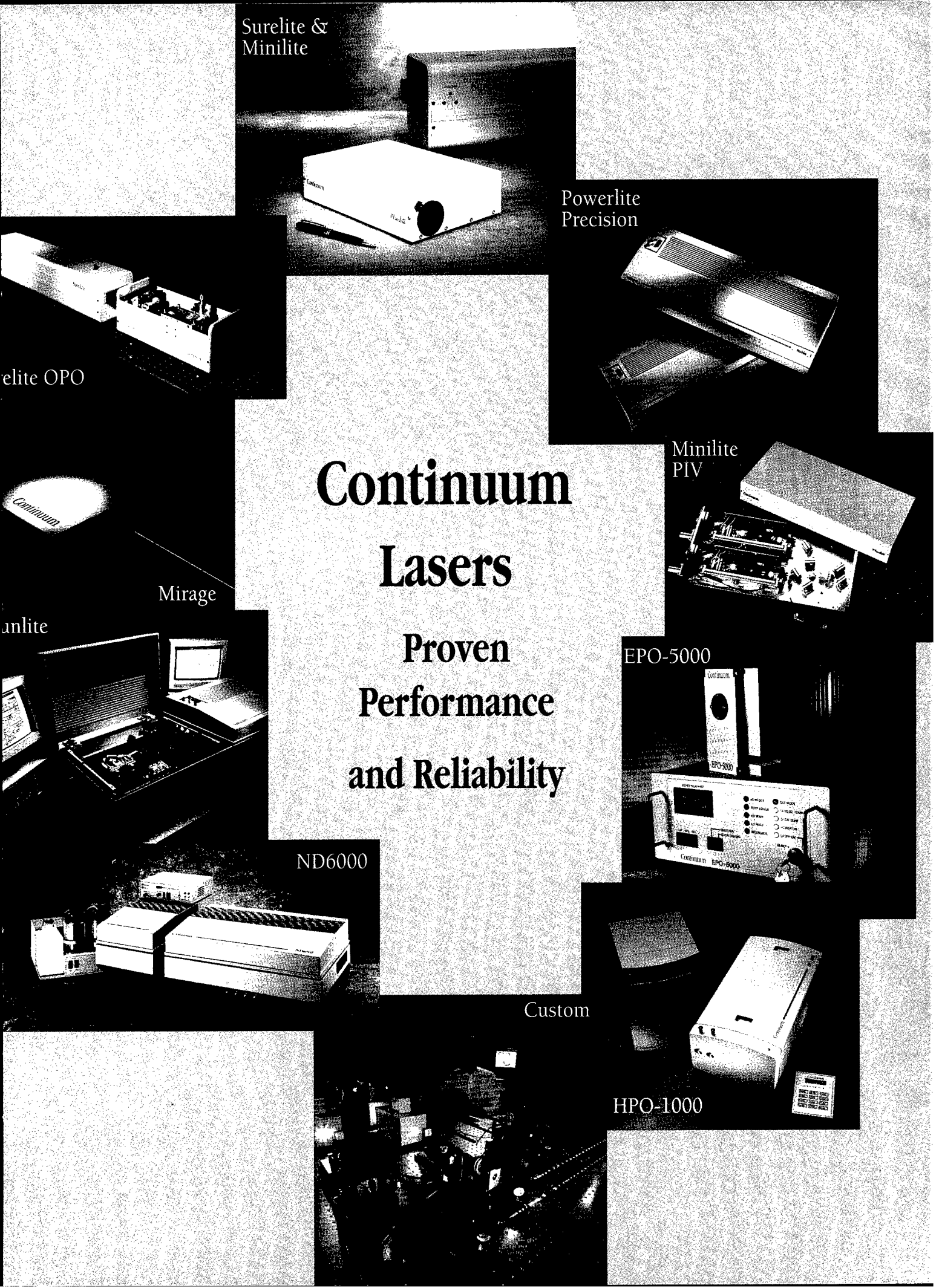
Surelite &
Minilite
Powerlite
Precision
elite OPO
Minilite
PIV
Continuum
Lasers
Proven
Performance
and Reliability
Mirage
unlite
EPO-5000
ND6000
Custom
HPO-1000

Continuum ..... *We take lasers personally.*

Continuum's global leadership in the scientific marketplace attests to our long standing tradition of truly listening to the needs of the scientist, and providing solutions with the highest levels of laser performance and customer service.

This continual customer orientation has led to the development of one of the largest and most diverse ranges of high peak power, advanced solid-state lasers and tunable sources in the world. Systems that continually distinguish themselves with leading edge performance, ease-of-use, rock-solid reliability and affordability.

Pulsed Solid-State Lasers and Tunable Sources

Q-Switched Nanosecond Nd:YAG

- Minilite Series (ML I & ML II)
- Surelite Series (SL I, II & III)
- Powerlite Precision Series
- Lasers for PIV (ML-PIV & SL-PIV)

Mode-Locked Picosecond Nd:YAG

- PY61 Series
- RGA60 Series

Nanosecond Optical Parametric Oscillator (OPO)

Broadband

- Surelite OPO, 410 - 2200 nm
- Mirage 3000B, 720 - 920 nm, <10 cm^{-1}

Narrowband

- Sunlite, 225 - 4000 nm, 0.1 cm^{-1}

Single Longitudinal Mode (SLM)

- Mirage 500, 426 - 2120 nm
- Mirage 3000, 710 - 840 nm & 1.4 - 4.0 µm

Picosecond Optical Parametric Generator (OPG)

- Mirage OPG 8000, 2.25 - 8.0 µm
- Mirage Visible OPG, 440 - 690 nm & 731- 2000 nm

Additional High Power Tunable Sources

- ND6000 Nanosecond Dye, 205 nm - 4.5 µm

Diode-Pumped Nd:YAG

- HPO-1000, 0-1 kHz
- EPO-5000, 0-5 kHz

Custom

- High Energy YAG, Glass & Ruby Systems
- Macro-Pulse Designs
- TR70 – Ti:sapphire Ultrafast Amplifiers
- TeraWatt Bench Top Lasers

Applications

- Ablation
- Cell Biology
- Geology
- Holography
- LIDAR
- LIF
- Machining
- Marking
- Mass Spectroscopy
- Microscopy
- Non-linear Optics
- Particle Image Velocimetry (PIV)
- Photolysis
- Remote Sensing
- Spectroscopy

Main Office
Continuum
Tel: (800) 956-7757
Fax: (408) 727-3550
continuum@ceoi.com
http://www.ceoi.com

Japan
HOYA-Continuum
Tel: 03 3353 5320
Fax: 03 3353 6673
ssalehcc@marinet.or.jp

Germany
Continuum GmbH
Tel: 49 89 800 6410
Fax: 49 89 800 1279
cntgmbh@ccn.de

France
Continuum, Paris
Tel: 69 36 3100
Fax: 69 36 3104
101511.2621@compuserve.com

4/97

MOLECULAR BEAM SESSION MB 1

Laser Cooling and Manipulation of Atoms and Molecules

CHAIR: J. Schmiedmayer (Innsbruck)

ROOM: LAVOISIER
TUESDAY, JULY 28, 1998
9:15 - 10:35

Making Molecules at MicroKelvin* †

William C. Stwalley, University of Connecticut,
Storrs, Connecticut, USA

The cooling and trapping of atoms and atomic ions is a rapidly advancing field of fundamental science (e.g. Bose-Einstein condensation). We are attempting to extend the field to neutral molecules (and also molecular ions) as well, e.g. for study of elastic, inelastic and reactive collisions in the highly quantum mechanical regime at extremely low energies. As a first step, we are employing single- and multicolor photoassociation to produce translationally ultracold $^{39}K_2$ molecules from ultracold (~300μK) ^{39}K atoms confined in a magneto-optical trap.[1-7] Photoassociation of ultracold atoms (as opposed to thermal atoms) includes sharp resonances with wavelength as long-range rovibrational levels (outer turning points of tens or hundreds of Bohr) are accessed from colliding atomic pairs with $\lesssim$10 MHz of relative kinetic energy and only a few partial waves (ℓ = 0, 1, 2). Potential energy curves derived from these spectra test electronic structure and long-range perturbation theory calculations of interatomic potentials. The molecules formed are translationally ultracold and rotationally cold.

Recently we have used two-color resonance enhanced multiphoton ionization to directly detect translationally ultracold molecules.[8] These molecules are formed in $v'' = 36$ of the ground $X^1\Sigma_g^+$ state of $^{39}K_2$ following spontaneous emission from $v' \approx 191$ of the $A^1\Sigma_u^+$ state, formed in turn by one-color photoassociation of ultracold ^{39}K atoms. In the near future, we will seek to produce translationally ultracold molecules in low rovibrational levels ($v'' \gtrsim 0$, $J'' \lesssim 3$) of the $X^1\Sigma_g^+$ state via two-color photoassociation as proposed by Band and Julienne.[9] We plan as a further step to cool the rovibrational distribution of ground state translationally ultracold molecules produced by two-color photoassociation using laser cooling.[10]

We also plan to directly study free → bound →bound stimulated Raman photoassociation to directly produce state-selected translationally ultracold K_2 molecules as recently proposed.[11] Note the application of this technique to an atomic Bose-Einstein Condensate may yield a coherent beam of state-selected molecules[12] (a "molecule laser").

Finally we note that translationally ultracold molecules can also be produced in metastable electronic states (e.g. the $a^3\Sigma_u^+$ and $b^3\Pi_u$ states of the alkali dimers). Indeed Fioretti et al. have recently observed translationally ultracold Cs_2 $a^3\Sigma_u^+$ molecules using one-color resonance enhanced multiphoton ionization.[13]

† In collaboration with Professors Phil Gould and Ed Eyler, Drs. He Wang, John Bahns, Paul Julienne, Eite Tiesinga and Carl Williams, and Jing Li, Xiaotian Wang and Anguel Nikolov. Supported in part by the National Science Foundation.

References:

[1] H. Wang, P. L. Gould and W. C. Stwalley, "Photoassociative Spectroscopy of Ultracold ^{39}K Atoms in a Vapor Cell Magneto-Optical Trap", Phys. Rev. A. 53, R1216 (1996).

* Abstract 7068 submitted to the 21st International Symposium on Rarefied Gas Dynamics, Marseille, France, July 26-31, 1998.

[2] H. Wang, P. L. Gould and W. C. Stwalley, "Photoassociative Spectroscopy of Pure Long-Range Molecules", Z. Phys. D 36, 317 (1996).

[3] H. Wang, J. Li, X. T. Wang, C. J. Williams, P. L. Gould and W. C. Stwalley, "Precise Determination of the Dipole Matrix Element and Radiative Lifetime of the ^{39}K 4p State by Photoassociative Spectroscopy", Phys. Rev. A 55, R1569 (1997).

[4] H. Wang, P. L. Gould and W. C. Stwalley, "The Long-Range Interaction of ^{39}K(4s) + ^{39}K(4p) Asymptote by Photoassociative Spectroscopy: Part I: The 0_g^- Pure Long-Range State and the Long-Range Potential Constants", J. Chem. Phys. 106, 7899 (1997).

[5] H. Wang, X. T. Wang, P. L. Gould and W. C. Stwalley, "Optical-Optical Double Resonance Photoassociative Spectroscopy of Ultracold ^{39}K Atoms near Highly-Excited Asymptotes", Phys. Rev. Letters 78, 4173 (1997).

[6] H. Wang, P. L. Gould and W. C. Stwalley, "Fine Structure Predissociation of Ultracold Photoassociated $^{39}K_2$ Molecules Observed by Fragmentation Spectroscopy," Phys. Rev. Letters 80, 476 (1998).

[7] X. T. Wang, H. Wang, P. L. Gould, W. C. Stwalley, E. Tiesinga and P. S. Julienne, "First Observation of the Pure Long-Range 1_u State of an Alkali Dimer by Photoassociative Spectroscopy," Phys. Rev. A, in press (1998).

[8] A. N. Nikolov, E. E. Eyler, X. Wang, H. Wang, J. Li, W. C. Stwalley and P. L. Gould, "Observation of Translationally Ultracold Ground State Potassium Molecules," to be submitted to Phys. Rev. Letters.

[9] Y. B. Band and P. S. Julienne, "Ultracold Molecule Production by Laser-Cooled Atom Photoassociation," Phys. Rev. A51, R4317 (1995).

[10] J. T. Bahns, W. C. Stwalley and P. L. Gould, "Laser Cooling of Molecules: A Sequential Scheme for Rotation, Translation and Vibration", J. Chem. Phys., 104, 9689 (1996).

[11] A. Vardi, D. Abrashkevich, E. Frishman and M. Shapiro, "Theory of Radiative Recombination with Strong Laser Pulses and the Formation of Ultracold Molecules via Stimulated Photo-Recombination of Cold Atoms," J. Chem. Phys. 107, 6166 (1997).

[12] P. S. Julienne, K. Burnett, Y. B. Band and W. C. Stwalley, "Stimulated Raman Molecule Production in Bose-Einstein Condensates, " submitted to Phys. Rev. A (Rapid Communication).

[13] A. Fioretti, D. Comparat, A. Crubellier, O. Dulieu, F. Masnou-Seeuws and P. Pillet, "Cs_2 Cold Molecules Formation through Photoassociative Scheme in a Cs Vapor-Cell Magneto-Optical Trap," Phys. Rev. Letters, 80 , 4402 (1998).

New Excitements in Molecular Optics: Squeezing, Waveguiding and Reflecting Molecular Beams with Light *

Tamar Seideman
Steacie Institute for Molecular Science
National Research Council of Canada
Ottawa, Canada

The application of light forces to control atomic motions has been the subject of intense activity for nearly three decades and is still rapidly evolving.[1] Recent theoretical work[2] proposed the possibility of spatially controlling also *molecular* motions. Although the techniques of atom optics cannot be extended to molecules, due to their complex level structure and weak transition dipole elements, it was shown possible to focus arbitrary molecules using a non-resonant (tuned far below all transitions of the molecule), moderately intense laser field. Spatial manipulation in that case is based on the nonlinear interaction of the intense field with the DC limit of the polarizability tensor, rather than on near-resonance interactions as in the atomic case.[1] Molecular focussing[2] extends to a general field of molecular optics. The possibilities of collimating and steering molecular beams and of separating species according to their mass, velocity, rotational state or electronic channel were shown analytically and numerically.[3]

Related recent studies illustrated the possibility of aligning molecules in an intense laser field,[4] raising the hope of simultaneously focussing molecules in space and aligning their figure axis along a given axis.[2] Both laser-focussing and laser-alignment were very recently realized also in the laboratory.[5,6]

An intriguing question that came out of the molecular optics work[3] is the possibility of devising *repulsive molecular optics elements*, that is, repealing the molecules from (rather than attracting them to) the high intensity regions. An crucial question concerning laser-alignment[4] is the possibility of preserving the effect under *field-free* conditions, sufficiently long after the laser pulse to be useful for studies of stereodynamics and gas-surface interaction.

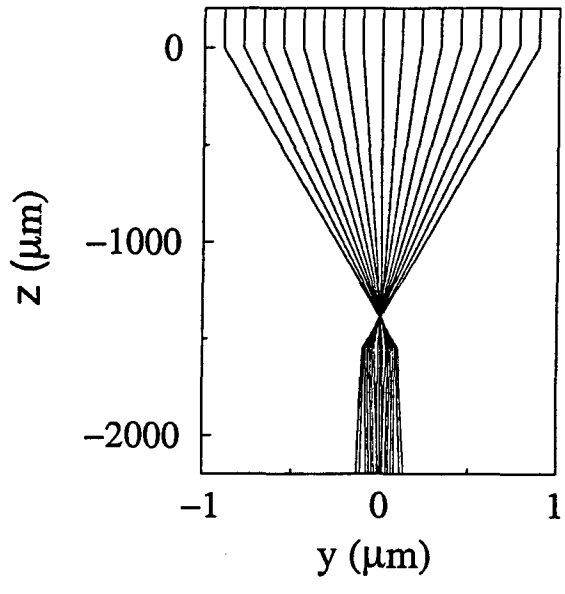

Figure 1: A complex positive lens: A molecular beam propagating along the negative z axis is focussed by means of one segment of the laser beam and subsequently collimated by means of a second segment, copropagating along the x axis.

Ongoing theoretical work addresses both (related) issues. A new molecular optics scheme is being developed, complementary to the scheme of Ref. 3 and based on repulsive interactions. An analytical model, supported by numerical calculations for realistic systems, derives the conditions under which alignment is preserved and significantly enhanced after the laser field, under perfectly field-free conditions.

The former study offers potentially a variety of new, exciting opportunities, including molecular reflec-

*Abstract a7061 submitted to the 21st International Symposium on Rarefied Gas Dynamics, Marseille, France, July 26-31, 1998

tion or partial reflection from (possibly curved) mirrors, trapping in a low intensity region, where long-time confinement is possible without risk of ionization, waveguiding along the low intensity axis of a TEM_{01}^{*}-mode laser-beam, building up complex molecular optics devices, focussing in a negative, partially reflecting molecular lens that allows improved demagnification ratios and studying problems in scattering theory, such as hard wall collisions. The latter study renders laser-alignment potentially useful for gas-phase and gas-surface stereochemical research.

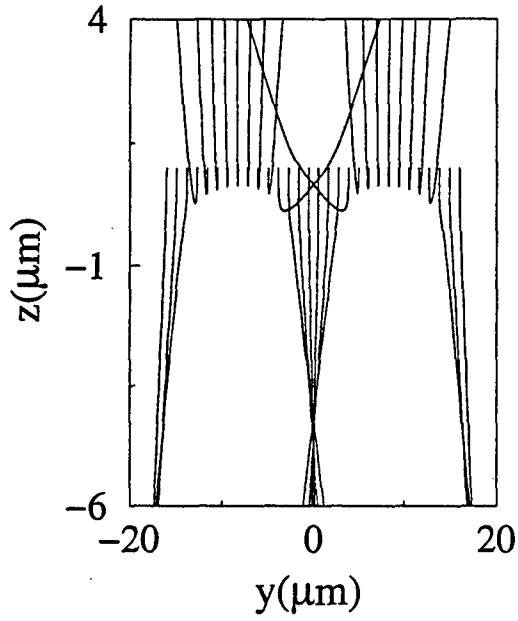

Figure 2: A negative lens selectively repeals part of the molecular beam, thus improving the demagnification ratio.

Combined, field-free alignment and molecular optics suggest a potential route to new materials, possessing predesigned electric or magnetic properties. An experimental realization of both schemes is currently being initiated.[7] Theoretical results supported by preliminary experimental evidence will be reported.

References

[1] P. R. Berman Ed., *Atom Interferometry* (Academic Press, London, 1997) and several abstracts in the present volume.

[2] T. Seideman, Phys.Rev. A **56**, R17 (1997); J.Chem.Phys. **106**, 2881 (1997).

[3] T. Seideman, J.Chem.Phys. **107**, 10420 (1997).

[4] Friedrich and D.R. Herschbach, Phys.Rev.Lett. **74**, 4623 (1995); T. Seideman, J.Chem.Phys. **103**, 7887 (1995).

[5] W. Kim and P.M. Felker, J.Chem.Phys. **104**, 1147 (1996).

[6] H. Stapelfeldt, Hirofumi Sakai, E. Constant and P. B. Corkum, Phys.Rev.Lett. **79**, 2787 (1997).

[7] R.J. Gordon, private communications.

Progress in Coherent Manipulation of Atoms and Molecules in Beams*

K. Bergmann, H. Theuer, and Th. Halfmann

Fachbereich Physik, Universität Kaiserslautern, Germany

We report on new applications of coherent radiation to manipulate atoms and molecules in beams.

One example is the coherent control of photoionization of He out of a metastable state [1]. A pulsed dressing laser allows the suppression of the ionization of helium by the pulsed ionizing laser by a factor of five or more, demonstrating unambiguously the formation of a trapped state in continuum coupling (laser-induced continuum structure, LICS). A spectral width of the LICS as narrow as 1 GHz or less has been observed. The underlying physics, possible applications and other implications will be discussed.

Another example will be the application of the technique of coherent population transfer by delayed interaction (STIRAP [2] for dissipation-free linear momentum transfer and deflection of a beam of Ne* atoms in a metastable state [3]. This is a demonstration of a crucial element (mirror or beam splitter for matter waves) of a STIRAP-based atom-interferometer, which is also applicable to molecules. The influence of a small magnetic field („Larmor velocity filter") will also be discussed.

[1] Th. Halfmann, L.P. Yatsenko, M. Shapiro, B.W. Shore, and K. Bergmann, *„Population Trapping and Laser-induced Continuum Structure in Helium: Experiment and Theory"*, Phys. Rev. A, Rapid Communication, July 1998

[2] K. Bergmann, H. Theuer, and B.W. Shore, *„Coherent Population Transfer Among Quantum States of Atoms and Molecules"*, Review of Modern Physics 70, 000 (July 1998)

[3] H. Theuer and K. Bergmann, *„Atomic Beam Deflection by Coherent Momentum Transfer and the Dependence on Weak Magnetic Fields"*, European Physical Journal D 2, 000 (July 1998)

* Abstract 6976 submitted to the 21st International Symposium on Racefied Gas Dynamics, Marseille, France, July 26-31, 1998

MOLECULAR BEAM SESSION MB 2

Effects of Molecule Alignment or Orientation
in Scattering Experiments

CHAIR: J. Fayeton (Orsay)

ROOM: LAVOISIER
TUESDAY, JULY 28, 1998
10:50 - 12:30

Aligned Molecules and Intermolecular Forces by Quantum Interference Scattering: O_2-rare Gases Interactions, Bonding in O_4 and Role of Spin Coupling *

V. Aquilanti[1], D. Ascenzi[1], M. Bartolomei[1], D. Cappelletti[1], M. de Castro[2], F. Pirani[1]
[1] Dipartimento di Chimica dell'Università, Perugia, Italy
[2] Instituto Pluridisciplinar, Universidad Complutense, Madrid, Spain

1 Introduction

Recently [1, 2], it was discovered that supersonic expansions of gaseous mixtures of molecular oxygen in lighter atomic carriers (seeded molecular beams) represent a natural and facile technique for obtaining alignment of molecular rotations, a striking result having been that such an alignment effect is remarkable for all studied carrier gases (in particular for H_2, He, Ne and their mixtures) but depends drastically on the final speed to which molecules are accelerated: so that, within a seeded supersonic expansion, fast molecules are much more aligned than slower ones. Specifically the alignment degree has been found to depend strongly on the ratio v/v_{max}, where v is the molecular velocity and v_{max} the peak of the beam velocity distribution. Such conclusion opens the way to prepare molecules with well-defined velocities and alignment properties, and to perform scattering experiments (at thermal energies corresponding to the glory interference effect) with oxygen molecules under a controlled alignment.
As shown in the case of N_2 [3], scattering experiments, particularly if leading to the observation of quantum interference effects (the "glory"), are also a sensitive probe of alignment.

2 Present results

The most important application is to study the anisotropy of intermolecular forces [4] and we present here total integral cross sections for scattering of O_2 on Kr and Xe atoms and on oxygen molecules. Data obtained with a "hot" effusive molecular beam, which contains fast rotating and randomly oriented O_2 molecules, mainly probe the spherical component of the potential energy surfaces.
Experiments with supersonic seeded beams, where molecules are cooled at $K = 1$ rotational level and selectively aligned probe the anisotropy of the potential energy surfaces. An example of cross section results for the scattering of "cold" supersonic beams of O_2 by Kr atoms at four different degree of molecular alignment is shown in Fig. 1.
The analysis of the experimental results, based upon close-coupling exact quantum mechanical calculations of the cross sections, provides an accurate characterization of the interactions at intermediate and large intermolecular distances for the Kr-O_2, Xe-O_2 and O_2-O_2 systems, the most stable configuration being for perpendicular approach of the rare gas atom, with energies 15.84 meV for Kr and 17.87 meV for Xe, at intermolecular distances of 3.72 and 3.87 Å, respectively.
Analysis of scattering data for the O_2-O_2 system yields a bond energy in the $(O_2)_2$ dimer of 1.65 kJ·mol^{-1} at an intermolecular distance of 3.56 Å, corresponding to parallel approach. The splitting of the triplet and the quintet states above the ground singlet state, and the angular dependence of all three surfaces are also given. These results indicate that most of the bonding in the dimer comes from van der Waals forces. This first complete characterization of the interaction, basic to the theory of weak chemical bonds, and relevant for the dynamics of atmospheric gases, leads also to quantify the (minor) role of spin-spin coupling between isolated molecules, of interest for modeling magnetism in solid O_2 and in O_2 clusters.
An adiabatic approximation and a semiclassical description of the scattering process contribute to shed light on some general features of the collision dynamics of aligned molecules, in particular on the observed effects of the interaction anisotropy on the glory interference phenomenon.

*Abstract 1721 submitted to the 21st International Symposium on Rarefied Gas Dynamics, Marseille, France, July 26-31, 1998

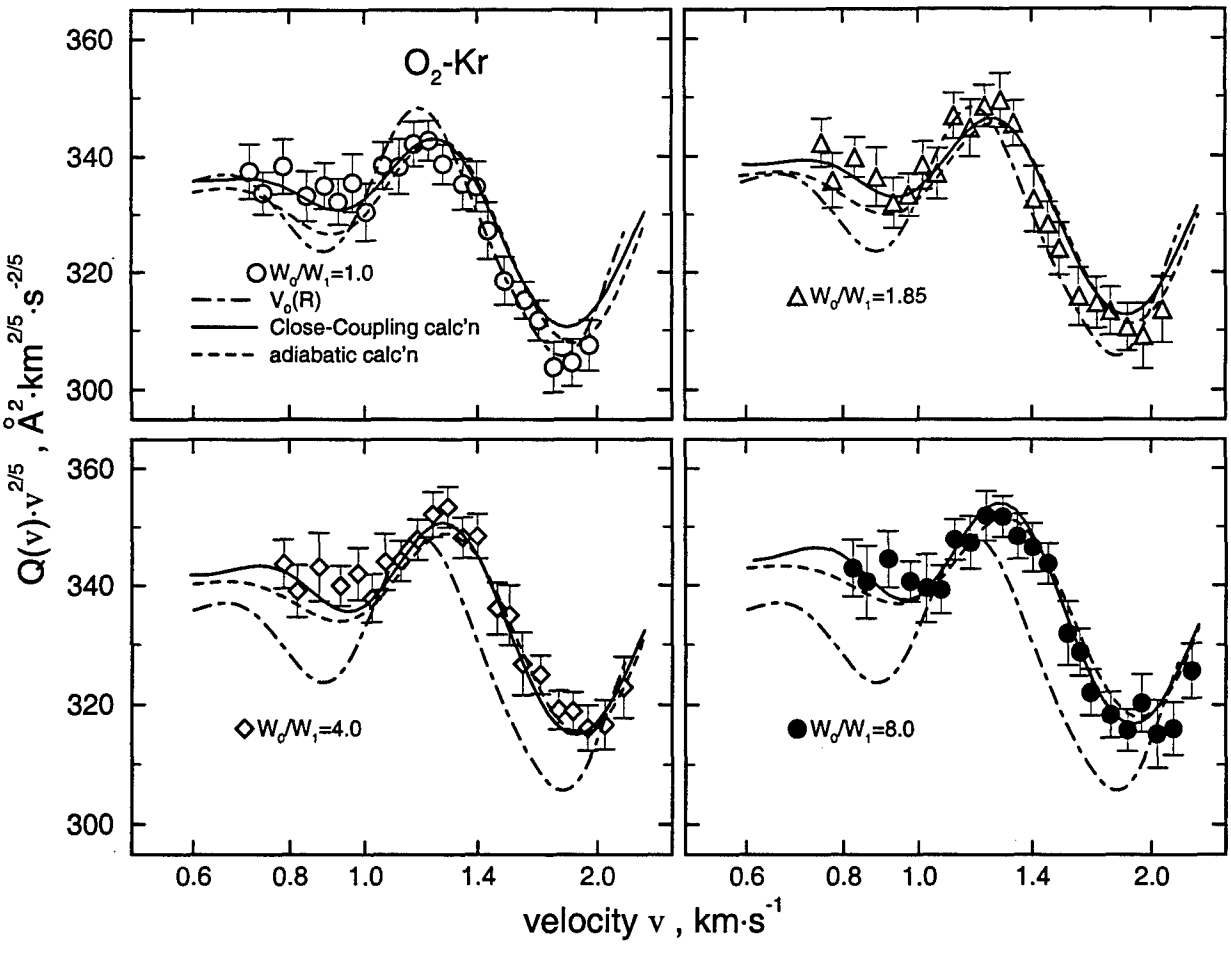

Figure 1: Total integral cross sections $Q(v)$ as a function of collision velocity v at the indicated degree of alignment W_0/W_1 for the O_2-Kr system. Dotted lines are calculations for scattering by an isotropic potential while solid lines are close-coupling calculations from the anisotropic potential energy surface and dashed lines are the results of an approximate adiabatic approach.

References

[1] Aquilanti V., Ascenzi D., Cappelletti D., Pirani F., *Nature* **371** 399 (1994).

[2] Aquilanti V., Ascenzi D., Cappelletti D., Pirani F., *J. Phys. Chem.* **99**, 13620 (1995).

[3] Aquilanti V., Ascenzi D., Cappelletti D., Fedeli R., Pirani F., *J. Phys. Chem.* **101**, 7648 (1997).

[4] Aquilanti V., Ascenzi D., Cappelletti D., Franceschini S., Pirani F., *Phys. Rev. Lett.* **74**, 2929 (1995).

Photodissociation of NO_2 at 212.8 nm Yields Aligned $O(^3P_j)$ atoms*

M. Ahmed, D. S. Peterka, O. S. Vasyutinskii[1] and A. G. Suits
Chemical Sciences Division, Berkeley National Laboratory
Berkeley CA 94720 USA
[1]Ioffe Physico-Technical Institute
Russian Academy of Sciences, 194021 St. Petersburg, Russia

The technique of velocity map imaging[1] has been applied to study the photodissociation of NO_2 at 212.8 nm. The translational energy and angular distributions of the three spin-orbit components of the ground state oxygen atom products ($O(^3P_2)$, $O(^3P_1)$, and $O(^3P_0)$) were measured using 2+1 REMPI around 226 nm in conjunction with ion imaging. The polarization of the probe light was rotated to be either perpendicular or parallel to the ion flight axis, the purpose being to study the phenomenon of atomic photofragment alignment (angular momentum polarization). This alignment provides information on the electronic rearrangement which occurs during optical excitation and dissociation of the parent molecule [2].

Fig. 1 shows angular distributions extracted from the raw ion-images for the three fine structure components of the ground state oxygen atom for two different polarizations of the probe laser obtained using the inverse Abel transform. The dominant contribution to the shape of the image is from the photofragment velocity anisotropy, the β parameter. A signature for atomic photofragment alignment is difference in the angular distribution with change of the probe laser polarization. We see a particularly dramatic effect for the $O(^3P_1)$ angular distribution. Comparing the angular distributions for the two different probe polarizations in Fig. 1, we see the intensity is reduced at the poles and increased at the equator when the probe polarization is perpendicular to the photolysis. This behavior is consistent with the alignment anticipated for adiabatic dissociation from a parallel transition. The change is much more subtle for the $O(^3P_2)$ fragment, and nonexistent for the $O(^3P_0)$ fragment (for j = 0, there is no total angular momentum and hence no alignment). The use of the Abel transform is not strictly valid for the crossed polarization case in the presence of atomic alignment, but it serves here only to document the presence of the

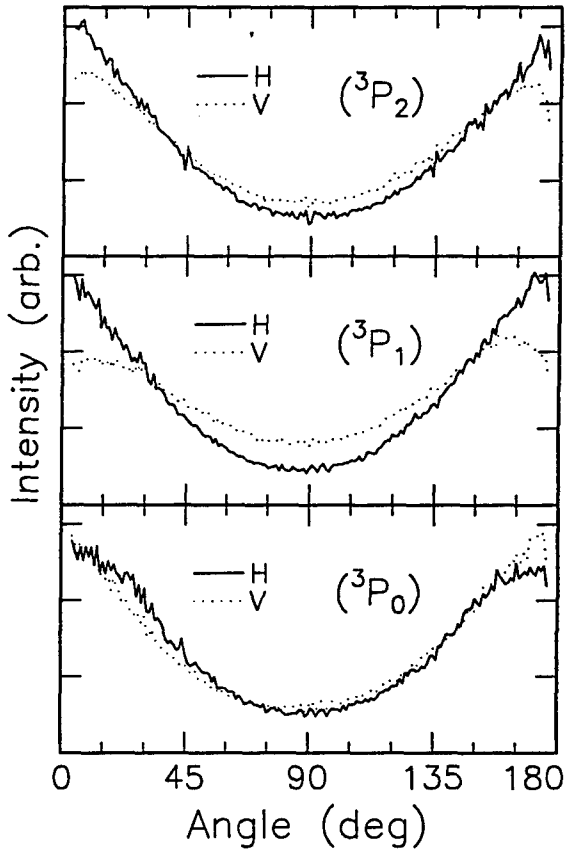

Figure 1: Angular distributions for the indicated spin-orbit states of $O(^3P)$ and indicated probe polarization direction. 'H' refers to probe polarization parallel to the photolysis polarization direction and to the plane of the detector. 'V' polarization is parallel to the ion flight axis, perpendicular to the photolysis laser polarization.

*Abstract 7066 submitted to the 21st International Symposium on Rarefied Gas Dynamics, Marseille, France, July 26-31, 1998

effect. Atomic photofragment alignment has been reported for $Cl(^2P)$ from Cl_2[2], $O(^1D)$ from O_3[3] N_2O[4], $S(^1D)$ from OCS[5], but this is the first observation of aligment of the ground state O atom.

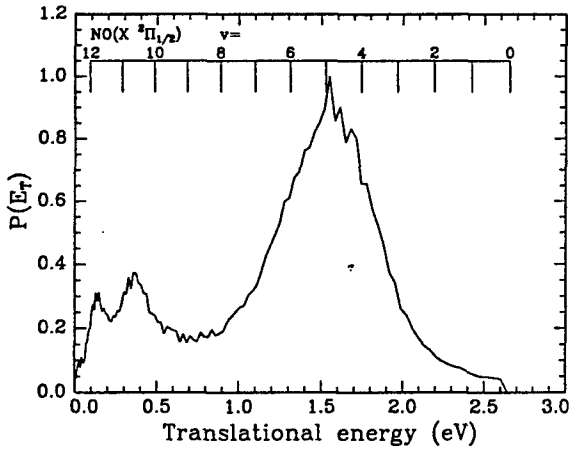

Figure 2: Total translational energy release obtained for $O(^3P_2)$ from photodissociation of NO_2 at 212.8nm. The comb indicates the corresponding vibrational level for the N=0 $NO(X\,^2\Pi_J)$ cofragment.

Examining the translational energy distributions of the oxygen atom provides a mapping of the internal state distributions of the NO co-fragment due to momentum conservation. Fig. 2 shows such a translational energy distribution for the $O(^3P_2)$ product. The main peak around 1.6 eV corresponds to a range of excited vibrational levels of the $NO(X\,^2\Pi_J)$ ground state peaking around v=4 or 5. The peaks near 0.4 eV and 0.1 eV correspond to a pair of highly excited vibrational levels around v=11. This bimodal vibrational distribution most likely arises from photodissociation via two distinct electronic states.

References

[1] Eppink, A. T. J. B., and Parker, D. H., *Rev. Sci. Instrum.*, Vol. 68, p. 3477, 1997.

[2] Bracker, A. S., Wouters, E. R., Suits, A. G., Lee, Y. T., and Vasyutinskii, O. S. *Phys. Rev. Lett.* Vol. 80, p. 1626, 1998.

[3] Miller, R. L., Suits, A. G., Houston, P. L., Toumi, R., Mack, J. A. and Wodtke, A. M. *Science*, Vol. 265 p. 1831, 1994.

[4] Suzuki, T. Katayangi, H., Mo, Y. and Tonokura, K., *Chem. Phys. Lett.*, Vol. 256, p. 90, 1996.

[5] Mo, Y., Katayangi, H., Heaven, M. C., and Suzuki, T., *Phys. Rev. Lett.*, Vol. 77, p. 830, 1996.

Inelastic Collisions with Oriented Molecules: A Quantitative Exploration of the Steric Effect

M.J.L. de Lange[1], M.M.J.E. Drabbels[1], J.Bulthuis[1], J.G.Snijders[2] and S.Stolte[1]

[1] Laser Centre and Department of Physical and Theoretical Chemistry, Vrije Universiteit, De Boelelaan 1083, 1081HV Amsterdam, The Netherlands

[2] Department of Chemical Physics and Material Science Centre, Rijksuniversiteit Groningen, Nijenborgh 4 9747 AG Groningen, The Netherlands

Despite the abundancy of scattering experiments involving NO, including those between NO and Ar [1,2], the NO molecule still conceals a few secrets. Recently, renewed interest in the NO-Ar system has emerged [3-8]. The present work forms a follow up of the tentative study of van Leuken et.al [7]. An incoming beam of NO molecules is state selected in the upper f-level of the λ-doublet of the $^2\Pi_{1/2}$ j= 1/2 rotational ground state by using an electric hexapole focuser. The state selected state posseses negative parity [9]. After state-selection, the NO molecules can be oriented in a homogeneous electric field. This enables us to study orientation effects along with the role of parity breaking on collision-induced rotational excitation of NO in a crossed beam geometry, using Laser Induced Fluorescence (LIF). The NO and Ar beams are both pulsed, with repetition rates of 10 Hz and 5 Hz, respectively. The LIF-excitation laser, tuned at the γ(0,0) band around 226nm operates with a pulse repetition rate of 10 Hz. The resulting fluorescence is detected by a photomultiplier and sampled by a gated integrator (see Fig.1). The Stark effect resulting from applying an electric (guiding) field brings about that the rotational states can not carry any longer a well defined parity.

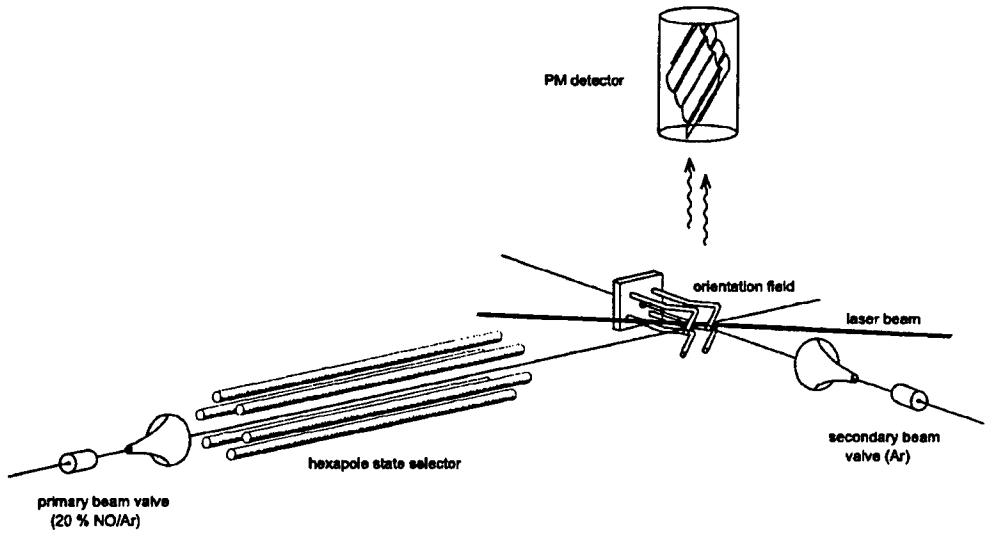

Figure 1: The experimental setup

[1]Parity breaking is demonstrated by using the electric dipole selections rules of LIF-transitions. The transitions R1 and Q21, which are forbidden to occur from the selected (f) parity component of the NO molecules, become allowed in an electric field due to the mixing of the e and f paritylevels of the λ-doublet. Quantitative analysis of the LIF intensity ratio measured for the zero field forbidden and allowed transitions (provided that saturation remains absent for all transitions) shows that the observed degree of parity breaking is proportional to the retrievement of the degree of prepared orientation, a necessary

[1]Abstract 7001 submitted to the 21st International Symposium on Rarified Gas Dynamics, Marseille, France, July 26-31, 1998.

prerequisite for quantitative exploration of the steric effect in inelastic collisions. The steric assymetry (the difference between the inelastic collision cross section with the N-end in front and the one with the O-end in front divided by twice the inelastic

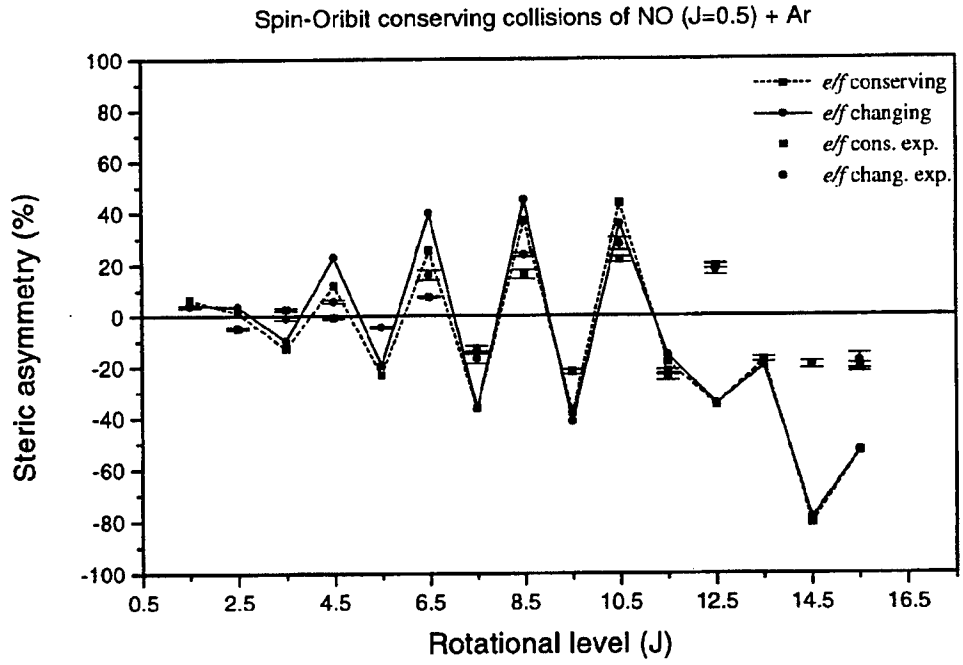

Figure 2

collision cross section with randomly oriented incoming NO molecules) as a function of the final rotational state J has been measured and calculated for spin-orbit conserving collisions at a collision energy of 442 cm^{-1}. Fig.2 shows these results from which the following remarks emerge. The steric asymmetry alternates its sign with $\Delta J=1$. Also the agreement between experiment and theory regarding the sign and strenght of the steric asymmetry, as well as its insensitivity for parity conserving/breaking final rotational states appears to be encouraging. The preference for O-end collisions to yield the highest, nearly 100%, transfer of incoming collision energy into rotation appears to be somewhat weaker experimentally than theoretically. Further work is in progress to elucidate these steric phenomena.

Ackmowledgements: Financial Support from SON and FOM turned out to be indispensable to carry out this work. The research of M.Drabbels was supported by the Royal Dutch Academy of Sciences (KNAW).

REFERENCES

[1] P. Andresen, H. Joswig, H. Pauly, and R. Schinke, J.Chem.Phys. 77 (1982) 2204.
[2] H. Joswig, P. Andresen, and R. Schinke J.Chem.Phys. 85 (1986) 1904.
[3] S.D. Jons, J.E. Shirly, M.T.Vonk, C.F. Giese, and W.R. Gentry, J.Chem.Phys. 97 1992) 7831.
[4] L.S. Bontuyan, A.G. Suits, P.L.Houston, and B.J. Whitaker J.Phys.Chem., 97 (1993) 1904.
[5] M.H. Alexander J.Chem.Phys. 99 (1993) 595.
[6] C.R. Bieler, A. Sanov, and H. Reisler Chem.Phys.Lett. 235 (1995) 175,
[7] J.J.van Leuken, J. Bulthuis, S. Stolte, and J.G. Snijders, Chem.Phys.Lett.260 (1996) 595
[8] S. Antonnova, A.Lin, A.P. Tsakotellis, and G.C. McBane Preprint (1998).
[9] F.H. Geuzebroek, M.G. Tenner, A.W. Kleyn, H. Zacharias and S. Stolte Chem.Phys.Lett. 187 (1991) 520.

Laser Cooling and Reaction Dynamics in Excited Electronic States *

E. Pollak, G. Gershinsky
Chemical Physics Department, Weizmann Institute of Science, 76100 Rehovot, Israel

The laser excitation of trans-stilbene from the S_0 state to the excited S_1 state and the subsequent isomerization is a prototypical example of laser induced unimolecular reactions in the excited state. Our recent theoretical investigations of this system have led to some new general observations. Previous theoretical and experimental investigations of the trans-stilbene isomerization reaction indicated that the gas phase thermal rate at room temperature is much smaller than the thermal rate in the liquid phase. This was based on the observations that: a) A combination of measured energy dependent rates and RRKM calculations led to an isolated molecule thermal rate at T=300K of $2 \cdot 10^9$ sec^{-1}; b) An experiment of Balk and Fleming (J. Phys. Chem. **90**, 3975 (1986)) in which stilbene vapor at 300 K excited at the S_0 to S_1 zero point to zero point electronic transition energy (0_0^0), gave a lifetime in the excited state of $\sim$ 750 psec. The liquid state lifetime in ethane is $\sim$ 30 psec.
In this paper we present theoretical computations of the rate in the gas and liquid phases, based on a new potential model of Vachev et al (J. Phys. Chem. **99**, 5247 (1995)). We find that:
a) RRKM rates are in agreement with measured energy dependent rates for trans-stilbene, deuterated isomers of trans-stilbene and hexane clusters of trans-stilbene.
b) Quantum effects at room temperature are negligible for this system, justifying the extensive use of classical molecular dynamics in investigating this reaction.
c) The thermal rate derived from the new RRKM rates is the same as the thermal rate in liquid ethane.
d) The laser excitation experiment of Balk and Fleming leads to *laser cooling of the excited state* suggesting that their measured lifetime is longer than the lifetime in the liquid. The liquid surrounding heats up the molecule on a time scale which is faster than the isomerization lifetime. Experiments are suggested to verify this interpretation.
e) The observation of laser cooling of the excited state suggests new models for interpreting the experimental measurement of the survival probability as a function of vapor pressure of a buffer gas at room temperature. The survival probability depends on three competing processes - heating of the excited state by the buffer gas, unimolecular reaction and spontaneous emission. A simple expression is derived for the survival probability. The competition between thermal relaxation and reaction may prevent the usual single exponential kinetics.

*Abstract 4066 submitted to the 21st International Symposium on Rarefied Gas Dynamics, Marseille, France, July 26-31, 1998

MOLECULAR BEAM SESSION MB 3

Gas-Surface I: Interactions of Clusters
and Fullerene with Surfaces

CHAIR: F. Huisken (Göttingen)

ROOM: LAVOISIER
TUESDAY, JULY 28, 1998
14:35 - 16:15

Femtosecond Neutralization Dynamics and Electron Emission in Cluster-Surface Collisions *

K. H. Meiwes-Broer[1], B. Wrenger[1], M. E. Garcia[2] and O. Speer[2]
[1] Fachbereich Physik, Universität Rostock, 18051 Rostock, Germany
[2]Institut für Theoretische Physik der Freien Universität Berlin,
Arnimallee 14, 14195 Berlin, Germany

In this talk we will rise the question whether the transient character of a collision process of a charged metal atom cluster with a solid surface might elucidate the dynamics of the electron motion between two partners.

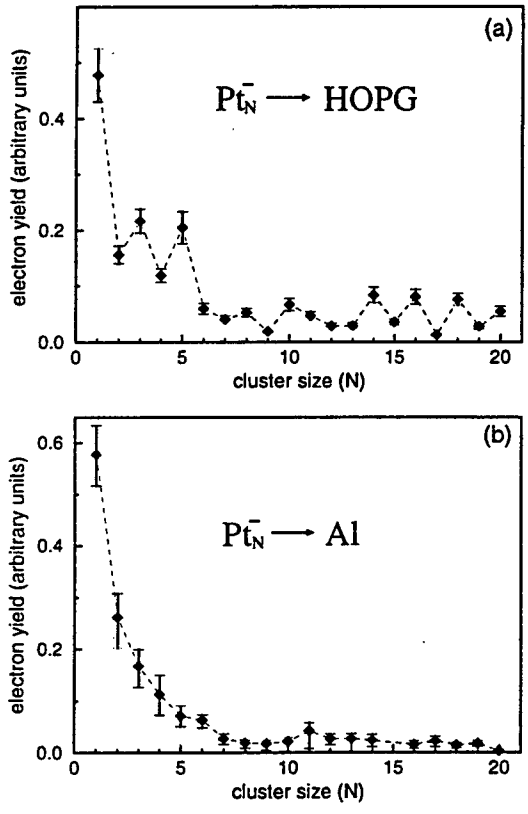

Figure 1: Experimentally determined relative electron yield γ as a function of size N for Pt_N^- clusters colliding with a (a) HOPG target, (b) Al-surface. The collision energy is $E_{coll} = 500$eV.

Experimental results for the relative electron emission yields $\gamma(N)$ of charged clusters colliding at low energies with different surfaces are presented[1]. For the measurement of the relative electron yield a Wien filter mass spectrum was recorded in order to assign a given filter setting to the corresponding cluster mass. The mass spectra of Pt_N^- were resolved up to $N = 20$.

For fixed collision energy a remarkable cluster size dependence of $\gamma(N)$ is obtained for clusters colliding with HOPG. $\gamma(N)$ changes completely if Aluminum is used as target.

A rough analysis of the known mechanisms for ejection of electrons upon particle-surface collisions does not help much to understand our experimental results. None of the known mechanisms for electron emission, in their simplest form, yields a consistent description of our observed $\gamma(N)$. We developed a model for the description of electron emission yields $\gamma(N)$[1].

With the help of a microscopic theory we describe the femtosecond neutralization dynamics during the collision process. It is shown that, for fixed collision energy, the size dependence of non-adiabatic survival probability $P_s(N)$ of the charged cluster is very sensitive to the density of states of the target. For instance, for targets with narrow densities of states $P_s(N)$ shows oscillations as a function of the cluster size, which reflect the time-oscillations of the neutralization process, as shown in the inset of Fig. 2(a). This effect resembles the well known Stückelberg oscillations,

By assuming that the collision induced electron emission is essentially determined by the femtosecond dynamics during the collision process a remarkably good agreement between the theoretical results for $P_s(N)$ and experimental results $\gamma(N)$ for different cluster types and surfaces is obtained.

*Abstract 6991 submitted to the 21st International Symposium on Rarefied Gas Dynamics, Marseille, France, July 26-31, 1998

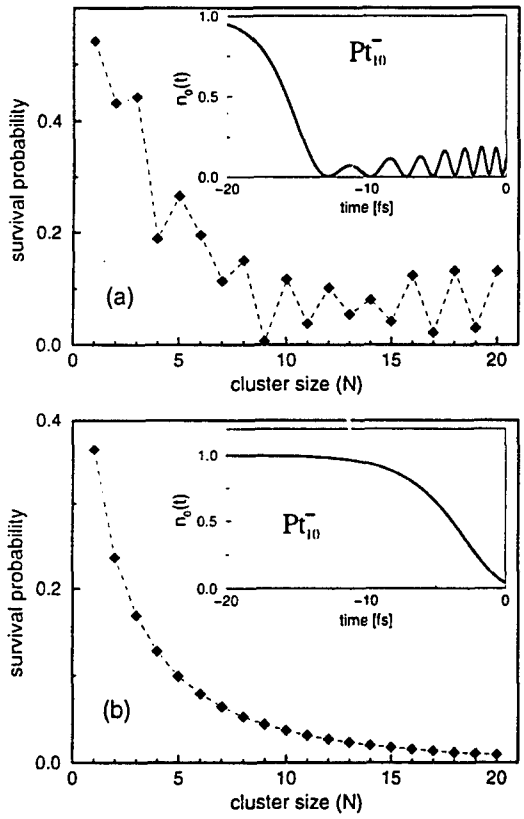

Figure 2: Theoretical results for the survival probability $P_s(N)$ of Pt_N^- clusters impinging on a (a) HOPG target, (b) Al-surface. E_{coll} = 500eV. In the inset figures, the time-dependent level occupation $n_0(t)$ of Pt_{10}^- colliding with both targets is shown.

References

[1] B. Wrenger and K. H. Meiwes-Broer, O. Speer and M. E. Garcia, Phys. Rev. Lett. **79**, 2562 (1997).

Catalytic Reactivity, Mobility and Electron Dynamics of Deposited Silver Clusters

T. Leisner, U. Busolt, E. Cottanzin, H. Röhr, L. Socaciu, S. Wolf, and L. Wöste

FB Physik, Freie Universität Berlin, Arnimallee 14, 14195 Berlin, Germany

1 Introduction

In this contribution we will present an overview over our work on deposited metal clusters. It includes experimental techniques for soft landing of mass selected clusters, chemical reactivity and catalytic activity of mass selected clusters and time resolved photoemission studies of cluster covered surfaces.

2 Experimental

Metal clusters are produced by bombarding four metal targets with xenon cations of 25kV kinetic energy. The secondary ions are introduced into a linear helium filled RF ion guide. In the high pressure (~10^{-2} mbar) helium, the clusters experience a friction force and condense to the minimum of the pseudopotential in the center of the ion guide. At the same time their kinetic energy is reduced and their temperature approaches room temperature. This preconditioning of the clusters reduces their spread in phase space and therefore sustantially increases the brightness of the ion source. After differential pumping, the cluster ions are mass selected in a quadrupole mass filter and fed into a second quadrupole ion guide. Here they pass a helium filled collision cell where their kinetic energy is further reduced. This quadrupole ion guide serves to transfer the clusters into a UHV chamber where the clusters are deposited on solid surfaces.

By careful adjustment of the helium pressure in the second gas cell, and of the offset voltages of the quadrupole and the sample it is possible to achieve a deposition with very low kinetic energy and therefore true soft-landing with overall kinetic energies around 1eV. As demonstrated in Fig. 1, the width of the kinetic energy distribution decreases from about 20 eV to below 1 eV after moderation in the gas cell.

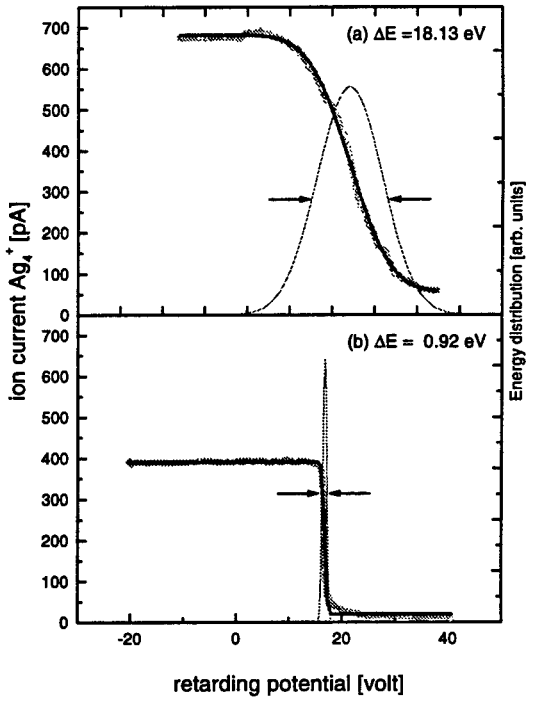

Figure 1: Distribution of the kinetic energies of silver tetramers at deposition (a) without- and (b) with moderation in a gas cell prior to deposition.

2 Results and Discussion

The energy of deposition is a crucial parameter which has to be controlled carefully if mass selected clusters are to be deposited on surfaces. As an example the catalytic activity of silver tetramers in the reduction of AgBr to elemental silver is given below. This reaction is catalyzed by silver clusters and therefore stands at the bottom of silver halogenide photography. We modeled this reaction by the deposition of size selected silver, gold, and silver/gold mixed clusters onto photographic AgBr grains.

*Abstract 6981 submitted to the 21st International Symposium on Rarefied Gas Dynamics, Marseille, France, July 26-31, 1998

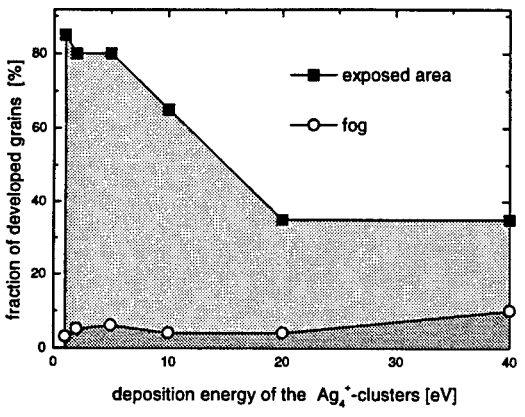

Fig. 2: Comparison between the developability of cluster-covered (exposed area) and pure (fog) AgBr crystals as a function of the deposition energy of the Ag_4^+ clusters.

After development of the sample at ambient conditions the fraction of developed grains was determined as a function of cluster size, composition, coverage and impact energy.

In Fig. 2 it is given for pure (fog) and Ag_4 covered (exposed area) samples as a function of the kinetic energy of the clusters. Catalyzed by Ag_4, the cluster covered samples are reduced more easily than the pure AgBr grains. With increasing deposition energy however, the catalytic activity of the Ag_4 centers decreases substantially, indicating progressive fragmentation of the clusters during the deposition. In our contribution, we will present data which demonstrate the amazing size sensitivity of this process. The results indicate that the noble metal clusters retain their identity on AgBr crystallites even at room temperature and under atmospheric conditions. Of course this stability is a property of the specific cluster/surface combination.

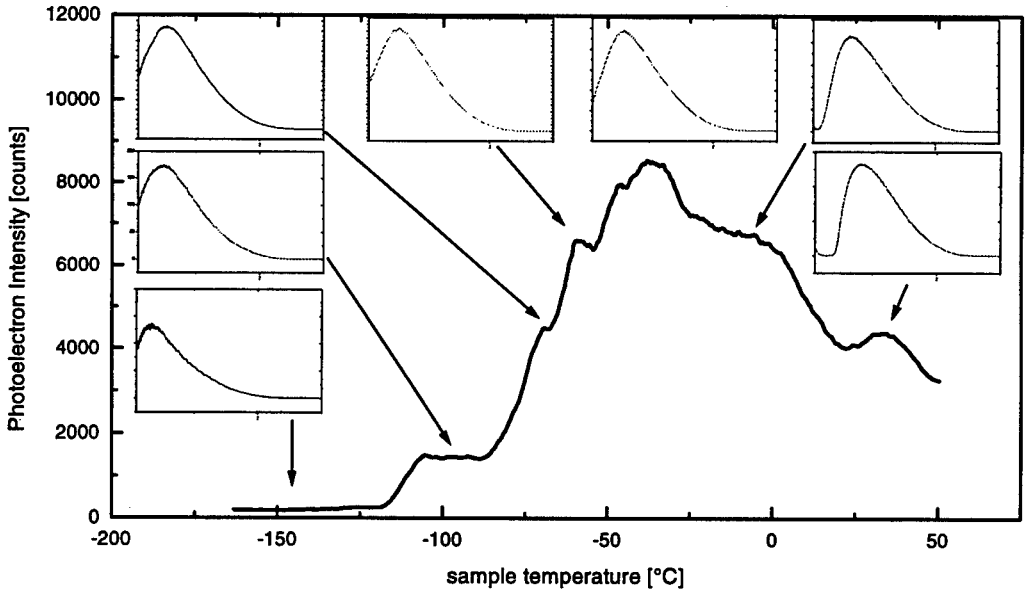

Fig.3 Total two-photon (λ= 400nm) photoelectron yield (thick curve) and photoelectron spectra (inserts) of a Ag_5 covered HOPG surface as a function of temperature. The x-axis of the inserts is the photoelectron energy in the range from 0.1eV and 3 eV, the y-axis the rescaled photoelectron intensity.

Recently we were able to observe the relaxation and coalescence of monodisperse silver clusters deposited on HOPG surfaces under UHV conditions by time-resolved two-photon photoemission. The photoelectrons are created by the subsequent absorption of photons from two ultrashort laser pulses at a controlled delay time. In this system the initially well separated clusters become mobile far below room temperature and form larger islands which are clearly discernible from the isolated clusters by their altered electron dynamics. As an example an annealing curve for highly oriented pyrolytic graphite (HOPG) samples is given in Fig. 3. Here the total photoelectron yield In our contribution we will present size dependent results on the dynamics of electronic excitations in the isolated silver clusters on HOPG as well as on their mobility as a function of temperature.

Rotational distributions of scattered molecules from van der Waals cluster-surface collision. *

E. Fort, A. De Martino, F. Pradère, M. Châtelet and H. Vach
Laboratoire d'Optique Quantique du CNRS, Ecole Polytechnique,
91128 Palaiseau Cedex, France
e-mail: fort@leonardo.polytechnique.fr

We have characterized in detail the translational and rotational distributions of nitrogen molecules scattered from $(N_2)_n$ clusters colliding with a graphite surface at an initial velocity of 750 m/s, for average cluster sizes n ranging between 200 and 1000, and for two surface temperatures T_S (450 K and 700 K), in ultrahigh vacuum conditions.

Angular density distributions and angularly resolved velocity distributions have been measured wih a quadrupole mass spectrometer (QMS) that can be moved about the graphite sample over 300°. Rotational population distributions have been characterized over a wide angular range by using another rotatable device involving laser induced ionization followed by ion detection on a stack of multichannel plates [1]. We used the (2+1) photon REMPI detection scheme proposed for N_2 by Lykke and Kay [2], which yields the rotational state populations directly (irrespective of the degree of orientation and/or alignment of the molecules to be detected), with a very high detectivity. The UV radiation tunable around 202 nm needed for this purpose was provided by frequency tripling a YAG-pumped nanosecond dye laser.

The QMS data turn out to be similar to those obtained previously for argon clusters (an example of angular density distribution is shown on fig. 1), and they are reasonably well fitted by a simple thermokinetic model [3]. These fits indicate that during the collision the cluster velocity component parallel to the surface is conserved to within ±15% typically, while the cluster "boiling" temperature ranges between 220 K and 360 K.

On the other hand, the measured rotational distributions are clearly non thermal : the temperature derived from the low J state populations is definitely lower than that describing the high J states. This

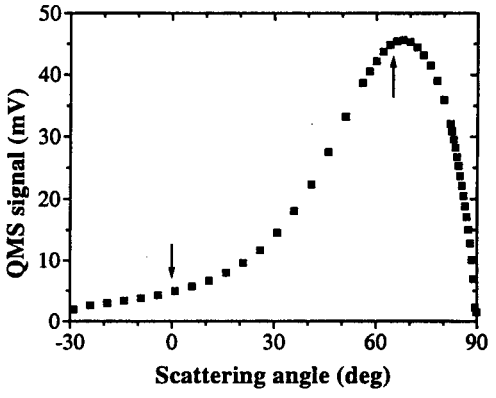

Figure 1: Angular density distribution of scattered nitrogen molecules. Incidence angle 45°, incoming cluster size 1000, surface temperature 700 K. Scattering angles are defined from surface normal. The arrows indicate the angles where the REMPI spectra shown in fig. 2 have been taken

behavior was mentioned without further details in the early (and, to our knowledge, the only) work reported to date on this topic [4]. The measured rotational distributions can be accurately fitted by the sum of two Boltzmann contributions with quite different temperatures : a cold one at about 60 K and a hot one around 350 K. The relative importance of the cold component increases with increasing incidence and/or scattering angles. It reaches 65% of the total population when both angles equal 70°.

According to the intuitive description of cluster-surface collisions as Leidenfrost processes [5], the outcoming particles can be divided schematically into three categories : first, residual clusters (in favourable conditions), second, monomers evaporated directly from the "top" surface of the colliding clusters without actually "touching" the surface, and third, monomers having undergone a trapping-desorption process (with a very short residence

*Abstract 6958 submitted to the 21st International Symposium on Rarefied Gas Dynamics, Marseille, France, July 26-31, 1998

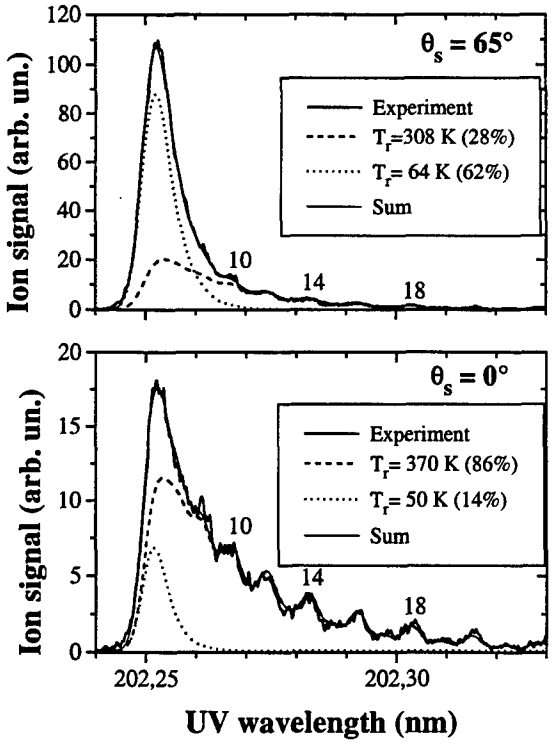

Figure 2: REMPI spectra taken in the conditions defined in fig. 1, shown with the two-temperature fits. The height of the lines is proportional to the populations of the rotational states, which are indicated for J = 10, 14 and 18.

time) on the surface.

Only monomers are detected by REMPI. In the rotational spectra, the cold and hot contributions might be assigned respectively to the second and third components. However, this interpretation would imply a surprisingly low rotational temperature for directly evaporated monomers, which is possible in principle but does not seem very plausible. Alternatively, the rotationally cold component might be due to the "post-evaporation" of monomers by the residual clusters after they leave the surface [6], while the rotationally hot molecules might come from the second and third components involved by the Leidenfrost process.

References

[1] F. Pradère, M. Château, M. Benslimane, M. Bierry, M. Châtelet, D. Clément, A. Guilbaud, J.C. Jeannot, A. De Martino and H. Vach, Rev. Sci. Instrum. **65**, 161 (1994).

[2] K.R. Lykke and B.D. Kay, J. Chem. Phys. **95**, 2252 (1991).

[3] H. Vach, A. De Martino, M. Benslimane, M. Châtelet and F. Pradère, J. Chem. Phys. **100**, 3526 (1994).

[4] R.J. Holland, G.Q. Xu, J. Levkoff, A. Robertson, Jr., and S.L. Bernasek, J. Chem. Phys. **88**, 7952 (1988).

[5] H. Vach, M. Benslimane, M. Châtelet, A. De Martino, and F. Pradère, J. Chem. Phys. **103**, 1972 (1995).

[6] M. Svanberg and J.B.C. Petterrson, Chem. Phys. Lett. **263**, 661 (1996).

Charge Transfer Processes in Hyperthermal (5 - 50 ev) Fullerene-Surface Collisions.

A. Bekkerman, B. Tsipinyuk and E. Kolodney.

Department of Chemistry , Technion - Israel Institute of Technology

Haifa, 32000, Israel.

1 Introduction.

Ion formation during low energy surface scattering or sputtering is of fundamental physical and practical importance. The charge transfer processes studied in the past were mainly neutralization and negative ion formation during collision of positive atomic ions with metal surfaces and positive / negative ion sputtering [1]. Charge inversion resulting in negative ion formation of both parent and fragments was observed for small molecular ions scattered off metal surface at impact energies of 200÷2000 eV [2]. During recent years there is an increased interest in the scattering of polyatomic molecular ions from surfaces at the energy range of 50 ÷ 200 electronvolt [3]. Surface scattering of neutral polyatomic molecules at the hyperthermal impact kinetic energy range of 1÷10 eV was also studied intensively [4]. The intermediate energy range of 10÷50 eV was rarely explored due to technical difficulties related to beam generation and energy analysis of the incident and scattered particles. We have recently bridged over this energy gap and studied in detail the scattering dynamics of neutral C_{60} molecules (aerodynamically accelerated in helium seeded beam) at hyperthermal impact energies of 5÷50 eV. We have studied kinetic energy transfer to the surface, vibrational excitation and initial vibrational energy effects. We have found nearly complete decoupling between normal and tangential energy losses to the surface and have measured low vibrational excitation probability [5]. Our results described the first real "bouncing" regime for C_{60} scattering off surfaces. Here we report the formation of the negatively charged C_{60}^- in near grazing scattering of hyperthermal neutral C_{60} from a carbonized (covered with monolayer graphite) nickel surface [6]. Hyperthermal negative surface ionization of large neutral organic molecules was observed and studied before at impact energies of 1÷15 eV [7]. The central role of image charge effects (down shifting the affinity level of the approaching molecule) was assumed but no experimental evidence was reported. We will describe our measurements of image charge effects in C_{60} surface scattering and discuss the implication of the measured image charge barrier in relation to possible collisional surface-molecule electron transfer mechanism.

*Abstract 3961 submitted to the 21st International Symposium on Rarefied Gas Dynamics, Marseille, France, July 26 - 31, 1998.

2 Experimental.

The molecular beam surface scattering apparatus was described before [5]. The hyperthermal C_{60} source is an all ceramic differentially heated nozzle oven typically operated at 1000÷1900 K. The C_{60} molecules were scattered from a fully carbonized polycrystalline nickel surface held in UHV chamber. Surface temperature was kept at 950 K. Both primary (E_o) and scattered beam (E_s) energies were measured using small electrostatic energy analyzers mounted between the ionizer and the entrance ion optics of a quadrupole mass spectrometer. A 90° cylindrical analyser served for measuring E_o and a retarding field analyzer served for E_s measurements of both neutral (post ionized) and the negative charge C_{60}^-. Special care was taken to ensure that the ion flight path between surface and the analyzer entrance was completely field free.

3 Results and discussion.

The graphite layered nickel was prepared by carbonization with C_{60} bombardment [5]. The scattered negative ions spectra from the carbonized nickel surface was totally dominated by the C_{60}^- molecular peak. No fragments were observed. The C_{60}^- signal showed strong increase with E_o above an apparent threshold at ~4 eV. The C_{60}^- formation yield is estimated as 0.1-0.5% at E_o=45 eV. In what follows, we will focus on the C_{60}^- angular and energy distributions

and their analysis in terms of image charge effects.

We have measured the energy distribution of scattered neutral C_{60}^{o} and negative ions C_{60}^{-} at the peaks of the corresponding angular distributions. All distributions measured in the range of E_o = 5÷45 eV consistently show that the peaks (most probable values) of the scattered C_{60}^{-} energy distributions (E_{sm}^{-}) are lower in energy than the corresponding peaks of the neutral C_{60} distributions (E_{sm}^{o}) by a constant shift of 0.5÷0.7 eV. The accuracy of the measured E_{sm} values is limited by the unknown contact potentials up to ±0.5 eV. Although the observed energy shift can be considered only semi-quantitatively it is clearly indicative of a retarding image charge effect. The image potential barrier E_{image} retards the outgoing C_{60}^{-} such that $E_{sm}^{o} = E_{sm}^{-} + E_{image}$. Assuming now that the image potential barrier has planar geometry one should expect a refractive behaviour manifested by a relative angular shift between outgoing trajectories of C_{60} and C_{60}^{-}. Indeed, a clear angular shift is observed between

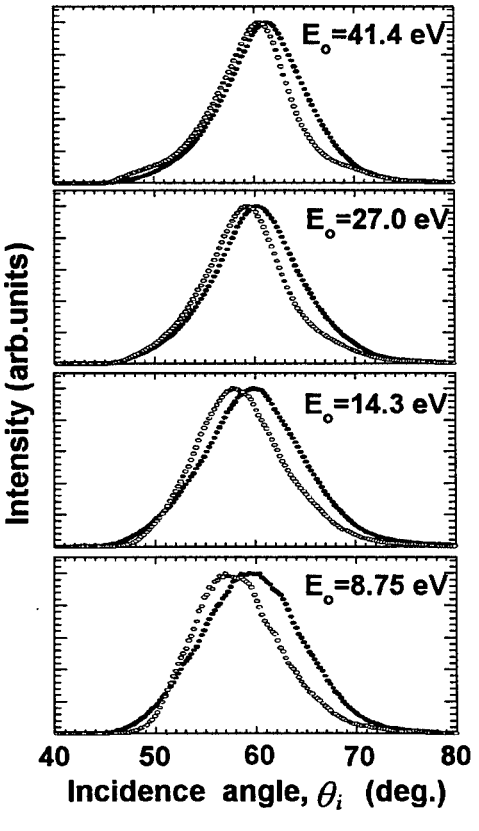

Fig.1 Scattered C_{60}^{o} (full circles) and C_{60}^{-} (empty circles) beam intensity vs. incidence angle $I(\theta_i)$ for Ψ = 45°, T_S=950 K and various primary energies E_o. Note the gradual shift (due to image charge deflection) between maxima in the $I(\theta_i)$ dependencies of C_{60}^{o} and C_{60}^{-} with decreasing E_o.

the $I(\theta_i)$ dependencies of neutral C_{60} (solid circles) and those of C_{60}^{-} (empty circles) as presented in Figure 1 for several E_o values. The shift is also increasing with decrease in E_o (and correspondingly $E_{S\perp}$) as expected. Being formed on the exit path the negative ion suffers an additional deflection (as compared with the scattered neutral) due to the attraction exerted by the image force in the surface normal direction (Z axis) along the outgoing trajectory from the instant of final formation of the ion, at some critical distance Z_C from the surface. For all distances larger than Z_C the formed ion continue on its outgoing trajectory subjected to the attractive image forces while scattered C_{60} that crossed Z_C as neutral continues unperturbed by image charge forces. We have analyzed the angular shifts over all the impact energy range studied and have obtained an image charge barrier of $E_{image}(Z_c) = 0.28 \pm 0.02$ eV corresponding to a critical "ion formation" distance of $Z_c = 13 \pm 1$ Å. The tunnelling width of the surface-molecule potential barrier at Z_c is therefore 8 ± 1 Å. The large value of Z_C as measured here is giving us with some indication regarding the mechanism for the negative ion formation. Since Z_C is much larger that the C_{60} radius, the incoming C_{60} can cross it at any of the E_o values. Under these conditions, a deeper (E_o dependent), impulsive penetration of the incident molecule into the surface is of no importance in increasing the negative ion yield and the final populations of the different charge states are therefore being determined on the exit path.

References.

[1] J.Los and J.J.C Geerlings. *Physics reports* Vol.190 p.133, 1990.

[2] W. Heiland in :"*Low Energy Ion-Surface Interactions*". *Edited by J.W.Rabalais*, Chichser 1994, p. 313 and references therein.

[3] R.G. Cooks, T. Ast, Md.A. Mabud *Int.J. Mass Spectrom. Ion Processes* Vol.100, p.209, 1990.

[4] A.Amirav, *Comm. At. Mol. Phys.* Vol.24, p.187, 1990.

[5] (a) A. Budrevich, B. Tsipinyuk, A. Bekkerman and E.Kolodney, *J.Chem.Phys.*, Vol.106 p.5771, 1997.

(b) E. Kolodney, B. Tsipinyuk, A. Bekkerman and A. Budrevich, *Nucl. Instr. Meth. B.*,Vol.125, p.170, 1997

[6] A. Bekkerman, B. Tsipinyuk, S.Verkhoturov and E.Kolodney, *J.Chem.Phys.*, submitted.

[7] A. Danon and A. Amirav, *J. Phys. Chem.* Vol. 93, p.5549, 1989.

MOLECULAR BEAM SESSION MB - P

Poster Session

CHAIR: A. González-Ureña

IN OPEN AIR
TUESDAY, JULY 28, 1998
16:15 - 18:15

Observation and Spectroscopy of Metastable O_4 *

D. S. Peterka, M. Ahmed and A. G. Suits
Chemical Sciences Division, Berkeley National Laboratory
Berkeley CA 94720 USA

Although speculation about novel tetraoxygen molecules dates back to a 1924 paper by G. N. Lewis[1], serious consideration of covalently bound O_4 species really began with Adamantides' 1980 prediction[2] of a bound cyclic (D_{2d}) form. This stimulated considerable theoretical effort as this cyclic O_4, nearly 4 eV higher in energy than two O_2 molecules, appeared to be a promising candidate for a high energy density material[3]. Subsequent theoretical studies have also identified a D_{3h} form analogous to SO_3 at a somewhat higher energy[4]. Although experimentalists have long observed evidence of van der Waals' complexes of O_2, no evidence has been found supporting the theoretical predictions of covalent O_4 species. We present resonant photoionization and photoelectron spectra of an energetic O_4 species that may represent one of these elusive covalent tetraoxygen molecules[6].

The experiment features a pulsed beam of oxygen which produces a discharge in the collision region of the expansion upon encountering an electrode at ±5kV. The resulting beam is skimmed before entering the main chamber where it is probed via a tunable laser between 280 and 330nm. We see very strong signals at m/e=64 (O_4^+) in ion time-of-flight using an unfocused laser and less than 100 microjoules/pulse (15 nanoseconds) on the resonant lines. This, combined with laser power studies, indicates a 1+1 resonant ionization process. Under these conditions, O_4^+ is the only ion observed. Spectra were obtained by scanning the laser while recording m/e=64 ion yield or total electron yield (Fig. 1). For the electron spectra, the polarity of the discharge was reversed and the total discharge current was lower. The differences between the ion and electron spectra may thus indicate the presence of more hot band contributions in the ion spectrum.

We see many vibrational lines throughout the region from 280 to 330nm. However, only those in the long wavelength region from 320 to 330nm show

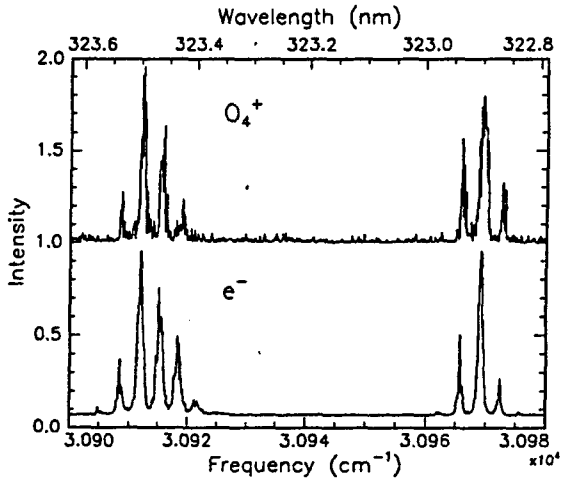

Figure 1: Total photoelectron and m/e=64 ion yield as a function of wavelength (see text).

the rotational structure apparent in Fig. 1. It is interesting to note that we also observe these spectra when the discharge is produced by focusing a laser at 248 or 266nm onto the collision region of an oxygen or ozone beam.

These spectra allow us to make some general statements concerning the energetics of O_4, summarized in Fig. ??. The persistence of the REMPI signal out to 327 nm indicates that the initial state of the O_4 produced lies at least 4.1 eV above two ground state O_2 ($X^3\Sigma_g^-$) molecules, while the intermediate state must lie at least 7.9 eV above two O_2's. The presence of well-resolved rotational structure indicates the lifetime of the intermediate must be relatively long, precluding strong predissociation of the intermediate state. These energy values are in accord with theoretically predicted covalently bound states of O_4 of various geometries[2-5]. Another candidate being investigated is a novel van der Waals' form (T shaped) resulting from combination of a ground state O_2 ($X^3\Sigma_g^-$) with a metastable Herzberg state of O_2 ($c^1\Sigma_u^-$).

We have also recorded photoelectron spectra on

*Abstract 7067 submitted to the 21st International Symposium on Rarefied Gas Dynamics, Marseille, France, July 26-31, 1998

the various resonant lines using velocity map imaging[7]. A range of behavior is observed, including both isotropic and anisotropic electron angular distributions and kinetic energy distributions showing resolved vibrational structure.

Possible interpretation and assignment of the REMPI and photoelectron spectra will be discussed in light of recent high-level ab initio calculations[5].

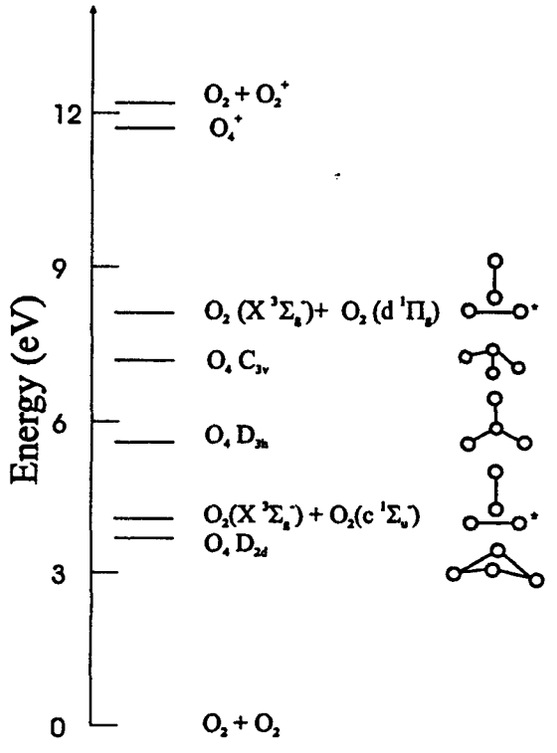

Figure 2: Relevant energies for the O_4 system from references [2-5].

References

[1] Lewis, G. N., *J. Amer. Chem. Soc.*, Vol. 46, p.2027, 1924.

[2] Adamantides, V., Neisius, D., and Verhaegen, G., *Chem. Phys.*, Vol. 48, p.215, 1980.

[3] Seidl, E. T. and Schaefer, H. F. *J. Chem. Phys.*, Vol. 88 p. 7053, 1988. Dunn, K. M. et al., *J. Chem. Phys.*, Vol. 92, p. 6077, 1990. Seidl, E. T. and Schaefer, H. F. *J. Chem. Phys.*, Vol. 96, p.1176, 1992.

[4] Roeggen, I. and Nilssen, E. W., *Chem. Phys. Lett.*, Vol. 157, p.409, 1989. Hotokka, M. and Pyykko, P., *Chem. Phys. Lett.*, Vol. 157, p.415, 1989.

[5] Korkin, A., Nooijen, M., Watts, J., Wilson, K. and Bartlett, R., Private Communication.

[6] Bevsek, H., Ahmed, M., Peterka, D., Sailes, F. C. and Suits, A. G., *Farad. Discuss. Chem. Soc.* Vol. 108, in press, 1998.

[7] Eppink, A. T. J. B., and Parker, D. H., *Rev. Sci. Instrum.*, Vol. 68, p. 3477, 1997.

Elastic Scattering of Metastable He($2^{1,3}$S) Atomic Beam by the Ground-State Na Beam: Phase Analysis of Scattering Mechanism

*

E.Yu.Remeta, V.I.Kelemen, A.V.Snegursky, A.N.Zavilopulo
Institute of Electron Physics, Ukr.Nat.Acad.Sci.
21 Universitetska, Uzhgorod 294016 Ukraine

The method of theoretical determination of the phaseshifts of elastic atom-atom scattering within the framework of the optical potential method has been developed. The technique uses the phase function equation [1,2]. The optical potential for He(^{1,3}S) + Na(^{1}S$_0$) scattering was found in [3] fy fitting the experimental data for the 5-105° LAB-scattering angles at five CM-collision energies from 52 meV to 207 meV. Using this potential, the theoretical studies of partial phaseshifts and partial, differential and total scattering cross sections were performed at the 80 and 92 meV collision energies. Two scattering models are considered - with real and complex potentials. The results of calculations of differential scattering cross sections at 92 meV are compared with experimental data of [3], while at 80 meV - with present experiment.

A detailed description of experimental technique can be easily found elsewhere [4]. The differential cross sections were measured within the 0-20°(LAB) anglular range at 0.6° angular resolution of metastable detector. The metastable He beam was produced by a supersonic nozzle source with axial electron excitation. This allowed the angular divergence of metastable beam to be minimized as compared with, say [3], where the transverse excitation scheme was applied. However, such nethod has almost negligible perturbation effect on the primary beam velocity distribution. This allowed us to perform the experimental studies of the differential elastic cross sections for the abovementioned partners.

It is well-known that the potential at low distances, being repulsive, has quite large value (1000 a.u.). Therefore, to integrate well phase equation in this region of distances the analytical formulae are used providing an evidence for the dependence of the complex phase function value on the wave-vector, orbital momentum and optical potential parameters. About 100 partial waves were calculated as the function of energy. The partial phase functions exhibit a leap-like (by π number) behaviour, indicating the large number of possible bound states in the He*Na quasimolecule due to the attractive part of the potential at 5.5-20 a.u. distances (see [1,2]). The calculated differential scattering cross sections reproduce the experimental behaviour at given collision energies. This testifies to a good (at least qualitatively) behaviour of the potential.

Present work was partially supported by the Ukrainian State Fundamental Research Foundation (Grant No F4/1675-97).

References

[1] F.Calogero. Variable Phase Approach to Potential Scattering. Acad.Press, N.Y. and London, 1967, 292p.

[2] V.V.Babikov. Phase Functions Method in Quantum Mechanics. Nauka, Moscow, 1968, 256p. (in Russian)

[3] H.Haberland, W.Weber. J.Phys.B:At.Mol.Phys.1980,v.13,4147-4155.

[4] A.V.Snegursky, A.I.Zhukov, A.N.Zavilopulo. Ukr.Fiz.Zhurn. 1994, v.39,N3,300-303. (in Ukrainian)

*Abstract 5767 submitted to the 21st International Symposium on Rarefied Gas Dynamics, Marseille, France, July 26-31, 1998

Energy Analysis and Model Calculations of Collisional Acceleration in Seeded Molecular Beams: A study of Xe / He and C_{60} / He.

B. Tsipinyuk, A. Budrevich, A. Bekkerman, and E. Kolodney.

Department of Chemistry , Technion - Israel Institute of Technology

Haifa, 32000, Israel.

A simple theoretical model for the aerodynamic acceleration of heavy particles in seeded molecular beams in the hyperthermal energy range of 1 - 60 eV is presented [1]. The model gives a microscopically detailed picture of the collisional acceleration dynamics in terms of the number of collisions at a given distance downstream from the nozzle aperture. The basic model applies to an ideal isentropic free jet centreline expansion with hard spheres collisions but is also modified to include capillary nozzle effects. The model predictions are compared with experimental measurements [1,2] of terminal kinetic energies of Xe accelerated in He in the constant flux mode up to 11.5 eV and C_{60} accelerated in He in the constant flux mode up to 56 eV and in the constant temperature mode up to 41 eV. Good agreement between calculation and experiment is obtained.

The C_{60} beam is expanded out of a two-stage differentially heated nozzle at temperatures (T_o) of up to 2000 K. For T_o=1200÷2000 K, the C_{60} molecule (before expansion cooling) contain average vibrational energy in the range of $< E_v >$=10÷21 eV. Aerodynamic acceleration of such a superhot specie is an intriguing process where the initial vibrational energy is as high as 21 eV and the vibrational cooling is of the same magnitude as the energy slip (as define by the velocity slip). We have applied a mass spectrometry based vibrational thermometry method (independently calibrated with effusive beams) for measuring the vibrational cooling of the superhot C_{60} [3]. Under extreme stagnation conditions (P_o,T_o) we obtain vibrational coolind of 6 - 8 eV but typical values are in the range 3 - 5 eV. The applicability of the hard sphere approximation for describing the acceleration dynamics of superhot C_{60} in He shows that C_{60} can be treated here as a "quasi-atom", and that the coupling between vibrational relaxation and velocity slip effect can be ignored in this case.

*Abstract 3962 submitted to the 21st International Symposium on Rarefied Gas Dynamics, Marseille, France, July 26 - 31, 1998.

The collisional acceleration dynamics of C_{60} molecules ($P(C_{60})$ = 0.1 Torr) seeding in He carrier gas is calculated in Fig.1 for two pairs of T_o, P_o values. These are the exact experimental conditions for the measured C_{60} kinetic energies as presented in Fig.2. Close inspection of the simulation in Fig.1 shows that for the initial conditions T_o=1130 K; P_o = 2100 Torr, the freezing point is achieved after 483 collisions at a distance of 129 nozzle diameters downstream (y_{483} = 129), and the terminal energy obtained is 28.6 eV. However, for the pair T_o=1795 K; P_o = 2100 Torr a freezing is achieved already after 435 collisions (y_{435} = 107), but the terminal energy is

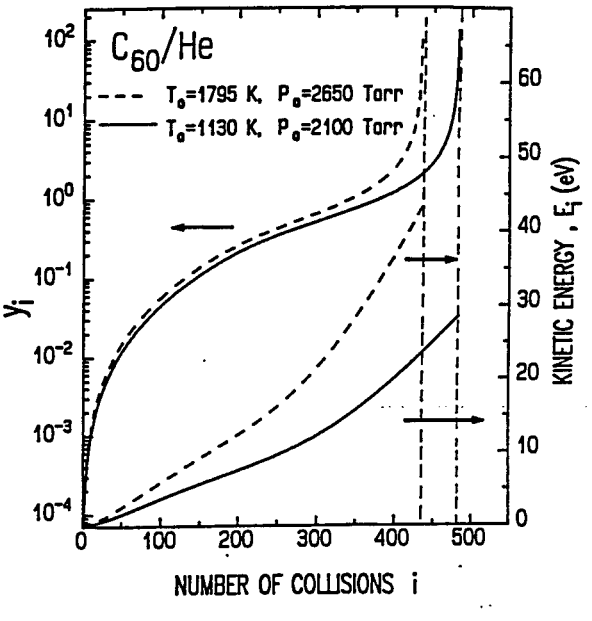

Fig.1 Calculated collisional acceleration dynamics for C_{60} molecules (0.1 Torr) seeded in He under constant flux conditions ($P_o / \sqrt{T_o}$ = 62.5 Torr·$K^{-1/2}$). The relative distance y_i (left ordinate) and the kinetic energy E_i (right ordinate) are presented as a function of the collision number i. $y_i = x_i / D$ where x is the distance from the nozzle orifice and D the nozzle diameter. The two vertical dashed lines stand for the maximal number of collisions ("freezing of the acceleration processes). The effective nozzle diameter D is 103 μm.

43.0 eV. It is also interesting to note that already after two nozzle diameters (T_o=1795 K; P_o = 2650 Torr, $y_{392} = 2$) the kinetic energy is 35.4 eV, which is 82% of the terminal value. This behaviour is a general characteristic of all the acceleration processes presented here and result from the behaviour of y_i,

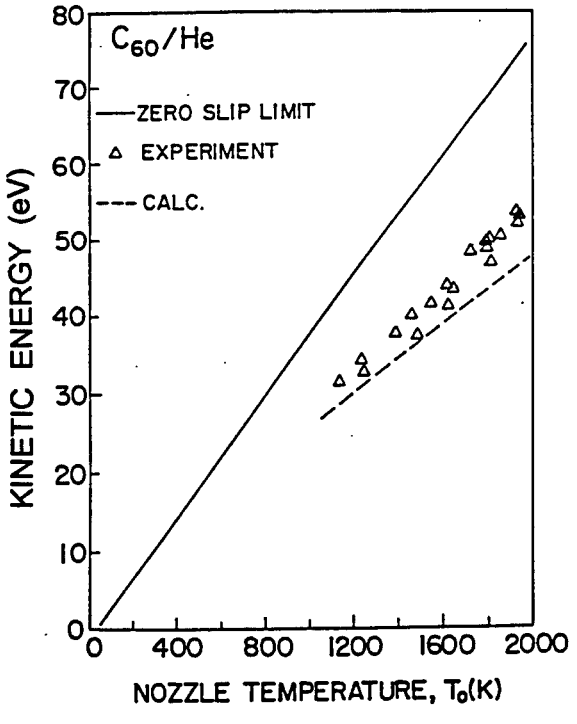

Fig.2 Measured and calculated kinetic energies of C_{60} molecules (0.1Torr) accelerated in He as a function of nozzle temperature T_o under constant flux conditions ($P_o / \sqrt{T_o} = 62.5$ Torr$\cdot K^{-1/2}$). Shown are experimental points (squares) and calculated energies (dashed lines). The effective nozzle diameter D is 103 μm. The straight solid line is the isentropic limit (zero slip).

which for C_{60} / He rise steeply only during the last 50 collisions, whose contribution to the terminal kinetic energy is relatively small.

Fig.2 presents the experimental measurements (triangles) under constant He flux conditions and variable nozzle temperature in the region of 1130-1930 K, for D = 103 μm. The solid thin line stands for the isentropic limit (dilution ration corrected) and the calculated values, lower by 7 - 8% than the measured ones, are given by the dashed line. Although the agreement obtained is quite good considering the simple model applied and various assumptions made, we believe that for this situation as well as for the case of Xe acceleration the difference between the calculated values and measured ones can be related to the capillary nozzle effects. Correcting the model for capillary nozzle effects we obtained approximately 10% increase in terminal energies, in agreement with experiment. However, due to the somewhat arbitrary nature of these corrections (new density function) this result should be considered only as a qualitative one.

In summary, we are presenting new experimental and theoretical tools for the generation, energy analysis and modelling of the collisional acceleration of large particles in the hyperthermal energy range 10÷100 eV.

[1] B. Tsipinyuk, A. Budrevich and E.Kolodney, *J. Phys. Chem.* Vol.100, p.1475, 1996.

[2] A. Budrevich, B. Tsipinyuk, E.Kolodney *Chem. Phys. Lett.* Vol.234, p.253, 1995

[3] B. Tsipinyuk, A. Budrevich, M. Grinberg E.Kolodney *J. Chem. Phys.* Vol.106, No.6 pp.2449, 1997.

REMPI Spectroscopy of internal state populations in HBr + Ar and HBr + Nitrogen free jets: Rotational relaxation of HBr Presentation of Abstracts Submitted to the 21st International Symposium on Rarefied Gas Dynamics *

Andrey E. Belikov[1], Michael M. Ahern[2], Mark A. Smith[2]
[1] Institute of Thermophysics, Russian Academy of Sciences, Novosibirsk, Russia
[2] Department of Chemistry, University of Arizona, Tucson, Arizona, USA

1 Introduction

A study was made of the terminal rotational states of HBr in free jets of Ar and N_2 under varying conditions of P_0D. These state-selective results provide valuable data for the study of temperature dependent rotational relaxation cross sections down to the extremely low temperatures within the jet. Such data can aid in the global understanding and modelling of temperature dependent molecular relaxation. They relate not only to problems in aerodynamics, molecular beam and free jet collision studies but also can be used to reveal anisotropies in the intermolecular potentials. In this paper, experimental results are provided for relaxation in both the Ar and N_2 buffers and a simple relaxation model is presented for the relaxation by Ar.

2 Experimental

Our free jet apparatus and diagnostic equipment is a modification of the apparatus used in earlier reports from this laboratory on reactive and inelastic collision processes of ions, radicals and molecules within the cores of free jets [1]. The terminal rotational state distributions for HBr seeded <10 percent in Ar or N_2 were obtained using resonance enhanced (2+1) multiphoton ionization (REMPI) of the HBr through the E $^1\Sigma^+$(0-0) state at excitation wavelengths near 256.6 nm. The REMPI line strength factors were determined by direct measurement of 300 K spectra. These allowed terminal rotational state populations for HBr to be obtained at distances greater than 50 nozzle diameters downstream of the orifice. The free jet was pulsed, with a pulse duration of 700 *mus*, the data being obtained from the center of the gas pulse.

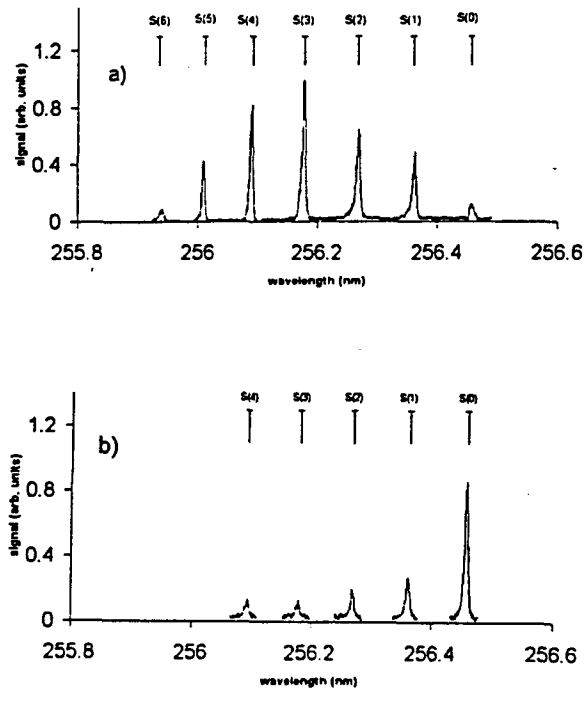

Figure 1. Top: (2+1) REMPI spectrum of the S branch of the E $^1\Sigma^+$ state of HBr, static gas at 300 K. Bottom: Same spectrum of terminally cooled HBr at 0.5 percent seeded in Ar buffer expanded through a 0.04 cm diameter pusle nozzle orifice with stagnation pressure and temperature of 103 torr and 298 K respectively. In the bottom spectra, only the lines were scanned to optimize signal-to-noise for reasonable scan times./medskip

*Abstract 6931 submitted to the 21st International Symposium on Rarefied Gas Dynamics, Marseille, France, July 26-31, 1998

3 Results and Discussion

Example spectra are shown in Figure 1. The rotational state distributions for HBr in N_2 are shown in Figure 2. From these distributions in Ar a power law relaxation model was employed to fit the data over P_0D ranges from 50 to 550. This allowed the rotational relaxation cross sections to be obtained as a function of temperature over the range present in the post-continuum zone of the free jet flows (180 to 15 K). This model will be presented and discussed as will the data for N_2 which is still under analysis and naturally requires a more sophisticated treatment of the scattering.

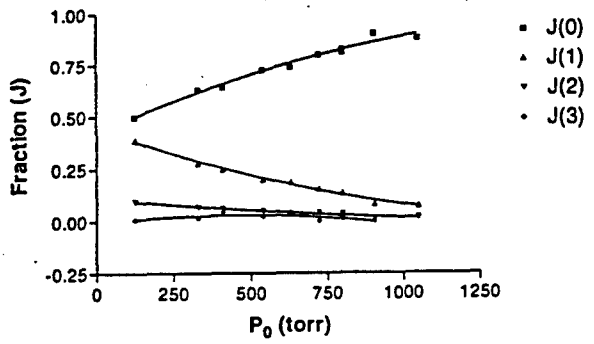

Figure 2. Terminal rotational state distributions for HBr in N_2 as a function of P_0D.

References

[1] Smith M.A., International Reviews in Physical Chemistry, Volume 17, no. 1, 1998.

Femto Second (imaging) Pump Probe Experiments with a High Repetition Rate in a Molecular Beam

Wim Roeterdink, Anouk Rijs, Piotr Wasylczyk, Arjan Wiskerke, Steven Stolte, Marcel Drabbels and Maurice Janssen

Lasercentre, Dept. of Physical and Theoretical Chemistry Vrije Universiteit 1083, 1081 HV Amsterdam

A femtosecond laser system has been installed last year and is currently tested in our laboratory. Its source, formed by a Titanium Saphirre oscillator (Tshunami), produces 80 fs pulses with a repetition rate of 82 Mhz and an energy of approximately 10 nJ per pulse. Its wavelength is slightly tunable around 800 nm. The femtosecond oscillator pulses are amplified in a regenerative amplifier (Regen). Due to the high intensity of the femtosecond pulses the oscillator pulses are streched approximately 10.000 times in the time domain. This is done by introducing linear chirp. The pulses are then amplified 100.000 times in energy by the regen. Subsequently these pulses are compressed to give 130 fs pulses of 1 mJ at a repetition rate of 1Khz and at a bandwidth of 8 nm at 800 nm, which is transform limited within experimental error.

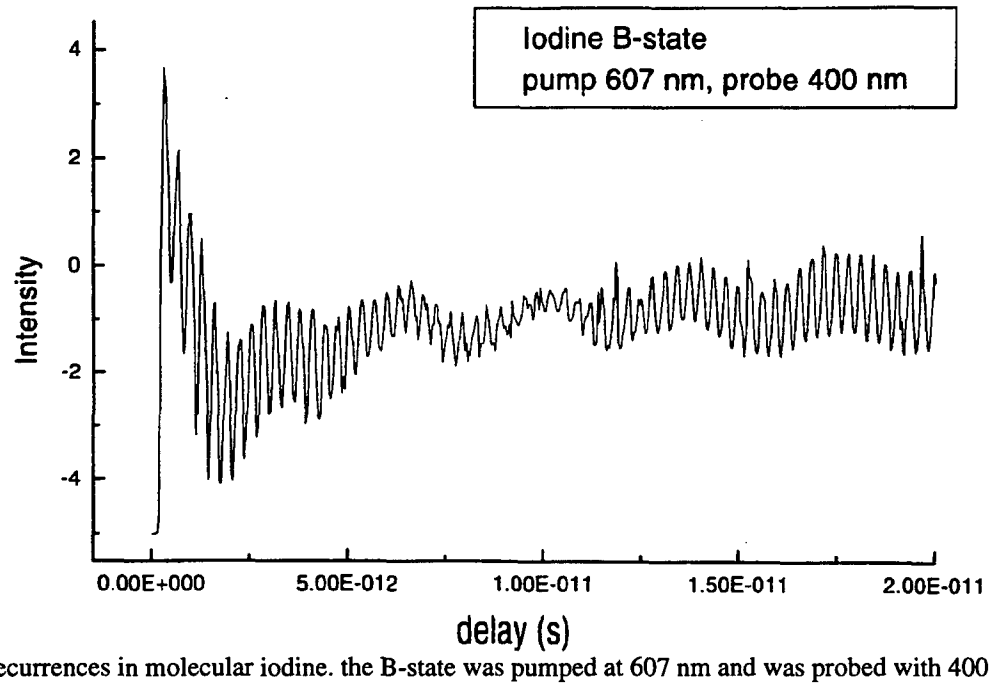

fig 1. recurrences in molecular iodine. the B-state was pumped at 607 nm and was probed with 400 nm

*The pulse duration was measured with a home build second harmonic single shot autocorrelator following [1,2]. Moreover a single shot monochromator was constructed to measure the spectral shape of the laser pulses. The tunability is achieved with an OPA, which can generate a signal from 1150 nm to 1700 nm, with its maximum power output around 1200 nm. This signal was doubled to 50 μJ at 600nm with a bandwith of 8 nm and a puls duration of 150 fs. Further compression with a beamwalk prism compensated compressor shortens this pulse to 95 fs. The alignment of the compressor is easily done with the help of home build FROG which enables us to minimize the linear chirp. To test the lasersystem pump-probe experiments were carried out in a Iodine duration of 150 fs and a energy of 30 μJ. A resulting interferogram (fig 1) reproduces the earlier findings [3] and its Fourier transform reproduces the vibrational

*Abstract 7002 submitted to the 21st International Symposium on Rarified Gas Dynamica, Marseille, France, July 26-31, 1998.

frequencies of the excited B-state of Iodine. To allow femto second experiments with our system in molecular beams a special ion-imaging machine is being build. Its source chamber is pumped by a 5000l/s diffusion pump with a liquid nitrogen baffle. Our seeded molecular beam is produced in a fast piezo pulsed valve [4], yielding gas pulses with a repetition rate of 1 kHz and a pulse width of 200 μs. Compared to CW operation a reduction in gas load of factor 5 has been achieved.To ensure a high particle density, LIF measurements are done directly behind the piezo valve. The molecular

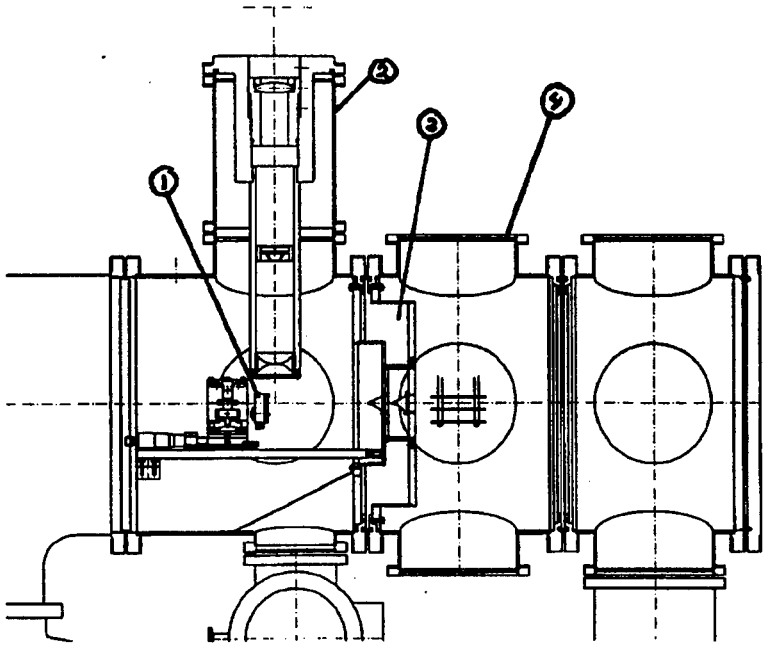

fig 2. cross section of the beam machine, 1) source chamber 2) LIF collection system 3) bufferchamber 4) ion imaging of molecular ions and photo-electrons

beam is double skimmed before entering the ion imaging chamber. This is done to prevent gasleakage from the source chamber and to ensure low beam temperatures. The imaging technique which is going to be used is the velocity map imaging with electrostatic lenses. [5] The advantage of this technique is that the ion image is not a convolution of the spatial profile of the molecular beam, because all molecules with the same velocity are imaged on the same place. The electrostatic lenses ensure that there is no need for an extracting grid, which causes blurring of the image. Femto second pump probe in small e.g. I_2, CH_3I and CF_3I are in progress.

Acknowledgements: Financial support from SON and FOM allowed the construction of our femto laser setup. We are grateful to the university to provide a special laboratory fitted for femto second laser experiments. Wim Roeterdink acknowledges his special PhD student position of the young chemist program of SON. The research of M.Drabbels was supported by the Royal Dutch Academy of Science (KNAW).

REFERENCES

[1] A. Brun, et. al., J. Phys. D: Appl. Phys. **24** (1991) 1225.
[2] J. Janszky, G. Corradi, R.N. Gyuzalian, Opt. Comm. (1977) 293.
[3] R.M. Bowman, et. al., Chem. Phys. Lett **161** (1989), 297
[4] D. Gerlich, Private Communication,
[5] A.T.J.B. Eppink and D.H. Parker, Rev.Sci. Instrum. **68** (1997) 3477.

Molecular beam studies of chiral molecules*

A. Giardini-Guidoni[1], S. Piccirillo[2], A. Latini[1], D. Toja[1], A. Paladini[1], A. Palleschi[1], M. Satta[1]
[1] Dipartimento di Chimica, Universita' "La Sapienza", Roma, Italy
[2] Dipt. STC, Universita' "Tor Vergata", Roma, Italy

1 Introduction

The molecules having the property of chirality [1], discovered in the early nineteenth century, have been since, the subject of innumerable experimental and theoretical investigations in the field of physics, chemistry and biology [2]. Such a large interest is due to the prominent role these molecules play in natural processes [3]. Many techniques to obtain enantiomerically pure compounds have been developed. However all traditional methods which provide the basis for enantiomeric discrimination involve measurements in condensed phase where the presence of the solvent may produce undesired effects in their differentiation. Recently, through resonant ionization and fluorescence techniques, the difference between the binding energy in ground and electronically excited states in gaseous diastereomeric complexes of a chiral chromophore with a chiral solvent as been measured. A different spectroscopic shift, ($\Delta\nu$), of the 0_0^0 electronic transition is found in case of clusterization of one enantiomer of a chiral alcohol with another R or S chiral molecule [4,5]. In this work we report on an investigation of spectroscopic properties as ionization potential (IP) of (R)-(+)-1-phenyl-1-propanol (P_R) and IPs and dissociation energies of its clusters with (R)-(-)-2-butanol (P_RB_R) and (S)-(+)-2-butanol (P_RB_S). We have also calculated the structures, binding energies and dissociation energies of these complexes using semiempirical calculations.

2 Experimental methodology

The experimental apparatus has already been described in previous publications [6,7]. Briefly, the clusters are produced in a supersonic expansion from a pulsed nozzle using argon as carrier gas at P=2-6 bar. The seeded molecular beam passes through a 1 mm skimmer into a second chamber and is probed by the laser radiation at a distance of 25 cm. The laser system consists of two tunable dye laser pumped by the same frequency doubled Nd:YAG laser. Neutral compounds in the supersonic beam are excited to the S_1 state through a first photon ($h\nu_1$), ionized by a second photon ($h\nu_2$) (2c R2PI) and detected by a time of flight (TOF) mass spectrometer. The dissociation energy of the clusters in the ground state (D_o'') is derived from the difference between the dissociative photoionization threshold of the adduct and the IP of the molecule. The dissociation energy of the ionized cluster (D_o^+) is given by the difference between its IP and its dissociative ionization threshold.

3 Results and discussion

From the excitation spectrum of the P_R molecule, already reported, it can be inferred that three different conformers are present [9]. Their occurrence is confirmed by ab initio calculations [8]. In the 2cR2PI absorption spectrum of the P_RB_S and of the P_RB_R the shifts of the most intense bands, assigned to the electronic band origin of the most stable clusters, are bathochromic. Moreover they are shifted 13 cm^{-1} one respect to the other, as already seen in 1cR2PI experiments [5,9].
In table 1 IPs and dissociative appeareance potentials of of P_RB_R and P_RB_S clusters are reported together with their D_o'' and D_o^+ energies.
It appears fromm the table that the binding energy of the clusters is, as expected by the presence of hydrogen bonding [10], larger than the binding energy of aromatic van der Waals clusters, where only dispersive forces are present [11]. The relative increase in dissociation energy upon ionization is about 40%. The dissociation energy of P_RB_R in the ground state is larger by about 360 cm^{-1} with respect to the analogous complex with P_RB_S. Since the pure hydrogen bond interaction should be essentialy the same in diastereomeric complexes, the measured

*Abstract 7030 submitted to the 21st International Symposium on Rarefied Gas Dynamics, Marseille, France, July 26-31, 1998

	$h\nu_1(cm^{-1})$	$h\nu_2(cm^{-1})$	$h\nu_3(cm^{-1})$	$D_o''(cm^{-1})$	$D_o^+(cm^{-1})$
P_RB_S	37485±1	33160±40	35540±40	1700±40	2380±40
P_RB_R	37498±1	32950±40	35890±40	2060±40	2940±40

Table 1: Photon energy for excitation ($h\nu_1$), threshold ionization ($h\nu_2$), and threshold dissociative ionization ($h\nu_3$), of P_RB_R and P_RB_S clusters and derived dissociation energies of fundamental (D_o'') and ionic state (D_o^+)

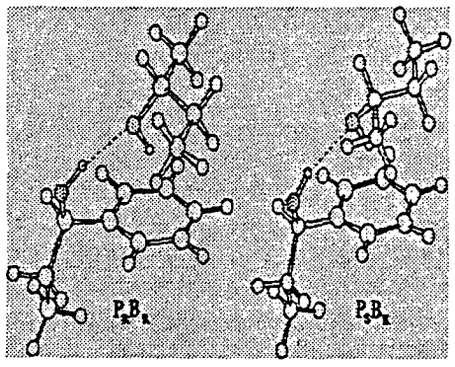

Figure 1: Predicted structures for P_RB_S and P_RB_R clusters.

difference between P_RB_R and P_RB_S bond energy can be mainly attributed to differences in attractive and repulsive dispersion forces. Fig. 1 displays the calculated structures of the most stable isomer of P_RB_R and P_RB_S in the ground state. It can be seen that the hydrogen atom of the hydroxylic group of the solvent is centrally bound above the benzene ring via hydrogen bond to the π electron cloud [12], and that the P_R molecule acts as the hydrogen bond donor, as expected from thermochemical data on proton affinity [13]. The calculated nuclear configurations for the two diasteromers can explain the measured difference of dissociation energy.

4 Conclusions

In this paper it has been shown that 2cR2PI technique is an excellent tool to enantiodifferentiate gas phase neutral and ionic diastereomeric compounds. New experimental information on the energetic and spectroscopy of this clusters are reported. The homochiral P_RB_R adduct is more stable both in the ground and ionic state than the heterochiral P_RB_S cluster in agreement with semiempirical calculations.

References

[1] L. Pasteur, Bull. Soc. Chim. France, 41, 215, (1884).

[2] S. F. Mason, Molecular optical activity and the chiral discriminations (Cambridge Univ. Press, Cambridge, 1982).

[3] C. F. Chyba, Nature, 389, 234, (1997)

[4] A. L. Al-Rabaa, E. Brèhèret, F. Lahmani, A. Zehnacker, Chem. Phys. Lett., 237, 480, (1995)

[5] S. Piccirillo, C. Bosman, D. Toja, A. Giardini Guidoni, M. Pierini, A. Troiani, and M. Speranza, Angev. Chemie Int. Ed. Engl., 36, 16, 1729, 1997

[6] Piccirillo S. , Consalvo D. , Coreno M. , Giardini-Guidoni A. , Douin S. , Parneix P. and Brechignac P. , (1994), Chem. Phys., 187, 97.

[7] Piccirillo S. , Coreno M. , Bosman C. , Giardini Guidoni A. , Mele A. Palleschi A. , (1995), Chem Phys Lett. 247, 577.

[8] S. Piccirillo, A. Latini, D. Toja, M. Satta, A. Giardini-Guidoni, M. Speranza, to be published.

[9] A. Giardini-Guidoni, S. Piccirillo, Israel Journal of Chemistry, 37, 439 (1997).

[10] T. Burgi, T. Droz, S. Leutwyler, Chem. Phys. Lett., 246, 291, (1995)

[11] T. Burgi, T. Droz, S. Leutwyler, J. Chem. Phys., 103 (17), 7228, (1995)

[12] S. Suzuki, P. G. Green, R. E. Bumgarner, S. Dasgupta, W. A. Goddard III, G. A. Blake, Science, 257, 942, (1992)

[13] S. G. Lias, J. E. Bartmess, J. F. Liebman, J. L. Holmes, R. D. Levin, W. G. Mallard, J. Phys. Chem. Ref. Data 17, Suppl. 1 (1988).

Mixed clusters produced in Argon-Nitrogen coexpansions as evidenced by two experimental methods. *

E. Fort, A. De Martino, F. Pradère, M. Châtelet and H. Vach
Laboratoire d'Optique Quantique du CNRS, Ecole Polytechnique,
91128 Palaiseau Cedex, France
e-mail: fort@leonardo.polytechnique.fr

G. Torchet, M.-F. de Feraudy and Y. Loreaux
Laboratoire de Physique des Solides (URA 002), Bt. 510, Université Paris-Sud,
91405 Orsay Cedex, France

We present two complementary techniques that provide detailed diagnostics of supersonic expansions involving several species, applied on a coexpansion of a gas mixture Ar 0.1 molar fraction (mf)-N_2 0.9 mf

The first technique involves scattering of the supersonic beam by a buffer gas or by a surface [1].

We use a rotatable quadrupole mass spectrometer (QMS), where the clusters are fragmented into monomers and dimers inside the ionization head. We measure the broadening of the beam profile for different QMS mass settings, and for different buffer gas pressures, from which we deduce the average size of the clusters, if any, present in the beam [2]. Fig. 1 shows the normalized beam profiles' broadening at the mixed dimer ArN_2 mass setting. Identical broadening are obtained for Ar and N_2 mass settings, proving the presence of mixed clusters. Average cluster size *vs* stagnation pressure for this gas mixture is shown in fig. 2 together with the results obtained for pure nitrogen gas. By using the QMS at different monomer mass settings within the beam it is also possible to deduce the beam composition.

Besides, monomers and clusters impinging on a surface yield quite different angular distributions of scattered particles. Hence, surface scattering, together with QMS detection, yields the percentage of uncondensed particles in the incident beam for each species. Eventually, it is possible to deduce mixed *cluster* composition present in the beam.

In the second technique, clusters produced during the expansion scatter a high energy (50 keV) electron beam, providing diffraction patterns which are characteristic of the state of condensation of each species.

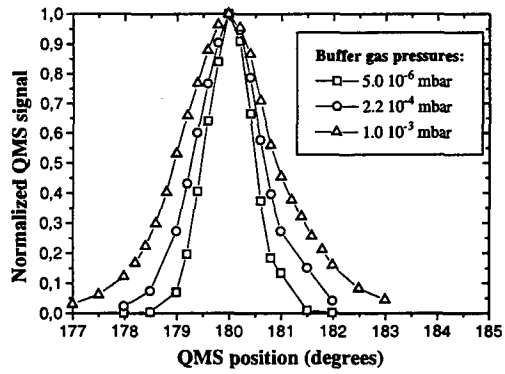

Figure 1: Broadening of mixed ArN_2 dimer profiles for different buffer gas pressures for a 0.1 mf argon-0.9 mf nitrogen mixed gas composition.

Applying these two techniques to the 0.9 mf nitrogen-0.1 mf argon mixture, we have evidenced the existence of mixed clusters, up to a few hundreds of molecules for stagnation pressures up to a few tens atmospheres. We have gathered significant results for a better understanding of the nucleation process. Nitrogen seems to help argon nucleation because of the Mach-number focusing effect and, conversely, argon atoms acting like seeds favor nitrogen condensation.

In the middle of fig. 3 is shown the diffraction pattern recorded from the 0.1 Ar + 0.9 N_2 gas mixture under the following experimental conditions: inlet pressure p=10 bar, inlet temperature T=300 K and

*Abstract 6959 submitted to the 21st International Symposium on Rarefied Gas Dynamics, Marseille, France, July 26-31, 1998

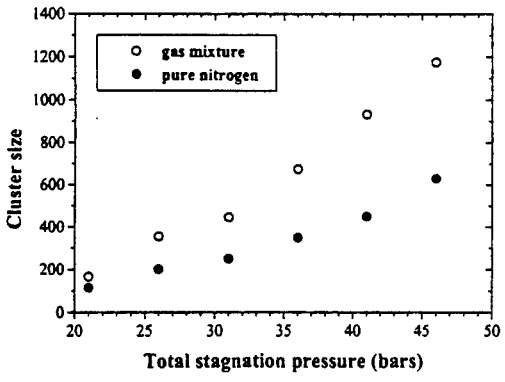

Figure 2: Evolution with stagnation pressure of the average cluster sizes for a 0.1 mf argon- 0.9 mf nitrogen mixture and a pure nitrogen beam.

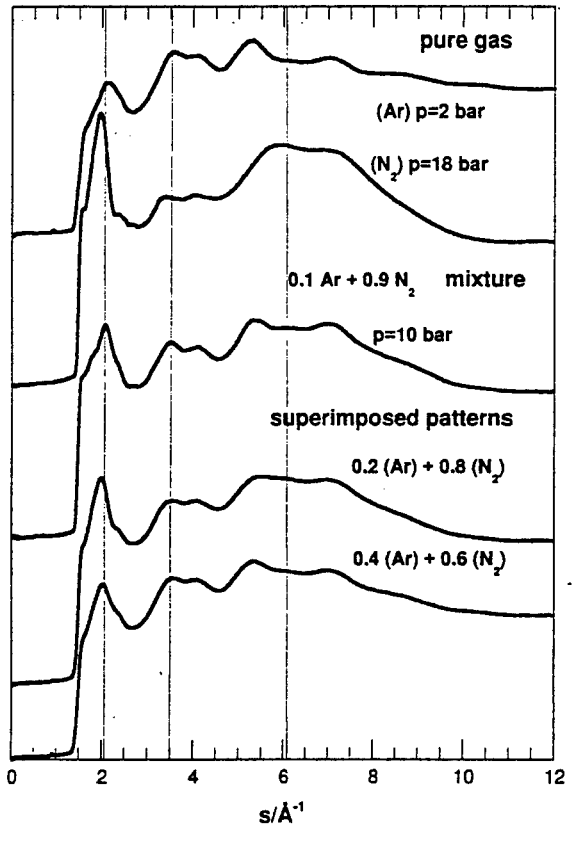

Figure 3: Upper curves: electron diffraction patterns (s^3I *vs* $s=4\pi/\lambda sin(\theta/2)$, with λ electron wavelength and θ diffraction angle) produced by pure Ar and N_2 gas expansions and by Ar+N_2 mixture. Lower curves: superposition of pure gas patterns. Vertical lines should make easier the comparison between curves.

0.2 mm nozzle diameter. This pattern is due to clusters made of a few tens of atoms or molecules. From previous studies on Ar [3] and N_2 [4] clusters, the two oscillations near 3 $Å^{-1}$ and 4 $Å^{-1}$ can be attributed to an amorphous structure.

Upper patterns in fig. 3 corresponding to pure Ar and N_2 gas expansions, obviously show some similarities with the mixture pattern. It is worthwhile to note that the inlet pressures needed to get this similarity, 2 bar (Ar) and 18 bar (N_2), are higher than the partial pressures in the gas mixture, 1 bar (Ar) and 9 bar (N_2) -pressures at which no condensation should be observed-. Mixing both gases thus favors nucleation phenomena. Lower curves in fig. 3 result from the superposition, in different proportions, of upper patterns, weighted according to the respective exposure times. Such curves correspond to diffraction patterns which should be produced by isolated Ar and N_2 clusters traveling together in the beam. Although the calculated curves well compare with the mixture pattern, it is clear that a good agreement cannot be found, whatever the proportion. Due to the opposite effect of Ar and N_2 characteristics in the patterns, it is, for instance, impossible to reproduce at the same time the first line height near 2 $Å^{-1}$ and the plateau near 6 $Å^{-1}$. The coexistence model has then to be discarded, proving that Ar and N_2 coexist inside the clusters produced by the gas mixture.

References

[1] E. Fort, F. Pradère, A. De Martino, H. Vach and M. Châtelet, Eur. Phys. J. D 1, 79 (1998).

[2] A. De Martino, M. Benslimane, M. Châtelet, C. Crozes, F. Pradère and H. Vach, Z. Phys. D **27**, 185 (1993).

[3] J. Farges, M.-F. de Feraudy, B. Raoult and G. Torchet, J. Chem. Phys. **78**, 5067 (1983).

[4] J. Farges, M.-F. de Feraudy, B. Raoult and G. Torchet, Ber. Bunsenges. Phys. Chem. **88**, 211 (1983).

Quantum Optics with Atomic Beam Spin Echo *

M.F.M. DeKieviet[1], R. Grimm[2], A. Reiner[1], M. Zielonkowski[2]
[1] Physikalisches Institut Universität Heidelberg, Heidelberg, Germany
[2] Max-Planck-Institut für Kernphysik, Heidelberg, Germany

Atomic Beam Spin Echo (ABSE) is a versatile and high intensity experimental technique, which allows for the study of very small changes in the atomic beam particles' kinetic energy. The first successful demonstration of the method involves the nuclear spin-$\frac{1}{2}$ system of ^{3}He atoms and operates in the field of surface science [1]. In this contribution, we report on the development of two ABSE setups for atoms having an electron spin: hydrogen and lithium.

We describe first Spin Echo (SE) experiments, performed on an atomic beam of hydrogen. In contrast to a single SE group, obtained for spin-$\frac{1}{2}$ particles, these data show three spin echo groups diverging for increasing spin echo fields. In the middle panel of Fig. 1, the occurence of three interference patterns is demonstrated. The lower panel displays the fact that the oscillation frequency within the two outer interference patterns is about twice as high as that for the middle SE group. Although the magnetic fields involved in this spin echo experiment are but a percent of the critical one for hydrogen, the nonlinear Zeeman effect of the atom can be made responsible for this phenomenon.
A quantum mechanically exact calculation of the hydrogen atom in an external magnetic field, taking hyperfine interaction into account displays excellent quantitative agreement with the data. A summary of the data and comparison with theory is presented in the top panel of Fig. 1. The interference patterns between the contributions of different hyperfine levels is resolved downto some 100 peV. Within this sensitivity, we experimentally confirm the Breit-Rabi formulae for atomic hydrogen.

For deuterium, however, the SE data show significant deviations from this formulae. The explanation for this discrepancy is believed to derive from a quadrupolar contribution of the nucleus (having $I = 1$).
A more illustrative description of the hydrogen spin echo experiment is given in terms of coherence volumes. This picture, first presented by Gähler et al. [2], is almost intuitive and brings about multiple spin echo groups naturally.

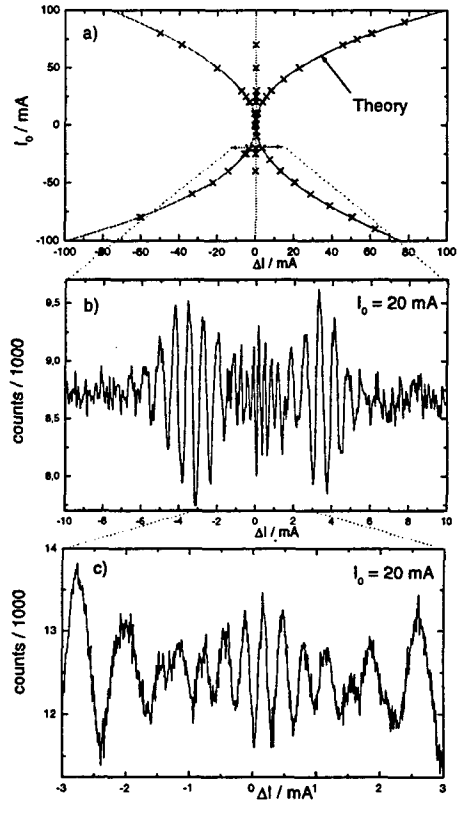

Figure 1: a) Location of all measured SE points (crosses); b) a typical hydrogen SE curve ($I_0 = 20$ mA), showing three clearly separated SE groups; c) a blow-up of the center part of b)

The second electronic spin system discussed in this contribution is that of lithium. With its easily accessible D lines, we have managed to construct an ABSE experiment, in which spin manipulation is achieved entirely optically.
A schematic of the experimental apparatus is shown in Fig. 2. The physical mechanisms involved are

*Abstract 6969 submitted to the 21st International Symposium on Rarefied Gas Dynamics, Marseille, France, July 26-31, 1998

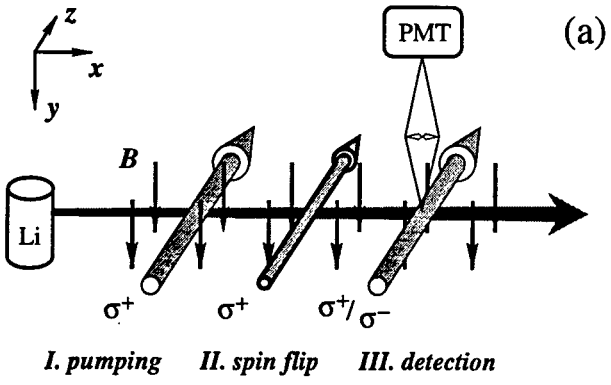

Figure 2: Schematics of the ^{7}Li spin echo apparatus. Three consequetive diode lasers, of σ^+ polarization cross the atomic and induce a $\frac{\pi}{2}$, π and $\frac{\pi}{2}$-pulse, respectively.

optical pumping (spin preparation and detection) and light induced Zeeman shift of atomic ground states (for spin flipping). The latter mechanism, responsible for a π-pulse here, was first described by Cohen-Tannoudji et al.[3] in terms of a *fictitious magnetic field.* We have systematically studied its behavior, as a function of laser power and frequency, and present experimental data on Larmor precession induced by this fictitious magnetic field. As a direct application, we show entirely optically induced spin echo signals on the beam of ^{7}Li atoms. In these data, the contribution of the various multipole components to the Larmor precession can be identified straightforwardly.

References

[1] M.DeKieviet, D.Dubbers, Ch.Schmidt, D. Scholz and U. Spinola, Phys. Rev. Lett. **75(10)**, 1919 (1995).

[2] R.Gähler, R.Golub, K.Habicht, T.Keller and J.Felber, Physica B **229**, 1 (1996).

[3] C. Cohen-Tannoudji and J. Dupont-Roc, Phys. Rev. A **5**, 968 (1972).

An experimental investigation of Debye-Waller factor in Hydrogen and Deuterium scattering from Cu [111] surface *

M.Varlam , D.Steflea, N.Chiriloaie
Vacuum Physics Department,
National Research Institute of Cryogenic Technologies, Rm.Valcea, ROMANIA

1 Introduction General theoretical basis

It is well-known that the elastic scattering of molecular beams from single crystal surfaces is a purely quantum idea.In classical physics, the zero energy exchange probability, between a surface and an incident particle is obviously zero. There is also a non vanishing probability for that events to occur and is usually called the *Debye-Waller* factor. In these scattering processes, of thermal molecular beams from surfaces, the *Debye-Waller*factor is a measure of the elastically scattered beams . An usual expression, generally accepted for the Debye-Waller factor is given on the basis of the dependence from the amount of the surface atoms motion and also from the momentum transfer value in the collision process, and it is shown below:

$$f_{DW} = \exp(-2W) = \exp(-(\delta k_z)^2 < u_s^2 >). \quad (1)$$

where $\delta k_z = k_f - k_i$ is the total momentum transfer to the surface and $< u_s^2 >$ is the well-known named mean square displacement vector of the surface atom in the δk direction. Also, it is necessary to remind that the expression for $< u_s^2 >$ is proportional to the surface *Debye* temperature θ_s by the following relation:

$$< u_s^2 >= \frac{3h^2T}{M k_B \theta_s^2}. \quad (2)$$

where M is the surface atom mass, k_B is the *Boltzmann* constant, T is the surface temperature and h is the *Planck* constant. Obviously, the quantity θ_s so defined has no an exactly physical signification. In our study we intended to investigate the validity of the general expression (Eq.3) for this *Debye-Waller* factor, which take into account the attractive potential depth for the scattering of H_2 and D_2 from Copper surfaces. The usual expression for this factor is given by:

$$2W = (((\delta k_o)^2 + \frac{8mD}{h^2}) \times \frac{3h^2T}{M k_B \theta_s^2}). \quad (3)$$

2 Experimental work

In a small Molecular Beam Scattering System, made in our laboratories, Hydrogen and Deuterium beams scattering experiments has been carried out. The general setup of our system follow, in a general manner, the characteristics of other bigger HAS machines, and it is already presented in our paper. The target surfaces investigated was Cu[111] single-crystal, placed in the center of the interaction chamber, and was maintained at a controlled temperature in the 100 - 400 K range. The Hydrogen and Deuterium beams were formed in a *pulsed* molecular gun with three differential pumped stages. The intensity of the Hydrogen or Deuterium beams was about 10^{15} atoms/str*s and the angular spread was below 5^0. The angular distribution of H_2 and D_2 scattered by the target investigated has been detected in the I - plane., with a quadrupolar gas analyzer. The detection system was mounted on a mechanical system which allow a rotational movement around the target surface. Therefore, in our report, only, results in the I - plane has been shown. The angular distribution obtained (shown already in our paper)for H_2 and D_2 beams scattered by the target surface consist of a broadened specular reflection peak and o more broadened skirt around it. The broad skirt is obviously regarded as a result of inelastic events in this interaction.
The experiments has been carried out for different surface temperatures and also, for different inci-

*Abstract 7091 submitted to the 21st International Symposium on Rarefied Gas Dynamics, Marseille, France, July 26-31, 1998

dent angle for the Hydrogen and Deuterium beams. The surface temperature dependence of the specular intensity of the scattered beam for Hydrogen and Deuterium has been plotted, and considered as a first base of discussion for our work. The deviations from the surface temperature linear dependence of the lnI_{sp} for these angular distribution, in the 120 - 400 K range has been numerically evaluated, both for Hydrogen and Deuterium beams. Therefore, an enough satisfactory polynomial dependence of the specular intensity from the surface temperature is estimated, in order to obtain an optimum fit for the experimental data. Based on these calculations, a $T^{1.09}$ dependence of the specular intensity was considered to be proper for our experimental data. According to the previous equations given for *Debye-Waller* factor , a $(\delta k)^2$ linear dependence of lnI_{sp} has been estimated and also, a deviation from that has been evaluated. In our work we tried to estimate a correction factor for that ideal expression (Eq.3) both for Hydrogen and Deuterium beams. The differences observed in the evaluated *Debye* surface temperatures, for Hydrogen and Deuterium incident beams, has been considered in order to find a difference between the interaction potential for these two particular scattering events. Also, an investigation of the adsorption of the Hydrogen and Deuterium at different surface temperatures has been made, in order to obtain a correction factor for specular intensity . So, an estimation of attraction scattering potential depth has been made for H_2- Cu[111] and D_2 - Cu[111]. It could be emphases that the $\Theta_T(K)$ value estimated from the surface temperature dependence of the specular intensity decrease with the increasing of the temperature for both incident Hydrogen and Deuterium beams. The decrement of $\Theta_T(K)$ was about 9.7 K for an increment of T_s. On the other hand, the $\Theta_{theta}(k)$ value estimated from the momentum transfer dependence of the specular intensity , increase with increasing of this momentum transfer , or with the decreasing of the incident angle value. A set of experiments at lower surface temperatures has been carried out (in the 20 - 50 K), but , as a results of an important level of Hydrogen adsorption on the Cu surface, the results for the specular scattered intensity are drastically distorted. However, a temperature dependence of the specular intensity for Hydrogen and Deuterium beams has been estimated, taking into account an approximation factor for the adsorption.

3 Conclusion

- A first conclusion we could made is focused on the so-named *Debye* surface temperature evaluated in our experiments which show an important difference between the values estimated from Hydrogen and Deuterium experiments.
- An isotopic reaction between Hydrogen and Deuterium was shown in a very small degree, by the measuring the isotopic ratio for the incident beam and specular scattered beam. (both for beams which are mainly Hydrogen and Deuterium).
- A correction factor expression has been evaluated for *Debye-Waller*factor in order to take into account a more complicate configuration for the interaction potential.
- The differences between the amplitude of the specular intensities for the scattering of Hydrogen and Deuterium beams has been extensively treated.
- The so-called *Debye* surface temperature has been determined and compared with other similar values obtained from LEED experiments.

References

[1] Lagally M.G., *Surface Physics of Materials* , Academic Press , 1975.

[2] Toennies J.P. *Experimental Determination of Surface Phonons by Helium Atom and Electron Energy Loss Spectroscopy*, Surface Phonons, Springer Series,Vol.21.

[3] Matsui J., Miyabe M,Matsumoto Y.*A Molecular Dynamics Study of Gas-Surface Interaction with Adsorbates*, Rarefied Gas Dynamics ,Proceedings of the 19-th International Symposium, Oxford, 1994.

Deposition of Platinum Clusters on HOPG *

A. Bettac, R.–P. Mayer, L. Köller, V. Rank, K.H. Meiwes–Broer
Fachbereich Physik, Universität Rostock, Universitätsplatz 3, D-18051 Rostock, Germany

1 Introduction

For thin Pb films it was shown that the electronic properties change as a function of the film thickness [1]. The same phenomenon should be seen at small metal clusters where the electron confinement is known to induce distinct electronic states as has been shown by photoelectron spectroscopy in the gas phase [2]. In this contribution we report on scanning tunneling microscopy (STM) and spectroscopy (STS) measurements of deposited Pt clusters on graphite. From electronic structure calculations of small Pt clusters on Ni (111) [3] it is known that the density of states at the Fermi level strongly depends on the cluster size and shape. Our clusters were produced by a Pulsed Arc Cluster Ion Source (PACIS) [4] and alternatively by the condensation of evaporated Pt atoms into preformed nanometer sized pits [5]. The STS-characteristics of the Pt clusters show distinct peaks at the Fermi level and depend on the height of the cluster.

2 Experiment

For the condensation of Pt clusters into nanometer sized pits we have modified the HOPG surface by Ar–sputtering and subsequent heating in oxygen. This treatment causes pits with several nm in diameter and a few monolayers in depth, depending on the heating parameters. After deposition of Pt atoms on this structured surface the clusters are condensed into the nanopits or at step edges (Fig.1). The STM images have to be taken at small tunneling currents and high gap voltages. Otherwise the tip pushes the clusters out of the pinning pits which shows the weak cluster–surface interaction.
In the case of the deposition from a beam the clusters grow in the PACIS and impinge on the surface with a kinetic energy of about $1\,eV$ per atom under high vacuum conditions. In contrast to the surface-condensed clusters, those which are deposited from a beam are bonded much stronger to the surface. They are fixed at their arrival points and can not been displaced by the tip. Furthermore, the platinum clusters often appear flat and in their vicinity a $(\sqrt{3} \times \sqrt{3})$–superstructure is occasionally observed. Similar superstructures have already been

Figure 1: Topography of the (0001)–HOPG surface covered with platinum clusters (image size: $80\,nm \times 90\,nm$). The clusters are located either in the nanopits or arranged along the step edges.

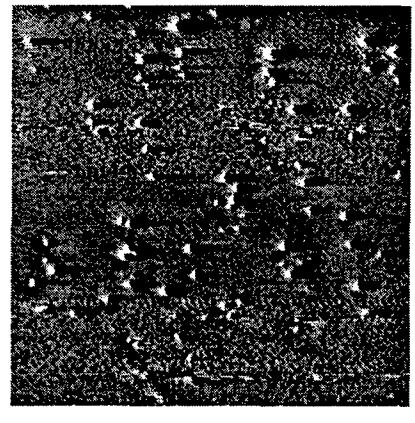

Figure 2: STM constant height image ($100\,nm \times 100\,nm$) of platinum clusters on a graphite surface. The clusters are genarated by the PACIS and deposited from a beam with a kinetic energy of about 1eV per atom.

*Abstract 6992 submitted to the 21st International Symposium on Rarefied Gas Dynamics, Marseille, France, July 26-31, 1998

seen in the area around point defects on HOPG [6]. We conclude that either there is a strong cluster–substrate interaction or the kinetic energy of the clusters in the beam is high enough to modify the surface locally (e.g. compression of the upper graphite layers).

For the spectroscopic measurements the tunneling current is recorded while scanning the sample bias from -0.6 to 0.6 Volts under open feedback conditions. During the investigations the samples are cooled either to liquid nitrogen or to liquid helium temperature (Fig.3).

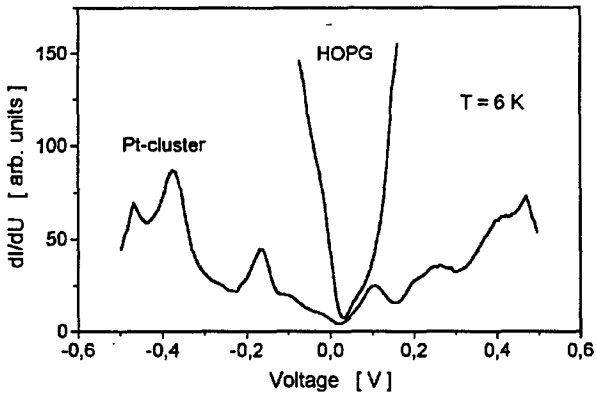

Figure 3: Tunneling conductance spectra measured at $6\,K$: a) on a clean HOPG surface (U–shape) and b) on top of a Pt cluster deposited from a beam on a HOPG surface (structured).

The parabola shaped curve shows the typical $\frac{dI}{dV}$ characteristic of the semimetallic graphite with a low density of states at the Fermi level. In constrast the spectra measured on top of a platinum cluster show peaks at about $-400\,mV$, $-200\,mV$, $100\,mV$ and $220\,mV$. For negative bias voltages the peak separations decrease with increasing height of the cluster d_z (Fig. 4). In a simple model [7] we obtain the following dependence of the energy spacing ΔE on the cluster height:

$$\Delta E = \frac{3\hbar\pi}{2d_z} v_F$$

Taking a linear fit which is forced to pass the origin, the slope gives the Fermi velocity, which is determined to $1 \times 10^7\,cm/s$. From the band structure of Pt bulk a value of $v_F = 1.1 \times 10^8\,cm/s$ can be extracted. The deviation could be caused by a higher effective electron mass in the cluster when compared to the respective bulk value.

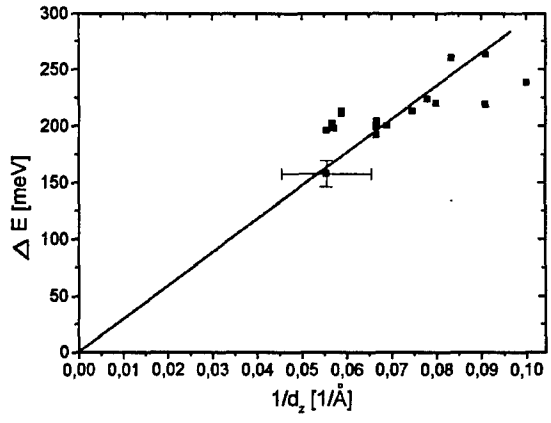

Figure 4: Dependence of the measured energy spacings between the first and the second peak (with negative bias voltage) on the reciprocal value of the cluster height.

3 Summary

The clusters deposited from a beam onto a clean HOPG surface are located at their impinging points, whereas the clusters condensed in the nanopits are weakly bonded. Spectroscopic measurements clearly show a peaked structure for the platinum clusters on HOPG. From the $1/d_z$ dependence of the energy spacings it is conceivable that the discrete levels in the spectra are caused by quantum size effects.

References

[1] Altfeder I.B., Matveev K.A., and Chen D.M., Phys. Rev. Lett., Vol.78, pp. 2815–2818, 1997.

[2] Meiwes–Broer K.H., Appl. Phys., Vol. A 55, pp.430–441, 1992.

[3] Castellani N.J., P. Lègarè P., Mikušík P., Pick Š., Demangeat C., Surf. Sci., Vol.307-309, pp.927–932, 1994.

[4] Ganteför G., Siekmann H.R., Lutz H.O., and Meiwes–Broer K.H., Chem. Phys. Lett., Vol.165, pp.293-296,1990.

[5] Hövel H., Becker Th., Bettac A., Reihl B., Tschudy M. and Williams E.J., J. Appl. Phys., Vol.81, pp. 154–158, 1997.

[6] Mizes H.A. and Foster J.S., Science, Vol.244, pp.559–562, 1989.

[7] Bettac A. , Köller L., Rank V. and Meiwes–Broer K.H., Surf. Sci., in press.

Collision Dynamics of Water Clusters on a Solid Surface: a Molecular Dynamics and Molecular Beam Studies *

Vostrikov A.A.[1,2], Kazakova I.V.[3], Belousov Yu.I.[1],
Dubov D.Yu.[1,2], Zadorozhny A.M.[2], Kazakov V.G.[2]
[1] Institute of Thermophysics, Novosibirsk
[2] Novosibirsk State University, Novosibirsk
[3] Institute of Computational Technologies, Novosibirsk

New results of the investigations of the cluster fragmentation and the ion formation at the neutral water cluster scattering by solid surface are reported. The appearance of the charged particles in a scattered beam of the water clusters was discovered in [1]. Later a series of experimental studies of this phenomenon were carried out, where the following facts were established:

1) The phenomenon was observed begining from the average size $\langle n \rangle \sim 330 \pm 70$ molecules per cluster, at the collision velosity equal to $1 km/s$ and the corresponding energy E_n=0.17·n eV.

2) Scattering by different targets (metals, semiconductors and dielectrics) was studied.

3) The ion current to the target and the reflected ion current depended on the surface material and on the incident angle α between the molecular beam and the normal to surface. The currents increased with the increase of $\langle n \rangle$ and α.

To elucidate the nature and the kinetics of this phenomenon we performed new beam and jet investigations of ion pairs formation and separation using new target's surfaces (carbon in the colloidal graphite form, fullerene C_{60} and ice). For simulating this process a calculation model based on a classical molecular dynamics technique was also elaborated. Clusters formed on the bases of Stillinger polarization model [2]. In this model a water molecule consists of two protons and negative oxygen ion carring two units of charge. The interaction potential consists of two components: one is the sum of potentials for each couple of particles and the other is non-additive potential that takes into account the polarization energy resulting from induced dipole momenta of oxygen particles in the field of other charges and dipoles. The parameters of Stillinger potential adopted in this model give a good description of geometry and bond energy of the isolated water molecule, water dimer and some ions. The cluster formed in the following way:

1) The initial configuration of the oxygen atoms corresponded to the usual ice structure. As for orientation of protons it was taken at random.

2) For getting a stable configuration of the water cluster a procedure of relaxation to a required temperature ($T \sim 80K$) was performed. The temperature of water clusters in the experimental gas-dynamic beam was the same.

The directed movement of cluster was set by adding to each atom a constant velocity vector. A normal and a tangential incidence were simulated. The step of integration was $2 \cdot 10^{-17}$ s. It gives a high precision of integration and a high kinetics resolution. The calculations were carried out for $(H_2O)_n$ clusters having $n = 32$ and 64 molecules and for the impact velocities $v = 1, 3.4$, and 10 km/s. For the normal incidence the interaction potential with the surface was taken purely repulsive: $V_i = C/z^9$, where z is the distance between the atom and the surface. The order of potential was taken according to [3]. The magnitude of C for oxygen atoms adopted was larger than that for hydrogen atoms by a factor of the mass ratio.

The following results were obtained: for cluster with $n = 32$ the ionic dissociation was observed only at $v = 10$ km/s, about 15 % of molecules being dissociated. However, the formed charges recombined, so the rebound particles were neutral. The absence of the charged particles in the scattered beam explained by the impossibility of the formation of the solvated shell around an ion because of a small number of molecules in the cluster. The phenomenon of the charges separation in cluster with $n = 64$ was

*Abstract 6711 submitted to the 21st International Symposium on Rarefied Gas Dynamics, Marseille, France, July 26-31, 1998

observed at all of the investigated velocities. In this sense the calculations corresponded to the experimental data. At the tangential collision the total capture of the first layer of the water cluster was assumed (the mass velocity of the first layer was taken to be equal to a zero). It provided the fast fragmentation of the cluster and the ejection of the charged particles. A charges scattering pattern had a lobe structure already at the 1 km/s velocity, in a good accordance with the experiment. It was interesting to observe the excitation of the internal degrees of freedom of molecules in the compressed layer of the cluster, the dissipation of energy during the process of dissociative ionization and solvatation in time.

The report will present the detailed analysis of the kinetic of the following processes: the cluster fragmentation, the dissociation of molecules, the ionization and separation of charged cluster ions in the scatterad beam.

References

[1] Vostrikov A.A., Dubov D.Yu., Predtechenskii M.R., *Chem. Phys. Lett.* **139, 124 (1987)**

[2] Stillinger F.H., David C.W., *J. Chem. Phys.* **69, 1473 (1978)**

[3] Barantsev R.G.,*Interaction of Rarefied Gases With Surfaces. Moscow; Nauka 1975*

INVESTIGATION OF FULLERENE THIN FILMS DEPOSITED WITH HELP OF SUPERSONIC MOLECULAR BEAM OF He.*

M.A.Khodorkovski, A.L.Shakhmin, S.V.Murashov, V.Yu.Davydov, Yu.A. Golod, A.M. Alexeev, T.O.Artamonova.

Institute of Applied Chemistry, Dobrolubova 14, St.Petersburg, 197198, Russia

The investigations of thin fullerene films deposited with the help of helium supersonic molecular beam seeded with neutral C_{60} molecules are presented. The peculiarity of the seeded molecular beam formation is in the passing-through the cell with fullerene vapor the impulse supersonic beam of helium formed by nozzle source [1]. For film deposition the axial part of the beam separated by skimmer is utilized.

Kinetic energy of fullerene molecules in the beam was changed in the range of 0.8-1.2 eV by varying parameters of nozzle source. The density of fullerene molecules in supersonic molecular beam permitted us to deposit films of 200-300 nm thickness during one hour exposition.

The obtained supersonic molecular beam deposited (SMBD) films were investigated using different methods of solid state analysis. This reveals that their properties differing greatly from the ones of the films deposited by usual thermal deposition (TD) method [2], in which the kinetic energy of fullerene molecules is much less and is determined by a temperature of an oven (400-450°C).

The binding energy of adsorbed molecules with the surface and intermolecular one in many respects is determined by energy parameters of interacting molecules [3]. It can be expect that within SMBD films the binding energy between C_{60} molecules will exceed the corresponding energy in TD films.

The simplest experimental confirmation of this assumption is the results of thermo-desorption experiments (TDS), which show, that the temperature of evaporation of C_{60} molecules from SMBD films is ~500°C, whereas the one for TD films never exceed 350°C. The obtained data permit to estimate the activation energy for the desorption processes. For SMBD films this energy is 0.5 eV higer than for TD films.

So evident modification of intermolecular binding energy within SMBD film can be explained in terms of polymer structure formation. The Raman spectroscopy data of mentioned structures in fullerene objects formed by HPHT techniques are presented in [4] in detail.

Our Raman spectroscopy investigation of SMBD films show that:

a) Only nonpolymerized phase of fullerene (pristine C_{60}) with characteristic frequency 1469 cm^{-1} was observed at low power density (up to 15.0 mW/mm^2) of probing laser radiation (488 nm);
b) At power density of laser radiation increase, the transformation of pristine C_{60} mode to linear polymers of O-type [4] was observed for SMBD films (Fig.1), whereas the pristine C_{60} mode in TD
a) films transformed to photopolymers [5,6]. It should be mentioned, that usually O-polymers (the intermolecular distance up to 9.1-9.2 Å) are observed in experiments utilizing very high pressure (4.8 GPa and more). Whereas the intermolecular distance in pristine C60 is near 10Å [4].

Fullerene molecules in SMBD films did not degraded right up to the power density of laser radiation of 85.0 W/mm^2., while C_{60} molecules in TD film destroyed into amorphous carbon at power density of laser radiation not more then 1.0 W/mm^2. Stability of SMBD films against laser

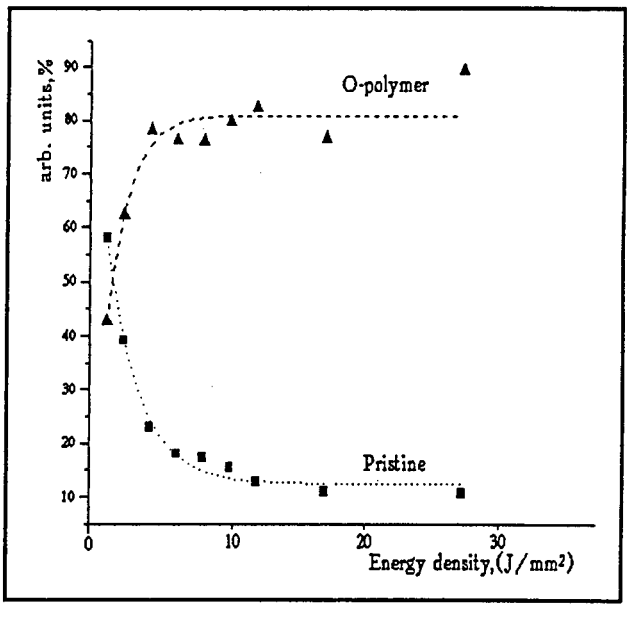

Fig.1 The dependence of pristine C_{60} and O-type polymer mode for SMBD film vs energy density of laser radiation.

* Abstract 7086 submitted to the 21st International Symposium on Rarefied Gas Dynamics, Marseille, France, July 26-31, 1998

radiation also have been confirmed during experiments on time-of-flight mass-spectroscopy with laser desorption. This made it possible to obtain mass-spectra of fullerene accumulating 100 and more probing laser impulses in one point of SMBD film, while TD film have been evaporated after 3-4 laser impulses of the same power.

As it is evident from the presented above results of TDS and Raman spectroscopy investigations, C_{60} molecules in SMBD films exist in nonpolymerised state notwithstanding the greater intermolecular binding energy comparatively to TD films.

The increasing of binding energy between neighboring molecules can also influence on the efficiency of excitation of valance electron density oscillations (π-plasmons), which can be evidently observed on spectra of Electron Energy Losses spectroscopy.

Analysis of spectra of energy losses of photoelectrons after C1s line, during X-ray photoelectron spectroscopy (XPS) investigation of fullerene films, showed that the spectrum feature corresponding to the energy losses with excitation of π-plasmon (6.1eV) have evidently smaller intensity for SMBD films in comparison with TD films (Fig.2). At the same time the electron structure of valance band obtained by XPS practically did not differ from one another.

On the base of the results of conducted investigations the following conclusion can be made. The intermolecular binding energy in SMBD fullerene films is greater than the one in traditional TD films. Intermolecular distance in SMBD films is close to the intermolecular distance in O-polymers. Formation of such a structure of SMBD films is possible due to overcoming the surface energy barrier by C_{60} molecules with relatively high kinetic energy (~1.0 eV). Formation of such a dense ensemble of C_{60} molecules in TD films is impossible as since the kinetic energy of deposited molecules is much less .

Acknolegments: The authors thank E.E.B. Campbell for help in TDS investigations and useful discussions. The work was supported by State Science-Technical program «Actual Directions in the Condensed Matter Physics», direction «Fullerenes and Atomic Clusters», grant No. 95066.

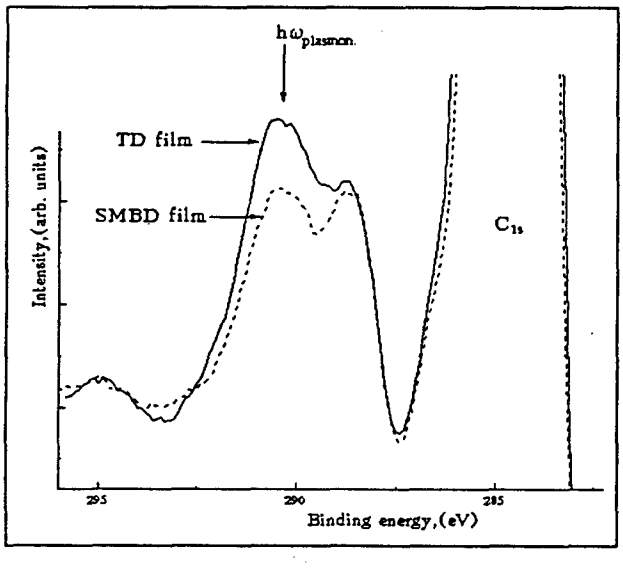

Fig. 2. Energy losses of photoelectrons after C1s line for SMBD and TD films.

References.

[1] Khodorkovski A.M. et al., Pis'ma v Zn. Tekh. Fiz, Vol.24, No10, pp.20-23, 1998 (in Russian).

[2] Prawer S. et al., Phys.Rev. B, Vol.52, No2, pp.841-849, 1995.

[3] Girard Ch. et al., Phys.Rev. B., Vol.49, No.16, pp.11425-11432, 1994.

[4] Rao A.M. et al., Phys.Rev. B, Vol.55, No.7, pp 4766-4773, 1997.

[5] Wang Y. et al., Chem.Phys.Letters., Vol.211, No4,5 pp.341-345, 1993.

[6] Akselrod L. et al, Chem.Phys.Letters., Vol.215, No1,2,3, pp.131-136, 1993

MOLECULAR BEAM SESSION MB 4

Structure and Relaxation in Molecular Free Jets,
Spectroscopy in Cold Molecular Beams

CHAIR: E.L. Knuth (UCLA)

ROOM: LAVOISIER
WEDNESDAY, JULY 29, 1998
9:05 - 10:55

Raman Studies of Free Jet Expansion *

S. Montero, B. Maté, G. Tejeda, J. M. Fernández, and A. Ramos
Instituto de Estructura de la Materia, CSIC.
Serrano 121, 28006 Madrid, Spain

Introduction

The potential of Raman spectroscopy as a diagnostics tool for rarefied gas dynamics has been recognized long ago [1-3]. Practical applications have been scarce, however. The intrinsic small cross section of the Raman process and the low density proper of free jet expansions have posed severe limitations until recently.

A new generation of light detectors based on charge coupled devices (CCD's), and improvements derived from computer assisted spectrometers, have lead to a sensitivity gain of two orders of magnitude [4]. Good quality Raman spectra from highly rarefied media can now be recorded routinely. In addition, expansion chambers specifically devised for Raman spectroscopy allow for three-dimensional probing of the expanding flow field [5].

The physical properties of a supersonic jet differ markedly from those of a gas under equilibrium conditions. Too, these properties depend strongly on the stagnation pressure and temperature, on the size and shape of the nozzle, on the residual pressure, and on the composition of the expanded gas. Hence, for most applications a diagnostics of the jet should be carried out in order to determine its local properties: Molecular density number, vibrational, rotational and translational temperatures, flow velocity, aggregation state, and geometrical configuration of confining shock front structures. As will be shown in the present contribution, the mentioned properties can be quantified by means of linear Raman spectroscopy, with some advantages over other diagnostic techniques used so far.

Quantitative Measurements

As primary data, Raman spectroscopy can provide absolute local density of any molecular species in the jet in the range

$$10^{14} < \mathcal{N} < 10^{20} \text{ molecules/cm}^3,$$

with accuracy on the order of 10 %. Rotational temperatures can be measured for several important species (N_2, O_2, H_2, CO_2, H_2O, CO, NH_3, light hydrocarbons,...) in a wide range of tempertures with accuracy to about 5 %. For most polyatomic molecules the population of some vibrational levels can be monitored along the expansion with fairly good accuracy. Combining these Raman data by means of the conservation principles of mass, momentum, and energy, information can be obtained about flow velocity, translational temperature, and condensation energy released in the jet [6].

Raman Mapping

A spatial resolution of few microns in a flowfield from $\approx$0.2 D (D = *nozzle diameter*) to $\approx$100 D along the jet, and $\approx$50 D across it, covering a wide range of temperatures and densities, allows Raman spectroscopy mapping jets with accuracy. A sample map of rotational temperatures in a jet of CO_2 is shown in Fig. 1. The map was generated with the data from 2200 Raman spectra recorded in a grid of points covering the flow field. Temperatures in barrell shock and in normal shock fronts, non-Boltzmannian regions of the jet, have been interpolated to allow for the visualization of the flow field.

*Abstract 7016 submitted to the 21st International Symposium on Rarefied Gas Dynamics, Marseille, France, July 26-31, 1998

Shock Fronts

At the shock fronts the actual distribution of rotational temperatures is bimodal. Jointly with the absolute densities this distribution contains a wealth of information about the collisional processes across these boundary regions. In particular, the gradual conversion of the set of *cold* molecules impinging onto the shock front, into the set of rethermalized *warm* molecules, can be tracked in space and time by means of Raman spectroscopy.

Non–isentropic Flow

The isentropic model for a perfect gas is an approximation widely utilized to characterize a free jet. However, to a major or lesser degree, real gases tend to depart from this model. This is caused by condensation, and by the contribution of the vibrational degrees of freedom. Both alter the energy balance in the jet and, consequently, the remaining physical properties. Vibrational cooling starts from the beginning of the expansion, and condensation a few nozzle diameters ahead. Both effects depend markedly on the stagnation pressure. So, the general properties of a real gas jet are conditioned along the first nozzle diameters of the expansion, a region not too accessible for most diagnostic techniques. Raman data presented here illustrate in detail these processes.

Summary

Several examples related to the aforementioned topics will be presented with the aim of showing to what extent, and under which experimental conditions, Raman spectroscopy is a mature diagnostics tool to investigate laboratory scale free jets at a quantitative level.

References

[1] I. F. Silvera and F. Tommasini, Phys. Rev. Lett. **37**, 136 (1976).

[2] G. Luijks, S. Stolte, and J. Reuss. Chem. Phys. **62**, 217 (1981).

[3] J. W. L Lewis. 16*th RGD*, Progress in Astronautics and Aeronautics **117**. 107 (1989).

[4] G. Tejeda, J. M. Fernández-Sánchez, and S. Montero, Appl. Spectrosc. **51**, 265 (1997).

[5] G. Tejeda, B. Maté, J. M. Fernández-Sánchez, and S. Montero, Phys. Rev. Lett. **76**, 34 (1996).

[6] B. Maté, G. Tejeda, and S. Montero. J. Chem. Phys. **108**, 2676 (1998).

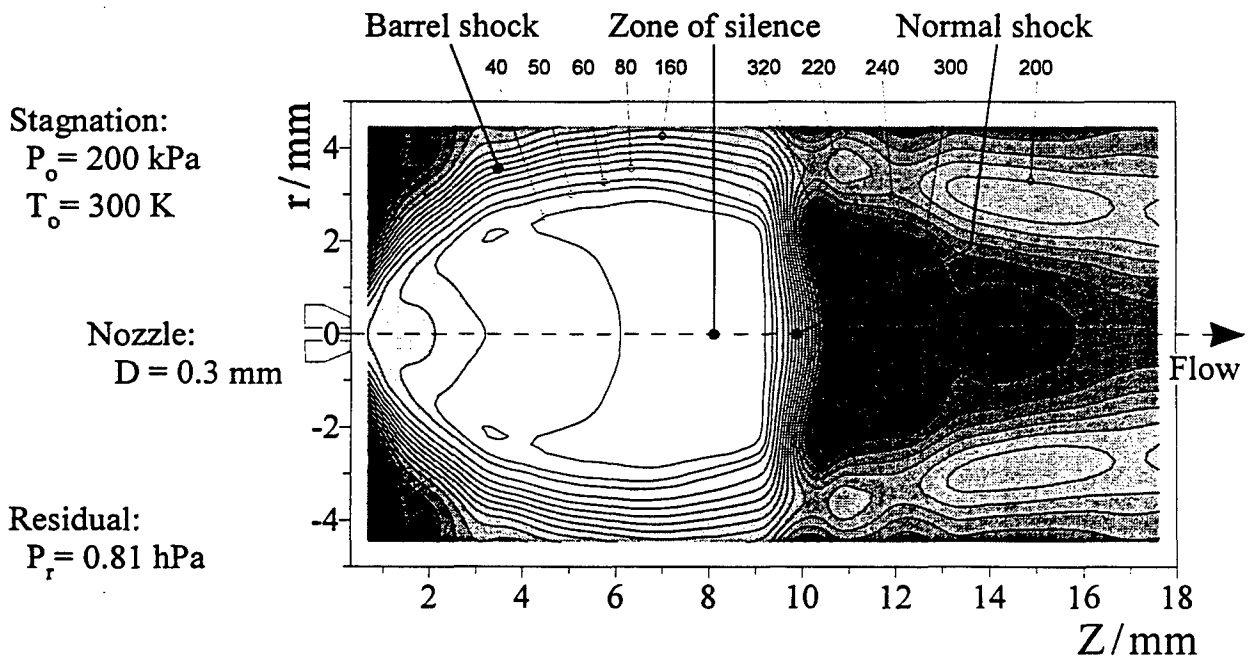

Fig. 1: Rotational temperature map of a supersonic jet of CO_2, in Kelvin.

Nonequilibrium distributions of rotational energies in a free-jet. *

H. Hulsman and J. Rozema
Physics Department, UIA, University of Antwerpen,
B-2610 Wilrijk, Belgium

In a supersonic free jet the expanding gas cools very fast. As a result, the distribution of molecules among the rotational and vibrational levels develops a non-equilibrium character. We have studied the evolution of the internal state distribution along the axis of the expansion for K_2 molecules seeded in argon. These experiments are an extension of earlier work on Na_2 seeded in argon under comparable conditions [1]. A large range of rovibrational levels of K_2 is thermally populated. Results are presented for a selection of these. The measurements extend from the nozzle exit down to a distance where the distribution is essentially *'frozen'*.

In the experiment we use a single-frequency laser to excite K_2 molecules from a single rovibrational level of the ground state. The intensity of the resulting fluorescence is measured as a function of the position of the laser beam in the jet. This has been done for a selection of rovibrational levels. The evolutions of the relative intensities as functions of the distance to the nozzle exit prove to be different for the various levels (fig. 1). In the first part of the expansion, the flow is expected to be near equilibrium. The local temperatures are fairly well known in this region. So, the internal state distribution at the first position of the experiment (at a distance of 0.22 nozzle diameters from the nozzle exit) is known. Consequently, the measured ratios of the *intensities* at other distances can be used to obtain the ratios of the *occupations* of the levels at these positions (fig. 2). We find that these distributions are Boltzmann distributions in the first few positions in the jet (fig. 3). The characteristic temperatures prove to be very close to the calculated values of the local translational temperatures.

At larger distances, however, appreciable deviations from equilibrium arise. These consist of relative over-populations for levels with higher internal energies. In figure 3 the occupations are shown as functions of the rotational energy for levels with $v = 0$ at different distances from the nozzle. One observes that the lower lines, which are those for larger distances become more and more curved. In such picture a Boltzmann distribution corresponds to a straight line with the slope $= -1/T_{rot}$. If one tries to associate a rotational temperature with the *average* slope of a distribution which is not a straight line, one introduces an uncertainty ΔT_{rot}. This reflects the arbitrary choice of the levels which had been included in the fit. In our data this uncertainty ΔT_{rot} proves to be remarkably large.

On the other hand, the distributions of fig. 3 can be

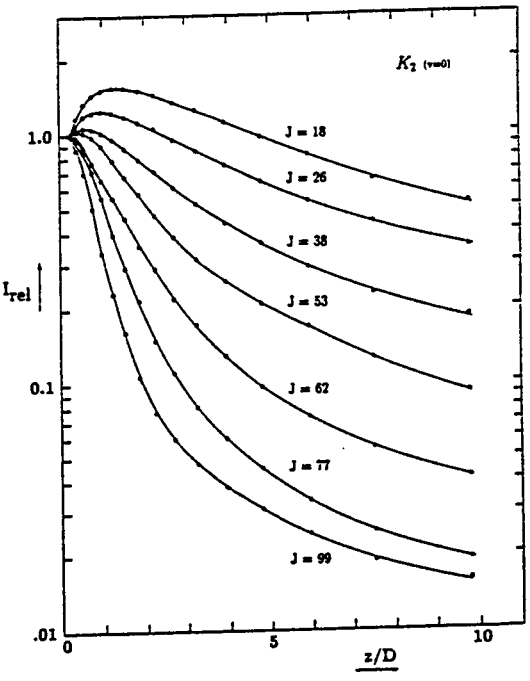

Figure 1: Reduced fluorescence intensities as functions of z/D, the reduced distance from the nozzle exit to the laser beam. Results are for transitions from various rovibrational levels of the electronic ground state of K_2. The stagnation conditions are: T_0 = 713 K, p_0 = 1778 Pa. The K_2 molecules are only some .15% of the gas. The expansion mainly consists of argon (about 80%). The rest is atomic potassium vapour.

*Abstract 2641 submitted to the 21st International Symposium on Rarefied Gas Dynamics, Marseille, France, July 26-31, 1998

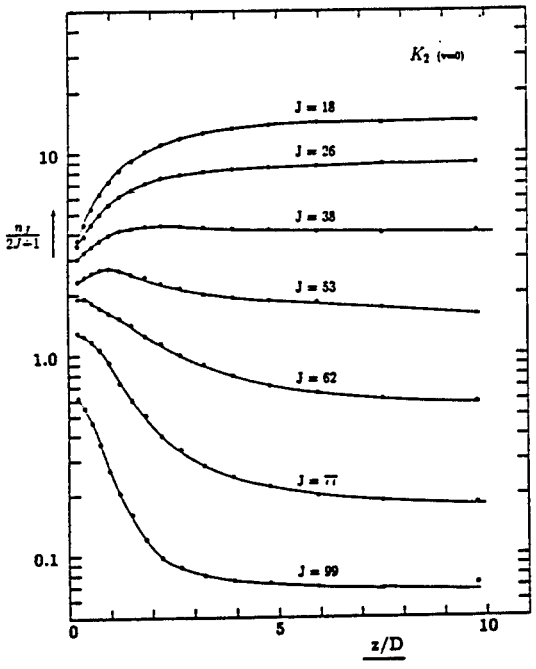

Figure 2: The occupations of various rotational levels along the axis of the expansion as functions of the reduced distance to the nozzle exit.

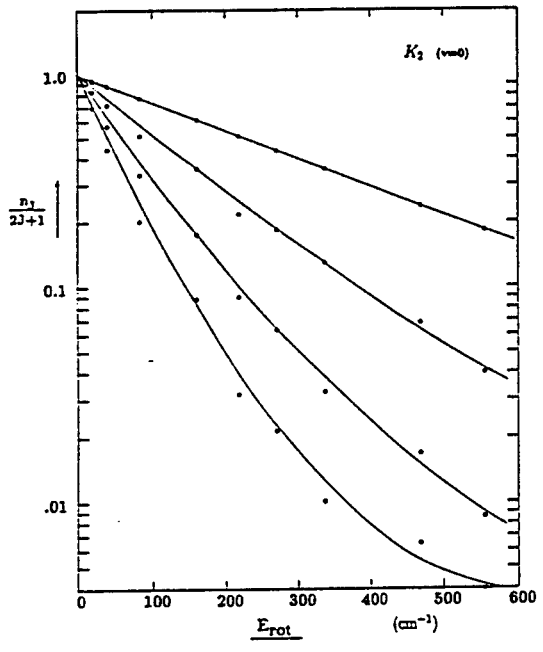

Figure 3: Normalized plots, showing the occupation of rotational levels divided by the statistical weight as functions of the rotational energy for various distances from the nozzle; $z/D = 0.22$, $z/D = 0.98$, $z/D = 2.24$ and $z/D = 9.80$

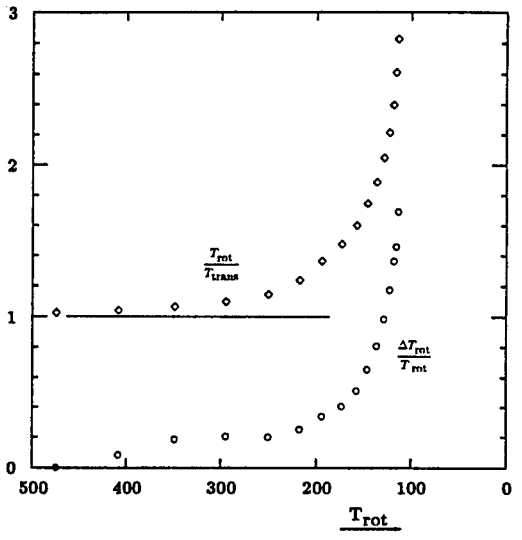

Figure 4: The experimental effective rotational temperature T_{rot} (= the average rotational energy divided by the Boltzmann constant) divided by the calculated translational temperature T_{trans} *vs* T_{rot} and the uncertainty of the fitted rotational temperature ΔT_{rot} over T_{rot} *vs* T_{rot}.

used to determine the average rotational energy of the K_2 molecules as a function of the position. This corresponds to the determination of the effective rotational temperature $T_{rot} = (E_{rot})_{average}/k_B$. The evolution of this T_{rot} may be compared with calculated values for the translational temperature. It may also be compared to results of calculations using the heat-conduction model.

In figure 4 the ratio T_{rot}/T_{trans} is shown as a function of T_{rot}. For comparison the relative uncertainty $\Delta T_{rot}/T_{rot}$ has also been plotted vs T_{rot}. One sees, that the deviations from the equilibrium distribution are present as soon as the energies of the internal degrees of freedom begin deviating from the equilibrium values. THerefore one may question the usefullness of the rotational temperature for the description of the internal state distribution in a jet.

References

[1] Hulsman H., *Nonequilibrium distributions of rotational and vibrational energies in a free-jet expansion*, Chem. Phys., Vol.217, pp.107–114, 1997.

The low temperature vibrational relaxation of OH in the $X^2\Pi$ and $A^2\Sigma$ states in an Argon free jet Presentation of Abstracts Submitted to the 21st International Symposium on Rarefied Gas Dynamics *

Michael M. Ahern[1], Mark A. Smith[1]
[1] Department of Chemistry, University of Arizona, Tucson, Arizona USA

1 Introduction

The OH radical is a key intermediate in a wide range of environments from low temperature planetary atmospheres to high temperature combustion processes. The understanding of both the chemistry and energy transfer processes of this radical over a wide range of temperatures is thus of great importance. In this study we have measured, under single collision conditions, integral and state-to-state absolute reaction rate coefficients for vibrational and rotational inelastic collisions of OH in the $A^2\Sigma$ and the $X^2\Pi$ states with Ar. This data, when combined with high temperature results [1] [2] provides insight into the mechanism for the various relaxation pathways. In particular, the behavior of vibrational relaxation in the 0 K limit, clearly shows a tendency towards the collision limit as has been seen in other free jet relaxation studies. [3]

2 Experimental

The experimental apparatus is similar to that used by this laboratory for numerous free jet collision studies of ions, radicals, and molecules. [4] In this study, radicals were generated in a pulsed free jet expansion by cold cathode discharge between an electrode plate (orifice diameter equal to 10 nozzle diameters) placed 3 nozzle diameters downstream and the nozzle orifice body. The flow gas consisted of between 0.1 and 1

3 Results and Discussion

An example dispersed LIF spectrum of the OH radical is shown in Figure 1. From analysis of similar spectra, considering a wide range of transitions, the absolute rate coefficients for the relaxation events are obtained and are given in Table 1.

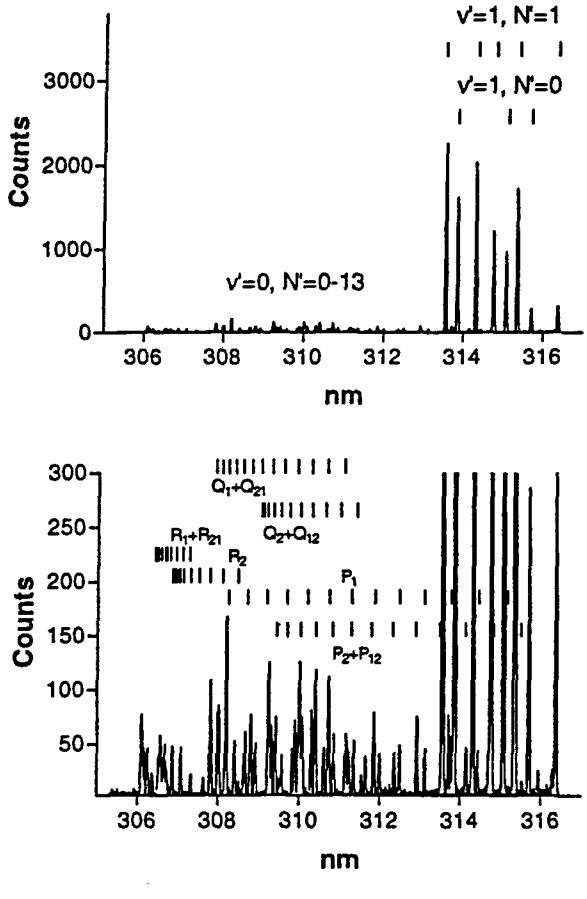

Figure 1. Dispersed LIF spectrum obtained by pumping the A-X (0-1) Q_1+Q_{21} N"=0 line producing initial population only in the A (v'=1, N'=1) state. The upper figure shows rotational redistri-

*Abstract 6932 submitted to the 21st International Symposium on Rarefied Gas Dynamics, Marseille, France, July 26-31, 1998

ing initial population only in the A (v'=1, N'=1) state. During the fluorescence lifetime of this state, the molecule undergoes on average less than one collision, but some population is transferred into both v'=1, N'=0 via rotational relaxation, as well as v'=0 N'=0 to 13, via vibrational relaxation. From the relative line strengths in comparison to the unrelaxed lines, absolute relaxation rate coefficients or cross sections are obtained applicable to the 5 K collisional environment within the free jet core.
All rates are observed to increase at low temperature. Of particular note, is the dramatic increase in the vibrational relaxation in the low temperature limit. At 300 K, OH X state is not observed to relax in an Ar buffer. The A state is observed to undergo slow vibrational relaxation at 300 K. At the near 5 K temperatures of the free jet, vibrational relaxation in the A state is observed to approach the collision limit. The rates of rotational and vibrational relaxation in the A state become comparable in this limit. This behavior is consistent with a long-lived collision complex mechanism for vibrational relaxation whereby vibrational predissociation of the collision becomes competitive with elastic separation as the temperature is lowered and the collision lifetime increases. The various features of such a mechanism and the relevance to a variety of other chemical processes at low temperatures will be discussed.

Table 1: Relaxation rate coefficients for OH $A^2\Sigma$ (v',N') with Ar.

	$k_{300}(10^{-11} cm^3\ s^{-1})$	$k_{5K}(10^{-11} cm^3\ s^{-1})$ *This work*
Rotational Relaxation		
v'=2 N'=2		20 ±4
v'=2 N'=1		13 ±4.5
v'=1 N'=2		11 ±2
v'=1 N'=1		6.7 ±1
v'=0 N'=2	N'→N'-1 6.0 ±1.0	N'→N'-1 12 ±2
	N'→N'-2 3.8 ±0.4	N'→N'-2 6.0 ±1
v'=0 N'=1		6.6 ±1
Vibrational Relaxation		
v'(2→1), N'=1		25 ±5
v'(2→1), N'=0		20 ±5
v'(1→0), N'=1	0.29 ±0.03	3.3 ±0.6
v'(1→0), N'=0		3.0 ±1.0

References

[1] Lengel, R.K., and Croseley D.R., Chem. Phys. Lett., Vol. 32, p. 261, 1975

[2] Jorg, A., Meier U., and Kohse-Hoinghaus, J. Chem. Phys., Vol. 93, p. 6453, 1990.

[3] Hawley M. and Smith M.A., J. Chem. Phys., Vol. 95, p. 8662, 1992.

[4] Smith M.A., International Reviews in Physical Chemistry, Vol. 17, no. 1, 1998.

Thermodynamic Properties of Argon Vapour in a Rarefied Flow at the Onset of Homogeneous Nucleation. *

P. Pal
Royal Holloway, University of London, Egham Hill,
Egham, Surrey TW20 0EX, ENGLAND

1 Introduction

This study focuses on the investigation of macroscopic behaviour of Argon vapour using a purely statistical mechanical treatment on its microscopic systems. At the onset of nucleation, the monomers of the vapour combine to form clusters of different shapes and sizes. The thermodynamic behaviour of the clusters is modelled by computing the canonical averages of their Helmholtz free energy using the well known Monte-Carlo (MC) technique.
The configurational component of the energy of an n -atom cluster was systematically evaluated using the additive property of the Lennard-Jones interaction potential in the size range $3 \leq n \leq 110$.

2 Methods

The initial configurations of the clusters in the chosen size range, were simulated by relaxing their constituent atoms under the Lennard-Jones interaction potential. The equilibration process generated a set of non- crystalline clusters with high stability and spherical symmetry. In the range $3 \leq n \leq 13$, the equilibrium configurations assumed recognisable shapes (e.g. Equilateral triangle for $n = 3$, Tetrahedron for $n = 4$, Trigonal bipyramid for $n = 5$, Pentagonal bipyramid for $n = 7$) leading to the one complete shell icosahedron for $n = 13$. Then the icosahedral growth scheme continued until it reached the two closed shell stage at $n = 55$, generating further intermediate structures of high symmetry at $n = 19$, 37, 43, and 49. Subsequent clusters were generated for up to $n = 115$, based on this scheme.
These equilibrated clusters were treated as the statically stable set at $T = 0$°K. By taking this set as the starting configuration, the thermodynamic behaviour at $T > 0$°K was investigated using the MC simulation.

T°K / n	13	55	110
10	-0.78	-5.2	-9.5
30	-0.82	-5.3	-10.6
50	-0.93	-5.8	-11.8
60	-1.18	-6.1	-12.7

Table 1: $\langle A(n,T)\rangle \times 10^{12}$ ergs of selected argon clusters

The simulation was performed using the Metropolis algorithm in which a Markov chain of states was set up for each cluster as a sequence of random walks representing the movement of its constituent atoms at a temperature T.
Based on this process, the potential energy surface for the clusters was explored generating a set of Boltzmann weighted configurational energies. By calculating the canonical average of this set of energies, the configurational component of the free energy was determined for a range of temperatures. Inherent in the averaging process was the objective of finding the thermodynamically stable clusters at a particular temperature T. Using the statically stable set of spherical symmetry as the initial configuration, the exploration of the energy surface became consistently efficient in the MC simulation.
Using the canonical averaging, suitable thermodynamic and structural parameters of these clusters were evaluated as part of the investigation of their thermodynamic behaviour.
In this context, the key parameter is the Free energy $\langle A(n,T)\rangle$ as a function of T, which is given by

$$\langle A(n,T)\rangle = \langle V\rangle + K$$

where V is the configuration energy and K is the kinetic energy. The $\langle A(n,T)\rangle$ values of a selection of clusters are given in Table 1.
The structural changes of the clusters as a function of T were examined by monitoring the pair separa-

*Abstract 5656 submitted to the 21st International Symposium on Rarefied Gas Dynamics, Marseille, France, July 26-31, 1998

tions of the constituent atoms from snapshots during the random walk process and computing the related Moment of Inertia matrix.
In addition, the radial distribution functions $g(r)$ of the clusters were calculated as a function of T, in order to investigate their transition to the liquid-like behaviour.
From the knowledge of the thermally averaged Helmholtz free energy of an ensemble, the next step was to evaluate the Gibbs free energy of formation of clusters on a purely statistical mechanical basis. The Gibbs free energy of formation of an n -atom cluster at a temperature T amounts to the reversible work involved in forming the cluster in the supersaturated vapour[1] and includes the intrinsic pressure and volume of the cluster.
By considering the supersaturated vapour in a free flow system as a mixture of ideal gases comprising monomeric and n -meric components, the Gibbs free energy of formation $\Delta G(n,T,P)$ may be expressed in a recognisable form which is given by

$$\Delta G(n,T,P) = \Delta G^{\circ}(n,T) + (1-n)kT \ln P$$

where $\Delta G^{\circ}(n,T)$ is the energy of formation at standard atmospheric pressure. The free energies of formation of clusters were calculated for a wide range of temperatures and pressures, from which the Gibbs free energy profile as a function of n was constructed. Each free energy propfile showed a typical maximum analogous to the classical liquid drop model. All the calculations were performed without invoking any bulk property.
The size of the cluster at the ΔG maximum represents the critical nucleus corresponding to the particular P and T. A plot of the trajectory of the P and T values at the ΔG maxima forms the well known Wilson zone. These values signify the appropriate external thermodynamic conditions in which nucleation may be expected.

3 Results

Different aspects of the results lend themselves for a range of comparisons. The following comparisons are reported here.

- Comparison of the $\langle A(n,T) \rangle$ values with Molecular Dynamics[2], Self-Consistent Phonon[3] and other MC[4] results and of the $\Delta G(n,T,P)$ values with [2].
- Comparison of the P, T values at the $\Delta G(n,T,P)$ maxima with the results [5] of a series of experiments on Argon nucleation at Yale University.

4 Conclusion

- By applying one of the well-tried simulation methods (MC) the present study has developed a comprehensive Gibbs free energy of formation treatment based on statistical mechanics for Argon clusters in the microscopic size range. This may be treated as the atomistic analogue of the classical liquid drop model.
- The treatment also brings successful confluence of the theory with experiments on Argon nucleation.

References

[1] Reiss H., Tabazadeh A. and Talbot J. , *J of Chem Phys, Vol 92, No 2, pp1266, 1990*

[2] McGinty D.J., *J. of Chem Phys, Vol 58, No 11 , 1973*

[3] Etters R, D, Kanney l., Gillis N. and Kaelberer J., *Phys Rev B, Vol 15, No 8, 1977*

[4] Lee J., Barker J.A. and Abraham F., *J. of Chem Phys, Vol 58, pp3166,1973*

[5] Wu J. C., Wegener P. P. and Stein G., *J. of Chem. Phys., Vol 69, No 4, pp78, 1978*

Electronic Spectroscopy of Cold Polycyclic Aromatic Cations in a Molecular Beam *

Philippe Bréchignac , Thomas Pino

Laboratoire de Photophysique Moléculaire, CNRS
Université Paris-Sud, Bât 210, F91405 Orsay Cedex, France

1 Introduction

Polycyclic Aromatic Hydrocarbons (PAHs) have been suggested to be present in the interstellar medium (ISM) since back to 1985. Since they could play an important role in this astrophysical environment many experimental and theoretical studies [1] have been developed to improve the understanding of the photophysics of such molecules in the ISM. Our work aims at the development of spectroscopic methods to obtain visible spectra of PAH cations and radicals in conditions close to the ISM conditions, i.e. cold and isolated. Such spectra are needed to test the suggestion that these species could be the carriers [2,3] of some of the diffuse interstellar bands (DIBs), which are observed throughout the visible spectrum and remain today after 50 years from their first discovery the longest-standing mystery of astrophysical spectroscopy.

2 Principle of the experiment

We have set up an experiment devoted to the search for the electronic spectra of gas phase cold PAH cations in the visible. Making large quantities of cold cations in the gas phase in order to measure absorption directly is very difficult. The principle of the technique we used consists to induce a fragmentation of the cation consecutive to the resonant absorption of laser photons, so that the change in the charge-to-mass ratio can be detected in a mass spectrometer. However it is well known that because of their stability PAHs (neutrals as well as cations) need a fairly large excitation energy before they begin to fragment on a reasonable timescale. This usually requires several laser photons, which means high laser flux, and then a number of experimental difficulties associated to saturation effects, power broadening, non resonant absorption and problems to control the number of photons involved in the process.

We have then used a trick, consisting to attach an argon atom to the PAH by forming van der Waals complexes in a molecular beam. This complex is photoionised by resonant two-photon absorption in the near UV. Then the binding energy of the complex cation is so small (about 500 cm-1) that it will fragment for every single photon absorbed. The use of two pulsed lasers of different colours in the ionisation step allows to control exactly the total energy, and to produce complexes which are cold both rotationally and vibrationally.

The technique has been tested first on a benzene derivative, the 4-fluorostyrene, and found to work. It was then applied to a larger aromatic hydrocarbon, the fluorene molecule C_{13} H_{10}. The technique works as follows. Monitoring the time-of-flight spectrum of fluorene$^+$ and its van der Waals complexes the wavelength of the first UV photon is tuned to optimise the formation of a given complex : the fluorene$^+$-Ar_2 for instance (see Figure). Some signal can be seen at the mass of the Fl^+-Ar complex, and a larger peak at the mass of Fl^+ since neutral fluorene is much more abundant but its cations are not formed

* Abstract 6943 submitted to the 21st International Symposium on Rarefied Gas Dynamics, Marseille, France, July 26-31,1998

efficiently. The pulsed visible laser inducing absorption by the cation is delayed with respect to the ionising lasers, so that the Fl^+ fragment produced by ejection of the two argon atoms appears separated in time from the rest of the Fl^+ ions.

3 Results

The spectrum is then obtained by monitoring the ion signal in the time window relative to this fragment while the laser wavelength is scanned. A spectrum is obtained similarly after optimisation of the Fl^+-Ar signal. They both exhibit an electronic origin at 628 nm, and several vibronic transitions. Two low-frequency vibrations of the fluorene skeleton can be recognized near 200 and 400 cm^{-1}.

The recording of these spectra required a relatively small energy (of the order of a few microjoules per pulse) for the visible laser, since it corresponds to a single photon process. On the contrary the recording of a spectrum, after optimisation of the Fl^+ signal, and adjusting the time window on the channels associated to the main fragment of the free ion, i.e. the ion formed by the loss of a single H atom, required a laser energy about two orders of magnitude larger. As a consequence the spectrum looks broader and presents less structure. Thus we should be in a case of lifetime broadening, as a result of intramolecular dynamics effects. The fact that both argon atoms are ejected from the Fl^+-Ar_2 is an indication that an ultrafast electronic internal conversion within the fluorene$^+$ moiety may have preceded the step of vibrational predissociation of the complex. Of course the technique gives access to the spectra of the van der Waals complexes rather than of the PAHs cations. But by using the van der Waals shift additivity rule, known to be obeyed by these aromatic clusters[4], one can easily recover the spectrum of PAH^+ from the spectra of PAH^+-Ar and PAH^+-Ar_2. In conclusion we hope that the production of electronic spectra for other gas phase PAHs cations will help to progress in the testing of their suggestion as DIBs carriers.

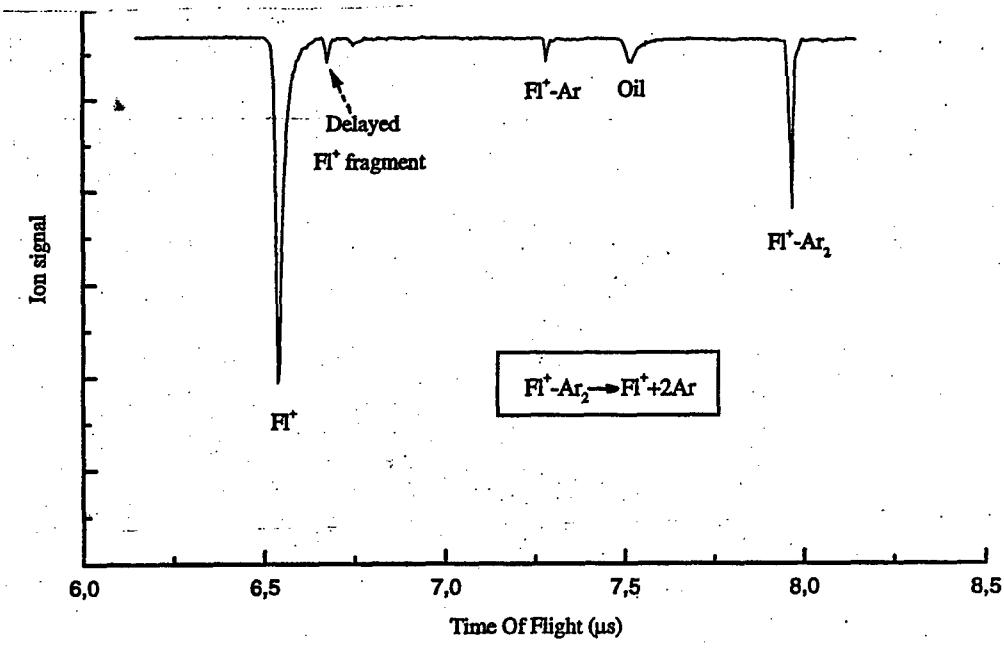

References

[1] A.Léger, L.d'Hendecourt and N.Boccara (eds) : 1987, Polycyclic Aromatic Hydrocarbons and Astrophysics, Reidel, Dordrecht.
[2] A.Léger and L.d'Hendecourt, Astron. Astrophys. 146, 81-85 (1985).
[3] G.P.van der Zwet and L.J.Allamandola, Astron. Astrophys. 146, 76-80 (1985).
[4] P. Hermine, P. Parneix, B. Coutant, F.G. Amar and Ph. Bréchignac, Z. für Physik D **22**, 529 (1992)

The Ultrafast Products Tree

Whatever your ultrafast laser requirements, you can pick a solution from our complete family of integrated, high-quality ultrafast products. Starting with the Tsunami, you can leverage your investment and grow your capabilities to meet your ever-changing needs. What's more, every solution is all-solid-state with the new Millennia pump sources. And they're all available now at Spectra-Physics, the solid-state laser company.

Call: 1-800-SPL-LASER (1-800-775-5273) E-mail: sales@splasers.com Web: www.splasers.com

Spectra-Physics

Spectra-Physics Lasers

Quanta-Ray®

Spectroscopy With MOPO.

Photoacoustics

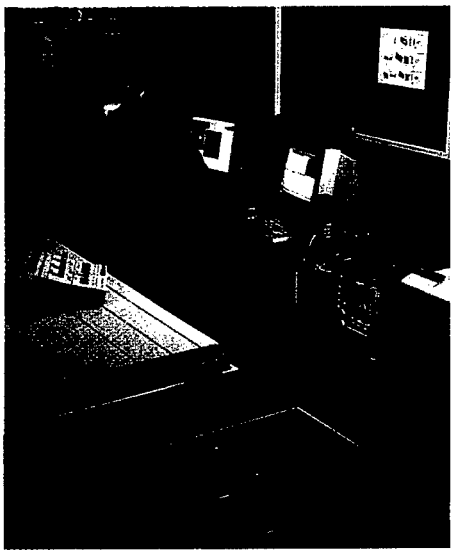

Dr. Doug Hunter uses MOPO to monitor a range of radioactive contaminants.

Broadly tunable high energy pulses with no need to change optics or dyes are some of the reasons why spectroscopists choose our MOPO-700 series optical parametric oscillators. Researchers tell us that the wavelength range, ease of tuning, and MOPO's superb performance help to enhance their results. We've worked hard to ensure that our customers get the performance we promise; for example OPO's require very stable energy and beam pointing from the pump laser, so our GCR series Nd:YAG lasers are designed specifically to meet these needs. Push your spectroscopy to new frontiers with MOPO, the world's only fully proven, state-of-the-art OPO. For more information call your Spectra-Physics sales engineer.

Photoluminescence

Prof. Chris Summers uses MOPO in the race to develop high definition emissive displays.

CARS

Prof. Peter Chen uses MOPO's signal and idler to improve phase matching by an order of magnitude.

MOPO tunability, only from

Spectra-Physics
Spectra-Physics Lasers

Spectra-Physics S.A. • **FRANCE** • Phone (33) 01 69 18 63 10 • Fax (33) 01 69 07 60 93

Lyon Office • Phone (33) 04 74 94 43 77 • Fax (33) 04 74 95 50 78

Web : http://www.spectra-physics.com

MOLECULAR BEAM SESSION MB 5

Atomic and Molecular Optics

CHAIR: W.C. Stwalley (Connecticut)

ROOM: LAVOISIER
WEDNESDAY, JULY 29, 1998
11:10 - 12:30

Optics and Interfrometry with Atoms and Molecules *

Jörg Schmiedmayer
Institut für Experimentalphysik, Universität Innsbruck

Experiments which investigate the wave character of the quantum motion of massive particles, especially interferometry experiments with matter waves have had a significant impact on our understanding of the fundamental principles of physics. Experiments with electron interferometers and neutron interferometers have provided demonstrations of many fundamental aspects of quantum theory [1].

Recently, experiments with matter waves have been greatly expanded by atom and molecular optics and the experimental realization of atom and molecular interferometers [2]. A variety of optical elements for atoms/molecules were proposed and realized in the last five years. These include, among others, diffraction from standing light waves, diffraction from nanofabricated structures, Fresnel lenses and lenses using a standing light wave, and beam splitters using Raman transitions, and adiabatic passage or the magneto-optic potential. An atom interferometer was patented in 1973 [3] and shortly afterwards several papers discussed the close similarity between multiple pulse laser spectroscopy and atom interferometers [4]. About half a dozen experiments that demonstrate atom interferometers have been performed. A good overview of the present status of atom optics and atom interferometry is given in [2].

In this talk I will give an overview of our own recent work in optics and interferometry with atoms and molecules at MIT [5] and in Innsbruck [6].

One of the main tools for these experiments are free standing transmission gratings constructed by nanofabrication techniques. Using these gratings we studied diffraction of atoms and molecules [8] and used the diffraction data to study the atomic and molecular sodium in this beam, building a mass spectrometer for neutral particles. Furthermore we investigated near field diffraction and interference by studying the atomic Talbot effect [9].

Using three of our nanofabricated gratings we have constructed an interferometer for atoms and molecules [7, 8] in which the two interfering portions of each particle's wavefunction are spatially separated and physically isolated by passing the arms if the interferometer on opposite sides of a stretched metal foil, $10\,cm$ long and $10\,\mu m$ thick. This has allowed us to develop general techniques for atom interferometry with separated beams which allow us to perform measurements on single states with spectroscopic precision.

We have performed several experiments probing interactions that shift the phase or energy of the ground state with better than 1% absolute accuracy. We have determined the coherence length of our beam, and developed a technique in which the contrast of the interference signal oscillates in proportion to the difference of the Zeeman interaction with a magnetic field applied differentially to the two sides of the interferometer [11]. We have made an accurate determination of the electric polarizability of the ground state of sodium [12] and measured both the attenuation and the phase shift (that is, both the imaginary and real parts of the index of refraction) of atomic sodium and molecular Na_2 matter waves in atomic and molecular gases [13].

Furthermore, we have used the possibility of scattering single photons from an atom to investigate the effect of a measurement on a coherently split, and spatially separated, atomic deBroglie wave [10]. We observed the decrease of the contrast of the atomic interference pattern (decrease of single particle coherence) with the increasing separation of the atomic deBroglie waves. In addition we could demonstrate that the lost single particle coherence can be recovered when one reduces the possible final states of the scattered photon. Finally we used our interferometer to test the applicability of atom interferometry as a high sensitivity inertial sensor [14].

In our atom optics work at Innsbruck [6] we focused on the fact that atoms interact strongly with electromagnetic fields which can be very precisely engineered using laser technology, diffractive optics and holography. The interaction between a light field and a two level atom with an additional decay

*Abstract 7036 submitted to the 21st International Symposium on Rarefied Gas Dynamics, Marseille, France, July 26-31, 1998

channel of the excited state to a third non interacting state, can be described by the complex optical potential [15]:

$$U(x,y) = \frac{1}{\hbar}\frac{(dE(x,y))^2}{\Delta + i\gamma/2}. \quad (1)$$

Here $E(x,y)$ is the electric field connected to the light, d is the dipole matrix element of the transition, Δ represents the difference between the light frequency and the resonance frequency of the transition, and γ is the loss rate from the excited level to the non interacting state. In matter wave optics any potential is equivalent to a complex index of refraction $n \simeq 1 - \frac{U}{2E_{kin}}$ for the propagating matter wave (with the kinetic energy E_{kin}). Hence any light field structure can be regarded as a complex refractive index structure like a hologram for atomic deBroglie waves. One can, in principle, build many different desirable structures in the laboratory. By changing the intensity and the frequency of the laser light one can change the interaction between the object and the atom at will, so that one may consider (a) very weak, elastic interactions such as those in dynamical diffraction, (b) very strong interactions as in channeling and (c) those interactions which are dominated by dissipative processes using onresonant light.

We performed our atom optics experiments using a metastable argon beam. We built a three-grating Mach-Zehnder deBroglie wave atom interferometer based on diffraction at standing light waves [16] and used classical ray atom optics to build a three grating Moiré imaging device [17]. We could show that this classical device is a very sensitive inertial sensor, capable even of surpassing present day commercial sensors. These two experiments demonstrate nicely the similarities between the classical Moiré apparatus and the quantum apparatus, the interferometer.

Recently we started investigate the coherent motion of atomic deBroglie waves in periodic structures made of light, which we call *"light crystals"*. Starting from the similar and well developed fields of dynamical diffraction in neutron, electron and x-ray physics, we investigated the atomic wavefields inside the light crystal in detail and demonstrated some basic effects like anomalous transmission [18] or a violation of Friedels law [19]. In addition we used the possibility to switch the light crystals quickly and at will to investigate time dependent matter wave optics [20].

Overall optics and interferometry with atoms and molecules became a mature field with many techniques and tools available for fundamental and applied experiments, especially in atomic and molecular physics.

References

[1] for an overview see: *Matter Wave Interferometry* Ed.: G. Badurek, H. Rauch and A. Zeilinger, Physica **B151**, (1988)

[2] for an overview see: *Atom Interferometry* Ed.: P.Berman, Academic Press (1997)

[3] S. Altschuler, L.M. Franz, (1973). US Patent Number 3,761,721

[4] V.P. Chebotayev, B.Y. Dubetsky, A.P. Kasantsev, V.P. Yakovlev, J. Opt. Soc. Am **B 2**, 1791 (1985); Ch. J. Bordé, Phys.Lett. **A140**, 10 (1989)

[5] J. Schmiedmayer *et al.* in ref [2] p.1-84

[6] H. Batelaan *et al.* in ref [2] p.85-119

[7] D. Keith, C. Ekstrom, Q. Turchette, and D. Pritchard , Phys.Rev.Lett. **66**, 2693 (1991)

[8] M. Chapman *et al.* Phys.Rev.Lett. **74**, 4783 (1995)

[9] M. Chapman *et al.* Phys.Rev. **A51**, R14 (1995)

[10] M. Chapman *et al.* Phys.Rev.Lett. **75**, 3783 (1995)

[11] J. Schmiedmayer *et al.* J.Phys. II **4**, 2029 (1994)

[12] C. Ekstrom *et al.* Phys.Rev. **A51**, 3883 (1995)

[13] J. Schmiedmayer *et al.* Phys.Rev.Lett. **74**, 1043 (1995)

[14] A. Lenef *et al.* Phys.Rev.Lett. **78**, 760 (1997)

[15] D.O. Chudesnikov and V.P. Yakovlev, Laser Physics **1**, 110 (1991)

[16] E. Rasel *et al.* Phys.Rev.Lett. **75**, 2633 (1995)

[17] M. Oberthaler *et al.* Phys.Rev. **A 54**, 3165 (1996)

[18] M. Oberthaler *et al.* Phys.Rev.Lett. **77**, 4980 (1996)

[19] C. Keller *et al.* Phys.Rev.Lett. **79**, 3327 (1997)

[20] St. Bernet *et al.* Phys.Rev.Lett. **77**, 5160 (1996)

Some New Effects in Atom Stern-Gerlach Interferometry *

R. Mathevet[1], K. Brodsky[1], F. Perales[1], K. Rubin[2], J. Robert[1], and J. Baudon[1]
[1] Laboratoire de Physique des Lasers (UMR 7538)
Université Paris-Nord, Av. J.B. Clément, 93430-Villetaneuse, France
[2] also at City College, New-York, USA

1 Introduction

The Stern-Gerlach (SG) interferometry is a polarization interferometry, basically like the optical polarization interferometer consisting of a birefringent crystal plate set in between crossed polarizer and analyzer. Any magnetic field plays the role of the birefringent plate and up to now a great deal of static inhomogeneous or pulsed fields had been studied. New investigations include (i) time and space dependent fields moving at atomic velocity (comoving fields), (ii) a double interferometer configuration and (iii) pulsed (non dispersive) Ramsey experiments.

2 Comoving fields with H*(2s) atoms

By using a set of helices of period λ supplied with alternative currents of frequency ν one obtains a transverse magnetic field of the form $B_0 \cos[2\pi(x - ut)/\lambda]\mathbf{y}$, the velocity of which, $u = \lambda\nu$, is easily tuned (by varying ν) to any value below 100 km/s, largely covering the whole distribution of atom velocities [1]. It is easily understood that, for a sufficient number N of periods, the phaseshift $\delta\phi$ is almost zero for all atomic velocities, except the resonant class $v = u$ for which the atom experiences a fixed field. The device is then highly v-sensitive and one can manage to first set the interferometer with orthogonal polarisers and, second, tune the field intensity so that $\delta\phi = \pi$. The device is then a de Broglie wave filter whose finesse equals to N (Fig. 1a). More one can add up currents of different frequencies to superpose such delta-like transmissions and build up any desired dispersion relationship $\delta\phi(v)$. We called "genericity" this ability of comoving fields to create a medium with any dispersion relation. In the end, it must be noticed that the genericity property holds for any comoving refraction index modulation and can be applied also in optics, e. g. to electrooptic modulators.

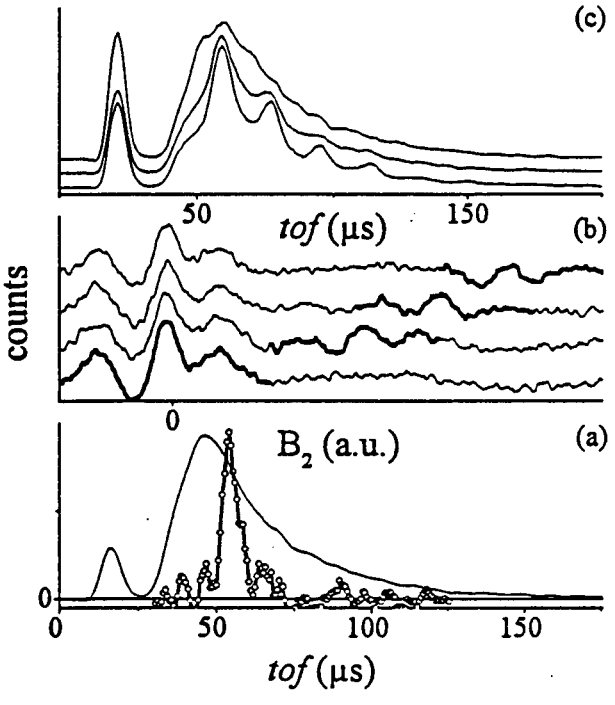

Figure 1: (a) Monochromator, double interferometer, (b) Signal for increasing values of $|B_1|$, (c) Effect of the inner polariser

3 A double interferometer with metastable H*(2s) atoms

With static fields, $\delta\phi$ is simply proportional to the atom-field interaction time and the field magnitude B. So, the interference pattern, as a function of the time-of-flight (tof), is a sine-type modulation of the

*Abstract 6938 submitted to the 21st International Symposium on Rarefied Gas Dynamics, Marseille, France, July 26-31, 1998

roughly Maxwellian incoming *tof*-distribution. On the other hand, as we are using a highly polychromatic source ($\delta v/\bar{v} \simeq 1$), the interference pattern, as a function of B, consists of a central and only two lateral fringes (Fig. 1b). One can then use a first SG interferometer (I_1) as a prepared source for a second one (I_2). Varying B_2 for a fixed B_1, one should observe the convolution of this last pattern by the Fourier transform of the modulation induced on the *tof*-spectrum by B_1, that is three δ-functions, one centred at 0 and two at values proportional to $\pm|B_1|$. Increasing B_1, ones sees these side bands moving away (Fig. 1b). The basic difference between this experiment and a spin-echo one [2] is readily seen by setting $B_1 = -B_1$ and varying the intensity in the intermediate polarizer from zero (spin echo) up to a nominal value for which its operation is complete: no modulation is seen in the first case whereas a super-modulation is observed in the second one (Fig. 1c). It may be noticed that $I_1 + I_2$ makes the two first step of a quantum Zeno effect.

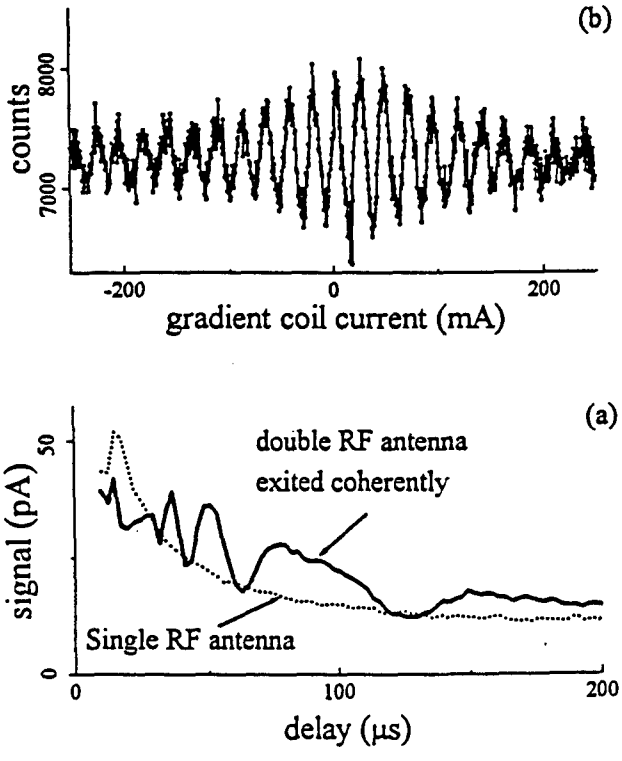

Figure 2: (a) Delay scan with 7 ms duration pulses, (b) B pulse (10 ms) gradient scan

4 Atomic interferometry with a monokinetic potassium beam with chronology control

In the potassium atom interferometer, polarizers are SG magnets, the beam splitters are RF antennas and a magnetic profile of overall amplitude B can be scanned in between. A first set of results present the Ramsey fringes and Rabi oscillations patterns in a pulsed regime where the pulse duration is made smaller than the transit time of the atom within each zone. In order to get time of flight analysis of the beam we have varied the delay between the periodic RF pulses (Fig. 2a). This technique is shown to work even with a slow response time detector. Then we show by controlling the relative delay between pulses of the RF and of the inner magnetic profile B, how it is possible to get an analysis of the overall magnetic profile (Fig. 2b).

References

[1] Mathevet *et al.*, Phys. Rev. A, **56**, 2954 (1997)

[2] De Kieviet *et al.*, Phys. Rev. Lett., **75**, 1919 (1995)

WAVE PACKET INTERFERENCES IN ALKALI ATOMS AND MOLECULES: COHERENT CONTROL AND WAVE PACKET DYNAMICS*

B. Girard, C. Nicole and M. A. Bouchène

Laboratoire Collisions, Agrégats, Réactivité, CNRS UMR 5589, IRSAMC,
Université Paul Sabatier, 118 Rte de Narbonne, 31062 Toulouse Cedex 4, France

Coherent control involves interferences between two (or more) quantum paths. Several schemes involving combinations of lasers at different frequencies have already been demonstrated [1,2]. Here, in temporal coherent control a sequence of two identical time delayed femtosecond pulses is used to create two different excitation paths in an atom or a molecule. Quantum interferences result in a scheme analogous to Ramsey fringes experiments [3,4]. These interferences are scanned by varying the time delay between the two pulses. The interference period is the reciprocal of the excitation frequency.

When the pulses can reach several excited states, each laser pulse creates a wave packet, coherent superposition of these excited states. The two wave packets can interfere when they overlap. The modulation of the interference pattern reveals the motion of this wave packet. An example is represented (Figure 1) in the (4s-4p) transition in potassium atoms, using a 110 fs laser operating at 769 nm. The long range scan was obtained with the low resolution device. Slow oscillations (period of 577 fs) result from beats between interferograms associated with the two excited states. The period is the reciprocal of the energy spacing between the two fine structure. The excited wave packets correspond to a precession of the electronic spin and of the electronic angular momentum around the total angular momentum.

The rapid oscillations (period of 2.6 fs), showed in the insets of the figure, are obtained with a high resolution device. Insets 1a and 1c correspond to short and long time delays respectively. They are associated to the optical interferences (total pulse overlap) and to quantum interferences (no pulse overlap) respectively.

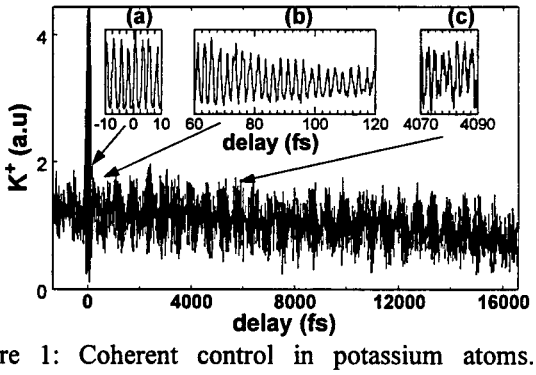

Figure 1: Coherent control in potassium atoms. Excitation of the 4s-4p transition.

It is not possible from the experimental data to distinguish between absorption lines belonging to different quantum systems or corresponding to different initial states of the same quantum system from the case where the absorption lines share the same initial state [5]. Only in this latter case is a wave packet created. We show that by introducing nonlinearities in the interaction, such as a two photon transition, this ambiguity is removed. An example will be given in two photon transitions in cesium atoms [6] where the quantum interferences period is clearly distinguishable from the optical interferences by a factor of two. An other way to

*Abstract 6961 submitted to the 21st International Symposium on Rarefied Gas Dynamics, Marseille, France, July 26-31, 1998.

introduce nonlinearities, is to increase the laser intensity. Then coherent control vanishes because of the ground state depletion. In this case, the second pulse cannot create a second wave packet, but can pump the first wave packet down to the ground state by stimulated emission. This stimulated emission depends on the evolution of the wave packet. It competes with ionisation which is reduced periodically. The ion signal reflects thus directly the wave packet dynamics.

An other way to distinguish quantum interferences from optical interferences without using strong field effect or multi-photon transition is to use chirped pulses. This, allows one to prepare tailored wave packet by induicing an additional dephasing to each frequency component. In our set up, the tailored wave packet is probed by interference with a reference wave packet prepared with a Fourier transform limited pulse. In a preliminary experiment, varying the wavelength around the transition frequency provides a shift of the optical interferences when the quantum interferences occurs for the same delay time.

This scheme of coherent control is extended to potassium and cesium dimers. Femtosecond pulses excitation induce vibrational wave packets. An example is represented in Figure 2, where the experiment is performed in the B state of Cs_2, at 768 nm, with 150 fs pulses [4]. Here, the two identical pulses create a coherent superposition of wave packets in the bound electronic state.

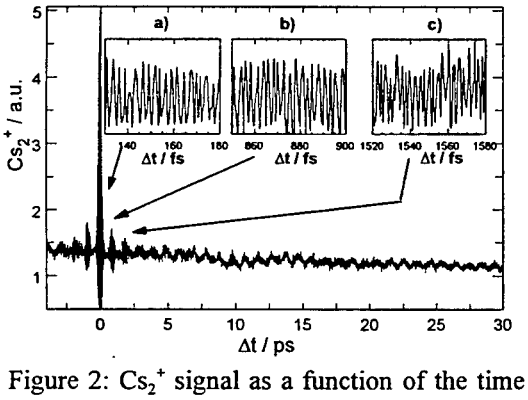

Figure 2: Cs_2^+ signal as a function of the time delay between the two pulses. The low-frequency oscillations (period of ca. 1 ps) correspond to pump-probe contribution reflecting the vibration of the wave packet.

The oscillations of these two wave packets are detected after photoionization of the system. Quantum interferences between them result in a temporal coherent control of the ionisation probability. The interferogram exhibits high-frequency oscillation corresponding to Ramsey fringes (at the Bohr frequency of the transition) modulated by a slow envelope corresponding to vibrational recurrences. It is found that this method is sensitive to the thermal distribution of initial states over rovibrational levels. The experimental "incoherent" averaging over this distribution results in a scrambling of the interferograms [7].

This technique can be used to extract information on the structure of the molecular excited states exactly as with high-resolution Fourier transform spectroscopy. As an interferometric technique, temporal coherent control provides a very sensitive tool to probe perturbations (ac Stark shifts, collision with an atom) which could affect the molecule between the pulses.

References:

[1] C. Chen, Y.-Y. Yin and D. S. Elliott, Phys. Rev. Lett. **64**, 507-10 (1990).

[2] M. Shapiro and P. Brumer, Int. Rev. Phys. Chem. **13**, 187-229 (1994).

[3] N. F. Scherer, A. J. Ruggiero, M. Du and G. R. Fleming, J. Chem. Phys. **93**, 856-857 (1990).

[4] V. Blanchet, M. A. Bouchene, O. Cabrol and B. Girard, Chem. Phys. Lett. **233**, 491-499 (1995).

[5] M. A. Bouchene, V. Blanchet, C. Nicole, N. Melikechi, B. Girard, H. Ruppe, S. Rutz, E. Schreiber and L. Wöste, Eur. Phys. J. D **2**, 131-141 (1998).

[6] V. Blanchet, C. Nicole, M. A. Bouchene and B. Girard, Phys. Rev. Lett. **78**, 2716-9 (1997).

[7] V. Blanchet, M. A. Bouchene and B. Girard, J. Chem. Phys. **108**, 4862-4876 (1998).

MOLECULAR BEAM SESSION MB 6

Exotic Session including Relaxation of Hot Atoms,
Reactivity at Low Temperature,
Structure and Dynamics of Molecules on Surface of Liquid Beam

CHAIR: A.A. Vostrikov (Novosibirsk)

ROOM: LAVOISIER
THURSDAY, JULY 30, 1998
9:05 - 10:55

Relaxation of Electronic Excitation during the Expansion of a Free Jet Generated from a Laser-Sustained Argon-Oxygen Plasma*

A. Lebéhot[1], R. Campargue[1], V. Lago[1], M. Dudeck[1], J. Kurzyna[1]
[1]Laboratoire d'Aérothermique du CNRS, Meudon, France
[2] IPPT-PAN, Academy of Sciences, Warsaw, Poland

1. Introduction

Relaxation phenomena are expected to be rather complicated during the expansion of a free jet generated from a plasma, due to electronic excitation with large number of states, ionization-recombination, dissociation, and radiative decay. These processes are now rather well analysed and understood when the plasma is generated in a pure gas, but the difficulty increases when the gas of interest is a mixture including one diatomic component.

2. Experimental

The apparatus is a free jet and molecular beam generator. A plasma is maintained in the vicinity of the waist of a continuous infrared laser beam, just upstream of the sonic nozzle [1], thanks to the inverse bremsstrahlung process. The gas used is a mixture of 7% oxygen in argon.

The radiation emitted spontaneously in the free jet structure is analysed locally [2]. After inverse Abel transform and geometrical deconvolution of the measured intensity, density maps are obtained for the electronic excited states which radiate spontaneously. This analysis is repeated with four states of argon and four states of atomic oxygen (Table 1).

3. Results

When reported in a Boltzmann diagram, the population densities appear in equilibrium at the nozzle exit, for all states investigated, and each component (argon and atomic oxygen). As the distance from the nozzle throat increases, only the upper levels remain in equilibrium for each species separately (Fig. 1), but the corresponding temperature is much higher for atomic oxygen than for argon (Fig. 2). The physical meaning of such a temperature becomes somewhat questionable. For a pure gas [2], the upper electronic levels can be generally assumed to be in equilibrium with the electron gas, so that the corresponding excitation temperature can be regarded as a good estimate of the free electron temperature [3]. Then, the excitation process is considered as governed prominently by the electron collisions. If such excitation temperatures are very different for the components of a mixture, what type of equilibrium can rule these temperatures? The excitation process can no longer be regarded as exclusively governed by the free electron gas, but also by quenching processes between heavy particles. This is also suggested when comparing the shape of the temperature maps obtained for argon and atomic oxygen. Fig. 3 shows that the local maxima of argon correspond generally to minima of oxygen, and the reverse; such a behaviour cannot be due to direct energy transfer with electrons.

It must be noted that the temperatures obtained for argon may be as low as 2000 K. Obviously, this temperature does not characterize the emission process itself, which should be negligible at such temperature: the detected emission occurs from upper states (which are between them at this low temperature) towards lower states which are much below the 2000 K regression law of the upper levels (see Fig. 1).

4. Conclusion

The measured excitation temperatures of argon and atomic oxygen suggest that the theoretical approach which was carried out for pure argon [2] is no longer valid for the argon-oxygen mixture. This approach assumed that the hydrodynamical behaviour is only coupled to overal energy exchanges while collisional-radiative processes can be treated separately. Also, it was assumed that the leading collisional processes are

* Abstract 3206 submitted to the 21st International Symposium on Rarefied Gas Dynamics, Marseille, France, July 26-31, 1998

the collisions between electrons and heavy particles. It appears that this kind of treatment must be considerably refined for a gas mixture.

Argon		eV	g_i	A_{ij} 10^{-8} s^{-1}
6965 Å	4p'[1/2]	13.33	3	0.067
4300 Å	5p[5/2]	14.51	5	0.00394
4158 Å	5p[3/2]	14.53	5	0.0145
6032 Å	5d[7/2]	15.13	9	0.0246
Oxygen				
7773 Å	^5P	10.74	15	0.34
4368 Å	^3P	12.36	9	0.0066
6455 Å	$^5S^0$	12.66	5	0.071
5330 Å	$^5D^0$	13.07	25	0.0197

Table 1

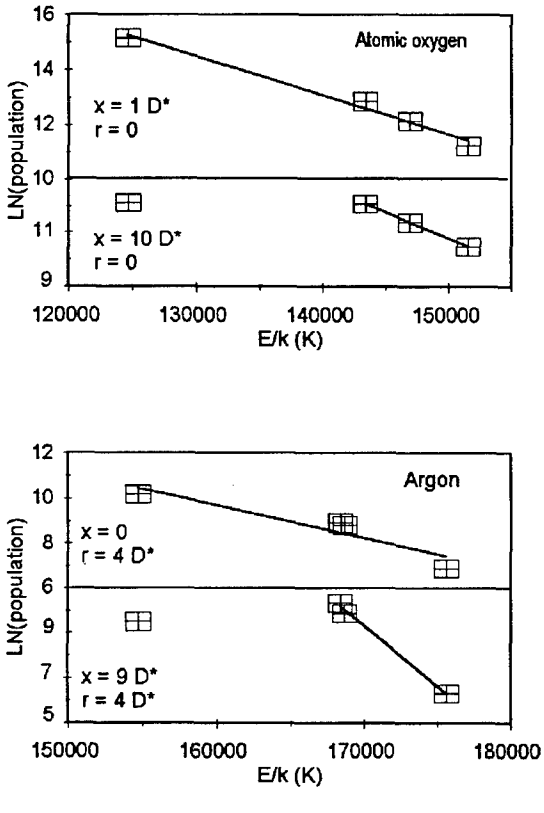

Fig. 1 Boltzmann diagrams for atomic oxygen and argon close to and far from the nozzle throat (diameter D*)

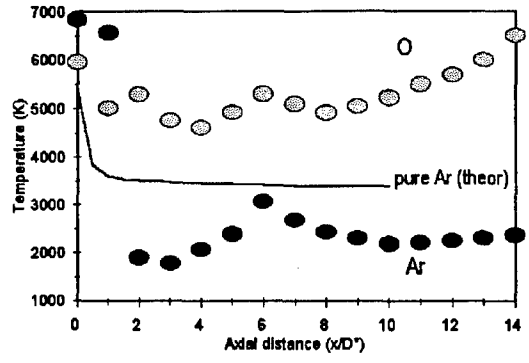

Fig. 2 Axial excitation temperatures as measured for O and Ar in the mixture, compared with the calculated electronic temperature for pure argon in the same conditions

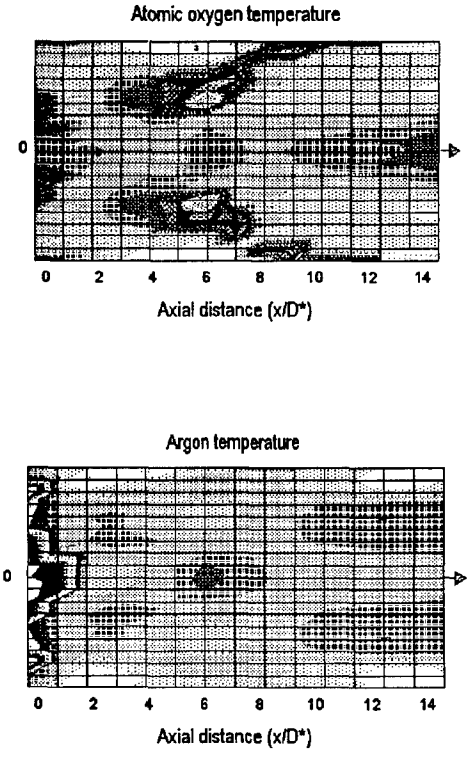

Fig. 3 Contour maps of the excitation temperatures for atomic oxygen and argon

References

[1] J.M. Girard, A. Lebéhot, and R. Campargue, J. Phys. D **26**, 1382 (1993)

[2] A. Lebéhot and R. Campargue, Phys. Plasmas **3**, 2502 (1996)

[3] B. van der Sijde and J.A.M. van der Mullen, J. Quant. Spectrosc. Radiat. Transfer **44**, 39 (1990)

Doppler Profiles of the Distribution of $O(^1D)$ Relaxing in Ne: Comparison of Classical and Quantum Cross Sections *

B. D. Shizgal[1], Y. Matsumi[2]
[1] Department of Chemistry, University of British Columbia, Vancouver, Canada
[2] Solar Terrestrial Environment Laboratory, University of Nagoya, Toyokawa, Japan

1 Introduction

The relaxation of hot atoms in a gaseous moderator remains a fundamental problem in rarefied gas dynamics [1]. The rate of relaxation of energetic particles to equilibrium has important applications in diverse fields. In addition to the calculation and measurement of relaxation times, in recent years there have been numerous measurements of the details of the relaxing velocity distribution functions by Doppler spectroscopy. For example, Park et al [2] have investigated the relaxation of H atoms produced in laser dissociation of H_2S at 193 nm. They measured the Doppler profiles of the H atoms at the Lyman-α line during the relaxation by collisions with the rare gases and some molecular moderators. Nan and Houston [3] monitered the velocity relaxation of $S(^1D)$ by He, Ar and Xe by measuring the Doppler profile of $S(^1D)$ created by pulsed laser photolysis of OCS at 222 nm. Cline et al [4] reported the relaxation of hot $I(^2P_{1/2})$ that was produced from photodissociation of of n-C_3F_7I at 266 nm in a background of He.

The distribution functions of $O(^1D)$ in the terrestrial atmosphere can be strongly non-Maxwellian owing to the production of these atoms by photodissociation of O_2 and O_3. The relaxation dynamics of $O(^1D)$ are important for a chracterization of the chemistry of the upper atmosphere. Matsumi et al [5] studied the velocity relaxation of $O(^1D)$ produced by photodissociation of O_2 with linearly polarized F_2 laser light at 157 nm. The velocity distributions of $O(^1D)$ were determined by Doppler profiles measured by VUV laser-induced fluorescence. They studied the relaxation of the energy as well as the rate of decay of the anisotropy of the distribution function.

The purpose of the present paper is to study theoretically the relaxation of anisotropic distributions of $O(^1D)$ in Ne with accurate quantum mechanical differential elastic scattering cross sections and to compare with both the measurements and the previous Monte-Carlo simulations that employ classical scattering cross sections [5].

2 Theory

We consider a nonequilibrium system of $O(^1D)$, density n, dilutely dispersed in a bath of Ne atoms, denoted by a subscript 1. We assume that the number density $n << n_1$, so that only (Ne,O) collisions need to be considered and the Ne distribution is a Maxwellian at the temperature T, that is $f_1^M(\mathbf{c}) = n_1(m_1/2\pi kT)^{3/2}e^{-m_1c^2/2kT}$. The Boltzmann equation for the time evolution of the $O(^1D)$ velocity distribution function is given by

$$\frac{\partial f}{\partial t} = 2\pi \int\int [f' f_1^{M'} - f f_1^M]\sigma(g,\chi) g d\chi d\mathbf{c}_1 \quad (1)$$

where $\sigma(g,\chi)$ is the differential elastic cross section, $\mathbf{g} = \mathbf{c} - \mathbf{c_1}$ is the relative collision velocity, and χ is the scattering angle in the center of mass frame. The quantities $\mathbf{c}$ and $\mathbf{c}_1$ are the velocities before a collision and $\mathbf{c}'$ and $\mathbf{c}_1'$ are the velocities after a collision.

The (Ne,O) system gives rise to to three different singlet potential curves, $^1\Sigma$, $^1\Pi$ and $^1\Delta$, and the detailed radial dependence is taken from the calculations by Langhoff [6]. The differential scattering cross section is calculated quantum mechanically following standard methods and the contribution from each interaction potential is given by the degeneracies of that state. The differential cross section is finite at zero scattering angle unlike the classical cross section and the small angle cut-off is not necessary [4]. A large fraction of the total cross section arises from integration of the differential cross section at small angles.

The Boltzmann equation can be rewritten in the

*Abstract 2777 submitted to the 21st International Symposium on Rarefied Gas Dynamics, Marseille, France, July 26-31, 1998

form

$$\frac{\partial f(\mathbf{c})}{\partial t} = \int K(\mathbf{c},\mathbf{c}')f(\mathbf{c}')d\mathbf{c}' - Z(c)f(\mathbf{c}) \qquad (2)$$

where the collision frequency is given by $Z(c) = \int K(\mathbf{c},\mathbf{c}')f_1^M(\mathbf{c}')d\mathbf{c}'/f^M(\mathbf{c})$. The kernel, $K(\mathbf{c},\mathbf{c}')$ is well-known [7]. The main objectives, as in the previous work [4], is to determine the time dependent velocity distribution function, the average energy,

$$E_{avg}(t) = \frac{1}{2}m\int f(\mathbf{c},t)c^2 d\mathbf{c} \qquad (3)$$

and the average anisotropy parameter, that is,

$$\beta_{avg}(t) = \int f(\mathbf{c},t)\beta(c,t)d\mathbf{c} \qquad (4)$$

In the analysis of the experimental results, $E_{avg}(t)$ and $\beta_{avg}(t)$ are fitted to single exponential decay curves.

In general, $K(\mathbf{c},\mathbf{c}')$ depends only on the magnitudes of the velocities $\mathbf{c}$ and $\mathbf{c}'$, and $\mu = \cos\theta$, where θ is the angle between $\mathbf{c}$ and $\mathbf{c}'$. We rewrite $K(\mathbf{c},\mathbf{c}')$ as $K(c,c',\mu)$. The $O(^1D)$ distribution function can be written as an expansion in Legendre polynomials, $f(\mathbf{c},t) = \sum_{l=0}^{\infty} f_l(c,t)P_l(\hat{\mu})$, where $\hat{\mu} = \cos\hat{\theta}$ and $\hat{\theta}$ is the polar angle between $\mathbf{c}$ and some fixed axis in velocity space. We can then decompose the kernel $K(\mathbf{c},\mathbf{c}')$ by the ℓth component $K_\ell(c,c')$, where $K_\ell(c,c') = 2\pi\int_{-1}^{+1} c'^2 K(c,c'),\mu)P_\ell(\mu)d\mu$. The μ-integration must be done numerically for all but the simplest cross sections. The Boltzmann equation then reduces to the set of uncoupled differential equations

$$\frac{\partial f_\ell}{\partial t} = \int_0^\infty K_\ell(c,c')f_\ell(c')dc' - Z(c)f_\ell(c). \qquad (5)$$

The initial distribution function in the experimental work is of the form,

$$f(c,\theta) = f(c,t)\left[1+\beta(c,t)P_2(\cos\theta)\right] \qquad (6)$$

where the anistropy parameter is, $\beta(c,0) \leq 2$ [5].

3 NUMERICAL SOLUTION OF THE BOLTZMANN EQUATION

We solve the Boltzmann equation, Eq. (5), numerically using the Quadrature Discretization Method (QDM). This method has been described in detail in other papers [8, 9]. It is convenient to consider reduced speed defined by $x = c/c_0$ where $c_0 = (2kT_s/m_1)^{1/2}$, and T_s is some arbitrary temperature parameter chosen so as to scale the reduced speed appropriately. The basis of the QDM is to use a set of convenient orthogonal polynomials to approximate the distribution function. All quantities are then evaluated at discrete points (the zeros of the N'th order polynomial), and integrals are evaluated using Gaussian quadrature. Here we use the "speed" polynomials, defined as the set of orthogonal polynomials $B_n(x)$ which satisfy $\int_0^\infty w(x)B_n(x)B_m(x)dx = \delta_{nm}$ where $w(x) = x^2e^{-x^2}$. With the change of variable to reduced speed, the integration in the right hand side of Eq. (5) can be performed with a quadrature of the form $\int_0^\infty w(x)g(x)dx \approx \sum_{i=1}^N w_i g(x_i)$ where x_i and w_i are the corresponding quadrature points and weights [10]. In this way, a direct solution of the Boltzmann equation is obtained and the distribution function and associated Doppler profiles are determined. This paper considers in detail a comparison of the use of quantum and classical cross sections.

References

[1] Shizgal, B. and Blackmore, R. Chem. Phys. **77**, 417 (1983).

[2] Park, J., Shafer, N. and Bersohn, R. J. Chem. Phys. **91**, 7861 (1989).

[3] Nan, G. and Houston, P. L. J. Chem. Phys. **97**, 7865 (1992)

[4] Cline, J. I., Taatjes C. A. and Leone S. R., J., Chem. Phys. **93**, 6543 (1990).

[5] Mastsumi, Y., Shamsuddin, S.M,, Y. Sato and M. Kawasaki. J. Chem. Phys. **101**, 9610 (1994).

[6] Langhoff, S. R. J. Chem. Phys. **73**, 2379 (1980).

[7] Kapral R. and Ross J. J. Chem. Phys. **52**, 3, 1238 (1970).

[8] Shizgal B. and Chen H., J. Chem. Phys. **104**, 4137 (1996).

[9] Shizgal B. D., Thoechem-J. Molec. Struc. **391**, 131-139 (1997).

[10] Blackmore R. and Shizgal B., J. Computat. Phys. **55**, 313 (1984).

Optical Emission Spectroscopy of Na Lines in Rarefied Air-Na Plasma Jets *

V. Lago[1], J.Benier[2], W.Röck[1], T.Olivier[1], M. Dudeck[1]
[1]Laboratoire d'Aérothermique du CNRS, Meudon France
[2]CEA /DCRE/SDE/Centre de Bruyères le Châtel, France

Introduction

In the frame of a CEA/CNRS collaboration, the sodium yellow doublet at 588.5 nm has been studied. The purpose was to analyze Na lines in rarefied air jet plasmas, and to calibrate a radiometer, manufactured by CEA by simulating a earth plasma reentry atmosphere in ground facility. In view to observe the sodium doublet, a small amount of sodium was added to the air plasma. Optical measurements of the emitted light were simultaneity observed with the CEA radiometer and the OMA system coupled to a monochromator and the atomic densities of sodium were deduced.

Experimental facility

The Laboratoire d'Aérothermique is equipped with three wind tunnels where low pressure arc jets (0.1 Torr) are generated to simulate the gas surrounding the surface of a vehicle during hypersonic re-entry. Stationary plasma jets are generated by an arc discharge generator. The arc is obtained between the cathode made of copper with a zirconium insert and the nozzle throat used as anode, also made of copper. The air is supplied directly along the cathode with a vortex effect. An injection of carbonate sodium powder was used to observe the sodium lines by optical emission spectroscopy. Carbonate sodium and air were injected together in the purpose to obtained an homogenous mixture.

Plasma parameters have to be known to a better understanding of the radiometer plasma measurements. So two different diagnostics were used in this purpose: optical spectroscopy emission to determine sodium atomic density and electrostatics double probes for the density and electron temperature.

Optical spectroscopy set up consists on a monochromator SOPRA, F of the Ebert-Fastie type, equipped with a 1800lines/mm grating. The intensified OMA detector (Princeton Instruments IRY 1024 scans 8.5 nm wavelength region simultaneously, and it is cooled by a Peltier element, allowing an operating temperature of –35 °C.

The radiometer measures the spectral flux in a specific solid angle. Several interferential filters allow to select the spectral ranges. The method is based on the differential measurement between the continuum (background) and the sodium doublet. The noise level has been reduced by look-in detection in order to detect the small signal.

A telescope is used as the optical head of three bundles of optical fibers: two bundles are connected to the radiometer and the spectrometer. The optical configuration of this set up allows the radiometer and the spectrometer to look at the same area of plasma.

The electrostatic double probes consists of a tungsten wire, 200 μm in diameter and 1 mm in length. The wires are polarized by a floating generator supplying a triangular signal (frequency: 100 Hz, amplitude: ±15V).

Measurements

The plasma conditions were chosen to have the more stable plasma during the measurements: arc current 100 A, static pressure 0.077 Torr and pressure source chamber 232 Torr.

Optical measurements were recorded during 60 s with the OMA and the radiometer at the same frequency (0.5s) [1]. The optical measurement point was located at a distance of 5 cm from the nozzle exit on the plasma axis (r=0 cm). The arc voltage fluctuations were also simultaneously recorded with optical measurements to control the plasma stability. The Figure 1 presents the sodium yellow doublet lines obtained with the OMA. Calculations for the determination of the atomic densities need a local measurement of the sodium emitted intensity, so an

* Abstract 3210 submitted to the 21st International Symposium on Rarefied Gas Dynamics, Marseille, France, July 26-31,1998

Abel inversion have been calculated from a radial sodium emission profile (r = -4 cm up to r = +4 cm).
The double electrostatic probe was inserted in a probe movement during the measurements.

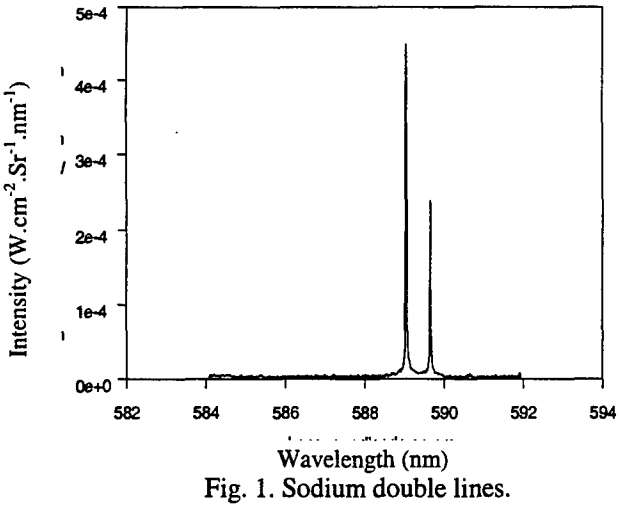

Fig. 1. Sodium double lines.

The radiometer measures the radiance fluctuation of the plasma. Figure 2 presents this evolution during 60 seconds.

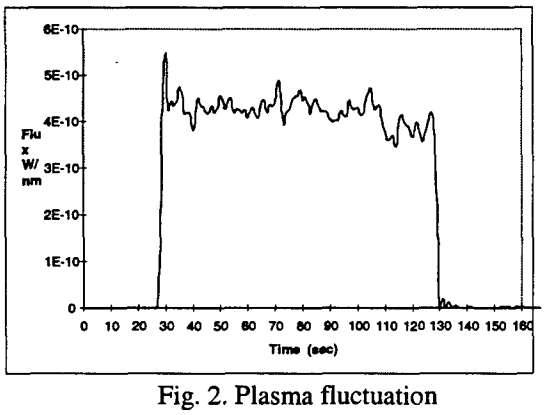

Fig. 2. Plasma fluctuation

Results

Under the assumption that the ground level is at Boltzmann equilibrium, we can consider only the spontaneous emission. So the intensity emission between levels m and n is done by [2]:

$$I_{mn} = N_m A_m x \frac{h\nu_{mn}}{4\pi}$$

Where I_{mn} is the spontaneous emission intensity ($W/m^3.sr$), A_{mn} is the probability emission (sec^{-1}), N_m is the number of emitting atoms, and $h\nu_{mn}$ is the energy between levels m and n (Joules).
Figure 3 presents the radial profiles obtained from each line of the sodium doublet.
The electron temperature and density were determined by applying the non-collisional probe theory. We optimize the experimental double probes characteristics using the algebraic equations proposed by Peterson and Talbot [3]. We obtained a value of 6000 K for the electron temperature and 0.6 10^9 cm^{-3} for the electron density.

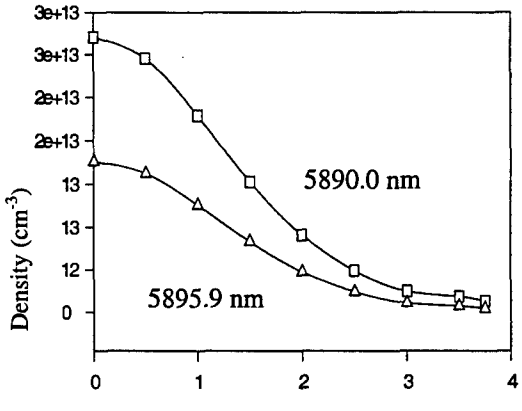

Fig. 3. Radial profile of atomic sodium density.

Acknowledgement

This study has been supported by CEA/DAM.

References

[1] Lago, V., De Graaf, M., Duten, X., Hulin, S., Dudeck, M., "Optical Spectroscopy and Probe Characterization of N_2-CH_4 Plasmas Jets", AIAA 96-2302.
[2] Brode, W. R., "Chemical Spectroscopy", John Wiley & Sans. Inc., June 1958.
[3] Peterson E., Talbot, L., "Collisionless Electrostatics Single-Probe and Double-Probe Measurements", AIAA Journal, Vol. 8, n°12, 1970, 2215-2219.

Recent developments with the uniform supersonic flow (CRESU) technique. *

B.R. Rowe
PALMS UMR 6627, Université de Rennes I, Rennes, FRANCE

1 Astrophysical motivations

One of the most fascinating problems in modern astrophysics is to understand how stars and planets are formed by the gravitational collapse of molecular cloud cores [1]. Molecular clouds are the densest part of the interstellar medium and typical conditions in a dense core are a kinetic temperature of around 10 K and a concentration of molecular hydrogen of 10^4 - 10^5 cm^{-3}. In the collapse of a rotating cloud core, a circumstellar disk is naturally generated in which planets, comets and various objects can be formed by accretion and this process is certainly not restricted to our solar system. If dust is present in various part of the interstellar medium as grains of sub-micron size, its concentration in dense clouds makes them opaque to the harsh UV and visible radiation field of neighbouring stars. With the striking developments of radioastronomy in the last few decades, it is, however, now possible to track the physical conditions prevailing inside these clouds mainly through the rotational spectra (most often in the sub-millimetre and millimetre range) emitted by polar molecules. Spin-orbit state transitions are also widely used and, most recently, infrared observations from space (with the ISO satellite) have yielded a great wealth of new information.
The observations have allowed more than one hundred molecules to be detected in the interstellar medium, and most especially in molecular clouds. Some of these molecules, such as highly unsaturated carbon chains, are quite exotic. This raises the question of their formation in conditions of extremely low temperature and pressure which look at a first glance to be quite unfavourable to molecule formation. Besides this fundamental question of how molecules are formed, it is now understood that the physics and the chemistry of the interstellar medium are highly linked and that the study of the chemistry of molecular clouds is important for our understanding of the process of the evolution of matter in the universe toward the formation of planets and of life. This field of science, which includes the study of the physics and chemistry of dense and diffuse clouds, and of planetary and cometary atmospheres, is now known as "molecular astrophysics" or "astrochemistry".
It is recognised that, in dense clouds, the chemistry is initiated by cosmic ray ionisation followed by a rich variety of processes, either in the gas phase (ion-molecule reactions, dissociative recombination of electrons with molecular ions, radical-molecule reactions) or on the surface of grains. The most recent numerical models of interstellar chemistry [2] now include hundreds of species and thousands of reactions. Such models are highly demanding of laboratory data obtained in the relevant temperature range.

2 Experimental techniques

To design an experiment able to study reaction or relaxation kinetics at a temperature well below that of liquid nitrogen, is a considerable challenge. Since the early 1980's, several experiments have been built for this purpose, most being restricted to the study of ion-molecule reactions, due to the fact that ions can be easily manipulated by electromagnetic fields and detected with a very high efficiency. An example is the cryogenically cooled RF ion trap of Gerlich and co-workers [3]. Such techniques are restricted generally to hydrogen as the molecular reactant at the lowest temperatures, due to heterogeneous condensation of other neutral species onto the walls of the apparatus.
The experimental methods that do not use cryogenic cooling rely on supersonic expansions in rarefied conditions to produce low temperatures, thus avoiding heterogeneous condensation. Merged beam techniques in which the cross section for a process is measured as a function of very low centre-of-mass energy [4], belong to this class of method,

*Abstract 6946 submitted to the 21st International Symposium on Rarefied Gas Dynamics, Marseille, France, July 26-31, 1998

however due to problems of energy resolution, it is very often difficult to obtain reliable rate coefficients at extremely low temperatures from such data. A free jet flow reactor has been used by the group of M. Smith at Tucson to provide extremely interesting results for the kinetics of ion-molecule reactions at temperatures close to zero Kelvin [6]. The first results on ion-molecule reactions down to very low temperatures (8K), however, were obtained by the author and his co-workers in the early 1980's at the Laboratoire d'Aérothermique de Meudon, using the so-called CRESU technique (french acronym for "Cinétique de Réactions en Ecoulements Supersoniques Uniformes" which means "Kinetics of Reactions in Uniform Supersonic Flows").

3 The CRESU technique

The idea behind the CRESU technique was born of the recognition by the author that the uniform supersonic flow obtained at the exit of a Laval nozzle, under rarefied conditions, is an ideal flow reactor in which one could perform chemical physics studies at extremely low temperatures. Such flows have been of course, widely used in rarified wind tunnels for aerodynamic studies [5] but curiously were ignored by the chemical physics community. Using this technique, a large body of data has been obtained on ion-molecule reactions down to 8 K. The technique has now been extended to radical-molecule reactions, relaxation processes and electron attachment reactions. Two apparatuses using steady flows are now in use world-wide, one in Rennes and the other at the University of Birmingham (UK) in the group of I.W.M. Smith [7]. Recently, an interesting extension to the technique which uses uniform supersonic pulsed flows, has been developed by M. Smith [8].

The aim of the presentation at the conference will be to present the technique and to illustrate how it compares to others methods, and especially to the merged beam technique. The most recent results concerning radical-molecule, electron attachment and relaxation processes at very low temperatures will be reviewed. For radical-molecule reactions, (which include reactions of radicals CN, CH, OH, C_2H, Al, Si with various molecules), the results obtained at Rennes and at Birmingham have shown that the rate coefficients for such reactions, very often increase strongly when the temperature decreases. As an example figure 1 shows the variation of the rate coefficient for the reaction of aluminium atoms with oxygen O_2 as a function of temperature. This has shed new light on the cold chemistry of space and modellers have now been forced to include neutral chemistry, to a much larger extent, in their models.

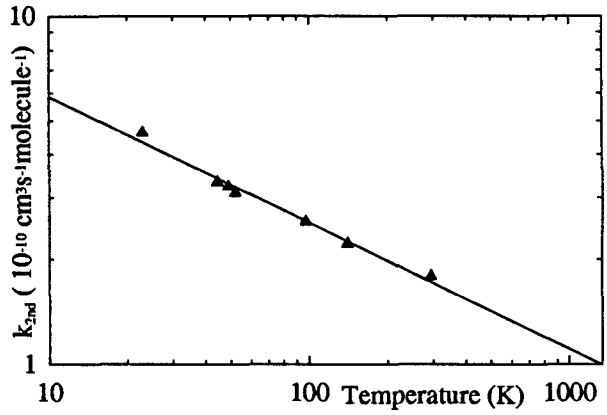

Figure 1: Rate coefficient for the reaction Al + O_2 as a function of temperature. Results are fitted using: $k(T) = 1.72 \times 10^{-10}(T/298)^{-0.36} cm^3 s^{-1}$

References

[1] Lewis J.S., *Cosmic abundances Matter*, AIP conference proceedings 183, p 17, 1989.

[2] Lee H.H., Bettens R.P.A. and Herbst E. , Astron. Astrophys. Suppl. Ser. 119, 111-114, 1996.

[3] Gerlich D. and Horning S., Chem. Rev. 92, 1509, 1992.

[4] Gerlich D. XII Int. Symp. on Mol. Beams, ed. Aquilanti V. Perugia, p 37, 1989.

[5] Owen J.M. and Sherman F.S., University of California, Technical Report HE 150-104, 1952.

[6] Hawley M., Mazely T.L., Randemiya L.K., Smith R.S., Zeng X.K. and Smith M., Int. J. Mass. Spectrom. Ion. Proc. 80, 239, 1990.

[7] Chastaing D., James P.L., Sims I.R. and Smith I.W.M., J. Chem. Soc. Faraday Trans II, in press.

[8] Atkinson D.B. and Smith M., Rev. Sci. Instr., 66, 4434, 1995.

Electronic Structure and Dynamics of Solute Molecule on Solution Surface by Use of Liquid Beam Multiphoton Ionization Mass Spectrometry *

T. Kondow, F. Mafuné
Cluster Research Laboratory, Toyota Technological Institute:
in Genesis Research Institute, 717-86 Futamata, Ichikawa
Chiba 272-0001, Japan

1 Introduction

Upon introduction of a liquid through a tiny aperture (ca. 20μm in diameter) into vacuum, a continuous laminar liquid flow is formed in it, if the Raynolds number of the flow is within a proper range. This flow is named as liquid beam [1-3]. The liquid beam provides us an unique opportunity to investigate the structure and dynamics of molecules on a liquid surface, since sensitive spectroscopic techniques successfully applied for the studies of molecules in the gas phase can be employed to detect and characterize the species from the liquid surface at a molecule level.

In this connection, we have developed a technique of a liquid beam. The surface of the liquid beam was irradiated with an ultraviolet laser with a nano- and femto-second pulse width, and ions and electrons liberated from the liquid surface are observed. In a single-color configuration, ions produced by multiphoton ionization of a surface molecule carries information on the solvation structures and the reactions induced by the ionization [4]. In a pump-probe two-color configuration, finer information such as ionization potential and relaxation of a surface molecule in an excited state are obtained. The kinetic energy of the photoelectrons is measured for obtaining information on the electronic structure of the molecule [5].

In this report, we present our recent studies on the electronic structure of a solute molecule on a liquid solution surface by use of the liquid beam multiphoton ionization mass spectrometry (LBMPIMS) in a pump-probe configuration (see Figure 1), and on the reaction dynamics involving solvated electrons produced by photoabsorption in a single-color configuration.

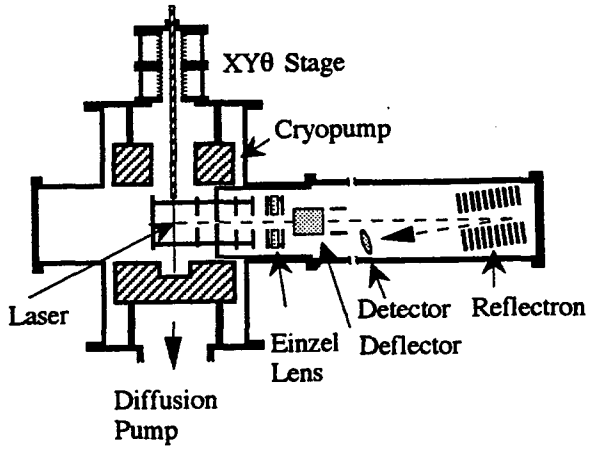

Figure 1: Schematic diagram of LBMPIMS apparatus

2 Ionization potential of a solute molecule on a solution surface.

A propanol solution of aniline was introduced into vacuum as a liquid beam and was exposed to laser in a pump-probe configuration: The first photon promote a solute aniline molecule on the sur-

*Abstract 7051 submitted to the 21st International Symposium on Rarefied Gas Dynamics, Marseille, France, July 26-31, 1998

face to the first excited state and the second photon with a variable delay time from the first one brings further the excited molecule into an ionization continuum. The solute ion accompanying solvent propanol molecules is ejected by Coulomb repulsion force exerted from neighboring ions on the solution surface. The ionization potential of a solute aniline molecule on the surface of the propanol solution was obtained to be 7.7 eV as the threshold energy determined by measuring the intensity variation of the solute and its cluster ions with the energy of the total photons involved in the ionization. In the determination of the threshold energy, the ion intensity is assumed to vary quadratically with the photon energy with respect to the threshold energy. The relaxation time for the $S_1 \rightarrow S_0$ transition of the solute molecule on the solution surface was measured to be 7.8 ± 2 ns by monitoring the intensity variation of the relevant ions with the pump-probe delay time. These findings are interpreted as that the solute molecule is incompletely solvated on the solution surface and is oriented in the direction so as to weaken greatly the hydrogen bonding between the NH_2 group of the solute molecule and an OH group of a solvent molecule.

3 Reaction dynamics involving solvated electrons.

In the LBMPIMS measurement of an NaI-ethanol (EtOH) solution in a single-color configuration, Na^+ is liberated from the surface as a result of photoexcitaion of the counter ion, I^-, into I and a solvated electron, e_s. Above the threshold laser power, Na^+ is ejected by accompanying EtOH and NaI molecules located in the vicinity of Na^+, as a cluster ion, $Na^+(NaI)_n\ (EtOH)_m$ as shown in Figure 2. In some cases, e_s recombines with I to resume I^- and the excess energy resulting from the recombination is released to the solution. The temperature rise due to the excitation-recombination cycles causes to rise the temperature of the ejecting cluster ions. A further analysis of the product ions containing NaI reveals that NaI aggregates are formed on the solution surface because of higher surface concentration of NaI and incomplete solvation of the surface.

In an ethanol solution of an iodide of a divalent cation, such as CaI_2, a dissociative charge splitting takes place in addition to reactions involving solvated electrons as is the case of an alcohol solution of NaI. Under laser irradiation, a bare divalent cation, Ca^{2+}, generated as a result of photoexcited electron release from I^- reacts with a neighboring ethanol molecule, EtOH, as

$$Ca^{2+} + EtOH \rightarrow CaOEt^+ + H^+ \qquad (1)$$

Each ion produced by reaction (1) is ejected with bringing neighboring solute and solvent molecules into vacuum.

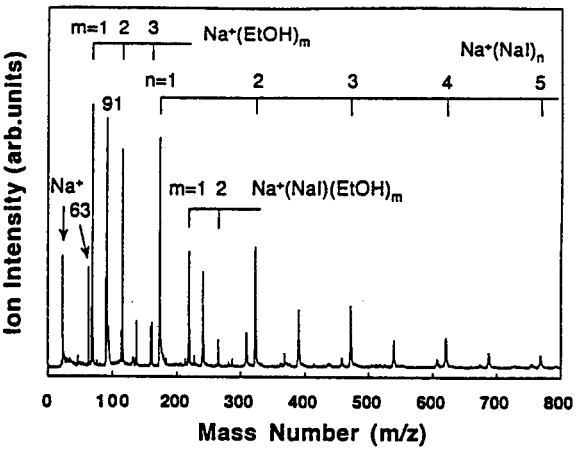

Figure 2: Mass spectrum of the ions produced from a 0.5 M NaI solution in ethanol under irradiation of a 220 nm laser.

The liquid beam technique will be applied in a variety of fields in a future.

References

[1] Mafuné F., Takeda Y., Nagata, T., Kondow T., *Chem. Phys. Lett.*, **199**, 615, 1992.

[2] Faubel M., Schlemmer S., Toennies J. P., *Z. Phys. D*, **10**, 269, 1988.

[3] Sobott F., Klinekofort W., Brutschy B., *Anal. Chem.*, **69**, 3587, 1997.

[4] Mafuné F., Hashimoto Y., Hashimoto M., Kondow T., *J. Phys. Chem.*, **99**, 13814, 1995.

[5] Faubel M., Steiner B., Toennies J. P., *J. Chem. PHys.*, **106**, 9013, 1997.

MOLECULAR BEAM SESSION MB 7

Crossed Molecular Beam Scattering

CHAIR: V. Aquilanti (Perugia)

ROOM: LAVOISIER
THURSDAY, JULY 30, 1998
11:15 - 12:30

New Directions in Reactive Scattering *

A. G. Suits, M. Ahmed, D. S. Peterka, N. Hemmi
Chemical Sciences Division, Berkeley National Laboratory
Berkeley CA 94720 USA

1 Introduction

Crossed molecular beam scattering remains the most powerful means of probing fundamental reactive encounters, and new techniques are opening new systems to investigation. We will present two distinct new approaches to reactive scattering recently developed in Berkeley.

2 Crossed-beam studies using synchrotron radiation

We will describe recent studies on the Chemical Dynamics Beamline at the Advanced Light Source using intense, tunable VUV synchrotron radiation (10^{16} photons/sec; 5-30 eV) as a universal yet selective probe of crossed-beam reaction products. We have used this technique to measure double differential cross sections for reaction of Cl atoms with saturated hydrocarbons. The use of tunable undulator radiation provides the unprecedented ability to probe the hydrocarbon radical fragment directly in these reactions. Our initial studies of the reaction of Cl with propane [1] suggested different dynamics for the forward and backward scattered products; we have now extended these studies to reaction of Cl with n-pentane to examine the underlying trends in the dynamics with an eye to the role of the extended carbon skeleton in these reactions.

The experimental results are summarized in Figs.1 and 2, which show, respectively, the laboratory and center-of-mass distributions obtained for the pentyl radical product in the experiments. Analogy with previous studies on the propane system suggest the forward scattered products are more likely associated with the formation of the lowest energy 2-pentyl radicals while the backscattered products arise from low impact parameter collisions preferentially involving the terminal carbons. Indeed the thermodynamic limits for the isomers shown in Fig. 2 clearly confirm this. The forward scattered products ('channel 1'), are formed extremely cold, largely beyond the limit for production of the 1-pentyl radicals. This indicates a 'stripping'-type mechanism and a loose transition state.

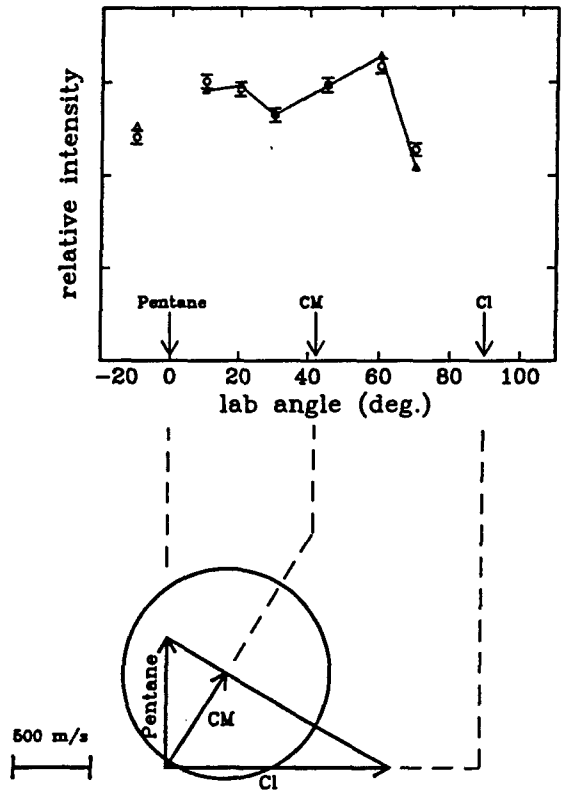

Figure 1: Newton diagram and measured laboratory angular distribution of pentyl radicals from the reaction Cl+n-C_5H_{12} → HCl+C_5H_{11}.

For the backscattered products, however, virtually all of the energy of the collision is deposited into the pentyl radical product, ('channel 2') producing extremely hot, reactive products. This is significantly different from what was observed in other systems, even differing significantly from the analogous propane reaction. In fact, previous laser-based studies relying on REMPI probe of the HCl have

*Abstract 7065 submitted to the 21st International Symposium on Rarefied Gas Dynamics, Marseille, France, July 26-31, 1998

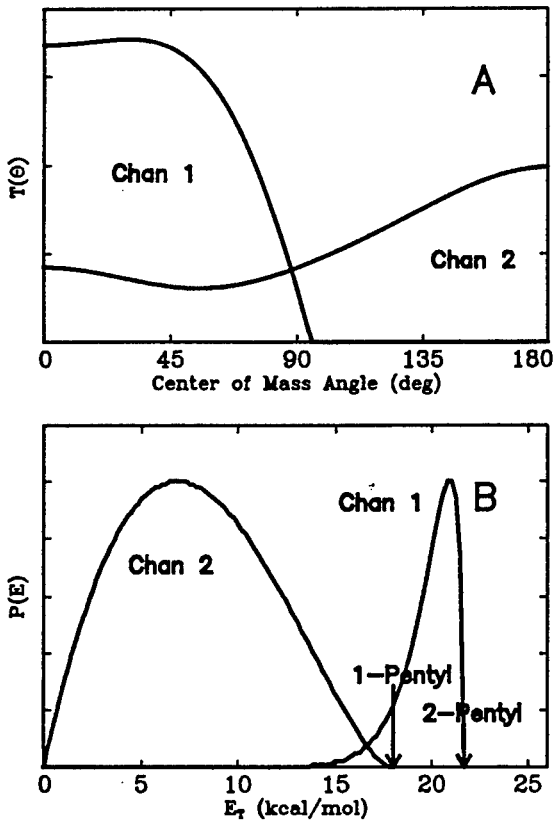

Figure 2: Center-of-mass angular and energy distributions obtained from the experiments. Arrows indicate limits for the production of the indicated radical isomer.

often assumed that no energy is deposited into vibration of the radical product. Figure 2B dramatically shows that this is incorrect. The origin of this behavior will be discussed. We suggest the important difference between propane and pentane is the presence of the extended carbon chain and the larger density of states for the pentane reaction. Estimates indicate that the timescale of the collision, about 20 femtoseconds, is very close to the timescale of the bending vibrations of the carbon backbone, making energy transfer from the collision to the C-C-C bends very efficient.

3 Velocity map imaging: $O(^1D) + D_2 \rightarrow OD + D$

We have adapted the technique of velocity map imaging [2] to application in crossed molecular beams in a study of the reaction $O(^1D) + D_2 \rightarrow OD + D$ under single collision conditions. Images of the reactively scattered D atom product were recorded, yielding the full double differential cross sections (energy and angle) for the reaction. Although the reaction $O(^1D)$ with molecular hydrogen and its isotopic variants has long been considered a prototypical insertion reaction, recent work [3, 4] has begun to challenge the notion of a simple insertion on the ground electronic potential energy surface (PES). The measured translational energy and angular distributions are foundd to be strongly coupled, with the forward scattered products showing the largest translational energy release, and the sideways scattered products the lowest translational energy release (Fig.3).

Although the overall translational energy distributions do not change significantly with E_{coll} we observe an increase in the contribution in the backscattering at the higher E_{coll}. These observations will be used to explore and contrast the dynamics of reaction on the excited state potential energy surfaces (1A", 2A') with that occurring on the ground state potential energy surface (1A').

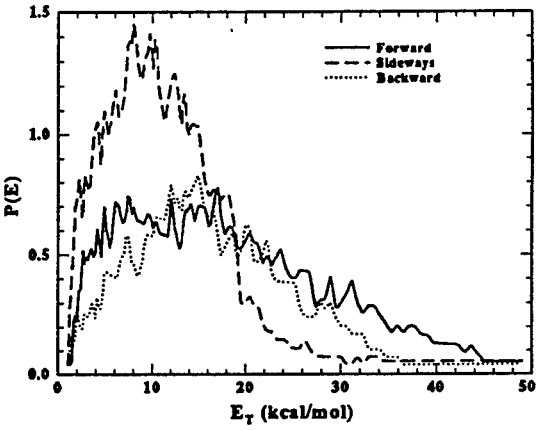

Figure 3: Center-of-mass translational energy distributions obtained from velocity map images of reactively scattered D atoms at a collision energy of 2.8 kcal/mol.

References

[1] Blank, D. A, Hemmi, N., Suits, A. G. and Lee, Y. T. *Chem. Phys.*, (in press) and references.

[2] Eppink, A. T. J. B. and Parker, D. H., *Rev. Sci. Instrum.*, Vol. 68, p. 3477, 1997.

[3] D. Che and K. Liu, *J. Chem. Phys.*, Vol. 103, p. 164, 1995.

[4] See, for example, the recent discussions in *Faraday Discuss. Chem. Soc.*, Vol. 108 (in press).

Ion–neutral collisions in crossed beams: nitrogen abstraction in the reaction of rare gas cations and dications with N_2 *

P. Tosi, R. Correale, S. Falcinelli, W.Y. Lu, and D. Bassi
Istituto Nazionale per la Fisica della Materia
and
Dipartimento di Fisica, Università di Trento, I-38050, Povo, Trento, Italy

1 Introduction

Ion–neutral collisions at low energies (below about 10 eV) play a central role in the physics and chemistry of low density plasmas and ionized gases. Interstellar clouds, planetary ionospheres, plasmas used for the deposition of thin films and gas discharges are relevant examples of systems where ion–neutral collisions are particularly important. At low energies, possible collision processes include chemical reactions, charge transfer, excitation and quenching of internal energy states. In this talk, we will consider a particular class of collisions, the so–called "atom abstraction" reactions *i.e.*:

$$X^+ + Y_2 \longrightarrow XY^+ + Y \qquad (1)$$

These reactions are particularly relevant for the synthesis of molecular ions. For example, the formation of NH^+ in the collision of N^+ with H_2 is the first step in the reaction chain which leads to the synthesis of ammonia in dense interstellar clouds [1, 2].
Reactions of rare gas cations and dications with molecular nitrogen have been extensively studied in recent years. However, most of these studies are limited to the investigation of charge–transfer channels [3]:

$$Rg^+ + N_2 \longrightarrow Rg + N_2^+ \qquad (2)$$
$$Rg^{2+} + N_2 \longrightarrow Rg + N_2^{2+} \longrightarrow Rg + 2N^+ \qquad (3)$$

where Rg indicates a rare gas atom. Very little information is available [4] on the energy dependence of nitrogen abstraction reactions *i.e.*:

$$Rg^{n+} + N_2 \longrightarrow RgN^{n+} + N \qquad (4)$$

where $n = 1, 2$. This is due to the fact that reactions (4) have cross–sections that are typically two orders of magnitude smaller with respect to the corresponding charge–transfer channels.
Accurate measurements of the energy dependence of cross–sections for reactions (4) provides interesting information on the structure and dynamics of the molecular ions RgN^{n+}. In this conference, we present some new results concerning nitrogen abstraction processes in the reaction of Ne^+, Ar^+ and Ar^{2+} with N_2.

2 Experimental

Experimental results have been obtained using two different machines [1, 5]. Both experiments make use of radio–frequency octopole ion guides both for guiding the primary ion beam and for collecting reaction products. In the first machine — hereafter called cell apparatus — the octopole is surrounded by a room–temperature scattering cell. This configuration provides high sensitivity allowing the precise determination of integral cross-sections. However, the influence of the random motion of the target gas produces a significant dispersion of the collision energy. The effective cross-section, measured at the nominal collision energy E_0, results from the convolution of the reaction cross–section $\sigma(E)$ — where E is the collision energy — with the energy distribution $f(E, E_0)$ of reactants:

$$\sigma_{eff}(E_0) = \int_0^\infty \sqrt{\frac{E}{E_0}} f(E, E_0)\, \sigma(E)\, dE \qquad (5)$$

If T is the temperature of the scattering cell, and assuming that $E_0 > k_B T$ the energy distribution function $f(E, E_0)$ is centered around E_0, with a FWHM given by:

$$\Delta E_0 \simeq \sqrt{11.1 \frac{m_I}{m_I + m_N} k_B T E_0} \qquad (6)$$

where m_I and m_N are the ion and the neutral mass respectively. As an example, the reaction of Ar^+

*Abstract 7026 submitted to the 21st International Symposium on Rarefied Gas Dynamics. Marseille. France. July 26-31. 1998

with N_2 producing ArN^+ is endoergic by about 8.5 eV. Using a room–temperature scattering cell, the energy resolution in the threshold region is about 1 eV. This may be a serious limit for the accurate determination of the energy threshold.
An alternative approach is based on the use of a crossed–beam apparatus where the scattering cell is replaced by a supersonic molecular beam [1]. The molecular beam is produce by supersonic expansion of neutral molecules through a nozzle cooled at 150 K. A collimator in front of the octopole, where the two beams cross at 90°, reduces the angular divergence of the supersonic beam to about 1°. The crossed-beam apparatus is much less sensitive with respect to the cell machine, and measurements may be very time consuming. However it provides a much better energy resolution which may be essential for the accurate determination of energy thresholds [1]
The combined use of the two apparatuses enable us to set-up a very effective measurement strategy. Ion-molecule reactions are first investigated using the high-sensitivity cell apparatus. The molecular beam apparatus is then used to repeat the measurements only at a limited number of collision energies, studying in more detail the regions where a better energy resolution is required. This allow us to save time, obtaining detailed information only when required. Moreover it is important to note that the use of two independent machines is also important to avoid possible systematic errors originating by variations of the detection efficiency at different collision energies [5].

3 Results

We have investigated the energy dependence for the following reactions:

$$Ne^+ + N_2 \longrightarrow NeN^+ + N \quad (7)$$
$$Ar^+ + N_2 \longrightarrow ArN^+ + N \quad (8)$$
$$Ar^{2+} + N_2 \longrightarrow ArN^{2+} + N \quad (9)$$

in the collision energy range from thermal to about 30 V. The production of ArN^+ has been investigated also for the symmetric reaction:

$$N_2^+ + Ar \longrightarrow ArN^+ + N \quad (10)$$

All the above reactions show an endoergic behavior, which corresponds to well defined thresholds in the energy dependence of the cross-section. Detailed results will be presented at the conference. Here we point out that reaction (9) is particularly interesting because ArN^{2+} is produced in a metastable state. In fact, ArN^{2+} is thermodynamically unstable with respect to the Coulomb explosion $ArN^{2+} \longrightarrow Ar^+ + N^+$ [6]. As far as we know, molecular dications have never been observed as a product of atom abstraction reactions. Our result open the way for the synthesis of molecular dications which do not have a stable precursor [7]. The possible applications of this method for the development of new experiments concerning molecular dications will be discussed at the conference.

References

[1] Tosi P., Dmitriev O., Bassi D., Wick O., Gerlich D., *Experimental observation of the energy threshold in the ion–molecule reaction $N^+ + D_2 \rightarrow ND^+ + D$*, J. Chem. Phys., Vol.100, pp.4300–4307, 1994.

[2] Tarroni R., Palmieri P., Mitrushenkov A., Tosi P., Bassi D., *Dissociation energies and heats of formation of NH and NH^+*, J. Chem. Phys., Vol. 106, pp.10265–10272, 1998.

[3] see for example: a) Tosi P., Dmitriev O., Bassi D., *The charge transfer reaction $Ar^+ + N_2 \longrightarrow N_2^+ + Ar$. Crossed-beam measurements of the integral cross section as a function of the collision energy*, Chem. Phys. Letters, Vol.200, pp.483–487, 1992; b) Störi H., Alge E., Villinger H., Egger F., Lindinger W., *Reactions of $Ar^{2+}(^3P)$ with CH_4, C_2H_2 and NO_2, of $Ar^{2+}(^1S)$ with H_2, N_2, O_2, CO_2, C_2H_2 and CH_4 and of Ar^+ with CH_4 and NO_2*, Int. J. Mass Spectrom. Ion Phys., Vol. 30, pp.263–270, 1979.

[4] Flesch G.D., Ng C.Y., *Observation of the formation of N^+ and ArN^+ in the collision of $Ar^+(^2P_{3/2,1/2})$ with N_2*, J. Chem. Phys., Vol. 92, pp.2876–2882, 1990.

[5] Bassi D., Tosi P., Schlögl R., *Ion–molecule–reaction mass spectrometer for on-line gas analysis*, J. Vac. Sci. Technol. A, Vol.16, pp.114–122, 1998.

[6] Pauling L., *The normal state of the Helium molecule-ions He_2^+ and He_2^{++}*, J. Chem. Phys. Vol.1, pp.56–59, 1933.

[7] Tosi P., Correale R., Falcinelli S., Lu W.Y, Bassi D., (to be published).

Crossed Beams Study of $(NaRb)^+$ Collisional System *

T. Romero, J. De Andrés, M. Albertí, J.M. Lucas, J.M. Bocanegra, A. Aguilar, J. Sogas
Departament de Química Física, Universitat de Barcelona, Barcelona, Spain

Among collisional systems forming one-electron quasimolecules, the study of those involving alkali ion-alkali atom collisions presents an added interest in that their potential energy surfaces can be described using relatively simple theoretical methods, which give quite good results with a moderate expenditure in calculation time. Thus, much experimental and theoretical work has been done on these systems (see [1] and references cited there).

In order to improve on the available knowledge about these systems, a crossed beam machine has been built in which neutral atom beams can be generated either by simply heating the metal or, in the case of Rb for instance, produced in situ via an exchange reaction (i.e. RbCl+Ba →BaCl+Rb). Beam intensity and stability have been controlled by means of an ionisation neutral atom detector. The alkali ion beam is produced by thermoionic effect, adequately focused and collimated. Both beams are the crossed. Short-lived, excited species are formed in the resulting collisions (via straight electronic excitation processes or by electron exchange) whose fluorescent emission is then analysed and measured.

Signal-to-noise ratio in these experiences was high enough to separate even such closely lying J-states as $Na(3^2P_{1/2})$ and $Na(3^2P_{3/2})$ [2], an example being given in Fig. 1 for the charge transfer process: $Rb(5^2S_{1/2}) + Na^+ \rightarrow Na(3^2P_{1/2};3^2P_{3/2}) + Rb^+$. The insertion of a polarising filter in the detector lightpath made also possible to make true polarisation fraction measurements (using data from the non-polarised transitions to compensate for deviations induced by the monochromator) from which cross-sections can be corrected to give the true emission values (this correction proved to have a quite negligible magnitude). Also, from those polarisation fraction values, the branching ratio between m_J states for some transitions was also obtained for the Na atom collisions with Li^+, Na^+ and K^+. In order to obtain data on processes involving the $(NaRb)^+$ quasimolecule, $Na+Rb^+$ [3, 4] and $Rb+Na^+$ [5] collisions have also been studied, as well as $Rb+Rb^+$ ones [6].

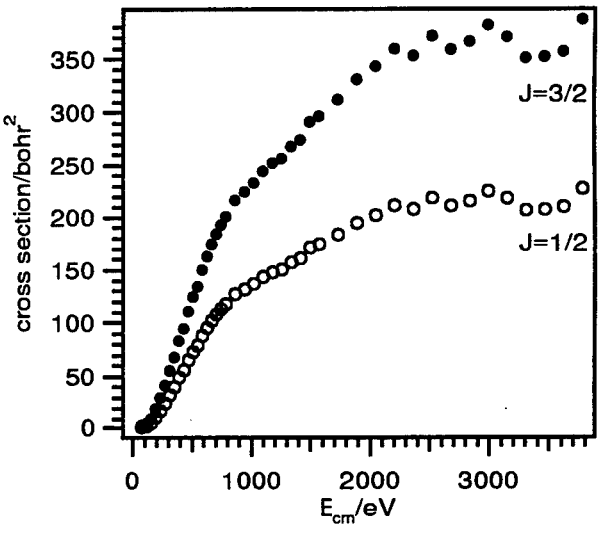

Figure 1: State-to-state excitation cross-section for the formation of $Na(3^2P_J)$ by collisions between Rb and Na^+

As simple two-state models did not give much information about the behaviour of these systems (although quite good results were obtained by fitting some of the experimental results to a rotationally-coupled Landau-Zener model), an ab initio calculation for the $(NaRb)^+$ system has been carried out [7] using pesudopotentials and taking into account the core polarisation. In this way it proved feasible to qualitatively justify such facts as the behaviour of diabatic orbital energies as a function of internuclear distance for relevant collision channels. Using the potential curves (see Fig. 2) the radial couplings (obtained by finite increment techniques plus an effective metric) and integrating the hemiquantal dynamic equations in a diabatic representation, excitation functions for processes leading to the formation of excited states having $J = 1/2$ have been determined. A comparison between experimental and computed cross-sections is presented in Fig. 3

*Abstract 7018 submitted to the 21st International Symposium on Rarefied Gas Dynamics, Marseille, France, July 26-31, 1998

for the electronic excitation process $Na(3^2S_{1/2}) + Rb^+ \rightarrow Na(3^2P_{1/2}) + Rb^+$.

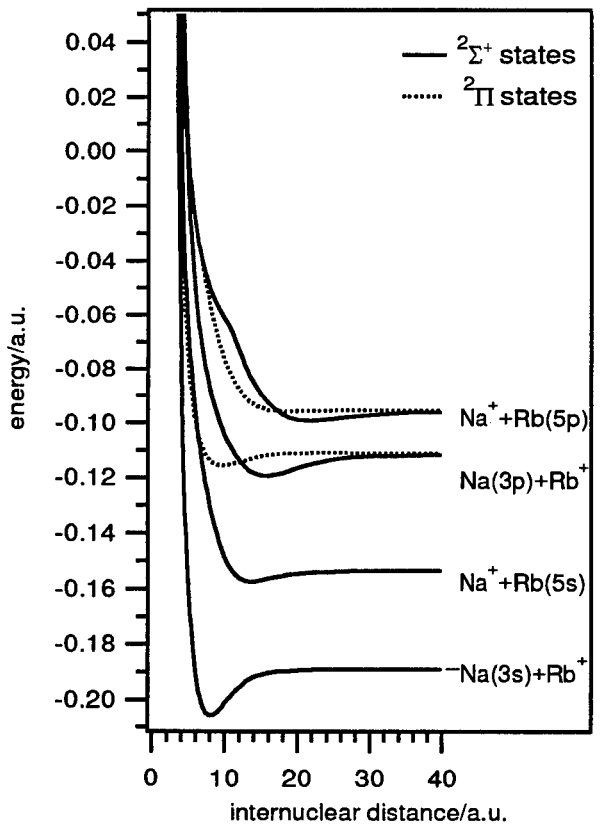

Figure 2: Potential energy curves for some relevant collision channels in the $(NaRb)^+$ collisional system

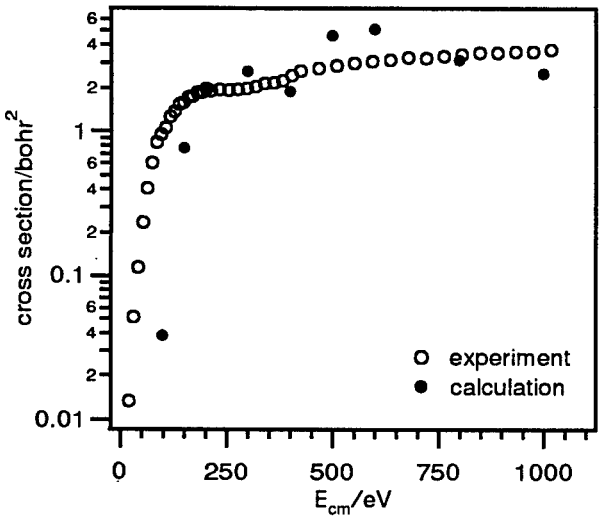

Figure 3: Computed and experimental cross-sections for the electronic excitation process $Na(3^2S_{1/2}) + Rb^+ \rightarrow Na(3^2P_{1/2}) + Rb^+$

Work at present in progress includes adding mass analysis capability to the experimental setup in order to study ion-molecule collisions and developing low-energy ion focusing devices. Also we would take into account the rotational couplings in the calculations for the ion-atom system.

References

[1] A. Aguilar, M.Albertí, M. Prieto, J. de Andrés, M. Gilibert, X . Giménez, M. González, J.M. Lucas, R. Sayós, A. Solé., Chem. Phys. Letters, 220 (1994) 267

[2] J. de Andrés, M. Prieto, T. Romero, J.M. Lucas, M. Albertí, A. Aguilar, Chem. Phys. Letters, 238(1995) 338

[3] T. Romero, J. de Andrés, M. Albertí, J.M. Lucas, A. Aguilar, Chem. Phys., 209 (1996) 217

[4] T. Romero, J. de Andrés, M. Albertí, J.M. Lucas, A. Aguilar, Chem. Phys. Letters. 272 (1997) 271.

[5] T. Romero, J. de Andrés, M. Albertí, J. Sogas, J.M. Lucas, J M. Bocanegra, A. Aguilar, Chem. Phys. Letters. 281 (1997) 74

[6] T. Romero, J. de Andrés, J. Sogas, M. Albertí, J.M. Lucas, J M. Bocanegra, A. Aguilar, (submitted)

[7] T. Romero, J. de Andrés, M. Albertí, J.M. Lucas, J. Rubio, J.P. Daudey, A. Aguilar, Chem. Phys. Letters., 261 (1996) 583

COHERENT®

LASERS SCIENTIFIQUES ET INDUSTRIELS

Tél. : 01 69 85 51 45 - Fax : 01 69 85 51 46

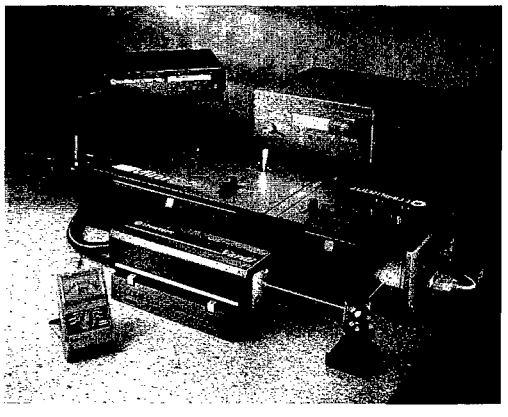

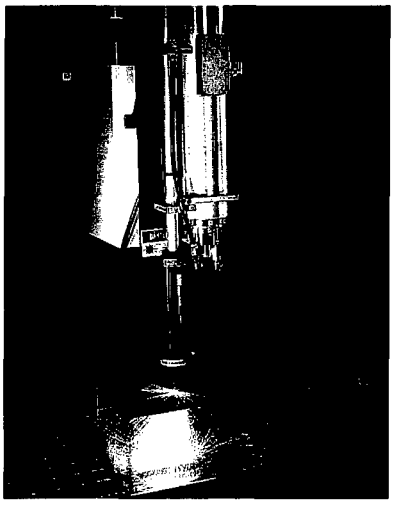

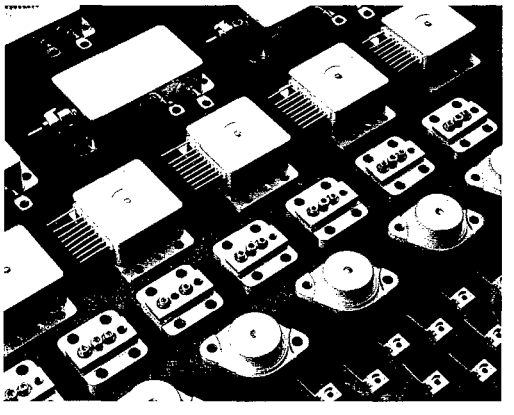

COHERENT·

OPTIQUE, OPTO-MECANIQUE ET INSTRUMENTATION LASER

Tél. : 01 60 19 40 40 - Fax : 01 60 19 40 00

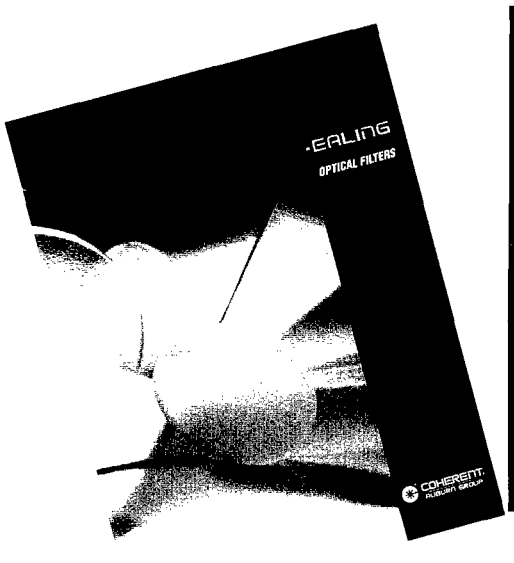

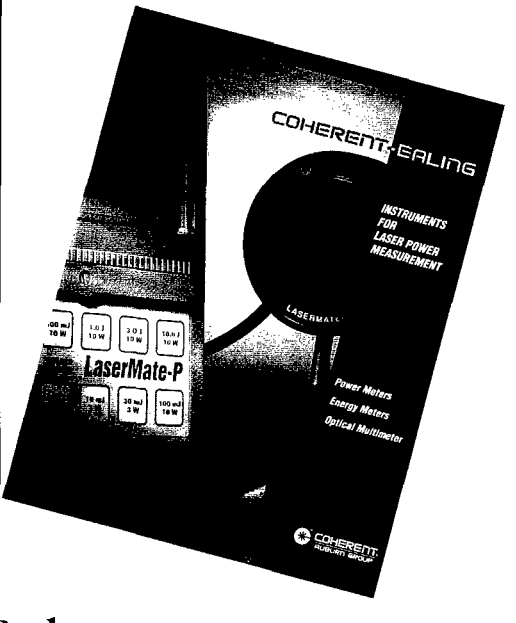

Domaine Technologique de Saclay
4, rue René Razel - Bâtiment Azur - 91892 ORSAY Cedex
www.coherent.fr

MOLECULAR BEAM SESSION MB 8

Reaction, Coagulation, and Electron
Attachment on Clusters or van der Waals Molecules

CHAIR: G. Meijer (Nijmegen)

ROOM: LAVOISIER
THURSDAY, JULY 30, 1998
14:00 - 16:00

Reaction between Barium and N_2O on Large Neon Clusters *

M.A. Gaveau, M. Briant, V. Vallet, J.M. Mestdagh, J.P. Visticot
CEA/DSM/DRECAM/SPAM, CE Saclay, France

1 Introduction

Over the past few years, we have developed in our laboratory a new method called CICR (for "Cluster Isolated Chemical Reactions"), with the goal to investigate the effect of a reaction medium on reaction dynamics [1]. CICR consists in performing chemical reactions on large van der Waals clusters in a very controlled way. Clusters provide an ideal medium for the study of solvation effects and heterogeneous chemistry at a microscopic level: They are free from any perturbations due to a substrate, they have a well defined internal energy and they have a finite size (from 10^2 to a few 10^3 atoms or molecules in our experiments). Reactants are deposited on the clusters by sticky collisions between the clusters and a low pressure buffer gas. This pick-up technique allows us a strict control of the reactant deposition onto the clusters. On the clusters, reactants will migrate, collide with each other and eventually react. Thus the clusters become true chemical nanoreactors. Reactions of Ba atoms and small Ba aggregates have already been investigated on various clusters, i.e. argon, methane and nitrogen clusters which have similar structures and internal temperatures (between 35 and 43 K) [2]. In particular, it has been shown that the mechanism of the chemiluminescent reaction

$Ba + N_2O \rightarrow BaO + N_2 + \Delta H = 4.1$ eV

is not substantially affected by the presence of the reaction medium. However, the cluster leads to specific effects. Firstly, there is a dramatic increase of the reaction rate compared to the gas phase reaction. Secondly, it leads to the formation of BaO molecules which can be either ejected from the cluster as free molecules or stay solvated on the cluster. As a solvent, it changes the energy levels of the solute so that the spectra of the solvated molecule is modified and shifted, and it relaxes the excess energy of the solvated product. The solvated BaO product has an interaction with the solvent which increases from argon to CH_4 and to nitrogen. In the latter case, the interaction is so strong that chemiluminescence is quenched. In argon, chemiluminescence consists in a band spectrum corresponding to the emission of vibrationally cold BaO in the $a^3\Sigma$ and $A^1\Sigma(v'=0)$ electronic states. In the case of methane clusters, the structure of the solvated BaO spectrum is completely washed out and its intensity is decreased, indicating a stronger interaction of the BaO product with the methane cluster. Even with argon, the interaction of BaO with the substrate is strong enough to lead to an important broadening of the vibronic bands.

Neon forms colder clusters (12 K) and is expected to have a smaller interaction with the product. This paper reports results on the Ba + N_2O reaction performed on large neon clusters.

2 Experiment

Neon clusters are grown by homogeneous nucleation in a supersonic free jet from a source cooled by liquid nitrogen. The stagnation conditions are P_0=30 bars; T_0= 77 K and the sonic nozzle has a 0.1 mm diameter. After extraction by a 1 mm skimmer, the cluster beam passes through a differentially pumped chamber, which can be used as a pick-up chamber for N_2O. We call it the early pick-up region. After a collimator, the beam enters the main chamber and fly through a heated barium cell, where barium atoms are deposited on the clusters. Then, it reaches the detection zone which is imaged onto the entrance slit of a monochromator. A second pick-up can be performed in this region (called late pick-up region) by crossing the beam with a N_2O beam effusing from a capillary tube. Downstream, the beam enters chambers, which house a quadrupole mass spectrometer and Time-Of-Flight Mass Spectrometer. The average size of the neon clusters measured with the latter one is about 9000 atoms under our experimental conditions.

Two types of experiments were performed depending on which pick-up region was used. In the first one, N_2O is deposited onto clusters in the late pick-up region, from which fluorescence sig-

*Abstract 6896 submitted to the 21st International Symposium on Rarefied Gas Dynamics, Marseille, France, July 26-31, 1998

nals are observed. Such experiments document the nascent distribution of electronically excited products within a time window of a few microseconds after the reaction, corresponding to the residence time of the clusters in the observation region. In the second type of experiment, the early pick-up region is used and fluorescence signals correspond to emission of excited products several tens of microseconds after the reaction. Figure 1 displays the chemi-

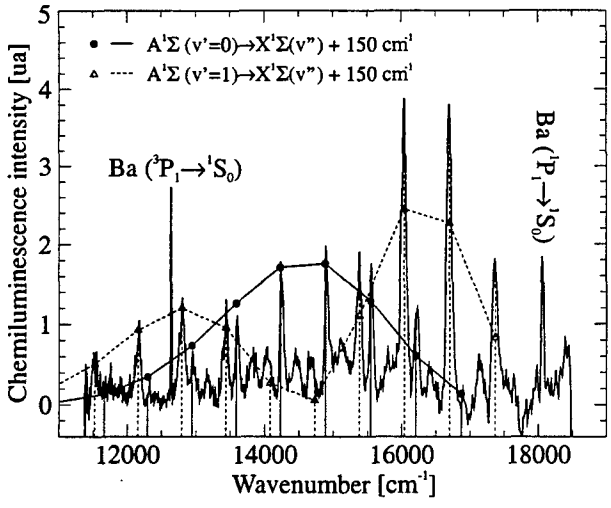

Figure 1: Solvated BaO chemiluminescence spectrum produced by the Ba+ N_2O reaction on large neon clusters with a late N_2O pick-up.

luminescence spectrum recorded in the late pick-up experiment, for solvated BaO specifically. It shows BaO molecular bands and two narrower atomic Ba($^1P_1 \rightarrow ^1S_0$) and Ba($^3P_1 \rightarrow ^1S_0$) lines. The two most intense molecular progressions correspond to two vibrational progressions of BaO : Emission of BaO $A^1\Sigma$ (v'=0) to the different vibrational levels of the ground state, and emission of BaO $A^1\Sigma$ (v'=1). For comparison, the corresponding line intensities calculated for the free BaO molecule are shown, but the emission must be blue shifted by 150 cm^{-1} to account for the solvation.These results are different from what is obtained on argon clusters: The bands are narrower (50 cm^{-1} instead of 150 cm^{-1}), the blue shift is smaller (150 cm^{-1} instead of 750 cm^{-1}) and the emission from v'=1 is predominant while only v'=0 is observed on argon clusters. Figure 2 displays the solvated BaO chemiluminescence spectrum recorded in the early pick-up experiment. It is composed of two vibrational progressions which can be assigned to the emission of the BaO $a^3\Sigma$ (v'=0) state and are respectively blue shifted by 770 and 1170 cm^{-1} from the corresponding lines of the free BaO molecule. Surprisingly, one progression exhibits narrow bands (40 cm^{-1}) while the other one presents wide bands (350 cm^{-1}). The position of the narrow band progression does not allow us to assign it to zero phonon lines associated to the wide band progression. It thus appears that they correspond to different locations of the BaO product: the latter one to BaO embedded inside the clusters, the former one to BaO less solvated but not really on the surface.

These results can be interpreted as progressive solvation of the BaO molecule produced by the Ba+ N_2O reaction on large neon clusters. During the first microseconds following the reaction, BaO stays in the short lived $A^1\Sigma$ state. It lies on the surface and keeps some vibrational excitation. After several tens of microseconds, only the long lived $a^3\Sigma$ state remains populated. BaO is much more solvated at two different locations, one embedded inside the cluster and the other one just below the surface.

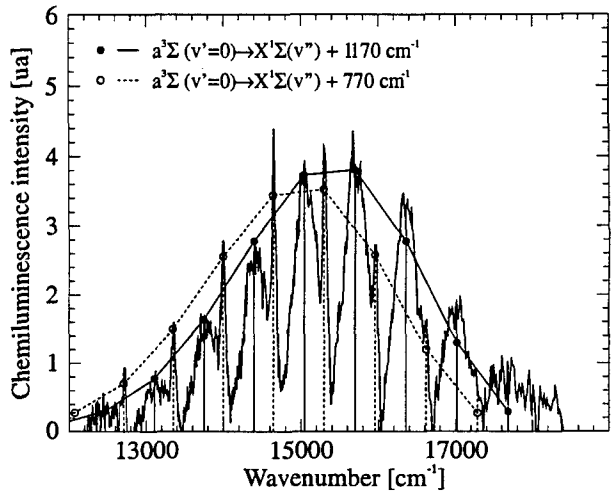

Figure 2: Solvated BaO chemiluminescence spectrum produced by the Ba + N_2O reaction on large neon clusters with an early N_2O pick-up.

References

[1] Mestdagh J.M., Gaveau M.A., Gée C., Sublemontier O., and Visticot J.P., Int. Rev. Phys. Chem., Vol.16, No. 2, pp.215-247, 1997.

[2] Gaveau M.A., Schilling B., Gée C., Sublemontier O., Visticot J.P., Mestdagh J.M. and Berlande J., Chem. Phys. Lett. Vol.246, pp.307-314, 1995.

Chemical Reactions in Small Molecular Clusters *

S. Martrenchard-Barra, D. Solgadi, C. Jouvet, C. Dedonder-Lardeux, G. Grégoire
Laboratoire de Photophysique Moléculaire du CNRS, Université Paris-Sud,
91405 Orsay, France

The study of chemical reactions within small molecular clusters produced in a supersonic expansion provides a way to get energetic and kinetic information without perturbation of the environment, which is important to disentangle the reaction mechanisms. Moreover, the effect of the solvation on bimolecular chemistry can be investigated step by step and comparison between dynamics in isolated molecules and in the condensed phase can be substantiated.

1 Solvent assisted intramolecular charge transfer

We have studied the role of the solvent (water, acetonitrile ...) on the intramolecular charge transfer in the case of Donor-Acceptor molecules such as substituted aniline derivatives (the model compound being the dimethyl-amino benzonitrile DMABN).

When they are excited in polar solutions, these molecules show an intramolecular charge transfer with a torsion of the donor moiety with respect to the acceptor moiety. This twisted intramolecular charge transfer (TICT) is characterized by a dual fluorescence, a blue shifted band corresponding to the non twisted conformation and a red one corresponding to the twisted charge transfer state.

In solution, the factors governing this photochemical behavior are :

- the polarity of the solvent which leads to a stabilization of the charge transfer state ;
- the torsion angle in the ground state : if the molecule is twisted, the torsion of the excited molecule will be easier ;
- the energy gap between the first and the second excited states corresponding to the locally excited state and to the charge transfer state.

In small clusters we have shown that for dimethyl-amino benzene methylester (DMABME) the transfer to the TICT state can be induced by one molecule of a polar solvent only (water or acetonitrile). When the cluster size is increased, the red fluorescence also increases.

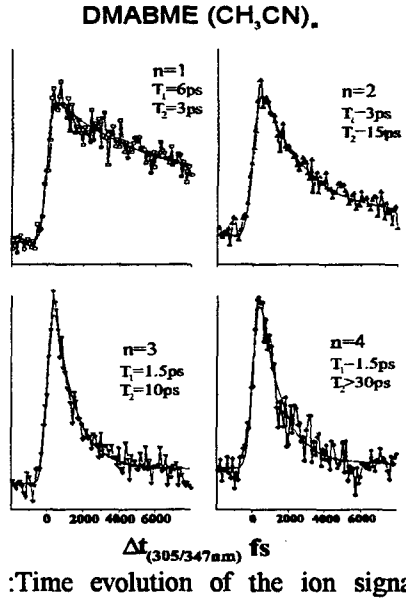

Figure 1 :Time evolution of the ion signal as a function of the delay between the pump (305nm) and the probe (347nm) laser for different cluster sizes.

* Abstract 6941 submitted to the 21st International Symposium on Rarefied Gas Dynamics, Marseille, France, July 26-31, 1998

A kinetic study of this process on the picosecond time scale shows that the crossing towards the TICT state is faster when the number of solvent molecules increases (figure 1). In this pump-probe experiment a first photon excites the complex and the second one delayed in time, leads to the ionizing continuum (figure 2). The biexponential decay of the ion signal has been assigned to the delocalization of the wavepacket initially prepared on the locally S_1 excited state to a mixed TICT/S_1 intermediate state. When the number of solvent molecules is increased, the wavepacket is more displaced towards the TICT state.

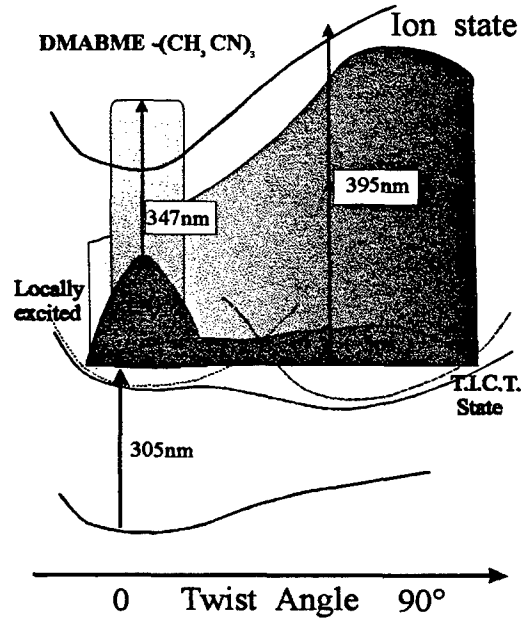

Figure 2 : Scheme of the potential curve along the twist angle coordinate. At time t=0 the femtosecond pulse prepares a wave packet (dark grey) at 0-0 which diffuses towards the TICT. This wavepacket can be probed by a 347 nm photon in the vicinity of the 0-0 or by a 395 nm at different angles

2 Chemical reactivity in small molecular clusters

An important effect of solvation on chemical reactions is to lower the barriers along the reaction coordinate. We have studied this kind of effect in clusters as a function of size.
For example, we have studied recently the polymerization reaction in vinyl chloride $(C_2H_3Cl)_n$ clusters and the proton transfer in the Phenol(ammonia)$_n$ clusters by Threshold PhotoElectron PhotoIon Coincidence (TPEPICO) experiments using the synchrotron radiation at LURE in Orsay.

The ionized vinyl choride dimer reacts leading to $C_4H_5Cl^+$ with loss of one HCl molecule. This reaction occurs after crossing a barrier of 0.2 eV. However, the energy content measured in the $C_4H_5Cl^+$ reaction product indicates a more complex mechanism involving a second barrier on the reaction path. Trimer and tetramer also polymerize.(figure 3). However for larger clusters the reaction products are no longer detected. This can be interpreted as an effect of thermal bath in the clusters where the reaction is in competition with energy redistribution in the vibrational modes of the system.

A second example is the study of the acid-base reaction occuring in the ground state of phenol-ammonia clusters. By measuring the ionization energies of the clusters we have been able to determine that at least 6 molecules of ammonia are necessary to allow the proton transfer. This can be directly correlated with the proton affinities of ammonia clusters which increase with the size and with the acidity of the phenol molecule.

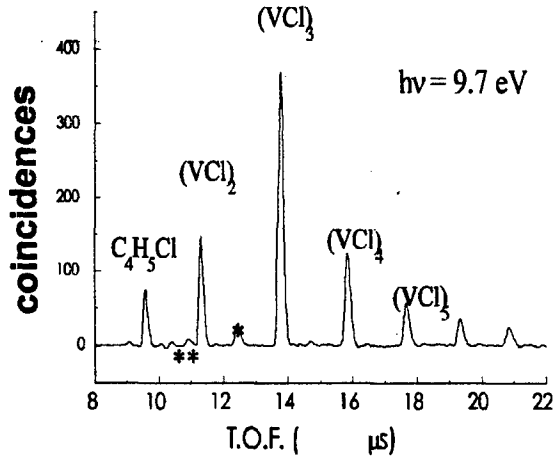

Figure 3 : Mass spectrum of ionized vinyl chloride clusters. C_4H_5Cl is the main reaction product resulting from the HCl elimination

Resonances in the Reaction Probability and Spectroscopyc Probing of the Transition-State Structure of a (van der Waals) Reaction

S. Skowronek, J.B. Jiménez, A. González Ureña
Unidad de Laseres y Haces Moleculares. Universidad Complutense de Madrid. Spain.

The spectroscopy and dynamics of the transition state constitutes one of the most exciting and expanding research fields in both modern molecular reaction dynamics and laser spectroscopy [1-12]. The present communication reports on simultaneous measurement of both the photodepletion spectrum of the Ba...FCH_3 weakly bound complex and the action spectrum of the BaF reactive channel in the range 16065-16340 cm^{-1}. Essentially these two pieces of information allow us to determine (see below) the reaction probability of the (excited) harpooning reactio, e.g.,

$$Ba...FCH_3 + h\nu \rightarrow |Ba...FCH_3|^* \rightarrow (Ba^+...FCH_3) \rightarrow BaF^* + CH_3$$

A detailed description of the experimental apparatus employed in this work has been reported elsewhere[12] so its description is omitted for brevety.

To obtain the photodepletion spectrum the disappearance of the species was monitored as a function of the dye laser wavelength. following the same procedure described in Ref.12. Figure 1 (top) shows the photodepletion spectrum obtained by monitoring the parent mass of the Ba...FCH_3 complex in the range 16065-16340 cm^{-1}. A well defined vibrational structure with a spacing of 150 cm^{-1} and a high cross-section can be noticed.

We have developed a method to extract the reaction probability from these spectra reatining only the dynamical part contained in the action spectrum. Such an interesting piece of information is displayed by the lower trace of Figure 2 for the BaF channel of the Ba...FCH_3 vdW photoinitiated reaction. A detailed analysis of the energy dependence of this reaction probabilty will be presented at the Symposium.

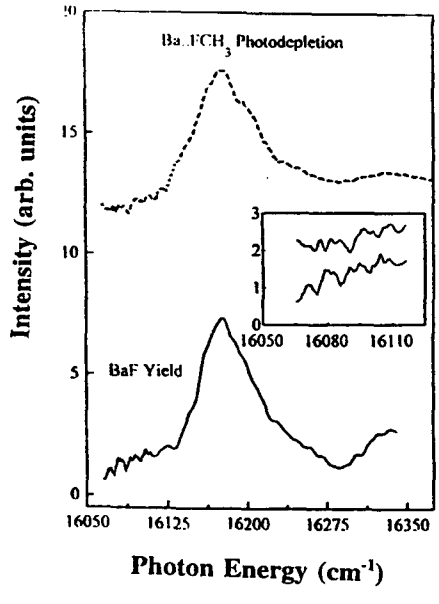

Figure 1. (Top). Photodepletion spectrum of the Ba...FCH_3 complex in the range 16065-16340 cm^{-1} . (Bottom). Action spectrum for the BaF reaction channel, i.e. BaF ion signal obtained by the 266 nm ionization wavelength as a function of the photodepletion laser wavelength tuned over the same range as in the top spectrum. Both: Top and Bottom signals are displayed in arbitrary units. The inset shows the near threshold part of both spectra for clarity. Notice the opposite phase of the BaF peaks with respect to those of Ba...FCH_3 depletion spectrum.

Abstract 7021 submitted to the 21st International Symposium on Reactied Gas Dynamics, Marseille, France, July 26-31, 1998.

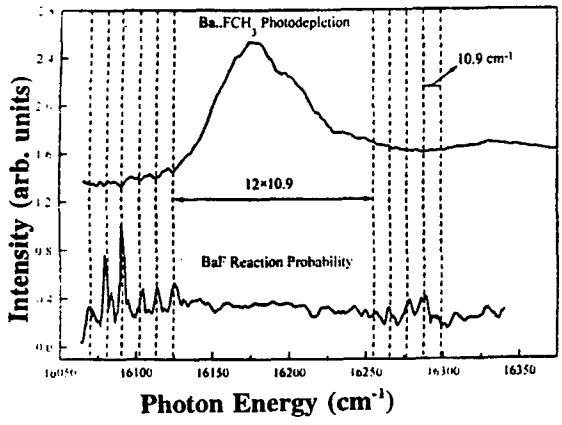

Figure 2. (Top) Same spectrum as in Figure 1 top. (Bottom) Reaction probability for the BaF photofragmentation channel. The ratio of the bottom to the top spectral signals of Figure 1 is displayed. Notice the energy spacing marked on the different peaks with the aid of vertical dashed-lines.

Conclusion

The simultaneous measurement of both the photodepletion action spectrum of the Ba...FCH_3 complex and the action spectrum of the reactive BaF photofragmentation channel over 16065-16340 cm^1 wavelength range allowed for the first time a direct determination of the reaction probability of a van der Waals reaction as a function of excitation energy. A key feature of this type of measurement is its high energy resolution due to the narrow bandwidth of the laser used to photoinitiate the chemical reaction. Thus energy resolution of ca. 0.01 m eV can be reached which makes possible the observation of quantal effects in an elementary reaction, a long-standing goal in chemistry. In this report the energy dependence of the Ba..FCH_3 + hν → $(Ba..FCH_3)^*$ → BaF^* + CH_3 reaction probability, $P_R(E)$, is presented showing a peak structure which may reflect *dynamical resonances* associated with excited quasi-bound states of the reactive intermediate. In addition the energy spacing between the peaks in $P_R(E)$ can provide direct information about the *vibrational structure* of the transition state of the reaction

Acknowledgments.

This work has received financial support from the DGICYT of Spain (grant PB95/391).

References

[1] J. C. Polanyi and A. H. Zewail, Acc. Chem. Res. **28**, 119, (1995).

[2] A. H. Zewail, Faraday Discuss. Chem. Soc. **91**, 207, (1991). ibid. A. H. Zewail, Science, **242**,1645, (1988).

[3] C. Jouvet and B. Soep, Laser Chem. **5**, 157, (1985).

[4] C. Jouvet, M. Boiveneau, M. C. Duval, and B. Soep, J. Phys. Chem. **91**, 5416, (1987).

[5] B. Soep, S. Abbes, A. Keller, and J. P. Visticot, J. Chem. Phys. **96**, 440, (1992).

[6] B. Soep, C. J. Whitham, A. Keller, and J. P. Visticot, Farady Discuss. Chem. Soc. **91**, 191, (1991).

[7] A. Keller, R. Lawruszczuk, B. Soep, and J. P. Visticot, J. Chem. Phys. **105**, 4556, (1996).

[8] G. Hoffman, Y.Chen, M.Y. Engel, and C. Wittig, Isr. J. Chem. **30**, 115, (1990).

[9] C. Wittig, S. Sharpe, and R. Beaudet, Acc. Chem. Res. **21**, 341, (1988).

[10] K. Liu, J. C. Polanyi, and S. Yang, J. Chem. Phys. **98**, 5431, (1993).

[11] C. Polanyi and Ji-Xing Wang, J. Phys. Chem. **99**, 13691, (1995).

[12] S. Skowronek, R. Pereira and A. González Ureña, J. Chem. Phys., **107**, 1668 (1997). See also ibid J. Phys. Chem., special issue on Stereodynamics, **101**, 7468-7475 (1997).

Capture and Coagulation of CO Molecules to Small Clusters in Large H2 Droplets*

E.L. Knuth[1], S. Schaper[2], J.P. Toennies[2]
[1]Chemical Engineering Dept., UCLA, Los Angeles, CA 90095
[2]MPI für Strömungsforschung, Göttingen, Germany

1. Introduction

Experimental studies of the properties of H_2 droplets formed in free-jet expansions have been described in papers [1,2] presented at earlier RGD Symposia. The objective of this series of studies is the production of metastable p-H_2 droplets in the liquid state with temperatures below 6.6K with the hope that such droplets would exhibit superfluid properties. In the first paper [1], cluster temperatures as low as 6K were deduced from measured values of terminal cluster velocities; evaporation provides additional cooling. In the second paper [2], dramatically higher terminal cluster velocities were observed for measurements made on p-H_2 which apparently had been inadvertently contaminated with some foreign substance; it was conjectured that this foreign substance provided sites for heterogeneous nucleation of solid p-H_2 and that the heat released in solidification was converted into additional terminal velocity. Time-of-flight measurements made with uncontaminated clusters passing through a scattering gas suggested that these clusters were liquid. In the measurements described here, a foreign substance, namely CO, was introduced deliberately into the H_2 droplets by passing the cluster beam through a scattering chamber containing CO at room temperature and various pressure levels. The sizes of the CO clusters formed by coagulation within the H_2 droplets were monitored.

2. Apparatus and Measurements

The apparatus used here is essentially the same as used by Schilling in his Dissertation [3] excepting that the length of the chopper chamber has been reduced from 125mm to 90mm. CO was bled into the chopper chamber so that this chamber served as a scattering chamber. CO was chosen for the scattering gas since its ionization potential is about 1.4 eV below that of the H_2. A p-H_2 free-jet cluster beam was formed by expansion from 20 bar and 45K through a 5 μm orifice. These source conditions yield clusters with an average size of about 5000 molecules. Mass spectra were measured for several values of CO pressure in the chopper chamber. Typical spectra are given in Fig. 1. CO clusters are observed up to $(CO)_{10}$ for 2.5×10^{-4} mbar CO in the scattering chamber, up to $(CO)_4$ for 1.2×10^{-4} mbar CO.

3. Characteristic Times

In order to place the time available for coagulation of the CO molecules within the H_2 droplets in perspective, we compare here several relevant characteristic times. For the given source conditions, a mean cluster speed of 891 m/sec was measured. Hence, for the existing flight distances, flight times of 0.05×10^{-3} sec and 2×10^{-3} sec are realized for the flight from the skimmer to the middle of the scattering chamber and for the flight from the middle of the scattering chamber to the ionizer respectively. The mean time between consecutive collisions of an H_2 cluster with CO molecules varies inversely as the product of the collision cross section, the mean cluster speed and the number density of CO molecules in the scattering chamber. The collision cross section for H_2 clusters containing 5000 molecules was measured to be about 8000 Å^2. Hence, for a CO pressure of 2.5×10^{-4} mbar, the mean time between consecutive collisions would be about 2×10^{-6} sec.

The characteristic time for coagulation depends upon whether the droplet is a normal fluid or a superfluid. A conservative (i.e., largest) value is realized for the normal fluid. For our purposes, we base this characteristic time on the diffusion-limited rate constant k_D. Starting with either Eq. (4-26) of Steinfeld, Francisco and Hase [4] or Eq. (7-11) of Friedlander [5], one obtains

$$k_D = (2/3)(kT/\mu)(1 + n^{1/3})^2/n^{1/3}$$

where k is Boltzmann's constant, T is temperature, μ is viscosity and n is number of CO molecules in the CO cluster. For one CO cluster and one CO molecule

* Abstract 6051 submitted to the 21st International Symposium on Rarefied Gas Dynamics, Marseille, France, July 26-31, 1998

moving randomly in an H_2 cluster of volume V, the characteristic time is simply V/k_D. Hence, the characteristic time for CO coagulation within an H_2 cluster of 5000 molecules is of the order of or less than $3x10^{-8}$ sec. We see that the CO has ample time for coagulation not only during the flight from the scattering chamber to the ionizer but also between consecutive collisions with CO molecules in the scattering chamber.

4. Discussion

Since the characteristic time for coagulation is two orders of magnitude smaller than the time between consecutive collisions with the scattering-gas CO molecules, one might expect every CO molecule colliding with an H_2 cluster to attach to the existing CO cluster and that the typical H_2 cluster emerging from the scattering chamber would contain one CO cluster consisting of average number of CO molecules equal to the average number of collisions experienced by the H_2 clusters in the scattering chamber. But, for a CO pressure of $2.5x10^{-4}$ mbar, the largest CO cluster observed contains only 10 CO molecules even though the H_2 cluster has collided, on the average, with 44 CO molecules. The observations reported in Ref. [2] suggest that the embedding of CO molecules initiates heterogeneous nucleation of a solid phase within the H_2 cluster, resulting in a decreased capture coefficient and a decreased mobility of the CO molecules within the H_2 cluster. Since heat is released by the solidification, this phase change requires a non-zero time lapse [6]. Then the maximum observed CO cluster size should be fixed by the number of collisions with scattering-gas molecules between the time at which the critical CO cluster size required for heterogeneous nucleation (a single CO molecule?) is reached and the time at which the H_2 cluster is solidified, and one would expect the maximum observed cluster size to be smaller than the number of collisions with CO molecules, a linear function of the scattering-gas pressure, and independent of the length of the scattering region. For the data shown in Fig. 1, the maximum observed cluster size does appear to be approximately a linear function of the scattering-gas pressure. Additional measurements, including measurements for another scattering-region length, are in progress.

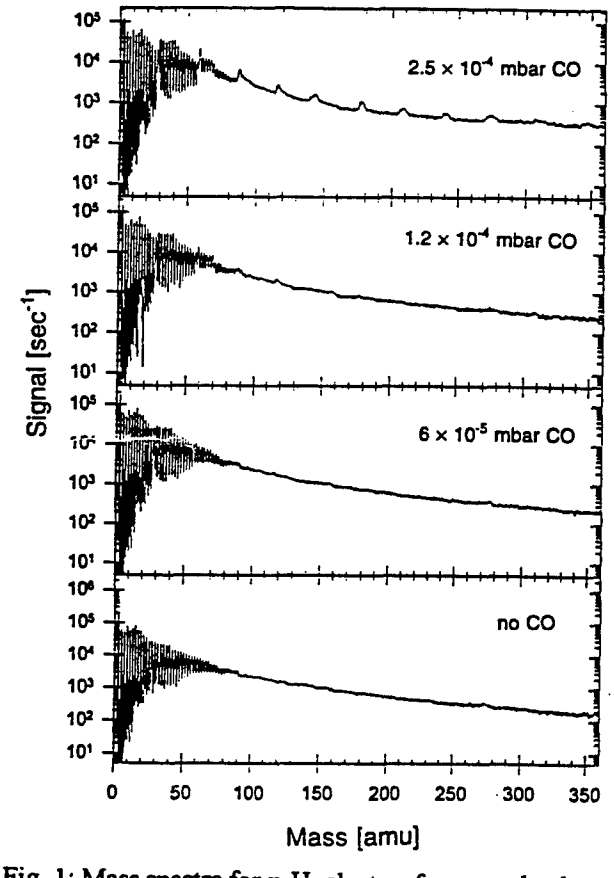

Fig. 1: Mass spectra for p-H_2 clusters for several values of CO pressure in the scattering chamber

The CO mobility required to produce CO clusters of the size observed here argues strongly in favor of the H_2 droplets being liquid until "contaminated" by the embedded CO. This evidence in favor of a liquid state maintains hope for seeing superfluid properties in metastable supercooled H_2 clusters.

References

[1] E.L. Knuth, B. Schilling and J.P. Toennies, *Liquid Clusters from Metastable Expansions: Quest for Superfluid H_2*, Rarefied Gas Dynamics (A.E. Beylich, ed.) 1035-1041. New York: VCH Verlagsgesellschaft mbH, 1991.

[2] T.P. Barrera, E.L. Knuth, L.S. Wong, F. Shünemann and J.P. Toennies, *Supercooled Liquid Clusters in Molecular Beams: Prospects for Superfluid H_2*, Rarefied Gas Dynamics (B.D. Shizgal and D.P. Weaver, eds.) 267-276. Washington, D.C.: AIAA, 1993. See also E.L. Knuth, F. Schünemann and J.P. Toennies, *Supercooling of H_2 Clusters Produced in Free-Jet Expansions from Supercritical States*, J. Chem. Phys. 102:6258-6271, 1995.

[3] B. Schilling, *Molekularstrahlexperimente mit Helium-Clustern*, Dissertation. Göttingen: University of Göttingen, 1993.

[4] J.I. Steinfeld, J.S. Francisco and W.L. Hase, *Chemical Kinetics and Dynamics*. Englewood Cliffs: Prentice Hall, 1989.

[5] S.K. Friedlander, *Smoke, Dust and Haze*. New York: Wiley, 1977.

[6] L.S. Bartell, L. Harsanyi and E.J. Valente, *Phases and Phase Changes of Molecular Clusters Generated in Supersonic Flow*, J. Phys. Chem. 93:6201-6205, 1989.

Electron Attachment to Ozone, Oxygen Clusters and Nitric Oxide Clusters *

G. Senn[1] S. Matejcik[2], J.D. Skalny[2], E. Illenberger[3], N. Mason[4], Y. Chu[6], A. Stamatovic[5], P. Scheier[1], T.D. Märk[1]
[1] Inst. für Ionenphysik, Universität Innsbruck, Austria
[2] Dept. Plasma Physics, Mlynska dolina, Bratislava, Slovakia
[3] Inst. Phys. Chemie, FU-Berlin, Germany
[4] London University Collage, United Kingdom
[5] Inst. Phys. Meteorology, Beograd, Yugoslavia
[6] Anhui Institute of Optics and Fine Mechanics, Hefei, Anhui, P.R. China

1 Introduction

Electron attachment studies are of fundamental importance to the understanding of electron-molecule and electron-cluster interaction and the mechanisms of negative ion formation. In addition these studies are important for the elucidation of atmospheric processes. It is known, that NO is involved in the destruction of ozone in the lower stratosphere. Besides this the catalytic destruction of ozone is also subject to dissociation by photons and electrons. As electron attachment and the properties of anions are involved in these processes we have recently started to study in detail, and with high accuracy the attachment cross section of some of these molecules and respective clusters.

2 Experimental

The measurements were carried out with a crossed beam experiment using a trochoidal electron monochromator (TEM) as the primary electron beam source. The best energy resolution achieved is about 5 meV (FWHM) and electron energies close to zero are possible. In combination with either a temperature controlled effusive molecular beam source or a supersonic nozzle source and with a quadrupole mass spectrometer for anlaysis of the anions produced, electron attachment spectra can be measured as a function of electron energy and target beam properties such as gas temperature and target composition. The zero energy position of the energy scale and energy resolution was calibrated and checked with the known cross section curve for Cl^- from CCl_4.

3 Results and discussion

3.1 Electron attachment to oxygen clusters

The measured relative attachment cross section function of the production of O_2^-, $(O_2)_2^-$ and $(O_2)_3^-$ in the low energy regime produced via reaction

$$(O_2)_n + e \longrightarrow (O_2)_m^- + \text{neutral products} \quad (1)$$

exihibits the same characteristic behaviour for all measured $(O_2)_m^-$ ions, i.e., the cross section is largest at about zero energy and then strongly decreases with increasing energy. Moreover, the decreasing cross section is structured by three additional peaks (1,2,3) whose maxima appear to lie (within the error bar of $\pm$10 meV) in all cases at the same energy. This strong decrease is compatible with the energy dependence predicted for s-wave scattering. Thus we conclude that the present observation indicates that s-wave electron capture is a likely mechanism in the electron attachment to oxygen clusters. After the initial s-wave capture of the electron by the entire $(O_2)_n$ cluster the energy gain from the positive electron affinity of O_2 (451$\pm$7 meV) leads, via monomer evaporation, to the final reaction product. Peaks at higher electron energies are attributed to the attachment of an incoming electron to a single oxygen molecule within the target cluster via direct Franck-Condon transition from the ground vibrational state to a vibrational excited state of the ensuing anion. Subsequent collisional stabilization of this anion within

*Abstract 7031 submitted to the 21st International Symposium on Rarefied Gas Dynamics, Marseille, France, July 26-31, 1998

number of peak	O_2^-	$(O_2)_2^-$	$(O_2)_3^-$	mean value	theoretical value
1-2	111	111	118	113	113
2-3	106	123	99	109	111

Table 1: Spacings between the peaks

the cluster enviroment to a vibrational state below the ground state of O_2 gives a stable O_2^-. Identification of these excited vibrational states populated in the anions can be achieved (besides other means [1]) by analysing the spacings between the different peaks, assuming similar spacings in the cluster and the monomer. The spacings between peak 1,2,3 fits to the vibrational levels 7,8,9 in the O_2^-.

3.2 Electron attachment to nitric oxide clusters

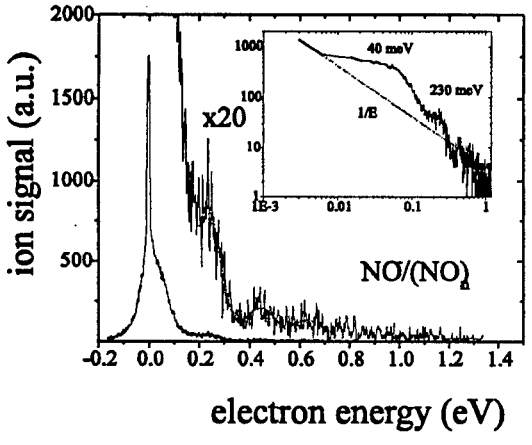

Figure 1: Measured NO^- signal as a function of the electron energy

The system NO is similar to O_2 in the way that the extra electron occupies an antibonding MO. However the adiabatic electron affinity of NO is only 26±5 meV and thus is considerably smaller than that of O_2. In contrast to O_2, NO has a dipole moment (0.16 D). In contrast to the O_2 an appreciable contribution of direct inelastic scattering may contribute to vibrational exitation of neutral NO. The relative attachment cross section for NO^- formation shows a very sharp peak close to zero eV and a series of further weak peaks having a spacing of about 190 meV. The zero energy peak is interpreted as s-wave capture. The spacings between the other peaks do not fit to the vibrational spacings in neutral NO (236 meV) or NO^- (159 meV). The vibrational frequency of a molecule bound in a cluster may be perturbed, in particular in the presence of appreciable coupling as in the case for a molecular ion like NO^-. Due to the very low adiabatic electron affinity of NO and the strong anion dimer bond, NO^- cannot be a result of evaporative attachment reaction of the form $e^- + (NO)_n \longrightarrow NO^- + (n-1)NO$. It is known that the weakly bound complex $NO^- \cdot NO$ correlates (probably without barrier) to a $[ONNO]^-$ which is about 2eV below the $NO^- \cdot NO$ system. The required energy to form a NO^- is possibly produced by an exothermic intracluster reaction which uses the $[ONNO]^-$ as catalyst.

3.3 Electron attachment to ozone

Electron attachment to ozone leads to the production of O^- and O_2^-. The present dissociative electron attachment cross section O_2^-/O_3 is in good agreement with measurements from Allan et. al. [2] disregarding a small difference in calibration of the electron energy. In the case of the formation of O^- from O_3 we measure the same three resonances as Allan et. al. [2], but we observe an additional "zero energy peak". This peak has an $1/E$ energy dependence which suggests a s-wave capture process. Due to the relative small intensity and the narrow structure this zero energy peak is only seen with the good energy resolution available with the present experimental setup.

Work was partially supported by FWF, ÖAW/EURATOM, ÖNB, BMWV , Vienna, Austria

References

[1] S. Matejcik et. al. Phys. Rev. Lett. **77** 18 (1996)

[2] M. Allan et. al. J. Phys. B. **29** (1996) 3487-3495

MOLECULAR BEAM SESSION MB 9

Diffraction, Polarizability, Fragmentation,
and Theoretical Properties of Clusters

CHAIR: J. Baudon (Paris-Nord)

ROOM: LAVOISIER
THURSDAY, JULY 30, 1998
16:15 - 18:25

Diffraction of Cluster Beams from Nano-Transmission Gratings *

Wieland Schöllkopf and J. Peter Toennies
Max-Planck-Institut für Strömungsforschung, Göttingen, Germany

1 Introduction

Van der Waals clusters produced in molecular beam expansions are characterized by a broad size distribution. Experimental techniques are therefore needed to select clusters of well defined sizes. With conventional mass spectrometers a size selective detection of these clusters is not possible because of cluster fragmentation and dissociation in the ionization process. To circumvent this problem we use an atom optical experiment in which cluster beams are diffracted by a 100-nm-period transmission grating leading to a non-destructive mass selection and detection of small clusters [1].

This method applied to small clusters of ^{4}He allowed for the unambiguous detection of He_2 and He_3 [1]. With a predicted binding energy of only 1.3 mK and a mean nuclear distance of about 55 Å the helium dimer is thought to be the weakest bound molecule. The bond is sufficiently weak to support an Efimov state in He_3. Efimov states are three particle bound states which occur only if the corresponding two particle system is sufficiently weakly bound.

2 Experimental Technique

A scheme of the experimental setup is shown in Fig. 1. The molecular beam is produced by expanding pure gas from a source chamber through a thin walled, 5 μm wide orifice into high vacuum. The temperature T_0 and the pressure P_0 inside the source can be varied from 4 to 300 K and 0 to 200 bar, respectively. After passing the skimmer the beam is collimated by two 10 μm wide slits to reduce the angular divergence before it impinges on the transmission grating that can be rotated to achieve off-normal incidence. The grating has a period of 100 nm and a nominal slit width of 50 nm. It is made out of silicon nitride by Tim Savas and Hank Smith from MIT, USA using the method of achromatic interferometric lithography [2]. The far-field diffraction pattern is measured by rotating the mass spectrometer detector precisely around an axis parallel to the grating slits with a 25 μm wide entrance slit in order to achieve a high angular resolution ($\approx 7 \cdot 10^{-5}$ rad).

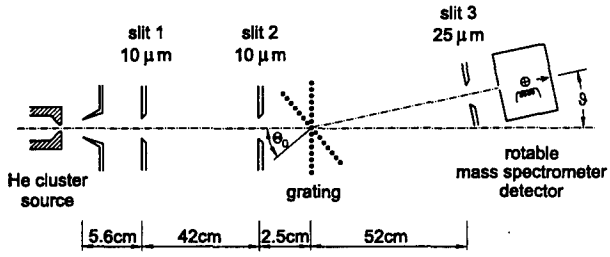

Figure 1: Experimental setup for the diffraction of a helium cluster beam by a 100-nm-period transmission grating. The grating can be inclined by rotating by Θ_0 to obtain narrower slits.

3 Diffraction of small helium clusters

The mass selection of the small clusters is based on the fact that clusters and atoms in the molecular beam have the same mean velocity determined mainly by T_0. Therefore, the de Broglie wavelength of a particular cluster He_N is inversely proportional to its mass $N \cdot m_{He}$. In the Fraunhofer limit the first order diffraction angles are thus inversely proportional to the mass leading to a separation of the clusters. Since only those clusters contribute to the diffraction pattern that do not hit the grating bars the technique is essentially non-destructive.

Fig. 2 shows a diffraction pattern of a helium cluster beam at $T_0 = 6$ K and $P_0 = 1$ bar including first order peaks of He_N, $N = 3, 4, 5, 6, 7$, measured with the mass spectrometer set to the He^+-ion mass (upper curve) and to the He_2^+-ion mass (lower curve). The comparison provides information on the fragmentation behavior in electron impact ionization.

The dependence of the mole fractions of small helium clusters in the molecular beam on P_0 shows an

*Abstract 6966 submitted to the 21st International Symposium on Rarefied Gas Dynamics, Marseille, France, July 26-31, 1998

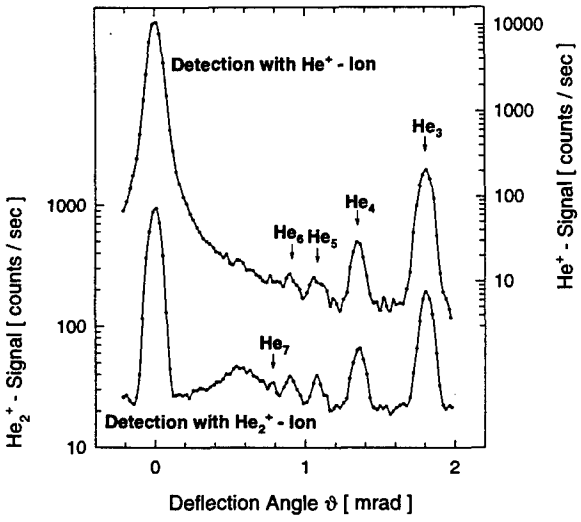

Figure 2: Mass analysis of a helium cluster beam by transmission grating diffraction showing the forward peak at $\vartheta = 0$ and the first order diffraction peaks of He_N ($N \geq 3$). The more intense He and He_2 peaks are off scale to the right.

interesting behavior. With increasing pressure first dimers then trimers and then tetramers are formed. The fraction of dimers shows a maximum when the trimer fraction increases. The later, in turn, reaches a maximum when the tetramer fraction increases. This behavior is decribed by a kinetic model of rate equations of the cluster formation in the jet expansion. The model allows for a microscopic understanding of the initial stages of condensation.

The intensity ratios of the n-th diffraction order divided by the 1st order for a given cluster depend on the respective molecular wavefunction i.e. the finite size of the cluster [3]. Therefore, it is possible to determine the sizes of He_2 and He_3 experimentally by a quantitative evaluation of the diffraction intensities. As a first approximation Kirchhoff's optical theory for an ideal grating was used to gain the mean nuclear distance of He_2 and the diameter of He_3 [4]. More refined calculations are in progress.

4 Diffraction of rare gas atoms, CH_3F and CHF_3 molecules

To investigate the influence of the van der Waals interaction between the beam particles and the silicon nitride grating bars on the diffraction patterns atomic beams of He, Ne, Ar, and Kr as well as molecular beams of CH_3F and CHF_3 were diffracted from normal and inclined gratings. As can be seen in Fig. 3 in addition to the anticipated decrease of the diffraction angles with increased mass of the particle there is a strong change in the relative intensities of the 2nd and 3rd order peaks. This behavior deviates from classical optics where, according to Kirchhoff's theory in the Fraunhofer limit, the diffraction pattern is determined solely by the Fourier transform of the grating.

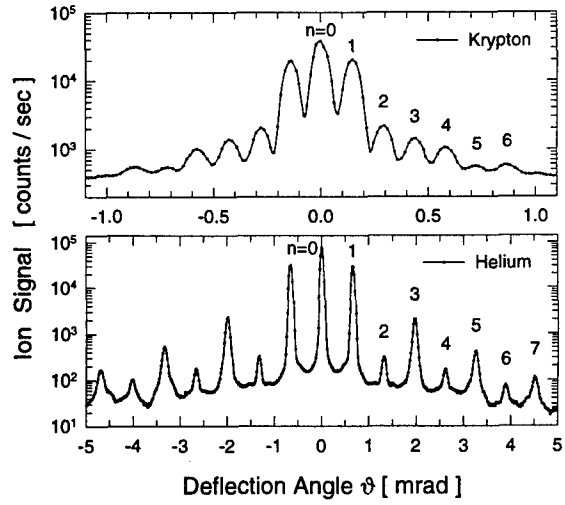

Figure 3: Diffraction patterns of atomic beams of He and Kr at $T_0 = 300\,K$ from the same grating at normal incidence.

By inclining the grating to off-normal incidence the effective widths of the grating slits can be reduced to less than 1 nm and the effective period can be decreased by more than 30%. As a result the relative intensities of the diffraction orders are altered and the diffraction angles are increased significantly. Using the variable slit widths it has been possible to filter larger clusters ($N \geq 10^4$) and determine their size distributions [5].

References

[1] Schöllkopf W. and Toennies J.P., Science, Vol.266, pp.1345, 1994.

[2] Savas T.A. et al., J. Vac. Sci. Technol. B, Vol.13, No.6, pp.2732, 1995.

[3] Hegerfeldt G.C. and Köhler T., Phys. Rev. A, Vol.57, No.3, pp.2021, 1998.

[4] Schöllkopf W. and Toennies J.P., 17th Symposium on Molecular Beams, Paris-Orsay, June 2-6, 1997.

[5] Schöllkopf W., Toennies J.P., Savas T.A., and Smith H.I., submitted to J. Chem. Phys. 1998.

Static dipole polarizability and permanent dipole of free clusters *

Ph. Dugourd[1], E. Benichou[1], R. Antoine[1], D. Rayane[1], B. Vezin[1], M. Broyer[1],
C. Ristori[2], F. Chandezon[2], B. A. Huber[2], C. Guet[2]
[1] Laboratoire de Spectrométrie Ionique et Moléculaire,
UMR 5579, CNRS and Université Lyon 1, Bât 205,
43 Bd du 11 Novembre 1918, F-69622 Villeurbanne Cedex, France
[2] DRFMC - Service des Ions, des Atomes et des Agrégats,
C E A Grenoble, 17 rue des Martyrs, F–38054 Grenoble Cedex 9, France

To what extent do clusters made of only a few atoms can behave as metallic objects ? The static dipole polarizability is a basic observable for discussing such a question since it is sensible to the effectiveness of the delocalization of valence electrons as well as the structure and shape of the cluster. We have recently built an apparatus to measure the static dipole polarizability of neutral clusters produced in a molecular beam.

First experiments have been carried out on lithium clusters. Despite numerous investigations of alkali metal clusters, polarizability measurements were only available for sodium clusters and for selected sizes of potassium clusters [1], while nothing was known about lithium clusters. However, the static and dynamic response of lithium clusters to electric fields is in many respects the most interesting and puzzling. Polarizabilities of sodium and lithium atoms are almost equal while corresponding values for the bulk differ by 50 per cent. Moreover, several experiments have shown that the optical response of lithium clusters is significantly redshifted as compared to the classical prediction for a finite metallic sphere. For a metallic sphere, the Mie frequency is directly related to the polarizability of the sphere. A direct determination of the electric polarizability is therefore crucial both for understanding the size evolution and for the interpretation of the optical response.

Briefly, the polarizability measurements are made by deflecting a well collimated beam through a static inhomogeneous transverse electric field (Fig. 1). Clusters are produced in a supersonic beam. Metal vapor (0.1 bar pressure) is co-expanded with argon (3 bars pressure) through an aperture of 100

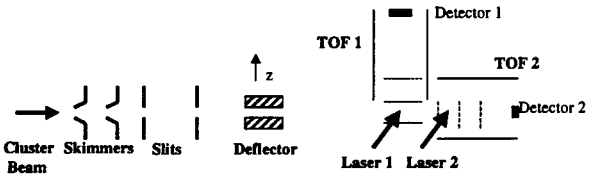

Figure 1: Schematic of the experiment

μm diameter. The colinear part of the beam is extracted by a skimmer and collimated by two 0.4 mm slits. The distance between the two slits is 1 m. The beam passes along the axis between the two cylindrical pole faces of a 15 cm long deflector. A difference of potential of 30 kV can be applied between the two pole pieces which are 1.7 mm apart. With the electric field magnitude along the z-axis denoted by E, the force acting on the passing cluster is

$$F_z = \alpha E \frac{dE}{dz}. \qquad (1)$$

Outcoming clusters are ionized by a low flux laser (λ = 308 nm or λ = 266 nm) at a distance of 1 m out of the deflector, and are subsequently mass selected in a time of flight (TOF 1) mass spectrometer. The set of voltages applied in the TOF is adjusted so that the arrival time on the detector is sensitive to the ionization position. The polarizability is proportional to the measured deflection in the z-direction: $\Delta z = KF_z/(Mv^2)$, where M is the mass of the cluster, v its velocity, and K a geometrical factor. The velocity is determined with a coaxial TOF (TOF 2).

The measured static dipole polarizabilities per atom for lithium clusters and sodium clusters are plotted in Fig. 2. For sodium, the polarizabilty per atom decreases slowly as a function of the cluster size.

*Abstract 6955 submitted to the 21st International Symposium on Rarefied Gas Dynamics, Marseille, France, July 26-31, 1998

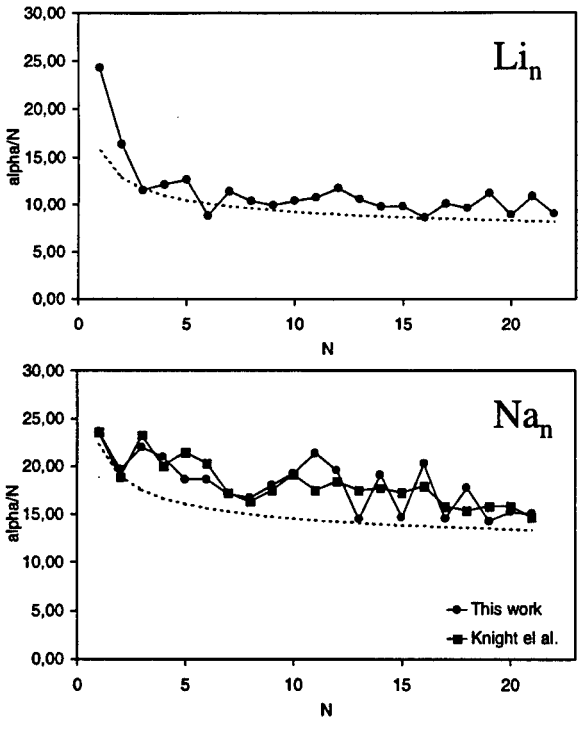

Figure 2: Static dipole polarizability per atom of lithium and sodium clusters as a function of the number of atoms in the cluster (Å^3). Experimental values are compared to the value calculated for a classical metallic sphere (dashed lines)

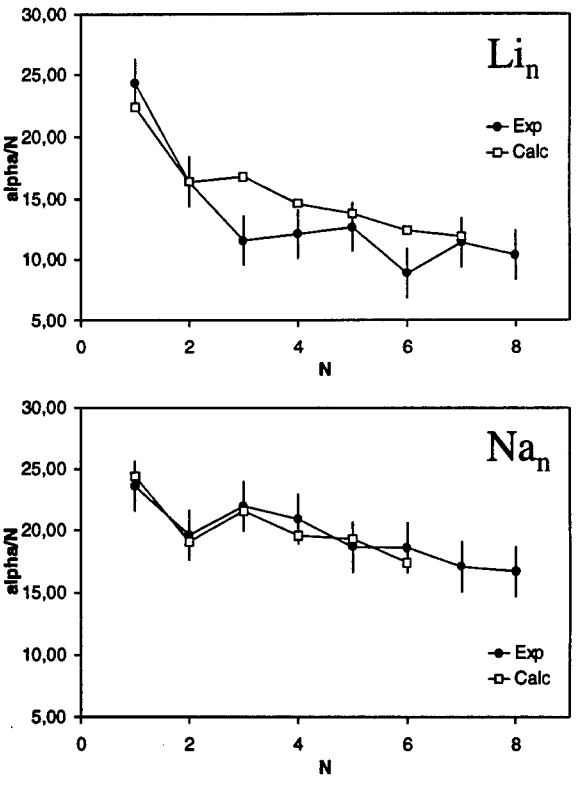

Figure 3: Calculated (empty squares) and experimental (black circle) static dipole polarizability per atom for lithium and sodium clusters as a function of the number of atoms in the cluster. (Å^3).

For lithium a sharp decrease between size 1 and size 3 is observed. The calculated values for classical metallic spheres :

$$\alpha = (N^{1/3} r_s + \delta)^3, \qquad (2)$$

where r_s is the Wigner-Seitz radius (1.75 Å, and 2.12 Å, for lithium and sodium respectively) and δ is the electronic spill-out (0.75 Å, and 0.69 Å, for lithium and sodium), are plotted in Fig. 1. For sodium, the experimental values, although globally higher, are relatively close to the calculated ones. For lithium, excepted for very small sizes, the same agreement is observed. This suggests that the metallic behavior already appears for sizes as small as 3 or 4. In conclusion, the static response of lithium clusters to an electric field is close to the response expected for a metallic sphere although the dynamic response is very different. The consistency of the present results with previous optical absorption measurements will be discussed at the conference.

Fundamental changes in the electronic properties of lithium clusters occur for very small sizes. To understand these changes we have performed Density Functional Theory calculations. Fig. 3 compares the calculated values to the experimental values both for sodium and lithium clusters (n=1 to 8). The overall agreement is very good. The analysis of the geometries and of the electron density maps allows to understand the specific electronic properties of lithium clusters.

We also present very recent measurements of permanent dipoles on small heterogeneous atomic clusters.

References

[1] W.D. Knight, K. Clemenger, W.A. de Heer, and W.A. Saunders, Phys. Rev. B **31**, 2539 (1985).

Properties of Clusters from the Random Matrix Theory *

V. M. Akulin
Laboratoire Aimé Cotton, CNRS II, Bâtiment 505, 91405 Orsay Cedex, France

The first principles theoretical consideration of quantum systems becoms more and more difficult with the increasing number of particles comprising the object, since the motion of such a system becomes chaotic and cannot be separated to independent motions of each of degrees of freedom. At the same time the number of the degrees of freedom may still be too small to ignore the statistical fluctuations of variables and employ the thermodynamical description based on the Gibbs distribution. Random matrix theory is a convinient tool for analysis of such objects. It makes use of the fact, that the universal properties of chaotic motion govern the main observable characteristics of the complex systems, in other words, the dynamics of a complex physical object resembles in main features the dynamics of another complex system, even if the latter has a very different physical origin. Recent results concerning optical and thermodynamic properties of metallic clusters and silicon powders obtained with the help of the random matrix theory will be reported. This analysis is done in the spirit of earlear works on polyatomic molecules in intense laser fields[1].

Indeed, the traditional models of Quantum Chemistry and Condensed Matter Physics [2] describe clusters of $N \sim 10 - 1000$ atoms at the limits of their applicability. The adiabatic separation of the electronic and nuclear degrees of freedom fails at $N \gtrsim 10$, when a typical distance between neighboring electronic terms $\Delta E[a.u.] \sim 1/N$ becomes comparable or smaller than a typical non-adiabatic interaction $V_{na}[a.u.] \sim \Lambda$, suggested by the Born-Oppenheimer parameter $\Lambda = (m_e/m_{at})^{1/4} \sim 1/10$. The concept of weakly interacting quasi-particles fails, in turn, for small clusters of $N \lesssim 1000$ atoms, when the mean free path of the electrons $l_f[a.u.] \sim \Lambda^{-1} \sim 10$ exceeds a typical cluster radius $R[a.u.] \sim N^{1/3}$.

A conceptually simple random matrix model[3], which considers the clusters as disordered pieces of solids, fills the gap between consistent molecular and the solid state descriptions. The approach relies on the transformation rule for an arbitrary quantum system perturbed by a random matrix[4]. There is a number of problems where the random matrix approach is very usefull: calculation of the optical absorption of alkali metal clusters of $N \sim 20$ atoms or determination of their dissociation energies are two of the examples. Another example is the optical luminescence of the porous silicon silicon nanostructures, [5] which is usually explained either by the effect of quantum confinement, or by the influence of the interface states. However, the

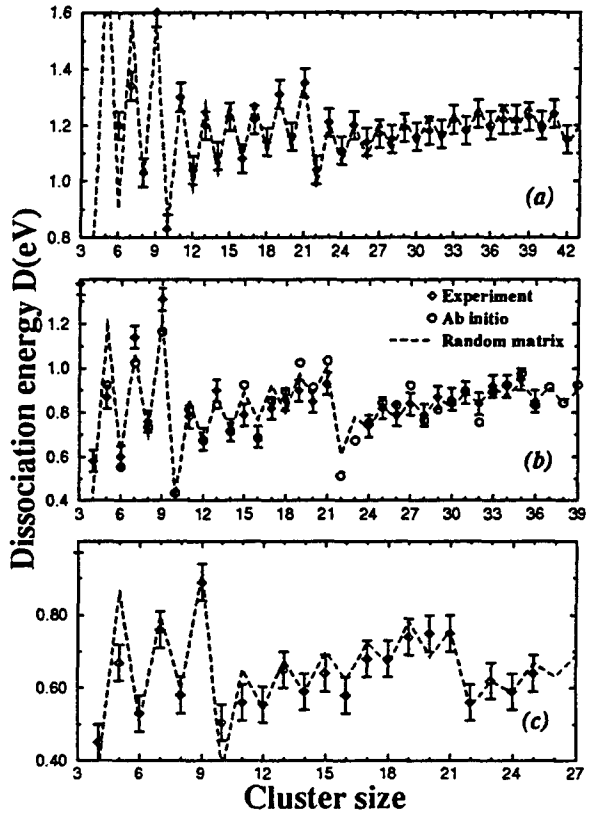

Figure 1: The dissociation energies of cluster ions for (a) Li,(b)Na, (c)K in function of size calculated with the help Random Matrix model along with the experimental data and *ab initio* calculations.

*Abstract 6936 submitted to the 21st International Symposium on Rarefied Gas Dynamics, Marseille, France, July 26-31, 1998

universality of the phenomemon suggests to look for a more general model.

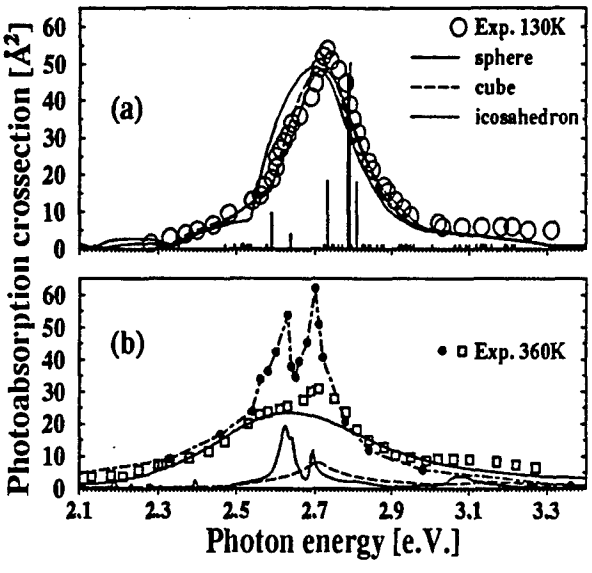

Figure 2: (a) Profiles of the absorption line in Na_{21}^{+}: Experimental at $T = 130K$ (circles) and the calculated for the spherical clusters: (solid line) perturbed by a cubic (doted line) or an icosahedral (dashed line) crystalin structure. (b) Two experimental profiles (squares and filled circles) at $T = 360K$ in slightly different conditions, and the simulated spectrum (solid line). Photo absorption (not to scale) from the first electronically excited state for $T = 50K$ (dotted line) and $T = 150K$ (dashed line).

The results of *ab initio* calculations of the dissociation energies of alkali metal clusters can be reproduced in the framework of the Random Matrix theory Fig.1 and give a very good agreement with the experimental data[6]. For the optical absorption spectra of the clusters it not only yields the correct positions of the spectral lines, but also allows one to simulate the line shapes, and thereby it reveals information about the clusters structure hidden in the optical absorption profiles Fig.2. Transformation of the optical spectra with an increase of the temperature[7] finds its explanation as well. A rather general view on the silicon luminescence mechanism could also be based on the random matrix model. Ballistic propagation of electrons and holes is randomly perturbed in silicon powders by the scattering at boundaries or interfaces, which lifts up the optical selection rules and thereby transforms the luminescence spectra as it is shown in Fig.3.

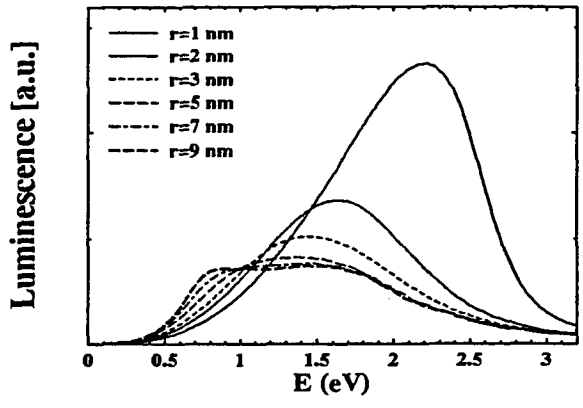

Figure 3: Silicon luminescence spectrum for different sizes of grains for the initial energy E=3.2 eV.

References

[1] V. M. Akulin and N. V. Karlov *Intense Resonant Interactions in Quantum Electronics*, Springer-Verlag, Berlin, 1991.

[2] G. Rajagopal, R. N. Barnett, and U. Landmann, Phys. Rev. Lett. **67**,727 (1991); M. Brack, Rev. Mod. Phys. **65**, 677 (1993).

[3] V. M. Akulin, C. Bréchignac, and A. Sarfati, Phys. Rev. Lett. **75**, 220 (1995).

[4] V. M. Akulin, Phys. Rev.**A 48**, 3532 (1993).

[5] L. T. Canham, Appl. Phys. Lett.,**57**,1046 (1990); Y. Kanemitsu, T. Ogawa, K. Shiraishi, and K. Takeda, Phys. Rev. **B 48**, 4883 (1993); S. Schupper, S. L. Friedman, M. A. Marcus, D. L. Adler, Y.-H. Xie, F. M. Ross, T. D. Harris, W. L. Brown, Y. J. Chabal, L. E. Brus, and P. H. Citrin, Phys. Rev. Lett., **72**, 2648 (1994); M. Voos, Ph. Uzan, C. Delalande, G. Bastard, and A. Halimaoui, Appl. Phys. Lett. **61**, 1213 (1992).

[6] C. Bréchignac, H. Bush, Ph. Cahuzac, and J. Leygnier, J. Chem. Phys. **101**, 6992 (1994).

[7] C. Ellert, M. Schmidt, C. Schmidt, T. Reiners, and H. Haberland, Phys. Rev. Lett. **75**, 1731 (1995).

Collision induced fragmentation of molecules and small Na_n^+ clusters: Competition between impulsive and electronic mechanisms *

J.A. Fayeton, M. Barat, J.C. Brenot, H. Dunet and Y.J. Picard
Laboratoire des Collisions Atomiques et Moléculaires
Bat. 351, Université Paris-Sud, 91405 Orsay cedex, France

1 Introduction

The interaction between particles and matter is governed by two basic mechanisms either via excitation of the electron cloud (EM for electronic mechanism) or via momentum transfer during collisions with the atomic cores (IM for impulsive mechanism). The collision-induced dissociation of molecules is a typical process in which these two mechanisms can be well identified. Extension of such investigation to clusters allows studying the more complex dissociation processes through the size dependence of the fragmentation patterns.

2 Na_2^+ dissociation

Fragmentation of small mass selected Na_n^+ (n<10) cluster ions induced by collision with He has been studied at 66 eV centre of mass energy, in a crossed beam experiment. The experimental technique [1] is based on the measurement of the velocity vectors of the ionic and neutral fragments that are detected in coincidence on two position sensitive detectors. This method provides information on the various dissociation parameters such as E_{rel}, the relative kinetic energy of the fragments, and the angles defining the orientation of the dissociation axis as a function of χ the deflection angle of the centre of mass of the cluster. Actually the χ angle dependence reflects the importance of the momentum transferred in the collision and therefore is a key parameter for analysing the impulsive mechanism.

Figure 1 illustrates how the IM and EM are identified in the $E_{rel}(\chi)$ correlation pattern for the simple case of collision induced dissociation of a diatomic molecule. Structures II and III appearing at $\chi \approx 0$ deg, without significant momentum transfer, signs EM corresponding to the excitation of the active $3s\sigma_g$ electron of Na_2^+, towards repulsive (III) and quasi-bound states (II). On the other hand, structure I at large χ angle reveals the impulsive mechanism as shown by the stretching of the contour along the $E_{rel}(\chi)$ curve given by a simple kinematic model describing a He Na binary elastic collision. In this model E_{rel} is given by :

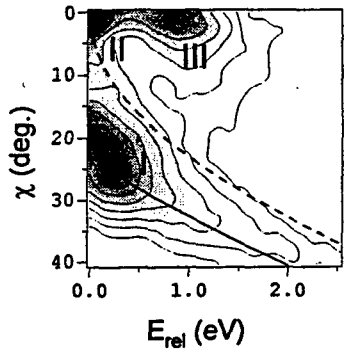

Figure 1: Typical contour maps illustrating the two basic CID mechanisms in the Na_2^++He collision at 66 eV collision energy. See text for explanation.

$$E_{rel} = E_T - E_D + E_{int}$$

where E_{int} is the rovibrational energy of the incident Na_2^+ ion and $E_D = 0.96$ eV the ground-state binding energy. The dependence of the transmitted energy E_T with χ can be calculated with :

$$E_T = \frac{M_T^2}{(M_T + M_{Na})^2} E_0 \sin^2 \frac{\chi_1}{2}$$

$$\tan \chi = \frac{\sin \chi_1}{M_T \backslash (M_T + 2M_{Na}) + \cos \chi_1}$$

The dissociation occuring in the collision plane, proved by the experiment, is also a typical signature

*Abstract 6951 submitted to the 21st International Symposium on Rarefied Gas Dynamics, Marseille, France, July 26-31, 1998

of the IM. This simple analysis has been theoretically confirmed by calculations based on a non adiabatic quantum molecular dynamics approach (NA-QMD) developed by the Dresden group [2]. However, even for such simple molecules more intricate dissociation mechanism also appears which combine IM and EM as discussed in [3].

3 Clusters fragmentation

For clusters, investigation of fragmentation mechanisms requires in addition to the combination of IM and EM, consideration of multiple collisions which in particular modify the simple $E_{rel}(\chi)$ relationship discussed above. The experimental findings can be summarized as follows. The dominance of IM mechanisms is clearly established. However a detailed analysis of $E_{rel}(\chi)$ and other correlations between the various parameters suggest several types of impulsive mechanisms schematically shown on figure 2 : (*i*) a one-step process in which the hit Na^+ core is directly ejected as a neutral particle without further interaction with the Na^+_{n-1} fragment or (*ii*) a two-step processes in which the transferred momentum is shared among the Na^+ cores through multiple intra-cluster collisions, a mechanism which dominates at low eV energy [4]. These two mechanisms are characterized by a large scattering of the dissociating cluster. But while in mechanism (*i*) the transferred energy is fully transformed in relative kinetic energy of the fragments, in mechanism (*ii*) the transferred energy is given to all degrees of freedom of the cluster, resulting in smaller relative kinetic energy. An additional two-step mechanism (*iii*) seems to involve multiple interactions between the cluster and the target as indeed suggested by the smaller scattering of the fragments and the lost of the collision plane reference in the spatial distribution of the fragments. Figure 2 shows that the relative contribution of both multi-step processes increases as a function of the size of the cluster. Notice also that process (*iii*) and (*ii*) become dominant as soon as the cluster geometry is no longer planar (Na^+_5) [5].

4 Conclusion

Up to now, dissociation in two fragments has been fully analyzed and only indirect information on multiple fragmentation has been extracted from the data [6]. In future, extension to the study of multi-fragmentation will be contemplated owing to the development of detectors able to localize several fragments simultaneously.

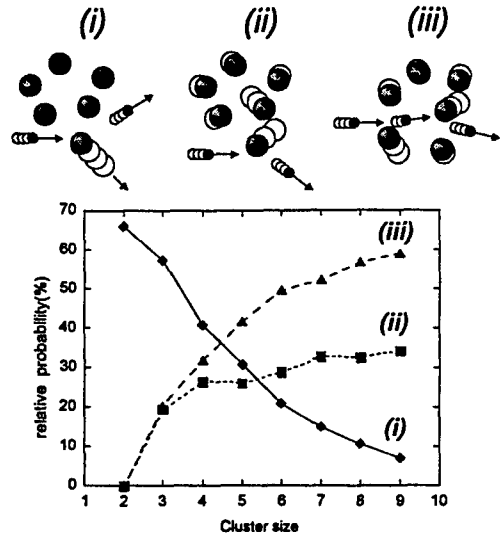

Figure 2: Schemes of the three impulsive mechanisms (see text) and their relative contribution as a function of cluster size. All data are given for a same collision energy.

References

[1] J.A.Fayeton, M. Barat, J.C. Brenot, H. Dunet, Y.J. Picard, R. Schmidt and U. Saalmann, Phys. Rev. A, Vol.57,.1058 1998

[2] U. Saalmann and R. Schmidt, Z. Phys. D. 38, 153, 1996

[3] M. Barat, J.C. Brenot, H. Dunet, J.A. Fayeton and Y.J. Picard, E. P. J. D. 1998, *in print.*

[4] S. Nonose, H. Tanaka, T. Mizuno,. N. J. Kim, K. Someda, and T. Kondow,J. Chem. Phys. 105, 9167, 1996.

[5] V. Bonacic-Koutecky, I. Boustani, M. Guest and J. Koutecky, J. Chem. Phys. 89, 4861, 1988.

[6] M. Barat, J.C. Brenot, H. Dunet, J.A. Fayeton and Y.J. Picard, *to be published,* 1998

Critical behaviour in cluster fragmentation *

B. Farizon[1], M. Farizon[1], M.J. Gaillard[1], F. Gobet[1], C. Guillermier[1],
J.P. Buchet[2], M. Carré[2], P. Scheier[3], T.D. Märk[3]
[1] Institut de Physique Nucléaire de Lyon, Villeurbanne, France
[2] Lab. de Spectrométrie Ionique et Moléculaire, Villeurbanne, France
[3] Institut für Ionenphysik, Leopold Franzens Universität, Innsbruck, Austria

Fragmentation of finite size systems is a wide spread phenomenon in nature, including such diverse phenomena as the break-up of submicroscopic objects or collisions between asteroids. Despite intensive research in various fields of science and technology complete analysis and understanding of fragmentation has not yet been achieved. Fragmentation of atomic or molecular cluster have been investigated by diverse excitation techniques. So far most of the studies concerning cluster fragmentation have been able to determine, besides other properties, average fragment size distributions without information on the size distribution of a single fragmentation event. We present the first account of a cluster fragmentation study involving collisions of high energy hydrogen cluster ions with fullerenes in which all the fragments of all collisions occurring in the experiment are mass analysed on an event by event basis using a novel multi-coincidence technique. The present experiment has been performed with the apparatus shown in Fig.1.

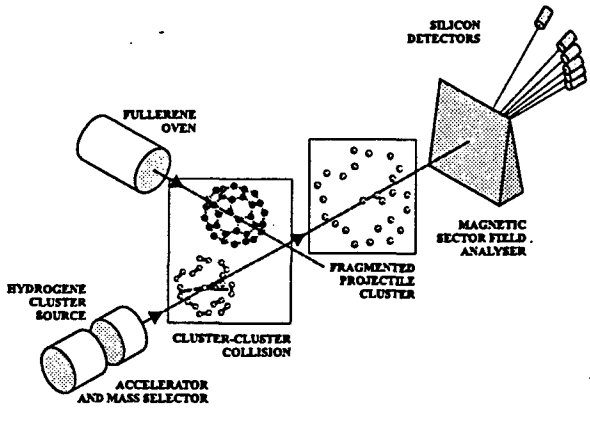

Figure 1: Schematic view of the experimental set-up.

Mass selected hydrogen cluster ions with an energy of 60 keV/u are prepared in a high-energy cluster ion beam facility consisting of a cryogenic cluster jet expansion source combined with a high performance electron ionizer and a two-step ion accelerator. Mass selected high energy projectile beam consisting in the present study of H_{25+} cluster ions is then crossed perpendicular by a C_{60} effusive target beam. One meter behind this collision region the high energy hydrogen collision products (neutrals and ions) are passing a magnetic sector field analyzer. Both, undissociated primary H_{25+} cluster projectile ions and neutral and charged fragments resulting from reactive collisions are then detected with a multi-detector device. This allows us to record simultaneously neutral and charged fragments detected in coincidence for each single collision event.

From the break-up in two fragments to the complete desintegration, we have observed different fragmentation patterns in high energy hydrogen cluster-atom or cluster-cluster collisions (Fig. 2).

In contrast to the earlier collision experiments with a helium target, the fragmentation studies of H_{25+} clusters induced by collision on a C_{60} cluster at high velocity (c/100) do not show a U-shaped fragment mass distribution, but a single power-law falloff with increasing fragment size p, i.e., $p^{-\tau}$ which has been observed with critical exponents in close proximity to the critical exponent 2.6 found in nuclear fragmentation experiments and with predictions (=2.23) from Fischer's droplet model. Although these observations have been taken as a strong hint for the occurrence of critical behaviour reminiscent of a second order phase transition in an infinite system, the mass yield shape alone cannot be considered as a conclusive proof.

*Abstract 6956 submitted to the 21st International Symposium on Rarefied Gas Dynamics, Marseille, France, July 26-31, 1998

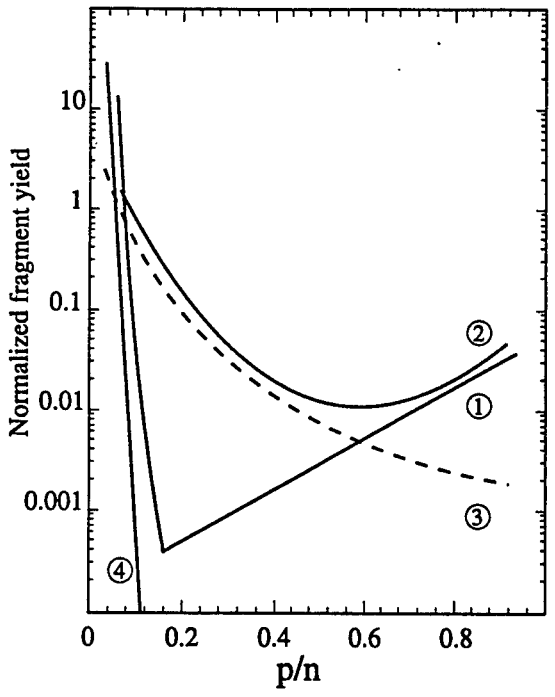

Figure 2 : Schematic representation of normalized fragmentation yield versus normalized fragment size p/n for different fragmentation regime. (1) Evaporation from low energy collisions between H_{n+} cluster ions and atoms after Reuss and coworkers [1]; (2) Bimodal regime (evaporation and multifragmentation) [2]; (3) Multifragmentation regime; and (4) Complete disintegration from high energy beam foil collision experiment with cluster ions.

Using a recently developed multi-coincidence technique for the measurement of the fragment mass distribution observed in the H_{25+} - C_{60} collision, we have been able to obtain a first set of approximately 6000 completely analyzed collision events. The statistical methods based on an event by event analysis of the fragment size distributions - conditional moments as well as scaled factoriel moments - can be applied on the experimental data in order to evidence a critical behaviour in these molecular systems [3].

References

[1] A. Van Lumig and J. Reuss, Int. J. Mass Spectrom. Ion Phys., 27, 197 (1978).

[2] S. Ouaskit, B. Farizon, M. Farizon, M.J. Gaillard, A. Chevarier, N. Chevarier, E. Gerlic et M. Stern, Int. J. Mass Spectrom. Ion Proc., 139, 141 (1994).

[3] V.N. Kondratyev and H.O. Lutz, Z. Phys. D40, 210 (1997).

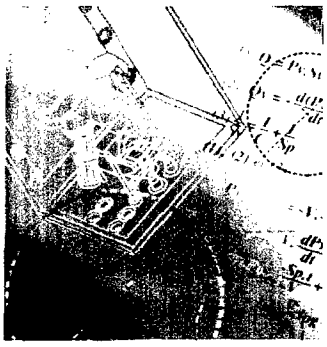

Physiméca technologie

14, rue de la Martinière
91 400 SACLAY
☎ : 01 69 35 17 30
Fax : 01 60 19 34 06

Visitez notre site internet :
http:\\www.physimeca-technologie.fr
Ecrivez nous :
Commercial@physimeca-technologie.fr
Technique@physimeca-technologie.fr

De la pièce mécanique à la machine entièrement automatique...

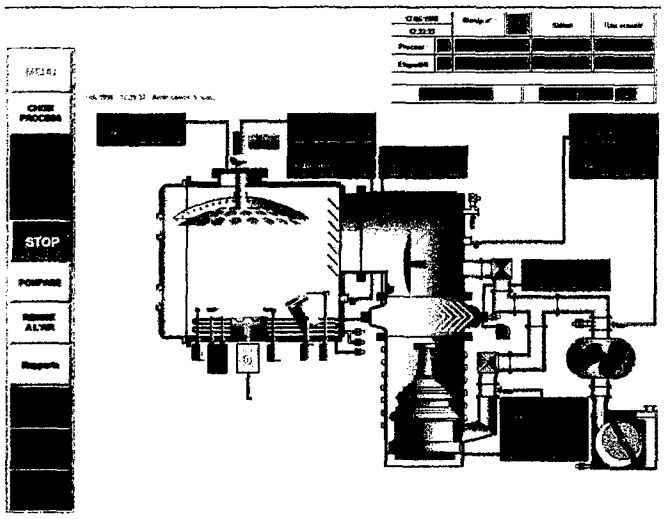

Modernisation d'équipement :automatisme et supervision didactique

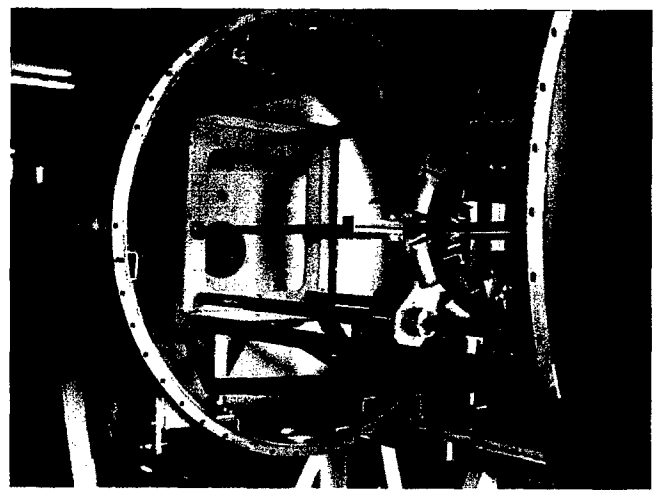

Equipement pour la physique des particules

Quatre métiers à votre service :

Bureau d'études : Conception et élaboration des dossiers de plans, calculs des systèmes de pompage, des structures, calculs thermiques...

Atelier Chaudronnerie/Mécanique : Réalisation des pièces sur plans. Montage des équipements.

Atelier Electrique : Réalisation des schémas électriques, programmation automates et supervision, câblage des équipements.

Service Qualité : Mise en place d'un plan Assurance-Qualité basé sur le référentiel ISO 9001. Définition des points de contrôles et d'arrêts, avant, pendant et en fin de fabrication.

... nous réalisons l'équipement adapté à vos besoins.

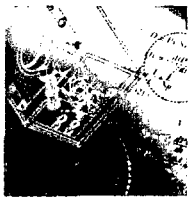

Physiméca technologie

DOMAINES D'APPLICATIONS

Semiconducteurs

Equipements de gravures
et de dépôts sous vide,
Implantation de matériels dans des bâtis existants,
Modernisation des automatismes.

Physique

Ensembles mécaniques
pour l'instrumentation scientifique,
Automatismes...

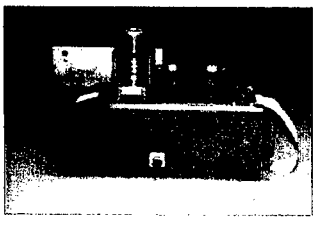

Optique

Equipements de dépôts sous vide,
Bancs de tests...

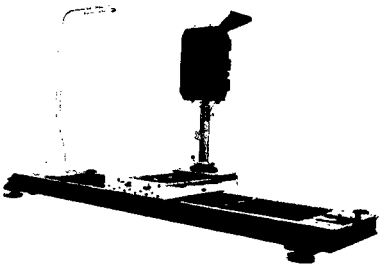

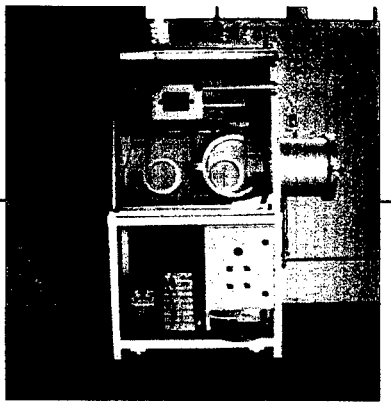

Nucléaire

Enceintes à vide,
Enceintes de confinement
(boîte à gants)...

Transport

Equipements de maintenance

Et tout autre domaine...

http:\\www.physimeca-technologie.fr
✍ Commercial@physimeca-technologie.fr ou Technique@physimeca-technologie.fr

MOLECULAR BEAM SESSION MB 10

Gas-Surface II: Deposition, Nanostructure Fabrication, Epitaxy, and Carbonization on Surfaces

CHAIR: S. Stolte (Amsterdam)

ROOM: LAVOISIER
FRIDAY, JULY 31, 1998
9:15 - 10:55

Molecular Beams of Silicon Clusters and Nanoparticles Produced by Laser Pyrolysis of Gas Phase Reactants *

F. Huisken, M. Ehbrecht, B. Kohn
Max-Planck-Institut für Strömungsforschung, Bunsenstr. 10
D-37073 Göttingen, Germany

1 Introduction

In recent years, there has been increasing interest in the synthesis and characterization of nanosized particles [1]. Due to their finite size, they often exhibit physical properties which may significantly differ from those of their bulk counterparts. Silicon is of particular importance for the microelectronics industry, and therefore much work has been devoted to the investigation of silicon clusters and nanoparticles. The development towards nanoelectronics requires a detailed knowledge of the physical and chemical properties of silicon in its mesoscopic state between the atom and bulk matter.

The observation of photoluminescence from porous nanostructured silicon at the beginning of this decade [2] has triggered an enormous increase in activity. The motivating force behind this kind of research is the ambition to integrate silicon nanostructures into future optoelectronic devices. While the early investigations were devoted exclusively to porous silicon produced by electrochemical etching of Si wafers, recent work is concentrating more and more on the production and characterization of silicon nanoclusters constituting zerodimensional quantum dots.

In the past, most experimental studies devoted to small Si_n clusters ($n < 100$) were carried out in molecular beams using a laser vaporization source to generate the silicon clusters [3]. An alternative technique, capable of producing much larger silicon clusters, is based on the pyrolysis if silicon-containing gas phase precursors, such as silane. This technique, commonly referred to as chemical vapor deposition (CVD), can be used to produce ultrafine powders and thin films. The energy necessary to decompose the gas phase molecules is usually provided by thermal heating. In particular, CO_2-laser-induced decomposition of SiH_4 in a gas flow reactor has been shown to be a very versatile technique for the production of ultraclean silicon particles in the nanometer size range [4]. However, with typical diameters above 10 nm, the particles are too large for many applications.

To close the gap between small silicon clusters ($n < 200$, $d < 2$ nm) and large nanoparticles ($n > 2.5 \times 10^4$, $d > 10$ nm) and to study the intermediate sizes, we have recently developed a novel cluster source which combines the laser-driven CVD reactor with a supersonic expansion of the nascent clusters into a high vacuum molecular beam apparatus [5].

2 Experimental

Silicon clusters and nanoparticles are produced by CO_2-laser-induced gas phase reactions in a gas flow reactor. In contrast to conventional techniques, the particles are expanded, directly after production, through a conical nozzle into a high vacuum chamber and then transferred into a molecular beam machine where they are analyzed *in situ* with a time-of-flight mass spectrometer (TOFMS) [5]. For high resolution mass spectrometry, a reflectron-type TOFMS is employed. The analysis reveals that the flow reactor emits high-purity silicon nanoparticles with diameters between 1 and 10 nm [6]. Peak and width of the size distribution are determined by the operating conditions. In addition, it is found that the particles' velocity strongly correlates with their mass. This feature and the fact that the particles are produced in a pulsed mode (by using a pulsed CO_2 laser) enable us to considerably reduce the dispersion of their size distribution by introducing a chopper into the cluster beam [7]. This tech-

*Abstract 6971 submitted to the 21st International Symposium on Rarified Gas Dynamics, Marseille, France July 26-31, 1998

nique has been successfully employed to perform size-selected low-energy cluster beam deposition on various substrates.

3 Results

The high resolution mass spectrometric analysis of the silicon cluster beam has confirmed that the laser-driven flow reactor is capable of producing hydrogen-free Si_n clusters and nanoparticles with n ranging from a few tens to several thousands. An investigation of the fragmentation behavior of the ionized silicon clusters as a function of the fluence of the ionizing ArF excimer laser reveals that intermediate-size Si_n clusters (n = 22 - 100) fragment by fission, yielding Si_6^+ - Si_{11}^+, while nanometric silicon clusters evaporate single Si^+ and Si_2^+ ions if the fluence of the ionizing laser is large enough [8]. At the same time, multiply charged nanoclusters are observed. The probability of multiple ionization scales with the size of the nanoclusters.
In addition to the mass spectroscopic characterization of the gas phase silicon clusters, we have deposited them on different substrates such as holey carbon films for high resolution transmission electron microscopy (HREM) as well as LiF and CaF_2 windows for Raman spectroscopy and luminescence studies. These condensed phase characterizations have been carried out by cooperating partners in various laboratories.
The high resolution electron transmission micrographs demonstrate that the silicon nanoclusters are monocrystalline with the same lattice parameters as encountered for bulk silicon. The monocrystalline core is surrounded by an amorphous, 1 - 1.5 nm thick layer of silicon oxide which has been formed after exposing the sample to the ambient [9]. The Raman studies confirmed the crystallinity of the silicon clusters and further revealed that the deposited particles had the same size as determined before by gas phase mass spectrometry [7]. Finally, the investigation of the luminescence behavior of the silicon nanoparticles upon irradiation with UV lasers showed that this phenomenon could be observed for silicon particles with diameters between 3.5 and 5 nm. As predicted by theoretical models, the peak of the luminescence curve shifted with decreasing particle size to smaller wavelengths (higher energies). In addition, it was found that the efficiency curve has a sharp maximum for particles with 4 nm diameter [10]. As a result, a bright orange-red luminescence could be observed with the naked eye from thin films composed of preselected 4 nm silicon nanoparticles. This strong luminescence, however, appeared only if the samples were exposed to ambient air for at least two days. Thus, surface passivation is very important for the luminescence to be effective.
The same technique has also been applied to produce silicon carbide as well as iron and iron carbide nanoparticles in the gas phase and deposited in thin films.

References

[1] See for example: *Nanophase Materials: Synthesis, Properties, Applications*, ed. by G. C. Hadijipanyis and R. W. Siegel, Kluwer Academic Publications (London, 1994).

[2] L. T. Canham, Appl. Phys. Lett. **57**, 1046 (1990).

[3] J. R. Heath, Y. Liu, S. C. O'Brian, Q.-L. Zhang, R. F. Curl, F. K. Tittel, and R. E. Smalley, J. Chem. Phys. **83**, 5520 (1985).

[4] W. R. Cannon, S. C. Danforth, J. H. Flint, J. S. Haggerty, and R. A. Marra, J. Am. Ceram. Soc. **65**, 324 (1982).

[5] M. Ehbrecht, H. Ferkel, V.V. Smirnov, O.M. Stelmakh, W. Zhang, and F. Huisken, Rev. Sci. Instrum. **66**, 3833 (1995).

[6] M. Ehbrecht, H. Ferkel, and F. Huisken, Z. Phys. D **40**, 88 (1997).

[7] M. Ehbrecht, B. Kohn, F. Huisken, M.A. Laguna, and V. Paillard, Phys. Rev. B **56**, 6958 (1997).

[8] M. Ehbrecht and F. Huisken, *Gas phase analysis of silicon nanoclusters produced by laser pyrolysis of silane*, Phys. Rev. B, submitted (1998).

[9] H. Hofmeister, F. Huisken, and B. Kohn, to be published.

[10] G. Ledoux, M. Ehbrecht, O. Guillois, F. Huisken, B. Kohn, M. A. Laguna, I. Nenner, V. Paillard, R. Papoular, D. Porterat, and C. Reynaud, Astron. Astrophys. **100**, 100 (1998).

Nanostructure fabrication by atom lithography *

F. Lison, D. Haubrich, D. Meschede
Institute for Applied Physics, Bonn University, Germany

1 Introduction

Optical lithography which is applied in industry at a large scale approaches a principal limit at a resolution below 100 nm. Lithography with neutral atom beams offers especially for parallel writing of periodic structures an interesting, still juvenile alternative. Through the interaction of atoms with light masks it is possible to generate periodic arrays of lines and various two-dimensional periodic patterns with a resolution below 100 nm. For this purpose atoms are directly deposited on a substrate or they are used to modify an organic resist.

2 Direct deposition via standing wave focusing

At the beginning of atom lithography there are experiments of two groups in the United States in which atoms from a thermal beam were directly deposited into a periodic nanostructure. An essential condition for this result was the transverse collimation of the atomic beam by radiation pressure light forces.
In the first experiments of Timp et al. [1] sodium was deposited on a glass surface under the action of a standing wave at the wavelength of the D2-line (589 nm). The sample could not be removed from the vacuum so that the authors only could identify the periodic structure indirectly by diffraction of a Helium Neon laser beam. Shortly afterwards, the problem of chemical instability was overcome at the NIST at Gaithersburg by replacing reactive alkali atoms with chromium. With a thermal atomic beam McClelland et al. [2] succeeded in writing chromium lines at the expected separation of $\lambda/2 = 213$ nm over several millimeters of a sample. Later on they also demonstrated how two write two-dimensional square lattices of dots [3].
With the method described here the growth of a layer is controlled by light forces in one or two dimensions. The substrate can be moved during the growth process so that parallel writing of many identical structures within a period of the light field is possible, too. It is furthermore conceivable that this control is extended to the third dimension if one uses several kinds of atoms and regulates the flux of their sources. It could become possible to fabricate superlattices at the scale of the wavelength used by applying the element selective light force in order to manipulate one component only during the growth of an alloyed layer.

3 Atom lithography based on resist techniques

The pet atoms of physicists dealing with laser cooling are alkali atoms (Na, Rb, Cs, ...) and metastable noble gas atoms (He*, Ne*, Ar*,...), since they can be prepared in an effective two level system, and since robust atomic beams and economic laser light sources are readily available. They were, however, apparently useless for further applications because, as demonstrated in the experiment by Timp et al. [1], alkali structures could not be removed from the vacuum without destruction, and because with noble gases deposition was impossible. A cooperative effort of chemists and physicists of Harvard University and NIST [4] succeeded in compensating this disadvantage. This group discovered that a hydrophobic self assembled monolayer (SAM) of organic molecules, which normally provides a highly inert surface, could be locally modified by a beam of metastable argon atoms such that a pattern could be transferred to the underlying layer by chemical procedures. The dose required for the alteration of the organic resist was about 10 metastable argon atoms per SAM molecule. Due to the low flux of metastable beam sources exposure times were extending into the hour regime, however. While all procedures for structuring of the SAM layer reported up to here are employing a material mask (so-called proximity printing) we have begun at Bonn to apply an immaterial mask in form of an optical standing wave for periodic patterning

*Abstract 6986 submitted to the 21st International Symposium on Rarefied Gas Dynamics, Marseille, France, July 26-31, 1998

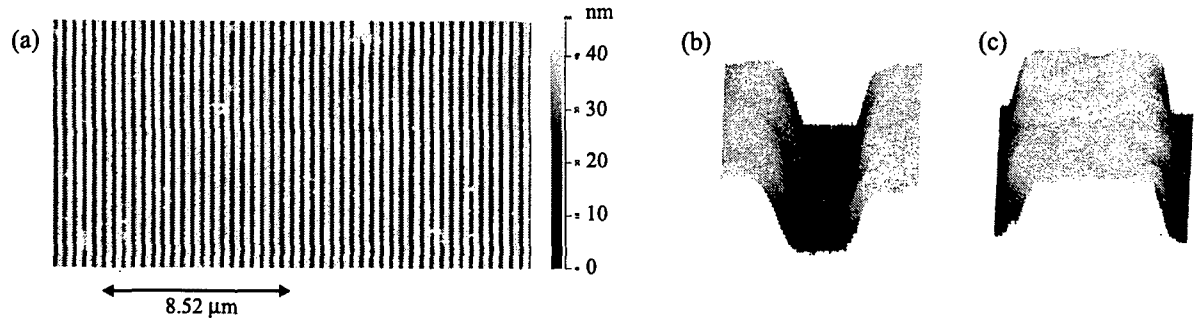

Figure 1: (a) Atomic force microscope image. The gold lines (bright) have a separation of 426 nm. (b) magnification of figure 1 ditch (FWHM 125 nm) and (c) bridge (FWHM 300 nm)

of these organic layers.
We are using a thermal cesium atomic beam which is cooled transversely by light forces and which has a diameter of 1 mm. The optical standing wave is generated by reflection of a laser beam with 160 mW power at 852,1 nm (cesium D2-line) off a mirror mounted within the vacuum apparatus. The frequency of the standing wave is detuned by +12,1 GHz relatively to the cesium transition from the ground state ($^2S_{1/2}$, $F = 4$) to the excited state ($^2P_{3/2}$, $F = 5$). Because the mirror surface determines the position of nodes and antinodes of the standing wave, the sample under preparation is fixed orthogonally to both the mirror surface and the atomic beam. The sample surface coincides with the middle of the Gaussian laser beam profile generating the standing wave. Following an illumination time of 6 to 8 minutes the samples are removed from the apparatus and etched afterwards. An atomic force microscopy image of the fabricated pattern can be seen in figure 1. The width of the ditches etched into the gold surface measures approximately 125 nm. By systematic variation of parameters we have been able to improve the resolution below 100 nm.
There exist additional ideas to use internal atomic degrees of freedom for pattern generation [7]. Laser radiation can for instance trigger the decay of metastable atoms to the ground state and hence suppress the interaction with the surface. This excitation can furthermore be locally confined if the resonance frequency is spatially controlled by inhomogeneous magnetic fields. With this technique very complex structures could be produced directly. With the self assembled monolayers there is now also a film for projection lithography with atoms available which we have demonstrated at a much coarser scale already. [8] The SAM layers provide a spatial detector with high resolution for atoms, too.

References

[1] G. Timp, R. E. Behringer, D. M. Tennant, J. E. Cunningham, M. Prentiss, and K. K. Berggren, Phys. Rev. Lett. **69** (1992), 1636–1639.

[2] J. J. McClelland, R. E. Scholten, E. C. Palm, and R. J. Celotta, Science **262** (1993), 877–880.

[3] R. Gupta, J. J. McClelland, Z. J. Jabbour, R. J. Celotta, Appl. Phys. Lett. **67** (1995), 1378

[4] K. K. Berggren, A. Bard, J. L. Wilbur, J. D. Gillaspy, A. G. Helg, J. J. McClelland, S. L. Rolston, W. D. Phillips, M. Prentiss, and G. M. Whitesides, Science **269** (1995), 1255; S. Nowak, T. Pfau, and J. Mlynek, Appl. Phys. B **63** (1996), 203–205.

[5] M. Kreis, F. Lison, D. Haubrich, S. Nowak, T. Pfau, and D. Meschede, Appl. Phys. B **63** (1996), 649–652.

[6] F. Lison, H.-J. Adams, D. Haubrich, M. Kreis, S. Nowak, and D. Meschede, Appl. Phys. B **65** (1997), 419–421.

[7] K. Johnson, J. H. Thywissen, N. H. Dekker, A. P. Chu, R. Younkin, K. K. Berggren, M. Prentiss, IQEC'98, Technical Digest, Paper QThD3.

[8] W. Kaenders, F. Lison, A. Richter, R. Wynands, and D. Meschede, Nature **375** (1995), 214.

Supersonic Free-Jet Epitaxy of Wide Bandgap Semiconductors *

V.M. Torres, D.C. Jordan, I.S.T. Tsong, and R.B. Doak
Department of Physics and Astronomy, Arizona State University
Tempe, AZ, USA

1 Introduction

The advent of wide band gap semiconductors is ushering in an era of high frequency semiconductor devices. These include LED's which emit blue light, high temperature/high power transistors, "visible blind" ultraviolet photodetectors, and solid state lasers operating in the blue to ultraviolet [1]. III-N nitrides are the materials of choice for such applications, particularly GaN with its direct band gap of 3.4 eV. Unlike conventional semiconductors, GaN cannot be grown from the melt but must be deposited expitaxially onto a suitable substrate under carefully controlled conditions. The established methods of doing this are Metal-Organic Chemical Vapor Deposition (MOCVD) and Molecular Beam Epitaxy (MBE) [2]. However, alternative techniques based on supersonic beams are now attracting considerable attention. Of specific interest are the energy selectivity, state selectivity, enthalpy storage, and high flux attainable in a supersonic free-jet expansion. This work will discuss two supersonic beam sources of particular relevance to III-N deposition, seeded supersonic free-jets [3] and corona discharge supersonic free-jets [4]. Recent developments in free-jet epitaxial deposition, both by our group and by others, will be presented.

2 Selected Energy Epitaxy

By expanding a gas mixture into vacuum through a supersonic nozzle, a heavy "seed" species in a light diluent can be aerodynamically accelerated to suprathermal translational energies. The terminal energy of the seed species can be tuned by adjusting the mixture and temperature of the nozzle. The supersonic seeded beam retains the high intensity and narrow energy distribution characteristic of a supersonic free-jet and, by virtue of its intensity, directionality, and energy specificity, offers the prospect of selectively altering gas-surface reactions. One reaction of particular interest in III-N semiconductor growth is the decomposition of NH_3 to supply nitrogen to a growing III-N thin film. NH_3 pyrolyzes on the GaN surface at temperatures above ca. 650 C ($kT = 0.08$ eV) and has become the nitrogen species of choice for both MOCVD and MBE growth of III-N compounds. With Ga supplied in the form of a metal-organic species or as the elemental metallic vapor, the reaction of NH_3 with Ga to deposit GaN is initiated heteroepitaxially on an appropriate substrate (sapphire, SiC, or an AlN buffer layer) then continues homoepitaxially on the growing GaN surface itself. Under standard MBE growth conditions, GaN grows successfully only over a narrow range of surface temperatures, which must exceed ca. 700 C in order to provide sufficient surface mobility of reactants yet remain below ca. 800 C to avoid GaN decomposition. By supplying NH_3 molecules in a seeded beam and tuning their translational energy to surmount the reaction barrier, an additional degree of freedom is provided in adjusting this balance.

We have used seeded beams of 10% NH_3 in helium to grow GaN epitaxially on both 6H-SiC(0001) and on AlN buffer layers deposited on SiC(0001). All deposition was carried out at a substrate temperature of 800 C. The incident NH_3 translational energy was varied from 0.034 to 0.44 eV with the beam impinging at 0°, 30°, or 75° with respect to the surface normal. Ga was supplied in over-abundance from an effusive evaporation source. The thickness and morphology of the resulting films was characterized *ex situ* using standard surface science techniques (RBS, Auger, TEM, and AFM). We find that the reaction chemistry can indeed be selectively influenced by adjusting the incident NH_3 translational energy. Selected energy epitaxial deposition (SEED) evidently occurs via a direct reaction channel over a barrier of 0.3 ± 0.1 eV. A low (thermal) energy reaction channel is also identified and ascribed to physisorption of the incoming NH_3 molecule followed by dissociative attachment of NH_x fragments.

*Abstract 7063 submitted to the 21st International Symposium on Rarefied Gas Dynamics, Marseille, France, July 26-31, 1998

Comparison of growth at the 0° and 30° beam angles indicates "total energy scaling," probably due to rotational coupling of the high and low energy reaction channels. Deposition at grazing angle (the 75° angle) yields facet growth oriented towards the incident beam. This allows an upper bound to be placed on mobility of the incident NH_3 and the attached NH_x fragments. These observations have clear implications for seeded beam epitaxy in particular but also for for GaN growth in general, demonstrating the versatility of supersonic beams as a tool for both fundamental and applied science.

3 Corona Discharge Free Jet

To grow nitrides from molecular nitrogen it is necessary to break or weaken the strong N_2 triple bond or namely, in chemistry parlance, to "activate" the nitrogen. Radio frequency (RF) and electron cyclotron resonance (ECR) discharges are the conventional means of activating nitrogen, yet both produce a broad spectrum of highly excited molecules, atoms, and ions. The more energetic and reactive of these may damage a growing GaN film [5]. Recent theoretical work indicates that the neutral excited molecular $A^3\Sigma_u^+$ state may be the ideal nitrogen reactant for GaN growth [6]. This lowest triplet metastable state de-excites to the ground state only via the forbidden Vegard-Kaplan bands and therefore has a very long intrinsic lifetime (ca. 1 s). Moreover as the $A^3\Sigma_u^+$ molecular state exothermically reacts with GaN, one N-atom attaches to the growing surface while the second departs and carries away the heat of reaction as kinetic energy. This leaves the first N-atom attached in a quiescent state.

A low energy electrical discharge supersonic free-jet is the ideal means of producing the $A^3\Sigma_u^+$ state. All higher electronic molecular states relax (primarily via the 1^{st} and 2^{nd} positive series) to collect in the the $A^3\Sigma_u^+$ state. Given a sufficiently abrupt expansion, as with a free-jet, a large percentage of the molecules survive in this state without being collisionally de-excited. We have built, tested, and characterized both arc-discharge and corona-discharge supersonic free-jet sources, operating with argon/nitrogen mixtures and with pure nitrogen. Of the two, the corona discharge is less expensive, easier to operate, and can be run under conditions which produce essentially only the desired the $A^3\Sigma_u^+$ excited state. Spectroscopic measurements made at the exit of the supersonic nozzle and at 1 and 3 cm downstream show the filling of this state through the 1^{st} and 2^{nd} positive series and allow estimates of the $A^3\Sigma_u^+$ density in the terminal free-jet. Epitaxial GaN growth with the corona-discharge free-jet is currently underway.

4 Acknowledgements

Support for this research by the U.S. Office of Naval Research under grants N00014-95-1-0122 and N00014-96-1-0962 is gratefully acknowledged.

References

[1] Mohammad S.N., Salvador A.A., and Morkoc H., *Emerging Gallium Nitride Based Devices*, Proc. IEEE, Vol. 83, No. 10, pp 1305-1355, 1995.

[2] Strite S. and Morkoc, H., *GaN, AlN, and InN: A Review*, J. Vac. Sci. Technol., Vol. B 10, No. 4, pp. 1237–1266, 1992.; Davis R.F., Weeks T.W. Jr., Bremser M.D., Tanaka S., Kern, R.S., Sitar, Z., Ailey, K.S., Perry W.G., and Wang C., *Growth of AlN and GaN Thin Films via OMVPE and Gas Source MBE and their Characterization*, Solid State Elec., Vol. 41, No. 2. Pp. 129-134, 1997.

[3] Torres V.M., Stevens M., Edwards J.L., Smith D.J., Doak R.B., and Tsong I.S.T., *Growth of AlN and GaN on 6H-SiC(0001) using a helium supersonic beam seeded with ammonia*, Appl. Phys. Lett., Vol. 71, No. 10, pp. 1365–1367, 1997.

[4] Jordan D.C., Burns C., and Doak R.B., *Inexpensive Corona Discharge Source for the Growth of III-N Semiconductors*, Proc. 45th Int. Symp. Am. Vacuum Soc., Baltimore, MD, USA, Nov 2-6, 1998.

[5] Botchkarev A., Salvador, A., Sverdlov B. Myoung J, and Morkoc H., *Properties of GaN films grown under Ga and N rich conditions with plasma enhanced molecular beam epitaxy*, J. Appl. Phys., Vol. 77, No. 9, pp. 4455 – 4458, 1995.

[6] Goddard W.W. III, *Theory of Selected Energy Growth Processes*, Proc. 45th Int. Symp. Am. Vacuum Soc., Baltimore, MD, USA, Nov 2-6, 1998.

Chemical Maps and SEM Images of The Reaction Products on Si Surfaces Irradiated with Cold and Hot C_2H_4 Beams *

I. Kusunoki[1]
[1] Research Institute for Scientific Measurements, Tohoku University, Sendai, Japan

1 Introduction

For a long time, reactive molecular beams have been detected using chemical reaction with a solid surface. For example, an atomic hydrogen beam is detected using the color change of molybdenum trioxide by reducing it. These techniques are, however, only used to observe the beam position by eye, or to measure the beam intensity qualitatively. Recently we have obtained quantitative chemical maps of the products on surfaces reacted with a molecular beam [1,2]. The intensity profiles on the surfaces are measured using scanning X-ray photoelectron spectroscopy (XPS). Especially the carbonization of a Si surface with C_2H_4 has been intensively studied using this technique [3,4]. We will show that the technique is useful to study gas–surface reactions.

2 Experimental

A homemade molecular beam apparatus is attached to the sample treatment chamber (STC) of a conventional multisurface analysis system (Shimadzu-Kratos XSAM 800)[3]. A molecular beam is produced by three-stage differential pumping. The temperature of the nozzle for expanding the beam gas can be varied from room temperature to 900°C. A quadrupole mass spectrometer in the STC provides measurements of the beam intensity and the components.

A sample is placed on the beam axis in the STC in which the vacuum is less than 2×10^{-10}Torr. It can be heated by electron bombardment. In the case of Si, the surface is cleaned by the bombardment in the ultrahigh vacuum. The sample reacted with the molecular beam is transferred under vacuum into the surface analysis chamber (SAC), which incorporates XPS and scanning Auger electron spectroscopy (SAM). The surface area that is reacted with the molecular beam is searched using scanning XPS with an electrostatic lens system. The largest analysis area is 10×10 mm^2. It can be divided into 250×250 elements at the maximum, with spatial resolution of 0.1 mm FWHM. However, we usually use 50×50 elements with a resolution of 0.6 mm to make the measurements feasible in a reasonable time (< 30 min). To observe the surface morphology at high resolution, a scanning electron microscope (SEM) is used. In these cases, however, the samples are exposed to air during transfer into the microscope.

In this presentation, we will show some experimental results in the cases of the carbonization of Si(100) surfaces using C_2H_4 beams produced from a room temperature nozzle and one at high temperature [3, 4].

3 Results and Discussion

A clean Si(100) surface at 675°C was irradiated with the room temperature C_2H_4 beam (flux: 3×10^{15} molecules cm^{-2} s^{-1}) for 30 min. A chemical map of the surface was drawn by C1s XPS of the reaction product (SiC). It is shown in Fig.1a. The line profile is given in Fig. 1b. Both reflect the beam profile clearly. The gradient of the beam flux in the tail provides a convenient method for studying the flux effect on the reaction.

When a hot beam produced from a 900°C nozzle irradiated the clean Si(100) surface at 650°C, two states of C atoms were observed using XPS. The state at the binding energy of 283eV is from SiC and another one (284.5eV) is from glassy (or graphitic) carbons. The line profiles taken through the beam irradiation center are shown in Fig. 1c. The glassy carbons exist only in the central region, while the intensity distribution of the SiC products has maxima at the edge of the region. These facts suggest that the beam flux and the beam temperature have effects on the reaction mechanism, resulting in the different products. Since the mass pat-

*Abstract 7056 submitted to the 21st International Symposium on Rarefied Gas Dynamics, Marseille, France, July 26-31, 1998

tern measured by the quadrupole mass spectrometer showed no difference between the room temperature beam and the high temperature one, the vibrational exitation of the impinging molecules may play a role. The population of the molecules exited vibrationally in the C=C stretching mode in the hot beam reaches 12% if the relaxation does not occur during the expansion. The exited molecules may dissociate more easily and futher the recombination of C atoms on the surface each other instead of the reaction with the surface Si atoms.

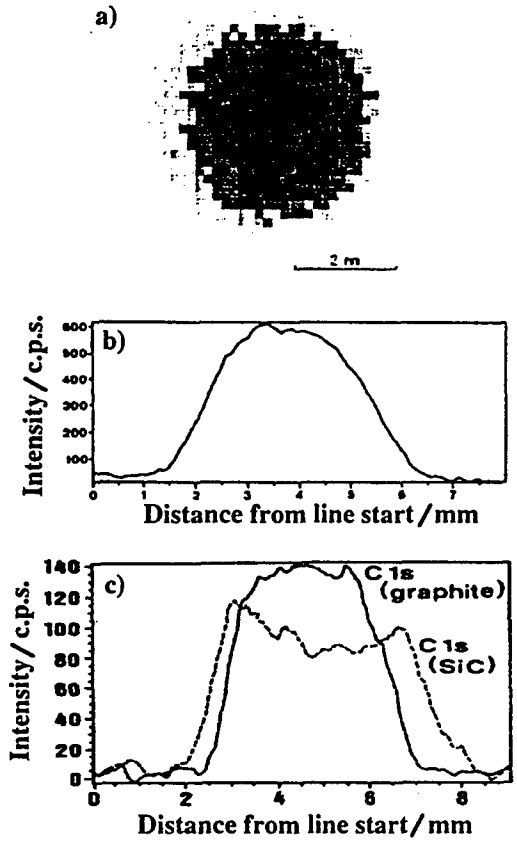

Figure 1: a) A chemical map of C1s(SiC) XPS of a Si surface reacted with a room temperature C_2H_4 beam, b) a line profile of the map drawn in a), c) line profiles of the chemical maps of the Si surface reacted with the hot beam

Highly magnified SEM images of the reacted surfaces showed that rectangular SiC crystals grow epitaxially on the Si(100) surfaces. This was confirmed by the reflection high energy electron diffraction (RHEED) pattern. Number density and the mean size of the SiC crystalline islands are dependent on the beam flux as well as on the surface temperature. In the case of the hot beam, the number of the SiC islands and their sizes in the central region covered with the glassy carbon film are smaller than at the maxima of the SiC intensity (see Fig. 1c).

4 Conclusion

- A molecular beam profile is measured from a chemical map of the surface reaction product using scanning XPS.
- This technique is useful to study the effects of the beam flux and the beam temperature on surface reactions.

References

[1] Kusunoki I., Igari Y., *XPS Study of a SiC Film Produced on Si(100) by Reaction with a C_2H_2 Beam*, Appl. Surf. Sci. Vol. 59, pp.95 - 104, 1992.

[2] Kusunoki I., *Scanning Auger Microscopy Study of Heterogeneous Growth of SiC Film on Si(100) by Reaction with a C_2H_2 Beam*, Jpn. J. Appl. Phys. Vol. 32, pp.2074 - 2077, 1993.

[3] Kusunoki I., Takagaki T., Ishidzuka S., Igari Y. Takaoka T., *Reaction of Si Surfaces with a C_2H_4 Beam*, Surf. Sci. Vol. 380, pp.131 - 144, 1997.

[4] Kusunoki I. Igari Y., Ishidzuka S., Mine T., Takami T. Takaoka T., *Growth Studies of β-SiC and Graphite Films on Si(001) Surfaces by Reaction with C_2H_4*, Advanced Materials '98 (Proceedings of The 5th NIRIM International Symposium on Advanced Materials), NIRIM, pp.121-124, 1998.

MOLECULAR BEAM SESSION MB 11

Ionization of Fullarenes and of Group III Metal-Ammonia Clusters

CHAIR: E. Kolodney (Haifa)

ROOM: LAVOISIER
FRIDAY, JULY 31, 1998
11:15 - 12:30

Infrared Resonance Enhanced Multiphoton Ionization of Fullerenes *

Gerard Meijer
Dept. of Molecular and Laser Physics
University of Nijmegen, The Netherlands

1 Introduction

For a long time, the microscopic equivalent of the thermal emission of electrons from a heated surface, the thermionic emission of electrons from neutral hot molecules, was not observed. For thermionic emission to be possible a large amount of internal energy, at least more than the energy needed for ionization, has to reside in a molecule. Such superheated molecules will often loose their energy preferentially via fragmentation and photon emission, the microscopic equivalents of the macroscopic cooling processes of evaporation and black-body emission. Thermionic emission can become a significant cooling channel when the energy needed for ionization is comparable to or smaller than the dissociation energy, as is the case for strongly bound molecules like the fullerenes as well as for clusters of transition metal atoms. To produce highly excited molecules, high power pulsed laser radiation in the visible (VIS) and ultraviolet (UV) region of the spectrum is commonly used. Although electronically excited states are initially prepared in this case, it is assumed that due to rapid thermalization and electronic-to-vibrational energy transfer, vibrationally excited, i.e. heated, molecules are created which can subsequently evaporate off an electron. A more direct insight into the processes involved can be obtained when exciting the vibrational modes directly, using intense infrared (IR) light. Over the last years Free Electron Lasers (FEL) have become available to users and their performance characteristics make them the ideal light sources for studies of this kind.

Here we present results from experiments where gas phase C_{60} is being resonantly excited by IR light up to internal energies where autoionization becomes efficient [1]. The experiments have been performed at the 'Free Electron Laser for Infrared eXperiments' (FELIX) user-facility in Nieuwegein, The Netherlands [2]. This laser produces pulsed IR radiation that is continuously tunable over the 100–2000 cm^{-1} range. The light output consists of macropulses of about 5 μs duration containing up to 100 mJ of energy. Each macropulse consists of a train of micropulses which are 1 ns apart. The macropulse repetition rate is 10 Hz. An effusive molecular beam of C_{60} is generated by evaporating C_{60} from a quartz oven. The FELIX beam enters the vacuum chamber and is focused onto the molecular beam in the region between the extraction plates of a Time of Flight (TOF) mass spectrometer. With an oven temperature of 875 K, the density of C_{60} in the interaction region can be estimated to be $(8\pm2) \times 10^9$ molecules/cm^3. After a delay of typically 30 μs after the FELIX pulse, ions are pulse extracted and detected in a TOF mass spectrum on a MCP detector.

2 Results and Discussion

Fig.1 shows the experimental setup and a typical mass spectrum obtained when FELIX is set to 19.2 μm. A strong peak of C_{60}^+ is observed. Surprisingly, the amount of fragmentation (C_{58}^+) is very small. It should be noted that the observation of fullerene ions, when exciting at this wavelength, results from the absorption of more than 500 IR photons by a single molecule!

By monitoring the amount of C_{60}^+ produced as a function of the FELIX wavelength, the IR REMPI spectrum, shown in the upper part of Fig.2, is obtained. Four peaks can readily be identified. In the lower part of the figure, the IR absorption spectrum of a thin film of solid C_{60} is shown. Again four lines can be seen and they correspond to the four well known IR allowed F_{1u} fundamental modes of C_{60}. The two spectra show a clear correspondence in both, their line positions as well as the relative intensities of the lines. Nonetheless, it can be seen

*Abstract 7006 submitted to the 21st International Symposium on Rarefied Gas Dynamics, Marseille, France, July 26-31, 1998

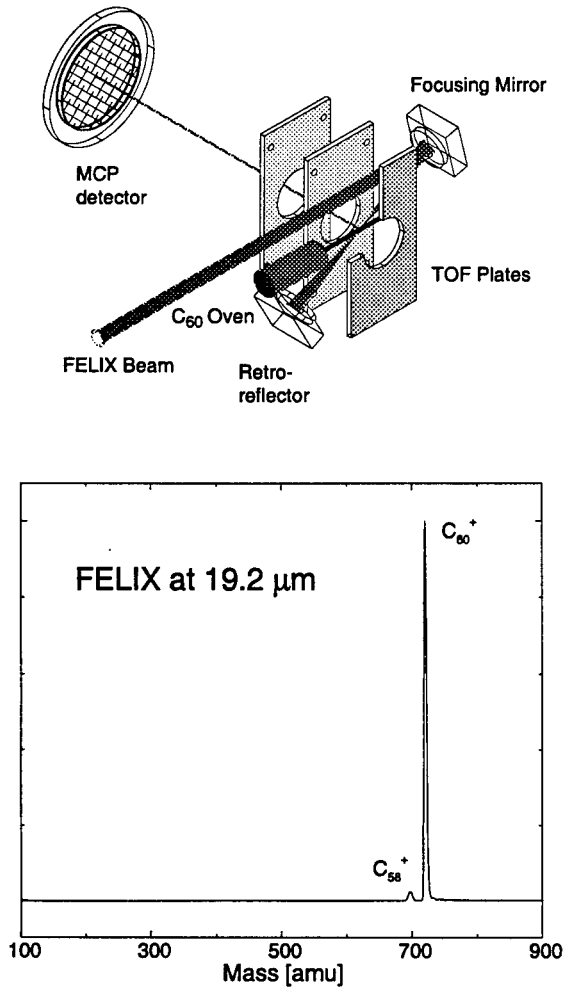

Figure 1: Experimental setup and TOF mass spectrum obtained when exciting at 19.2 μm

that the resonances in the IR-REMPI spectrum are systematically shifted to slightly lower frequencies than in the thin film absorption spectrum and that the lines in the IR-REMPI spectrum are slightly asymmetric. Further, the strongest lines in the IR REMPI spectrum are those which show the least frequency shift with respect to the corresponding lines in the thin film absorption spectrum.

The observation that C_{60} can be resonantly ionized by only IR photons seems astonishing. At least several hundred IR photons need to be absorbed by a single C_{60} molecule before it will ionize in the experimental time window and this might therefore appear to be a rather unlikely process. One also might expect that, after absorption of a few IR photons, the molecule runs out of resonance with the IR laser due to the intrinsic anharmonicities of the vibrational modes. The observation that so many

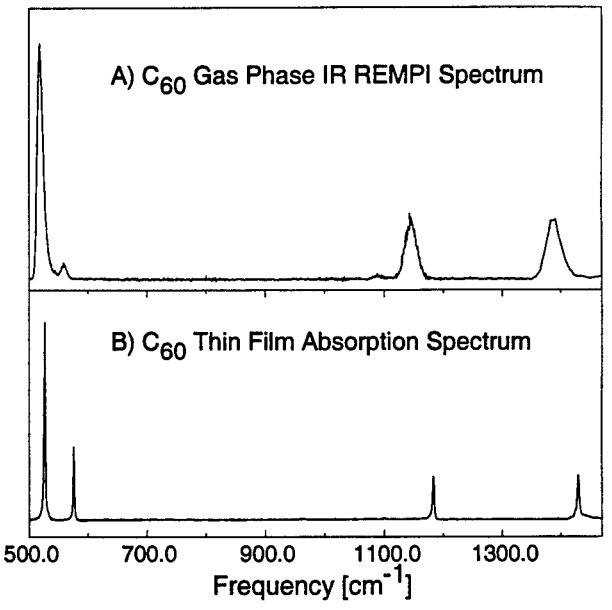

Figure 2: Shown is **a)** the IR-REMPI spectrum of gas-phase C_{60} effusing from the oven. Shown in **b)** is the thin film absorption spectrum of solid C_{60}, showing the four well known IR absorption lines.

IR photons can be absorbed by the molecules can be explained by IVR in combination with the pulse structure of FELIX. The molecule can therefore absorb one IR photon in a FELIX micropulse and, by the time the next micropulse arrives, the energy of the previous photon is completely randomized in the molecule. With 174 internal degrees of freedom and with an averaged vibrational frequency of 950 cm^{-1}, on average less than two quanta need to be put in each vibrational mode of C_{60} to reach the required energy of 35-40 eV. By sequential pumping of IR photons into the molecule, accompanied by thermalization via fast internal vibrational redistribution, the C_{60} molecule can then be resonantly heated up to energies at which ionization becomes efficient.

References

[1] G. von Helden, I. Holleman, G.M.H. Knippels, A.F.G. van der Meer, G. Meijer, *Phys.Rev.Lett.* **79**, 5234 (1997).

[2] D. Oepts, A.F.G. van der Meer and P.W. van Amersfoort, *Infrared Phys.Technol.* **36**, 297 (1995);
G.M.H. Knippels, R.F.X.A.M. Mols, A.F.G. van der Meer, D. Oepts and P.W. van Amersfoort, *Phys.Rev.Lett.* **75**, 1755 (1995).

Radiative cooling of C_{60} and C_{60}^+ in a beam *

Vostrikov A.A.[1,2], Dubov D.Yu.[1,2], Agarkov A.A.[1], Drozdov S.V.[1], and Galichin V.A.[1]
[1] Institute of Thermophysics, Novosibirsk, Russia
[2] Novosibirsk State University, Novosibirsk, Russia

1 Introduction

Cluster C_{60} is a unique object of the fundamental and the applied investigations, especially in a rarefied gas dynamics. Large mass ($M = 720$ *a.e.m.*) and approximately equal cross sections of the electron impact ionization and of the electron attachment $\sigma^{+,-} \sim 0.5\ nm^2$ at the corresponding electron energy $45 < E_e < 60\ eV$ and $0,5 < E_e < 6\ eV$ [1, 2], make the C_{60} cluster a promising working substance for the rocket ion engines. The C_{60} cluster has high stability against the dissociation (the reaction $C_{60} + e \rightarrow C_{58}^+ + C_2 + 2e$ is observed at an energy $E_e \geq 45\ eV$) . At this energy the temperature of C_{60} cluster reaches a value equal to 3000 K [3, 4]. It allows to use C_{60} as a probe particles for the diagnostics of the supersonic jets and the energy transfer in particle-particle and particle-surface collisions.

This report presents the results of the energy dissipation kinetics studies at the electron impact excitation of C_{60} in the molecular beam. We observed also the C_{60} cooling as a result of a thermionic emission and a thermal radiation:
$C_{60} + e \rightarrow C_{60}^* + e \rightarrow C_{60} + e + h\nu.$
$C_{60} + e \rightarrow C_{60}^* + e \rightarrow C_{60}^{+*} + 2e \rightarrow C_{60}^+ + h\nu + 2e$

2 Experimental technique

In short, molecular beam experimental arrangement was the following. The C_{60} vapor was allowed to effuse out of a cylinder oven containing a fullerene sample through a round orifice. The sample temperature, T_0, was 800 K. The electron beam from an oxide-coated cathode was collimated by a set of diaphragms and by magnetic field and crossed at right angles with the fullerene beam. In the set of these experiments the electron current was lower than 100 μA. The radiation from the fullerene and electron beam crossing region was collected in a direction normal to the electron beam. The angle with the molecular beam direction was about 40^0. The radiation was focused with the aid of a short-focal length objective lens onto the input slit of a grating monochromator and recorded with a photomultiplier (PM). The system of the radiation registration and the electron beam collimation of the longitudinal magnetic field precluded the cathodoluminescence. The electron beam was modulated by applying a negative potential to one of the diaphragms, and the signal from PM was measured in a lock-in mode. The output from a calibrated spectral source (quartz-tungsten lamp) was used to determine the combined spectral efficiency of the optical system. The raw spectra were then corrected by this response curve. For registration of UV-radiation the entrance lens was covered with luminophore.

In order to separate the contribution to the radiation of neutral C_{60}^* and C_{60}^+, we applied electric field to the two plates placed along the axes of molecular and electron beam. The distance between the plates was 10 *mm* and they were equidistant from the electron beam. The residence time of ions in the observation region was reduced with increasing voltage. Our system parameters were checked in the measurements of electron-induced radiation of $N_2^+(B_2\Sigma^+)$ ion and $N_2(C^3\Pi_u)$ molecule depending on the electron energy. The radiative lifetimes of these states are less than 0.1 μs, and while radiating these ions and neutrals do not leave the observation region. Thus this radiation is determined only by the parameters of electron beam.

3 Results

We have measured the spectra of radiation and excitation functions of radiation induced by the electron - fullerene collision in crossed beams. To obtain an emission spectrum, the electron energy, E_e, was fixed and the emission intensity as a function of

*Abstract 6712 submitted to the 21st International Symposium on Rarefied Gas Dynamics, Marseille, France, July 26-31, 1998

wavelength was recorded in 50 to 800 nm spectral region. We have observed a quasi-continuous (at spectral resolution 3 nm) spectrum of black body radiation and found that the ions C_{60}^{+} gives the major contribution to this radiation. To obtain the excitation function, we fixed the detection wavelength and scanned the electron impact energy. The excitation function of radiation C_{60} increases with the electron energy increase from $E_e \approx 30\ eV$ and reached the maximum at $E_e \approx 60\ eV$. From the spectra of C_{60} radiation at different E_e using the Plank's formula for radiation of small particle we have obtained the radiative temperature of C_{60}, T, depending on E_e. It turns out that the temperature increases with the electron energy increase up to the 50 eV and reaches the value of $T \approx 3000\ K$. The appearance of competitive processes, namely, evaporation, dissociative and fast ionization explains the existence of maximum on the excitation function of radiation C_{60} and on the C_{60} radiative temperature function depending on E_e. Note, that in the case of the direct ionization cold C_{60}^{+} ions seems to be formed, since after ionization the main part of energy carries away by primary and secondary electrons.

We measured the C_{60}^{+*} radiation intensity as a function of the electric field, which extracts the C_{60}^{+*} charged particles from the observed region, that is as a function of the residence time in the radiation observed region. It turns out that the ions give a contribution to the registrated radiation (in the absence of the extracting electric field) approximately 7 times larger than neutrals.

Based on these results and on the calculated data of the C_{60}^{+*} residence time in the observed region, t, we have obtained the radiation intensity, I, as a function of t. This dependence has a maximum. The relevant constants were obtained from the solution of kinetic equations for the formation and the radiation decay of C_{60}^{+*} and C_{60}^{*} which was compared with the experimental data. The maximum on the $I(t)$ dependence is explained by the fact, that the C_{60}^{+*} formation time and the photon radiation time are approximately equal.

Furthermore, the results of the energy transfer and the C_{60}^{+*} neutralization by the interaction with surface will be also presented.

References

[1] A.A. Vostrikov, D.Yu. Dubov, and A.A. Agarkov: *Tech. Phys. Lett.*, **21**, *517 (1995).*

[2] A.A. Vostrikov, D.Yu. Dubov, and A.A. Agarkov: *Tech. Phys. Lett.*, **21**, *681 (1995).*

[3] A.A. Vostrikov, D.Yu. Dubov, and A.A. Agarkov: *JETP Lett.*, **63**, *963 (1996).*

[4] E. Kolodney, B. Tsipinyuk, and A. Budrevich: *J. Chem. Phys.*, **102**, *9263 (1995).*

Molecular Beam Studies of Ammonia Clustered with III Group Metals Produced by Pulsed Laser Reactive Ablation*

T. M. Di Palma[1], A. Latini[1], M. Satta[1], A. Giardini-Guidoni[1,2]
[1] Dipartimento di Chimica, Universita' "La Sapienza", Roma, Italy
[2] CNR, Istituto Materiali Speciali, Tito Scalo (PZ), Italy

1 Introduction

The study of neutral and ionized clusters has developed rapidly in recent years [1]. The size dependent properties of these aggregates have been investigated by numerous spectroscopic methods [1]. Specific information on energetics, dynamic and structure of free clusters have been obtained from the supersonic expansion coupled with laser techniques and time of flight mass spectrometry [1, 2, 3]. The $Me(NH_3)_n$ are suitable models to investigate the interaction in metal-ligand bonding, metal-ion solvation and even in the absorption on metal surfaces and nitride deposition [4, 5]. In this paper a short review of the work performed on III group atoms solvated by a small number of ammonia molecules is reported. The photoionization spectra of $Me(NH_3)$ clusters are interpreted on the basis that the excess energy, absorbed above threshold, can lead either to a specific ionic vibrationally excited state or to autoionizing states. The photoionization measurements of $Me(NH_3)_n$ show that the NH_3 molecules can stabilize the excess electron. Features observed are discussed in connection with DFT calculations of the structures and energetics of these clusters.

2 Experimental

The experimental apparatus we have employed in the reported work is an instrument constructed in our laboratory [4] which consists of a laser ablation chamber where the metal is vaporized in NH_3 atmosphere, then expanded in vacuum forming a supersonic jet. The jet, where $Me(NH_3)_n$ clusters are present enters between the extraction plates of a time of flight mass spectrometer, where it is ionized by a Nd-YAG Quantel pumped dye laser ($5\,ns$ time duration) whose fluence is kept low (few mJ) in order to avoid multiphoton ionization processes. The ionization and excitation spectra of the clusters are measured by scanning the photon energy in the range $3 \div 5\,eV$ using different dyes.

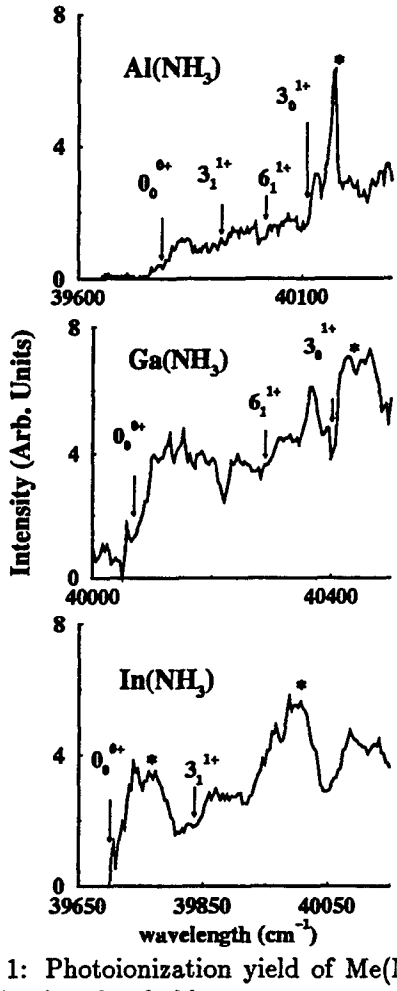

Figure 1: Photoionization yield of $Me(NH_3)$ near the ionization threshold.

3 Result and Discussion

The photoionization spectra of $Me(NH_3)$ corrected for the direct ionization field effect [6] are reported

*Abstract 7028 submitted to the 21st International Symposium on Rarefied Gas Dynamics, Marseille, France, July 26-31, 1998

n		$Al(NH_3)_n$	$Al(NH_3)_n^+$	$Ga(NH_3)_n$	$GaNH_3)_n^+$	$In(NH_3)_n$	$In(NH_3)_n^+$
1	R_{Me-N}(Å)	2.36	2.26	2.54	2.40	2.68	2.56
	$\theta_{Me-\widehat{N}-H}$	110.9	112.6	108.1	110.6	107.9	110.4
	IP (eV)	4.92	4.93*	4.84	4.98*	4.65	4.92*
2	R_{Me-N}(Å)	2.39	2.28	2.45	2.37	2.60	2.53
	$\theta_{N-\widehat{Me}-N}$	83.0	85.0	86.2	87.8	83.8	85.9
	IP (eV)	4.1	3.86*	3.82	$\leq$ 4.59*	3.75	$\leq$ 4.59*
3	IP (eV)	3.55*		$\leq$ 3.69*		$\leq$ 3.69*	
4	R_{Me-N}(Å)	3.75	2.78	3.80	2.93	3.40	2.90
	IP (eV)	3.39*		-		-	

Table 1: Calculated geometrical parameters and IPs of $Me(NH_3)_n$ clusters (* Experimental)

in fig. 1 in a range of about 600 cm^{-1} above the ionization threshold. The first step in each spectrum is associed with the $\Delta v = 0$ transition from the neutral complex to the vibronic ground state of the cation. The onset of one photon ionization process occurs at 39740±20 cm^{-1} for $Al(NH_3)$, at 40170±20 cm^{-1} for $Ga(NH_3)$ and 39700±20 cm^{-1} for $In(NH_3)$. Other steps observed at higher energy are assigned to direct ionization leading to two excited vibrational levels of the ion i.e. the stretching ν_3 and the bending ν_6 intermolecular ionic vibrations. Other observed bands (*) are attributed to high excited Rydberg states, autoionizing to ionic vibrational levels with a propensity rule $\Delta\nu = -1$ [6]. It should be noted that the autoionizing band appears blue shifted with respect to the assigned ionic transitions because the field induced shift for the Rydberg levels is lower than for the direct ionization process [6].

The IP thresholds for the $Me(NH_3)_n$ clusters, already reported [5, 7], are significantly less than the IPs of the ground-state atoms . The binding energies of $Me(NH_3)_n^+$ are found higher than that of the neutral and the relative Me-N bonds are stronger in the ionized cluster then in the neutral. Calculated equilibrium geometrical parameters and experimental IPs for small neutral and ionic $Me(NH_3)_n$ are reported in table 1. The IP appears to decrease by increasing the number of ammonia molecules in the cluster. A rapid IP cluster decrease up to n=3 is observed, and in Al $3 \leq n \leq 13$ the IP decreases less rapidly [7], and at very large n tends to reach the 1.45 eV bulk value of the solvated electron [8].

4 Conclusion

Photon ablation of metals in presence of ammonia, under suitable conditions, gives rise to metal ammonia clusters. The measured IPs of $Me(NH_3)$ clusters are found to be 1 eV lower with respect to that of the bare atoms. We have interpreted the photoionization spectra of third group $Me(NH_3)$ clusters through vibronic and autoionizing Rydberg transitions. We have obtained specific information on energetic and structure of these adducts. The experimental data are consistent with calculated values of binding energies of neutral and ionized $Me(NH_3)$ and $Me(NH_3)_2$ [7]. The measurement of the ionization potentials of $Me(NH_3)_n$ clusters shows that, when a third group metal is surrounded by a large number of ammonia molecules, its valence electron tends to be separated from the atom and form a solvated electron, as already observed for alkali and alkaline earth metals.

References

[1] E. R. Bernstein, *Atomic and molecular clusters*, Elsevier, 1990, Amsterdam, Netherlands.

[2] F. Misaizu, K. T. Sukamoto, M. Sanekata, K. Fuke, Chem. Phys. Lett. **188**, 241 (1992).

[3] I. V. Hertel C. Huglin, C. Nitsch and C. P. Schultz, Phys. Rev. Lett. **67**, 1767 (1991).

[4] T. M. Di Palma, A. Latini, A. Giardini Guidoni, A. Mele, S. Piccirillo, V. Marotta, A. Santagata, Nucl. Inst. Meth. in Phys. Res. B **122**, 415 (1997).

[5] A. Giardini Guidoni, A. Mele, T. M. Di Palma, M. Coreno, R. Teghil, and A. Morone, Appl. Surf. Sci. **106**, 154 (1996).

[6] D. R. Rodham, G. A. Blake, Chem. Phys. Lett. **264**, 522 (1997).

[7] T. M. Di Palma, A. Latini, M. Satta, M. Varvesi and A. Giardini-Guidoni, Chem. Phys. Lett. **284**, 184 (1998).

[8] J. Hasing, An. Phys. **37**, 509 (1940).

MOLECULAR BEAM SESSION MB 12

Gas-Surface III: Chemisorption, Beam Focussing,
Quantum Reflection, and van der Waals Cluster Enrichment

CHAIR: I. Kusunoki (Tohoku)

ROOM: LAVOISIER
FRIDAY, JULY 31, 1998
14:35 - 16:30

Probing the dynamics of chemisorption through scattering and sticking*

A.W. Kleyn
FOM-Institute for Atomic and Molecular Physics,
Kruislaan 407, 1098 SJ Amsterdam, The Netherlands,
kleyn@amolf.nl

The dissociative chemisorption of molecules is the key and rate determining step in many catalytic reactions. Although dissociative chemisorption is energetically favorable, the probability of dissociative chemisorption can vary over many orders of magnitude. We have studied a number of dissociative and molecular chemisorption systems over the years using molecular beam scattering.

Even for a very simple system such as non-activated molecular NO adsorption on Pt(111) our studies show that chemisorption is dominated by the deep chemisorption well. Surprisingly, there is a strong orientation dependence for the trajectories that do not lead to sticking [1]. Clearly the chemisorption well depth is orientation dependent. Similar effects may be important for many other systems.

Chemisorption is also dependent on the coverage of the surface. Passivation by hydrogen turns Ru(0001) into a flat mirror for molecules, sometimes with small holes in the mirror [2]. Covering the surface by molecules makes it a diffuse scatterer.

Activated dissociative chemisorption involves barriers, the nature of which is often unknown. N_2 dissociation on Ru(0001) is extremely difficult. Theoretical and molecular beam studies show that there is a metastable intermediate involved [3]. This may be one of the reasons why the dissociation process is hard to unravel: It involves intermediates that are non accessible to surface spectroscopies. For the dissociation of O_2 on Ag(111) a similar metastable intermediate was found by molecular beam methods [4, 5].
Molecular beam methods are very appropriate to determine barrier heights and the importance of metastable states. In many cases the process of dissociative chemisorption is hindered by other factors, such as diffusion at the surface. In this case molecular beam studies as such are not very informative. We found this when studying the coverage dependence of dissociative chemisorption of O_2 on Ag(110). Here diffusion of molecularly chemisorbed O_2 to a step is another rate limiting step. The diffusion is hindered by the presence of added Ag-O- rows at the surface. These rows form a kind of fences at the surface that induce desorption of the intermediate molecularly chemisorbed O_2. This information cannot be extracted from the molecular beam data, but was obtained from a scanning probe. Using this information the coverage dependence of the dissociative sticking coefficient could be modeled easily. It was found that a combination of energetic barriers and fences for diffusion were the rate limiting steps in this process [6]

Very recently we have studied the chemisorption of CO on 90% passivated H-Ru(0001). This gives another example of the power of the molecular beam method when studying chemisorption problems. From measurements of He scattering during displacement we could deduce that CO forms islands in the hostile sea of H-atoms on the Ru-surface. This process, which is well known from surface structural studies,

* Abstract 7012 submitted to the 21st International Symposium on Rarefied Gas Dynamics, Marseille, France, July 26-31, 1998.

occurs already at extremely low coverages, lower that 0.01 of a monolayer.

In the talk the number of examples discussed above will be presented to illustrate the use of molecular beam techniques to study the dynamics of chemisorption.

References:

[1] R.J.W.E. Lahaye, S. Stolte, S. Hollo way, and A.W. Kleyn, J. Chem. Phys. **104** (1996) 8301.

[2] D.A. Butler, B. Berenbak, S. Stolte, and A.W. Kleyn, Phys. Rev. Lett. **78** (1997) 4653.

[3] J.J. Mortensen, B. Hammer, and J.K. Norskov, Phys. Rev. Lett. **80** (1998) 4333.

[4] A. Raukema, and A.W. Kleyn, Phys. Rev. Lett. **74** (1995) 4333.

[5] A. Raukema, D.A. Butler, and A.W. Kleyn, J. Chem. Phys. **106** (1997) 2477.

[6] D.A. Butler, J.B. Sanders, A. Raukema, A.W. Kleyn, and J.W.M. Frenken, Surf. Sci. **375** (1997) 141.

Focussing Helium Atom Beams Using Single Crystal Surfaces

W. Allison and B. Holst†
Cavendish Laboratory
University of Cambridge, CB3 0HE, UK
† Present address: Max-Planck-Institut für Strömungsforschung,
Bunsenstr. 10, D-37073 Göttingen, FDU

1 Introduction

Focussed beams of thermal energy atoms offer several new opportunities for experimental development. We have recently shown that inert atoms, at thermal energies, can be focussed using reflection from a single crystal surface [1]. The main purpose of the present work is to provide further experimental details on the method and to discuss the factors that limit the quality of the focussed atom beams. Our approach has been to use helium atoms from a conventional molecular-beam source [2] operating at room temperature. The atoms are scattered from a hydrogen passivated silicon surface, Si(111)-(1x1)H, and focussing is achieved by deforming the surface into a concave profile. The use of a solid surface gives true elastic-scattering in the specular direction, thus the temporal coherence of the helium beam is preserved and small spot sizes can be achieved.

Focussed beams of helium atoms offer the prospect of significant improvements over current experiments. If these new possibilities are to be explored it is important to understand the factors, such as the atom source and scattering surface, that may limit the mirror performance. The results presented here are consistent with a mirror profile that is close to an ideal parabola and we show that the transverse velocity distribution in the molecular beam, which determines the effective source disk, is the dominant factor in determining the spot-size in the focussed beam.

*Abstract 7015 submitted to the 21st International Symposium on Rarefied Gas Dynamics, Marseille, France, July 26-31, 1998

2 Methods

The focussing mirror was created from a passivated Si(111)-(1x1)H wafer, with a thickness of 50 microns. Preparation of the surface consisted of cycles of oxide stripping and hydrogen passivation, which were performed ex situ [3]. The sample was transferred to the vacuum in an inert atmosphere and the quality of the surface remained unchanged over periods of several months. Figure 1 shows a schematic diagram of the sample mounting, in cross section. The sample, A, is mounted on a precision ground

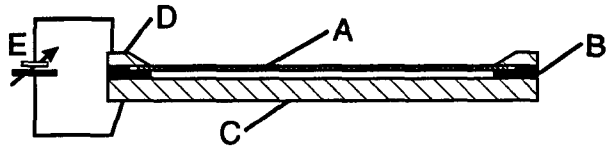

Figure 1: Sample mounting

sapphire insulator, B, which separates it from a lower electrode, C. The central part of the sample is free standing and deforms under electrostatic pressure when a potential difference, E, is applied between the sample and lower electrode. A metal ring, D, acts as an electrical contact and a clamp for the top of the sample.

The mirror is arranged to scatter atoms through a right angle to a fixed mass spectrometer, which acts as detector. The soure to mirror and mirror to detector distances are 0.7 m and 0.9 m respectively. The nozzle source was operated at a stagnation pressure of 150 bar, at room temperature, giving a helium beam wavelength of 0.052 nm. The spatial resolution of the ion source was increased to the desired level by placing a moveable pinhole, diameter 0.1 mm, between the mirror and the detector. The beam profile was obtained by scanning the beam across the pinhole.

3 Results

The scattering geometry is necessarily astigmatic. Thus the image formed in the scattering plane occurs at a different electric-field setting from that used to produce an image in the plane normal to the scattering plane. Between these settings lies the disk of least confusion. In our system this corresponds to a radius of curvature, R, equal to 0.78m. The beam profile obtained at the disk of least confusion is shown by the solid curves in fig. 2. The spot

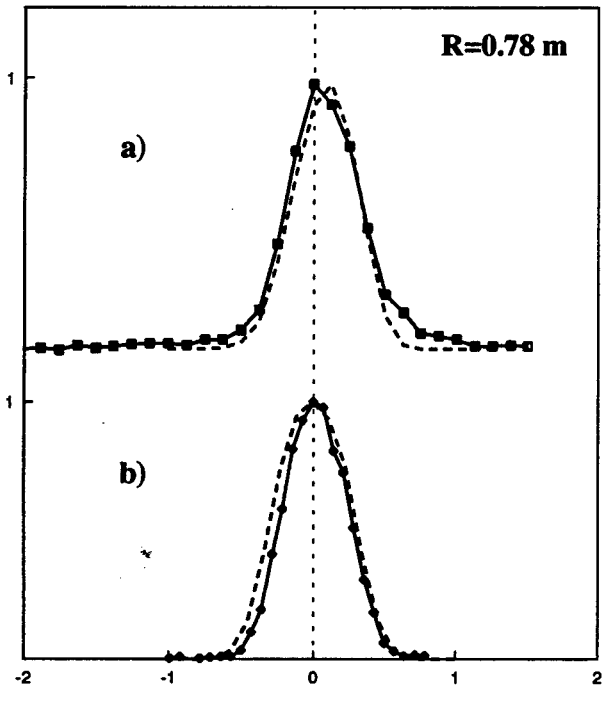

Figure 2: Spot profile

diameter of the disk of least confusion is 210+/-50 micron, where the uncertainty arises from the effect of the finite size of the pinhole (100 micron). The diameter is a factor of ten smaller than that of the unfocussed beam.

In order to assess the limits on the spot size, we have performed extensive ray tracing calculations. Three main factors affect the shape of the focussed spot-profile: the mirror profile; the effective object provided by the nozzle source; and the collimating apertures. All are included in the ray tracing. The profile of the mirror was taken to be a perfect paraboloid with a curvature given by the known applied field and known mechanical properties. The nozzle source was taken to be radially symmetric and the atom trajectories were assumed to start at a virtual source obtained by back projecting trajectories from the last collision surface, which separates the continuum and quasi-molecular-flow regimes [4].

Beyond the last collision surface, the perpendicular velocity distribution in the beam will continue to change as occasional collisions can transfer relatively large amounts of energy from the parallel to the perpendicular distribution. For the conditions in our experiment this latter effect dominates and it determines the effective source size.

The measured spot profile, at the disk of least confusion, are fitted to the simulations with a single variable parameter: the radius of the effective virtual source. The results of both measurement and fit, with an effective source-radius of 0.2 mm, are shown in fig. 2, where the fitted simulations are shown as a dashed curve. The agreement between simulation and experiment is excellent showing that the assumptions in the modelling are valid. Furthermore, spot profiles obtained at other values of the applied field have be compared with the simulations and similar good agreement has been obtained. At very small applied fields, where the calculated radius of curvature is large (> 1.5 m), we observe systematic deviations of the simulation from the measurements; however, these differences can be explained by small deviations from perfect planarity in the initial, zero-field, shape of the mirror.

In summary, we have demonstrated focussing of neutral helium atoms in the thermal energy regime. The quality of the optical "image" of the effective nozzle source has been shown to be of a high order and appears to be determined by the properties of the source itself, rather than any unexpected optical aberrations from the mirror. This fact alone shows that significant further improvements in image size can be obtained using smaller source sizes.

References

[1] B. Holst and W. Allison, Nature 390, 244 (1998).

[2] J.R. Buckland, R.L. Folkerts, R Balsod and W. Allison, Measurement Sci. and Technol. 8, 933 (1997).

[3] G.S. Higashi, R.S. Becker, Y.J. Chabal and A.J. Becker, Appl. Phys. Lett. 58, 1656 (1991).

[4] H.C.W. Beijerinck, G.H. Kaashoek, J.P.M. Beijers and M.J. Verheijen, Physica C 121, 425 (1983).

Sufficient Conditions for Quantum Reflection with Realistic Gas-Surface Interaction Potentials *

R.B. Doak† and A.V.G. Chizmeshya‡
†Department of Physics and Astronomy and ‡Materials Research Group
Arizona State University, Tempe, AZ, USA

1 Introduction

In complete contradiction to intuitions of classical mechanics, an atom striking a solid surface at extremely low velocity does not stick. Understanding of this non-sticking emerges through quantum theory, whereby the sticking probability $S(k)$ of the atom is found to vanish linearly with decreasing incident wave vector k for sufficiently small k [1]. Accordingly, this non-sticking of ultra-slow atoms has come to be known as "quantum reflection." Considerable theoretical effort [1]-[3] has been devoted to the subject over the last two decades. To keep the calculations tractable, this work has been limited to fairly simplistic modeling of the atom-surface interaction. Consequently it is not clear whether the results offer meaningful numbers to guide real-life experimentation, specifically to answer the question of how small k must be in order for quantum reflection to ensue. As experimental techniques are developed to generate ultra-slow atom beams [4] and as the first ultra-slow atom-surface scattering experiments emerge [5], this question has become quite relevant. In this paper we present a simple characterization of quantum reflection for real systems.

2 Spatial Decoupling

The quantum theory underlying quantum reflection is far less intimidating than might be supposed at first glance [2]. In its most basic form, the phenomenon derives from a simple spatial decoupling at small k of the $\hbar^2k^2/2M$ total energy term and the $V(x)$ potential energy term in the Schrödinger equation, M being the mass of the impinging atom. The decoupling yields distinct portions of the scattering wavefunction in an inner region near the surface (small atom-surface separation x) and in an outer region far removed from the surface (large x). The boundary $x = x_{</>}(k)$ between the two regions is defined by $|U(x_{</>}(k))| = k^2$ where $U(x) = 2MV(x)/\hbar^2$. The two portions must join asymptotically near $x_{</>}(k)$. In the outer region the scattering wavefunction adopts a simple sinusoidal behavior as $k \to 0$ and thereby a linear dependence kx at small x provided $\lambda = 2\pi/k$ exceeds $x_{</>}(k)$ and all other characteristic lengths of the potential. In the inner region the wavefunction becomes independent of k for $k^2 << U(x)$ and it is easily shown [6] that for a potential decaying at large x as $\sim C_s/x^s$ with $s > 2$, the inner wavefunction becomes linear in x for $x >> B$ where

$$B = \left(\frac{8MC_s}{(2-s)^2\hbar^2}\right)^{\frac{1}{(s-2)}}. \qquad (1)$$

Under appropriate conditions it then follows that the small x region of the outer wavefunction is linear in x upon approaching $x_{</>}(k)$ from above and that the large x region of the inner wavefunction is linear in x upon approaching $x_{</>}(k)$ from below. Asymptotic boundary matching at $x_{</>}(k)$ then transfers the kx-dependence of the outer portion of the wavefunction onto the inner portion. The slope of the inner wavefunction must therefore vanish linearly with k at $x_{</>}(k)$ and, since the inner portion of the wavefunction is independent for $k << |U(x)|$, this forces the same linear k-dependence onto the amplitude of the scattering wavefunction for all $x < x_{</>}(k)$. This vanishing of the scattering wavefunction near the surface is illustrated in Fig. 1 with Numerov calculations for helium scattering from Cu(111). This potential supports eight bound states as evidenced by the eight stationary zeros as $k \to 0$. The bound state wavefunction for the most weakly bound state would display seven zeros at very nearly the same x-values as the inner seven zeros of the scattering wavefunction and it would decay exponentially in amplitude at large x.

*Abstract 7064 submitted to the 21st International Symposium on Rarefied Gas Dynamics, Marseille, France, July 26-31, 1998

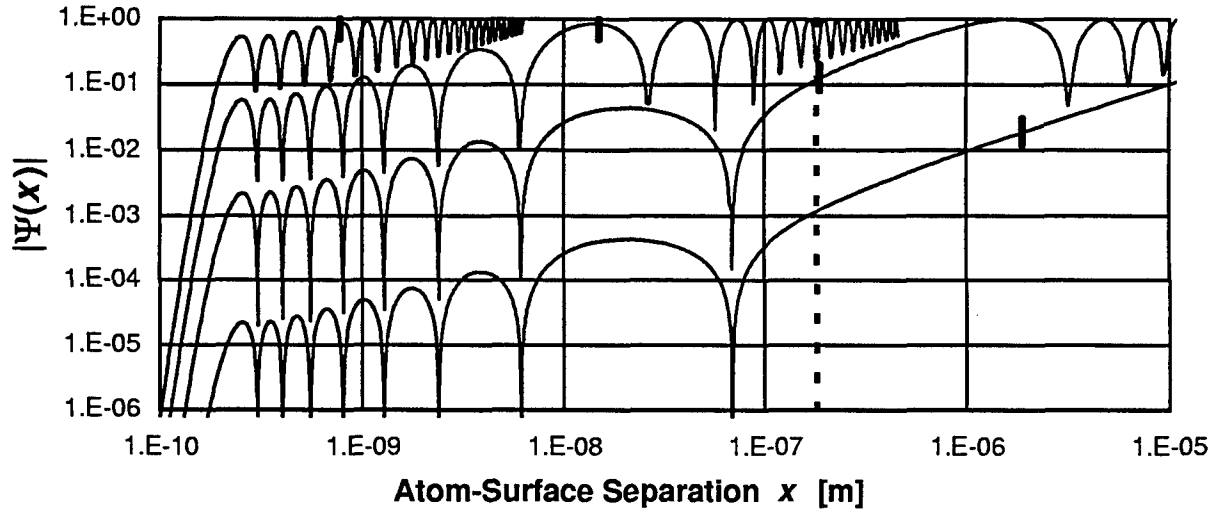

Figure 1: Scattering wavefunctions demonstrating near-surface dimunition with decreasing k for, top to bottom, $k = 10^{10}, 10^8, 10^6$, and 10^4 m^{-1}. Numerov calculations for a retarded He:Cu(111) potential. Short vertical bar on each curve marks decoupling boundary $x_{</>}(k)$ at that k. Dashed vertical line marks separation B beyond which $k \to 0$ form of the inner wavefunction is asymptotically linear in x.

3 Sticking Coefficient

Sticking of the incident atom onto the surface requires a transition from the Ψ_k scattering state into some Ψ_n bound state. Within the DWBA, the probability of this transition is proportional to $| < \Psi_n|V'|\Psi_k > |^2/k$ where V' is the perturbative potential mediating the transition [1], [6]. Ψ_n is independent of k and thus, for k-independent $V'(x)$ and given the linear k-dependence of Ψ_k in the overlap region, the sticking coefficient must decrease linearly with k. This is the hallmark of quantum reflection and the conditions giving rise to this behavior therefore constitute a set of sufficient conditions for quantum reflection. Those conditions are enumerated in detail elsewhere [6] and the dominant restrictions are generally (1) that $x_{</>}(k) > B$ and (2) that $x_{</>}$ be the largest characteristic length scale of the interaction potential. As $x_{</>}(k)$ moves outward with decreasing k, it eventually exceeds B, whereupon the vanishing inner wavefunction (Fig. 1) gives rise to quantum reflection. Explicitly, this requires

$$k << [2MC_s/\hbar^2 B^s]^{1/2} \quad . \qquad (2)$$

Knowledge of M, s, and C_s thus suffices to specify sufficient conditions for quantum reflection.

4 Acknowledgement

This work was supported in part under grant PHY-9223053 of the U.S. National Science Foundation.

References

[1] Clougherty D.P. and Kohn W., *Quantum theory of sticking*, Phys. Rev. B. Vol. 46 II, No. 8, pp. 4921–4937 (1992).

[2] Böheim J., Brenig W., and Stutzki J., *On the Low Energy Limit of Reflection and Sticking Coefficients in Atom Scattering*, Z. Physik B Vol. 48, pp. 43–49 (1982).

[3] Brenig W., *On the Low Energy Limit of Reflection and Sticking Coefficients in Atom Scattering.*, Z.Physik B Vol. 36, pp. 227-233 (1980).

[4] Lawall J., Kulin J.S., Saubamea B., Bigelow N., Leduc M., and Cohen-Tannoudji C., *Three-dimensional subrecoil laser cooling*, **Laser Spectroscopy. 12th Int. Conf., World Scientific, Singapore, 1995, and other papers in those proceedings.**

[5] **Yu I.A., Doyle J.M., Sandberg J.C., Cesar C.L., Kleppner D., and Greytak T.J., *Evidence for Universal Quantum Reflection of Hydrogen from Liquid ^{4}He*, Phys. Rev. Lett. Vol. 71, No. 10, 1589–1592 (1993).**

[6] **Doak R.B. and Chizmeshya A.V.G., *Quantum Reflection for Realistic Interaction Potentials: Sufficiency Conditions and Fundamental Understanding*, submitted, (April 1998).**

Surface Dynamics Studies using ^{3}He Spin Echo: Coronene on Gold *

M.F.M. DeKieviet[1], D. Dubbers[2], S. Hafner[1], F. Lang[1]
[1] Physikalisches Institut Universität Heidelberg, Heidelberg, Germany
[2] Institut Laue Langevin, Grenoble, France

We describe a novel technique, atomic beam spin echo, which aims at measuring extremely small changes in the kinetic energy in a flux of atoms (or molecules) carrying a magnetic moment.
For the study of 2-D dynamics, we constructed a ^{3}He Spin Echo (^{3}HeSE) spectrometer, which is schematically shown in Fig. 1. The difference in the Larmor precession angle of the nuclear spin of the He atoms in during their flight through the spin echo coils B_1 and B_2, before and after interaction with the probe surface, respectively, is a measure of the energy transfer during scattering. The macroscopic atomic beam polarization P_x of the echo signal, as a function of the magnetic field strengths B_1 and B_2, gives the time correlation (and therewith the dynamics) of the system. Our ^{3}HeSE spectrometer has an energy resolution of 10 neV with a coherence length up to 10μm [1].

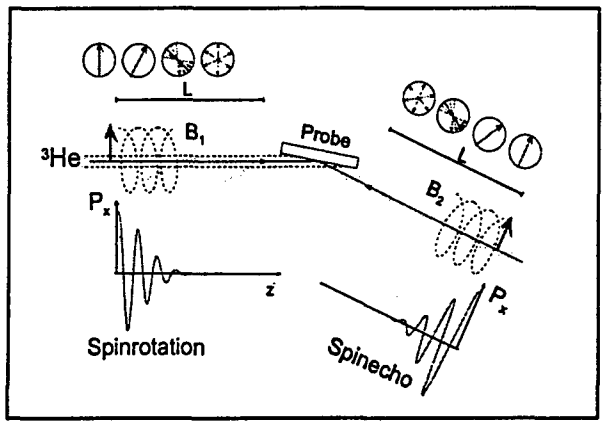

Figure 1: Classical picture of the ^{3}He spin echo experiment.

In this contribution, we show ^{3}He scattering data illucidating the structure and dynamics in and on the surface of gold. Of all fcc centered cubic metal (111) surfaces, Au is the only element showing reconstruction, with a rectangular unit cell topping the triangular bulk symmetry. The ^{3}He diffraction patterns, we obtained from a single crystal gold sample along the $[1\bar{1}0]$azimuthal direction, confirm the dimensions of this reconstruction to be $(p \times \sqrt{3})$, with $p = 21.5 \pm 0.5$ expressed in the bulk nearest neighbor distance $a = 2.885$ Å.

The dynamics of this reconstruction was captured with the ^{3}HeSE method, by following the two lowest-lying branches in the dispersion curve for Au(111). Calculations by Benedek et al. [2] have shown that the frequencies of these two branches for the reconstructed surface become zero at finite momentum $\vec{k}$. This is experimentally demonstrated by our data.

In addition, the thus characterized crystal serves as a substrate for the adsorption of coronene, which represents the nano-scale analogue of a puck-on-ice. At complete monolayer coverage, we find a commensurate $C_{24}H_{12}(4x4)/Au(111)$ superstructure, in which the coronene molecules have an equilibrium distance of 11.5 Å, and fit together like gears.
At a very dilute adsorbate concentration ($\ll$ 1 ML), the diffusive motion of coronene molecules was studied through quasi-elastic ^{3}He scattering. Since the ^{3}HeSE spectrometer was particularly built for studying slow, 2-D diffusion, we explicitly discuss the experimental details concerning this measurement. In Fig. 2, we schematically show how the intermediate scattering function, which fully describes the observed dynamics of the system in the time domain , is obtained from the spin echo data.

SE curves were measured for several incident angles and for surface temperatures ranging from 95 K upto 435 K. A representative set of these, taken at $\theta_i = 53.5°$ and $T_{surface} = 294$ K, is displayed in Fig. 2. The intermediate scattering function $I(\Delta K, \tau_{SE})$ (lower panel) is composed of the measured polarization in the SE point for each SE curve, i.e. for each SE time τ_{SE}. For coronene on gold(111) it contains

*Abstract 6968 submitted to the 21st International Symposium on Rarefied Gas Dynamics, Marseille, France, July 26-31, 1998

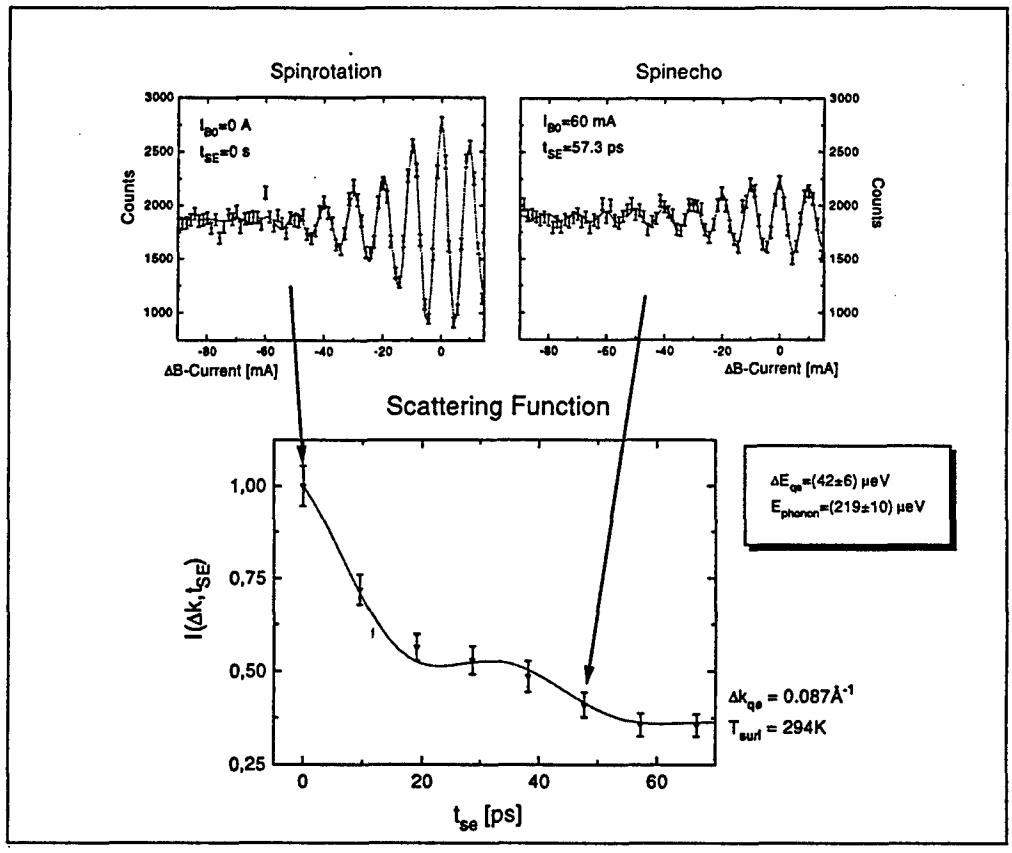

Figure 2: Compositon of the intermediate scattering function $I(\Delta K, \tau_{SE})$ for $C_{24}H_{12}/Au(111)$.

two contributions: An exponential decay, describing the quasi-elastic part, which results from the diffusion of the adsorbate. From the decay constant as a function of the surface temperature we obtain an activation barrier to diffusion of $E_A = (35 \pm 6)$ meV. The oscillatory part in the intermediate scattering function in figure 2 stems from the phonon dispersion curve for the reconstructed Au(111) surface, discussed above. The smallest phonon energy measured here is of the order of 20μeV.

References

[1] M.DeKieviet, D.Dubbers, M.Klein, Ch.Schmidt and M.Skrzipczyk, Surf. Sci. **377-379**, 1112 (1997).

[2] J.P.Toennies in: *Surface Phonons*, Eds. W.Kress and F.W.de Wette, Springer Series in Surface Science **21**, Springer (1991).

Enrichment of binary van der Waals clusters surviving surface collision. *

E. Fort, A. De Martino, F. Pradère, M. Châtelet and H. Vach
Laboratoire d'Optique Quantique du CNRS, Ecole Polytechnique,
91128 Palaiseau Cedex, France
e-mail: fort@leonardo.polytechnique.fr

When colliding with a hot surface at thermal kinetic energies, large van der Waals clusters undergo a kind of Leidenfrost process [1]. They slide on the surface, isolated by a cushion of atoms. Their normal kinetic energy is converted into heat and released by the evaporation of thermalized small fragments. Their average tangential velocity is approximately conserved. When the normal kinetic energy is not sufficient to evaporate the whole cluster, large fragments survive and are detected at grazing angles [1, 2].

We present results obtained for mixed Ar_nKr_m and Ar_nXe_m clusters produced by xenon picked up on pure argon clusters. The clusters are scattered off a hot (T_S = 500 K) graphite surface. Like pure clusters, these binary clusters undergo the same evaporation regime collision dynamics. Fig. 1 shows angular distributions of scattered particles obtained with a rotatable quadrupole mass spectrometer (QMS) for mixed $Ar_{4000}Xe_{600}$ clusters impinging on a HOPG surface. The QMS was operated at xenon and argon masses. The broad evaporation component and the narrow grazing one are fitted respectively by the thermokinetic model [3] and by a Gaussian function. From these fits, it is first possible to evaluate the total flux together with the relative fluxes of the scattered particles for both components. The total flux is know with a relative precision of ±20 % (limited by out of plane undetected particles). Typically, for the experimental conditions considered, the surviving cluster represents about 10 % of the incoming one. Then, the coincidence of the Gaussian function parameters (width and position) for both mass settings gives an unbiased criterion for the presence of a surviving binary cluster.

The evaporation process is species selective as clearly shown in fig. 1 where argon evaporates more easily than xenon. Consequently, the cluster undergoes a change of composition upon collision [4]. We

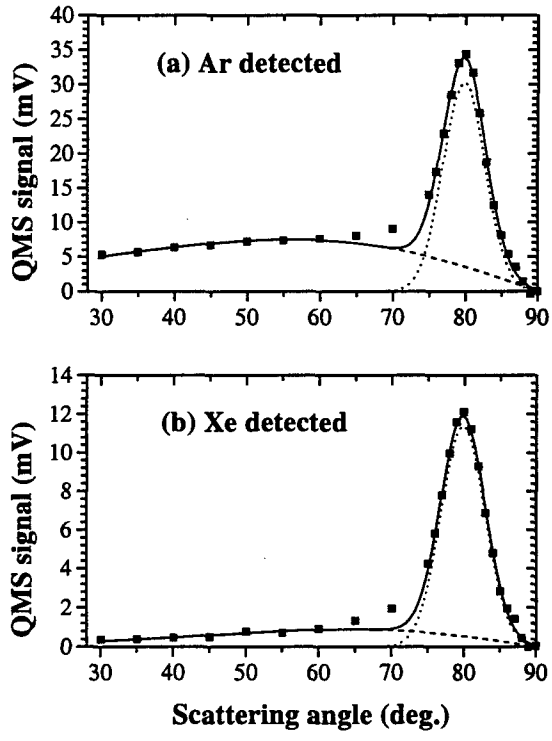

Figure 1: Density profiles obtained for mixed clusters $Ar_{4000}Xe_{600}$ colliding with a HOPG surface at T_S=500 K for argon (a) and xenon (b) QMS mass settings. The incident angle is $\theta_{inc} = 40°$ and the incident cluster velocity is 430 m/s. The evaporation component fits obtained with the thermokinetic model, the grazing component Gaussian fit and their sums are represented respectively in dashed, dotted and full lines.

*Abstract 6957 submitted to the 21st International Symposium on Rarefied Gas Dynamics, Marseille, France, July 26-31, 1998

characterize this change by the enrichment factor E(X) in the dopant species X. It is defined as the ratio of the dopant molar fraction (mf) in the surviving cluster over mf in the incident cluster.

We have studied the influence of the incident cluster composition, incidence angle and incident cluster size on the enrichment factor. As expected from simple bonding energy considerations, E(Kr) and E(Xe) are always larger than one. Nevertheless, the evaporation process cannot be considered as a classical distillation process. Indeed, we find E(Kr) to be always larger than E(Xe), in disagreement with bonding energy ordering. Besides, for high dopant concentrations (0.15 mf), xenon has a much more dramatic effect on the size and composition of the surviving cluster than krypton: for low enough incidence angles, no surviving cluster is detected for xenon, contrary to krypton. Fig. 2 shows the variations of E(Xe) and E(Kr) *vs* dopant molar fraction.

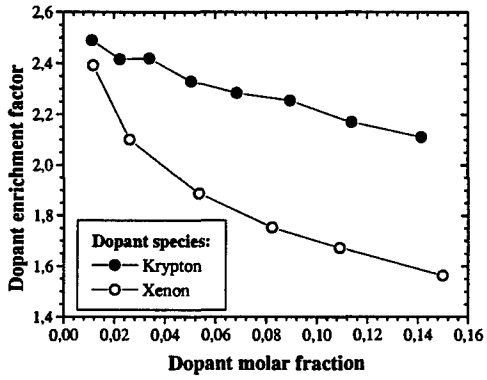

Figure 2: Variations of the enrichment factors vs. cluster composition for $Ar_{4000}Kr_n$ and $Ar_{4000}Xe_n$ mixed clusters with $30 < n < 600$ colliding with a HOPG surface at $T_S = 500$ K at a velocity of 430 m/s and a incidence angle of 60°.

We think that the incident cluster structure must play a crucial role in the enrichment results, which implies that the collision process does not reorganize completely the incident cluster. These results prove that it is possible to use surface scattering as a sensitive cluster structure probe technique since krypton and xenon have similar atomic properties but give quite different enrichment results. Also, binary clusters can help elucidate the cluster surface collision dynamics.

References

[1] H. Vach, M. Benslimane, M. Châtelet, A. De Martino, F. Pradère, J. Chem. Phys. **103**, 1972 (1995).

[2] M. Svanberg, J.B.C. Pettersson, Chem. Phys. Lett. **263**, 661 (1996).

[3] H. Vach, A. De Martino, M. Benslimane, M. Châtelet, F. Pradère, J. Chem. Phys. **100**, 3526 (1994).

[4] F. Pradère, M. Benslimane, M. Châtelet, A. De Martino, H. Vach, Surf. Sc. Lett. **375**, L375 (1997).

MOLECULAR BEAM SESSION INDEX

Your Reliable Partner in China

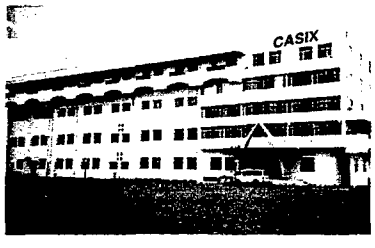

CASIX Corporate Heaquarters

Leading Technology
Mass Production
High Quality
Low Cost

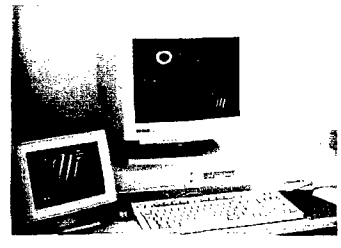
Zygo Interferometer

CASIX


Crystals & Optical Components

Optics
Crystals
Fiber Optics
Lasers & Accessories

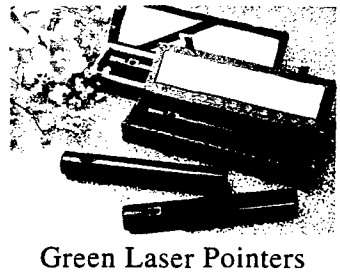
Green Laser Pointers

☞ Crystals

Nd:YV04, YV04, BBO, LBO, KTP
*a-BBO, KD*P, Nd:YAG, Cr:YAG,*
$LiNbO_3$, etc.

☞ Optics

Lenses, Prisms, Windows, Waveplates,
Polarizers, Laser Optics, Mirrors,
Beamsplitters, Substrates, etc.

☞ Diode Pumped Green & IR Lasers

Nd:YVO_4+KTP, Miniature design,
1-100 mW Green, 1-400 mW Infrared,
NEW! 1-5 mW battery powered POINTER.

☞ Fiber Optics Components

GRIN Lens, Birefringent Wedge, Filter,
Polarization Beamsplitter, Coupler,
Collimator, Pigtail Fiber, etc.

☞ OPO/OPA Systems & Doublers

Wide Tunability from 0.2 to 4.5 um,
Unique Design, Low Threshold & High,
Efficiency Doublers, Mixers & Others .

☞ Ti:Sapphire Doubler & Tripler

High Conversion efficiency,
Patended Time Plate Design,
Easy Operation & Tuning.

Please contact TECHNOSCIENCE
CASIX's representative in France

TECHNOSCIENCE
24, rue Charles de Gaulle, 91400 Orsay, France
Tél. : 01 69 28 01 05 - Fax : 01 69 28 00 78 - E-mail : Tchnscfr@aol.com
S A R L au capital de 210 000 F - R.C.S. Corbeil B 339 966 152 - Siret 339 966 152 00029

FC CASTECH

Fujian Castech Crystals, Inc.
P. O. Box 143. Fuzhou. Fujian 350002. P. R. China

Tel : — (86) 591 3710533
Fax : — (86) 591 3711593

BBO & LBO

The best choice to use your budget efficiently and economically!

●High Quality ●Low Price ●Fast Delivery

Optics Functional Crystal

- ***Nonlinear Optical/E-O Crystal:***
  *BBO, LBO, KTP, KD*P, KDP,*
  $LiNbO_3$, $LiIO_3$, ADP.
- ***Acousto-Optical Crystal:***
  $PbMoO_4$, TeO_2, $LiNbO_3$, $LiTaO_3$.
- ***Laser Crystal:***
  $Nd:YVO_4$, Nd:YAP, NYAB, Nd:YAG
- ***X-ray crystals:***
  PET, KAP
- ***Superconductive substrates:***
  $MgAl_2O_4$
- ***Angular Tuning Crystal Position Stage.***
- ***Hermetically Sealed Crystal House.***
- ***Free Crystal-Mirror mount Adaptor For BBO and LBO crystal.***
- ***Free Technical Consulting and Catalog.***

Backed by the first class R&D ability of Fujian Institute of Research on The Structure of Matter, and other Institutes of Chinese Academy of Science, Fujian CASTECH has become a world leading innovator and supplier of advanced optics functional crystals, especially in the line of nonlinear optical crystals. Through optimizing her fabrication procedure, and establishing strict quality control system, Fujian Castech now market her crystal products in stable high quality and low price with fast delivery.

Optical Components

- ***Windows ●Prisms ●Lenses ●Quartz plate***
  α-$NiSO_4$, CaF_2, BK7, UV-Fused Silica
  SF-2, SF-6, SF-10, SF-11, SF-14, SF-57
  Sapphire, LiF, MgF_2, ZnSe, ZnS, KBr, NaCl

Along with the developing of her business, Fujian Castech has established a production line of optical components, and has very strong ability to better service OEM users.

Please contact TECHNOSCIENCE
CASTECH's representative in France

TECHNOSCIENCE
24, rue Charles de Gaulle, 91400 Orsay, France
Tél. : 01 69 28 01 05 - Fax : 01 69 28 00 78 - E-mail : Tchnscfr@aol.com

S A R L au capital de 210 000 F - R.C.S. Corbeil B 339 966 152 - Siret 339 966 152 00029